Regulation of the Mevalonate Pathway by the Deubiquitinase USP28 in Squamous Cancer

Regulation des Mevalonat Stoffwechselwegs durch die Deubiquitinase USP28 in Plattenepithelkarzinomen

Doctoral thesis for a doctoral degree
at the Graduate School of Life Sciences,
Julius-Maximilians-Universität Würzburg,
Section - Biomedicine

submitted by

Carina Ramona Maier

from

Heidenheim a.d. Brenz, Deutschland

Würzburg **2023**

Submitted on: ……..……..

Office stamp

Members of the Thesis Committee

Chairperson: Prof. Dr. Alexander Buchberger

Primary Supervisor: Prof. Dr. Almut Schulze

Supervisor (Second): Dr. Grzegorz Sumara

Supervisor (Third): Dr. Nikita Popov

Supervisor (Fourth): Dr. Markus Diefenbacher

Date of Public Defence: ……..……

Date of Receipt of Certificates: ……

Du hinterlässt Spuren in unseren Herzen – Mögen sie uns in die Zukunft führen.

Table of Contents

1 Summary

The reprogramming of metabolic pathways is a hallmark of cancer: Tumour cells are dependent on the supply with metabolites and building blocks to fulfil their increased need as highly proliferating cells. Especially *de novo* synthesis pathways are upregulated when the cells of the growing tumours are not able to satisfy the required metabolic levels by uptake from the environment.
De novo synthesis pathways are often under the control of master transcription factors, which regulate the gene expression of enzymes, involved in the synthesis process. The master regulators for *de novo* fatty acid synthesis and cholesterogenesis are sterol regulatory element-binding proteins (SREBPs). While SREBP1 preferably controls the expression of enzymes involved in fatty acid synthesis, SREBP2 regulates the transcription of the enzymes of the mevalonate pathway and downstream processes namely cholesterol, isoprenoids and building blocks for ubiquinone synthesis.
SREBP activity is tightly regulated at different levels: The post-translational modification by ubiquitination decreases the stability of active SREBPs. The attachment of K48-linked ubiquitin chains marks the transcription factors for the proteasomal degradation. In tumour cells, high levels of active SREBPs are essential for the upregulation of the respective metabolic pathways. The increased stability and activity of SREBPs were investigated in this thesis.
SREBPs are ubiquitinated by the E3 ligase Fbw7 which leads to the subsequential proteolysis of the transcription factors. The work conducted in this thesis identified the counteracting deubiquitination enzyme USP28 which removes the ubiquitin chains from SREBPs and prevents their proteasomal degradation.
It further revealed that the stabilisation of SREBP2 by USP28 plays an important role in the context of squamous cancers. Increased USP28 levels are associated with a poor survival in patients with squamous tumour subtypes. It was shown that reduced USP28 levels in cell lines and *in vivo* result in a decrease of SREBP2 activity and downregulation of the mevalonate pathway. This manipulation led to reduced proliferation and tumour growth.
A direct comparison of adenocarcinomas and squamous cell carcinomas in lung cancer patients revealed an upregulation of USP28 as well as SREBP2 and its target genes. Targeting the USP28-SREBP2 regulatory axis in squamous cell lines by inhibitors also reduced cell viability and proliferation.

In conclusion, this study reports evidence for the importance of the mevalonate pathway regulated by the USP28-SREBP2 axis in tumour initiation and progression of squamous cancer. The combinatorial inhibitor treatment of USP28 and HMGCR, the rate-limiting enzyme of the mevalonate pathway, by statins opens the possibility for a targeted therapeutic treatment of squamous cancer patients.

2 Zusammenfassung

Die Reprogrammierung metabolischer Stoffwechselwege ist ein Kennzeichen von Krebs: Tumorzellen sind abhängig von der Versorgung mit Metaboliten und Bausteinen, um ihren wachsenden Bedarf als hoch proliferierende Zellen zu decken. Vor allem die *de novo* Stoffwechselsynthesewege sich hochreguliert, wenn die Zellen des wachsenden Tumors nicht mehr in der Lage sind, ihr erforderliches metabolisches Niveau mithilfe der Aufnahme aus der Umgebung zu erfüllen.
De novo Synthesewege sind oft unter der Kontrolle von zentralen Transkriptionsfaktoren die die Genexpression von Enzymen, die im Syntheseprozess beteiligt sind, regulieren. Die vorherrschenden Regulatoren, für die *de novo* Fettsäuresynthese und der Cholesterogenese sind die Steroid-regulatorisches-Element-bindende Proteine (SREBPs). Während SREBP1 bevorzugt die Expression von Enzymen die an der Fettsäuresynthese beteiligt sind kontrolliert, reguliert SREBP2 die Transkription von Enzymen des Mevalonat Stoffwechselwegs, sowie Prozesse unterhalb, namentlich die Cholesterol-, Isoprenoid- und die die Synthese von Bausteinen für die Ubiquinonsynthese.
Die Aktivität von SREBP ist streng reguliert auf verschiedenen Ebenen: Die post-translationale Modifikation mittels Ubiquitinierung reduziert die Stabilität von aktiven SREBPs. Das Anhängen von K48-verlinkten Ubiquitinketten markiert die Transkriptionsfaktoren für den proteasomalen Abbau. In Tumorzellen sind hohe Niveaus von aktiven SREBPs essentiell für die Induktion der entsprechenden metabolischen Stoffwechselwege. Die erhöhte Stabilität und Aktivität von SREBPs wurden im Rahmen dieser Arbeit untersucht.
SREBPs werden von der E3-Ligase Fbw7 ubiquitiniert, was zur Proteolyse der Transkriptionsfaktoren führt. In dieser Arbeit wurde gezeigt, dass das entgegenwirkende Deubiquitinierungsenzym USP28 die Ubiquitinketten von SREBPs entfernt und deren proteasomalen Abbau verhindert.
Diese Forschungsarbeit zeigt weiterhin, dass die Stabilisierung von SREBP2 durch USP28 eine wichtige Rolle im Kontext von Epithelkarzinomen spielt. Erhöhte USP28 Niveaus werden mit einem schlechten Überleben von Patienten in der Krebs-Untergruppe der Plattenepithelkarzinomen verbunden. Es konnte gezeigt werden, dass reduzierte USP28 Niveaus, in Zelllinien und *in vivo,* niedrigere SREBP2-Aktivität und eine Herunterregulierung des Mevalonat Stoffwechselwegs ergeben. Diese Manipulation führte zu reduzierter Proliferation und Tumorwachstum.
Ein direkter Vergleich von Adenokarzinomen und Plattenepithelkarzinomen in Lungenkrebspatienten zeigte zudem eine Hochregulierung von USP28 ebenso wie SREBP2 und dessen Zielgenen. Der gezielte Einsatz von Inhibitoren gegen die USP28-SREBP2 regulatorische Achse in Plattenepithelzellen reduzierte die Lebensfähigkeit und Proliferation der Zellen.

Abschließend berichtet diese Forschungsarbeit von der Bedeutung des durch die USP28-SREBP2 Achse regulierten Mevalonat Stoffwechselwegs bei der Tumorinitiation und dem Fortschreiten von Plattenepithelkarzinomen. Die

kombinatorische Behandlung mit USP28- und Inhibitoren der HMGCR, dem Schlüsselenzym des Mevalonat Stoffwechselwegs, mithilfe von Statinen eröffnet die Möglichkeit für eine gezielte therapeutische Behandlung von Patienten mit Plattenepithelkarzinomen.

1 Introduction

1.1 Post-translational regulation of protein stability and activity

Gene expression is a tightly regulated cellular process and transcription factors (TFs) play a pivotal role in protein homeostasis and cell survival. Many TFs involved in cell proliferation are short-lived proteins and show a high turnover rate to accommodate rapidly to specific circumstances. The fast degradation of the TFs is predominantly mediated by the post-translational attachment of ubiquitin chains. However, ubiquitination can also lead to enhanced transcriptional activity. The various different types of ubiquitination signals specifically regulate the stability and activity of transcription factors.

1.1.1 The post-translational modification of proteins by ubiquitination

Ubiquitination, the attachment of the small 76 amino-acid protein ubiquitin to specific amino acid residues or the N-terminus of proteins, is a common post-translational modification. The C-terminal carboxyl group of ubiquitin (Gly76) thereby reacts with either the N-terminal amino group or the amino group of an internal lysine residue to form a stable isopeptide bond, a cysteine residue to form a thioester bond or serine and threonine residues through an ester bond. The ubiquitination of proteins involves three main steps: the activation, the conjugation and the ligation of ubiquitin with the substrate protein. These biochemical steps are catalysed by a sequential cascade of ubiquitin-activating enzymes (E1s), ubiquitin-conjugating enzymes (E2s) and ubiquitin ligases (E3s), respectively (Pickart *et al.* 2004, Komander *et al.* 2012):
In the first step, ubiquitin is activated by E1 enzymes in an ATP-consuming reaction. The formation of a highly active ubiquitin-adenylation intermediate causes the transfer of ubiquitin to the cysteine residue in the active site of the E1 enzyme to form a thioester linkage between the C-terminal carboxyl group of ubiquitin and the E1 cysteine sulfhydryl group. In the second step, the E2 enzyme catalyses the transfer of ubiquitin from the active site cysteine of the E1 to the active site cysteine of the E2 via a transthioesterification reaction. The specificity of the ubiquitin transfer to a substrate protein is determined by the E3 ligases in the third step of the cascade. E3 ligases function as substrate recognition modules and bind the activated E2 enzymes as well as the substrate protein. The ligases are divided into two classes dependent on the possession of either a “homologous to the E6-AP carboxyl terminus” (HECT) domain or a “really interesting new gene” (RING) domain. The family of HECT E3 ligases transiently bind the ubiquitin moiety at the catalytic cysteine in their active site forming a thioester intermediate, whereas RING E3 ligases function as scaffold proteins bringing E2-Ub and substrate protein into close proximity and mediate the direct transfer of ubiquitin from E2 to the substrate protein.
RING E3 ligases can function as monomers, dimers or multi-subunit complexes. The SCF complex consists of the S-phase kinase-associated protein (SKP), a cullin (CUL)

and a variable F-box protein. Cullins form the major structural scaffold of the complex. They link the RING domain, which binds the E2 enzymes, to the SKP adaptor, the recognition and binding site for the F-box protein. Various F-box proteins mediate the specific substrate binding and ubiquitination of target proteins (Komander *et al.* 2012, Swatek *et al.* 2016).

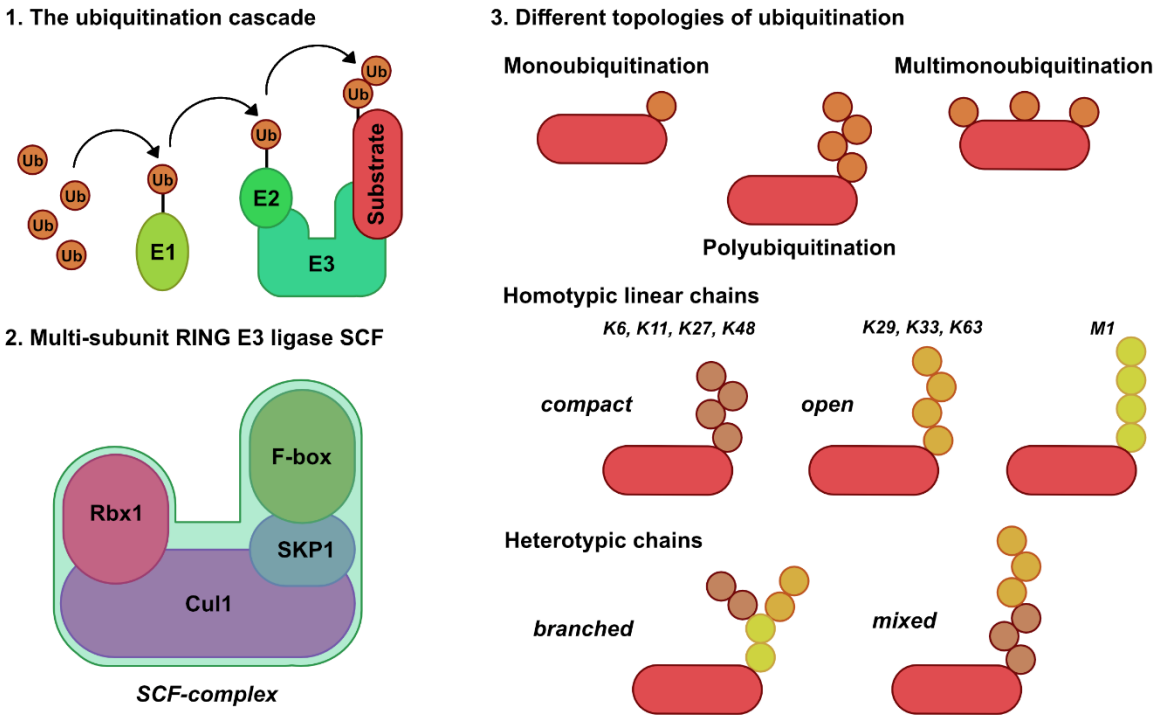

Figure 1-1: Ubiquitination is catalysed by an enzyme cascade and forms different fates of ubiquitination pattern.

Ubiquitin is bound to the E1 enzyme and transferred to the ubiquitin-conjugating enzyme (E2). Dependent on the different families of E3 ligases, the ubiquitin moiety is either first bound by the E3 ligase or directly transferred to the substrate (1). The family of RING E3 ligases are multi-subunit enzymes, e.g. the SCF complex. Rbx1 contains the RING domain and binds the E2 enzyme while the F-box protein specifically binds to the substrate protein. Cul1 and SKP function as scaffold proteins (2). Substrate proteins can show different ubiquitination fates. Beside monoubiquitinated proteins, the substrate can be ubiquitinated at different residues (multi-monoubiquitination) or the ubiquitin itself is again ubiquitinated (polyubiquitination). Polyubiquitination forms either compact or open homotypic linear chains or heterotypic branched or mixed ubiquitin chains (3).

The enzymatic cascade of E1, E2 and E3 is hierarchical: One E1 enzyme can bind dozens of E2s and these can bind hundreds of E3s. The specificity for substrate ubiquitination derives from the specific recognition and binding of the E3 ligases to the substrate.

Ubiquitin attachment can occur at a single lysine residue of the target protein (monoubiquitination). The attachment of several single ubiquitin moieties at different lysine residues of a substrate protein leads to multimonoubiquitination. However, ubiquitin itself harbours seven lysine residues and all of them can be ubiquitinated, which gives rise to isopeptide-linked ubiquitin chains. Dependent on the lysine residue (Lys6, Lys11, Lys27, Lys29, Lys33, Lys48, Lys63), different chain types are favoured (homotypic linear chains). Ubiquitin chains that are linked via different lysine residues

form heterotypic chains. Further, one ubiquitin moiety can be ubiquitinated at several lysine residues which results in branched ubiquitin chains.
The various combinations of ubiquitin linkage determine the fate of the substrate proteins: While mono- and multi-monoubiquitinated proteins are associated with protein interactions and localisation, K6-linked and K1-linked chains play a role in cell cycle regulation. K11-, K27- and K48-linked polyubiquitin chains prime substrate proteins for proteasomal degradation and the open conformation polyubiquitination of proteins with M1-, K63- K33- and K29-linked chains are important cell signalling molecules and mediate protein interactions. The specificity of the various linkage types of polyubiquitin chains are still under investigation.

1.1.2 The ubiquitin proteasome system (UPS) regulates the turnover of proteins

Proteolysis of cellular proteins is a highly complex and tightly regulated process and play a pivotal role in the balance between survival and cell death. The degradation of K48-linked polyubiquitinated proteins is mediated by the ubiquitin-proteasome pathway. Prominent cell cycle regulating proteins are often targeted for ubiquitination and subsequent proteasomal degradation (Dang *et al.* 2021). Beside controlling cell cycle as well as replication processes, the UPS regulates the proteasomal degradation and activity of transcription factors (Geng *et al.* 2012): transcription factors like c-Jun and p53 were found to be substrates for the ubiquitination cascade and the regulation of c-Myc and NF-κB transcriptional activity was a starting point for unravelling the role of ubiquitination in controlling gene expression.
Degradation of transcription factors via the ubiquitin pathway proceeds in two successive steps: Ubiquitin chains are covalently attached to the substrate proteins (see 1.1.1) and the subsequent degradation of the targeted protein by the 26S proteasome. At least four moieties of ubiquitin chains are necessary for efficient binding of the substrate protein to the proteasome (Thrower *et al.* 2000). The structure of the ubiquitin polymer is critical for the successful recognition: K48-linked polyubiquitin chains show an exact spatial relationship between each ubiquitin molecule and also K6- and K11-linked polyubiquitin chains are bound to the intrinsic proteasomal ubiquitin recognizing Rpn10/S5a family which are subunits of the 26S proteasome and function as adaptor molecules (Deveraux *et al.* 1994). Rpn10/S5a contains an ubiquitin-interacting motif (UIM) at its C terminus that mediates ubiquitin binding. However, extrinsic ubiquitin receptor proteins can also function as substrate adaptors for the proteasomes. The adaptor proteins have ubiquitin-like (UBL) domains that are recognised by the 19S proteasome and ubiquitin-associated (UBA) domains binding the ubiquitin moieties (Elsasser *et al.* 2005). These receptors are thought to escort ubiquitinated proteins to the proteasome.
The proteasome is a protein complex with a cylindrical “core” of four stacked rings forming a central pore and the 19S regulatory particle, the so-called “lid”. While the 19S regulatory particle forms the gate where ubiquitinated proteins are recognized and bind to the proteasome, the proteolytic function is mediated by the active sites of the core subunits. Here, the unfolded polypeptide chains are hydrolysed at the

isopeptide bond into short polypeptides, typically of 7-9 residues in length. Eventually, the ubiquitin-primed proteins are degraded by the proteasome and the resulting small peptides and single amino acids are reused for protein synthesis.

1.1.3 Deubiquitination – removal of ubiquitin from proteins

The ubiquitination of proteins is a reversible process and deubiquitinating enzymes oppose this post-translational modification by removing ubiquitin from the substrates. Deubiquitinases (DUBs) are cysteine or zinc metalloproteases, which cleave the bond between ubiquitin and its substrate protein. DUBs are highly specific and each DUB is only recognizing a small group of substrates.
DUBs are divided into seven distinct subfamilies based on their sequence similarity and mechanisms of action: While the members of the JAMM/MPN+ subfamily bind zinc and act as metalloproteases, the remaining six subgroups contain an active cysteine as part of the catalytic triad in their active centre and thus function as cysteine proteases. Among these, the family of ubiquitin-specific proteases (USP) is the largest and most diverse subfamily with around 60 enzymes. USPs contain two short but well-conserved motifs – the cysteine and the histidine boxes, which define the active site pocket. If the catalytic cysteine in the active site pockets is mutated the protease is rendered inactive (Amerik *et al.* 2004, Snyder *et al.* 2021).
The cysteine proteases hydrolyse the isopeptide bonds between ubiquitin and mostly the ε-amino group of lysine residues. In the absence of an ubiquitinated substrate, the enzymes are in an inactive conformation. Specific substrate binding causes structural rearrangements in the DUB, which switches the protease into an active configuration. This structural change brings the catalytic residues into their correct positions and the thiol group of the active cysteine gets deprotonated by a histidine residue. In the second step, the anionic sulphur in the deprotonated cysteine mediates a nucleophilic attack on the carbonyl carbon of the isopeptide bond between ubiquitin and its substrate. The histidine gets deprotonated and releases the substrate protein with an amine group. The ubiquitin is linked with the carboxy terminus to the cysteine thiol group of the DUB and forms a thioester intermediate. This thioester bond is eventually hydrolysed to release the ubiquitin moiety with a fully functional carboxy terminus at Gly76 ready to be attached to another substrate protein via the E1-E2-E3 enzymatic cascade (Snyder *et al.* 2021).
Subsequentially, deubiquitination negatively regulates protein degradation by the UPS and has major effects on the half-life and steady-state level of proteins. The stability of prominent transcription factors like p53 or c-Myc is controlled by ubiquitin-specific proteases, including USP7 and USP10 or USP28, respectively (Li *et al.* 2002, Popov *et al.* 2007, Yuan *et al.* 2010).

1.1.4 The interplay of E3-ligases and deubiquitinating enzymes finetunes the regulation of transcriptional activity and gene expression

Many DUBs are associated with specific E3 ligases to form functional pairs and several DUB-ligase pairs interact directly, e.g. USP7 and the E3 ligase MDM2 regulating p53 stability (Li *et al.* 2004).

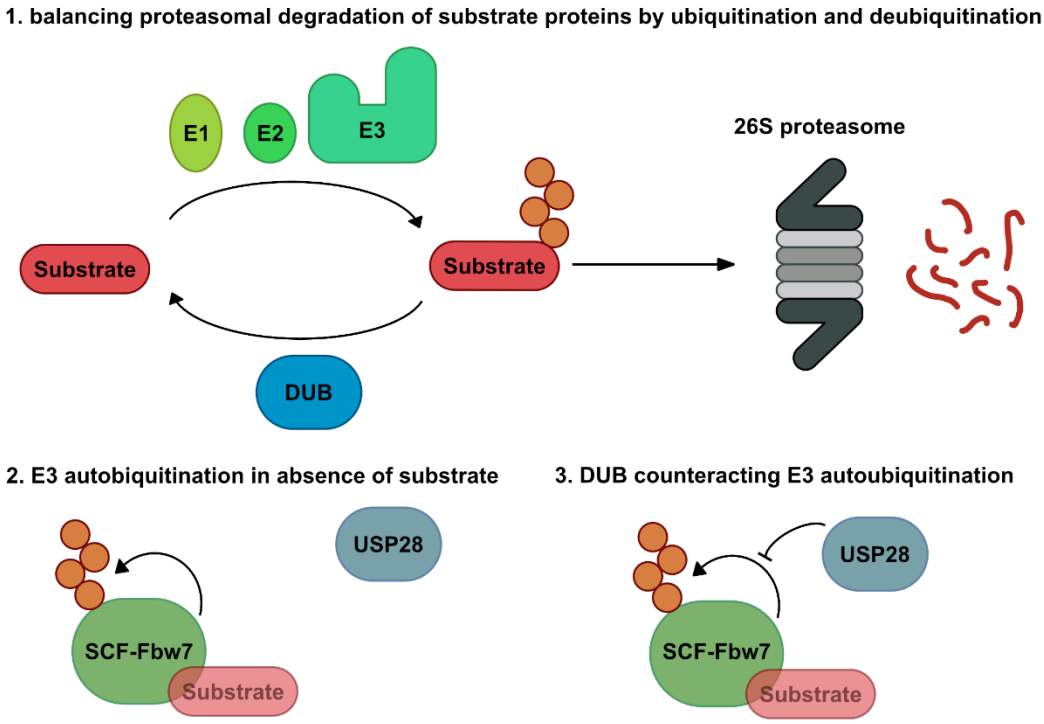

Figure 1-2: Regulation of proteasomal degradation of substrate proteins and E3 ligases by ubiquitination and deubquitination.

Deubiquitinating enzymes catalyse the hydrolysis of the isopeptide bond between the C-terminus of ubiquitin and its substrate thereby removing K48-linked ubiquitin chains and rescuing their targets from proteasomal degradation via the 26 S proteasome. The balance of ubiquitination by the E1-E2-E3 enzymatic cascade and deubiquitination by DUBs determines the stability and steady-state level of proteins. The effects on the steady-state levels of substrates of K48-linked ubiquitination therefore are specific to the relative amounts of the protein levels and activity of the E3 ligase and the respective DUB (1). In the absence of substrate proteins, E3 ligases like SCF-Fbw7 are targeting themselves for ubiquitination (autoubiquitination), which results in subsequential proteasomal degradation of the E3 ligase (2). The DUB USP28 was shown to counteract not only the ubiquitination of many substrate proteins of SCF-Fbw7 but also the autoubiquitination of the SCF-Fbw7 to prevent its degradation (3).

The association of the E3 ligase and DUB results in a competition of ubiquitination and deubiquitination of the substrate protein. The formation of pairs or complexes therefor counteracts the regulatory functions towards the substrate protein. Further, many E3 ligases showed in absence of other substrates the ability to regulate their stability by autoubiquitination and subsequent proteasomal degradation. Moreover, the binding or association of the respective DUB can counteract this autoubiquitination to stabilise the E3 ligase. Lastly, many associated DUBs were also shown to be substrates of their respective E3 ligase which ubiquitinates the DUB and leads to its degradation via the proteasome. Eventually, the interaction partners not only regulate their substrate proteins but are also transregulated by each other (Wilkinson 2009).

This complex mode of substrate ubiquitination and deubiquitination was investigated for the E3 ligase SCF-Fbw7 and USP28 (Schulein-Volk *et al.* 2014). The degradation of various Fbw7 substrates, including c-Myc and c-Jun, is reversed by USP28 (Popov *et al.* 2007, Diefenbacher *et al.* 2014). Fbw7 regulates its turnover by *trans*-autoubiquitination in a dimeric structure (Welcker *et al.* 2013) and USP28 stabilises Fbw7 by deubiquitination (Schulein-Volk *et al.* 2014). *Usp28* knockout studies in mice revealed that low USP28 levels result in reduced deubiquitination of substrate proteins and these are then favoured for proteasomal degradation. However, a complete loss of *Usp28* mediates the destabilisation of Fbw7 and, consequentially, results in the accumulation of target proteins (Taranets *et al.* 2015). The dual mode of regulation of the E3-DUB pair Fbw7-USP28 represents a finetuned process and the imbalance of this system affects the homeostasis of multiple substrate proteins.

1.2 Cancer Metabolism

1.2.1 Metabolic reprogramming of glycolysis in cancer cells – The Warburg effect

Reprogramming energy metabolism is a hallmark of cancer (Hanahan *et al.* 2011). Cancer cells are highly proliferating cells and are dependent on the supply of energy and biomolecules. To fuel the cell growth and division of cancer cells cellular biosynthesis pathways and transporters for metabolite uptake are often upregulated.
The reprogramming of the glucose metabolism was observed by Otto Warburg already 90 years ago. He published his worked on “the metabolism of tumours” 1930 in London. Under aerobic conditions, normal cells use glucose to synthesize pyruvate, which is further oxidized in the mitochondria to carbon dioxide and results in the production of ATP. Under anaerobic conditions, cells favour the glycolysis and only little pyruvate is transported to the mitochondria, a phenomenon called Pasteur Effect. Warburg observed in tumours that cancer cells reprogram their glucose metabolism favouring glycolysis also in the presence of oxygen. This principle of the so called “aerobic glycolysis” was henceforth named the Warburg effect (Warburg *et al.* 1927, Warburg 1956).
Such metabolic switches in cancer cells to upregulate *de novo* metabolic pathways of biomolecules or to increase the expression of transporters to import metabolites were explored by scientist over the following decades and are still of great interest in the field of cancer metabolism research.
The regulation of synthesis pathways or nutrient transporters is often under the transcriptional control of master regulators, such as c-Myc or HIF1α, and these proteins were found to be master inducers of cancer glycolysis. Especially, c-Myc and hypoxia-inducible factors (HIFs) are transcriptional regulators of key glycolytic genes, e.g. *LDHA* under normoxia and hypoxia, respectively (Semenza *et al.* 1994, Shim *et al.* 1997). These master inducers are often mutated or deregulated in the context of cancer.

The coordination and reprogramming of metabolic pathways provides tumours with a constitutive supply of metabolites for supporting their rapid proliferation and accelerated biosynthesis.

1.2.2 Enhanced lipid metabolism by upregulation of *de novo* lipid synthesis in tumours

The key question after observing the Warburg effect was why the aerobic glycolysis is advantageous for tumour growth. One proposed explanation was the increase in glycolytic intermediates from glycolysis but also from the tricarboxylic acid (TCA) cycle, which can funnel into anabolic processes. These side pathways would then support *de novo* synthesis of nucleotides, lipids and amino acids, which are all essential macromolecules for cell proliferation.
Tumour cells increase the uptake of glucose and convert its six-carbon backbone into two moieties of the three-carbon molecule pyruvate, which is translocated into the mitochondria and converted within the TCA cycle to citrate. Citrate in turn can be exported to the cytoplasm and is converted to acetyl-CoA, which is a central player in numerous *de novo* metabolic pathways to synthesize macromolecules, e.g. fatty acids.

Lipids are important building blocks for organelles and cell membranes. The *de novo* fatty acid synthesis is a multi-step process involving various enzymes, which convert cytoplasmic citrate to acetyl-CoA and further to saturated and mono-unsaturated fatty acids. Cancer cells frequently show increased *de novo* fatty acid biosynthesis to satisfy their demands for structural elements of membrane lipids, energy storage and signalling molecules.

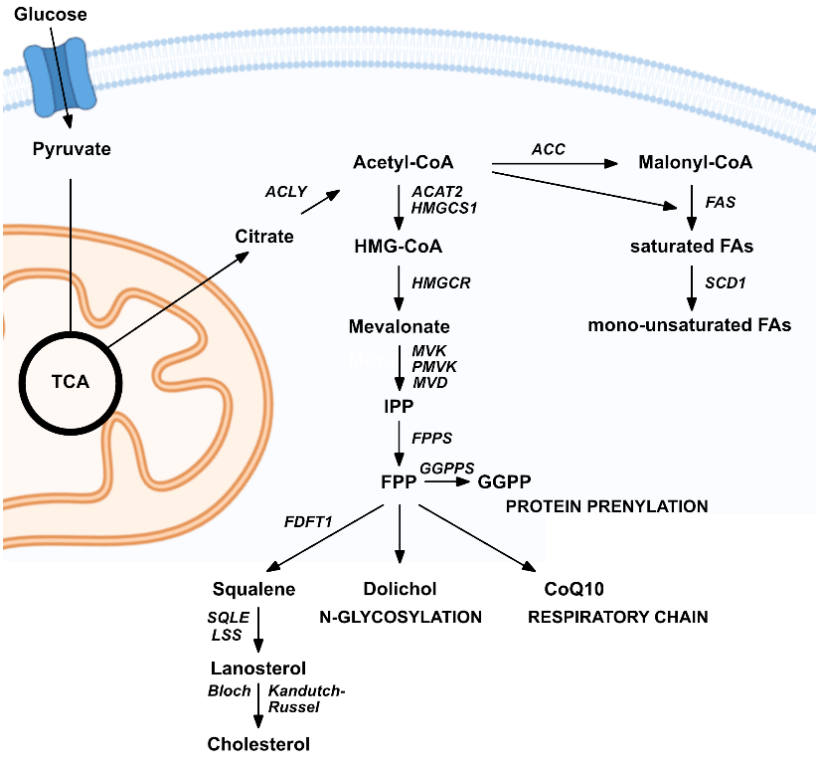

Figure 1-3: Increased glycolysis results in enhanced metabolic flux into the mevalonate pathway and de novo lipid synthesis.

Imported glucose is converted into pyruvate that is translocated to the mitochondria and feeds into the TCA cycle. Citrate is exported into the cytoplasm and further converted to acetyl-CoA, a central player in the cellular metabolism. Acetyl-CoA on the one hand is used for the synthesis of lipids and secondly is converted to mevalonate and further to farnesyl pyrophosphate (FPP). FPP and Geranylgeranyl pyrophosphate are building blocks for protein prenylation. Additionally, FPP is used for the synthesis of Coenzym Q10 (CoQ10), a complex of the respiratory chain and dolichol which serves as a membrane anchor for the formation of oligosaccharides for N-glycosylation of proteins. Lastly, FPP can be used for the synthesis of cholesterol and steroids.

ATP citrate lyase (ACLY) enzymatically controls the first step of the *de novo* fatty acid synthesis. Hereby, ACLY catalyses the conversion of cytoplasmic citrate and CoA into acetyl-CoA and oxalacetate (OAA). Acetyl-CoA is subsequently carboxylated by the acetyl-CoA carboxylase (ACC) in an ATP-dependent reaction and results in the formation of malonyl-CoA. The synthesis of long-chain saturated fatty acids (C16:0, palmitate) from malonyl-CoA and acetyl-CoA requires a series of condensation reactions catalysed by the multi-enzyme protein fatty acid synthase (FASN). Once the 16:0 carbon fatty acid has been formed, it can be desaturated and/or elongated by several membrane-bound enzymes located in the endoplasmic reticulum. The Stearoyl-CoA desaturase 1 (SCD1) catalyses the rate-limiting step in the formation of mono-unsaturated fatty acids (MUFAs). Free fatty acids can be combined with glycerol to form triglycerides (TAGs) for energy storage or phospholipids that form the phospholipid bilayers of membranes. Sphingolipids produced from fatty acids coupled to a sphingoid base play important roles in membranes, signal transduction and cell recognition.

1.2.3 The Mevalonate Pathway and cholesterol biosynthesis

Cholesterol synthesis via the mevalonate pathway (MVA) is also an important aspect of lipid biosynthesis, since cholesterol is a major component of membranes controlling the membrane fluidity and formation of lipid rafts of cell membranes.
The MVA pathway uses acetyl-CoA, NADPH and ATP to produce sterols, isoprenoids for isoprenylation and dolichol for the N-glycosylation of proteins that are essential for tumour growth. Further, isoprenoids are also used to produce the quinone co-enzyme Q10 (CoQ10) which is localised to the inner membrane of the mitochondria and transfers the electrons from complex I or II to complex III of the electron transport chain, thus enabling ATP production in cells which rely on oxidative phosphorylation to produce energy.
In the first step of the MVA, two acetyl-CoA molecules are condensed to yield acetoacetyl-CoA by the cytoplasmic enzyme acetoacetyl-CoA thiolase 2 (ACAT2). This is followed by a second condensation reaction with another acetyl-CoA molecule to form 3-hydroxy-3-methylglutaryl-CoA (HMG-CoA) which is catalysed by the HMG-CoA synthase (HMGCS1) In the next step, HMG-CoA is reduced by NADPH to mevalonate and this is catalysed by the HMG-CoA reductase (HMGCR). HMGCR is the rate-controlling enzyme of the mevalonate pathway and the enzyme is the target of statins, which are cholesterol-lowering drugs to treat dyslipidaemia. HMGCR is anchored in the ER membrane via its transmembrane domains and contains a sterol-sensing domain (SSD). Via this SSD HMGCR senses increased metabolite supply and this feedback control involves accelerated ER-associated degradation (ERAD) of the enzyme (Ravid *et al.* 2000). Mevalonate is further di-phosphorylated by two ATP-consuming steps at the 5-OH position by mevalonate-5-kinase (MVK) and phosphomevalonate kinase (PMVK), respectively. The resulted mevalonate-5-pyrophosphate is converted to isopentenyl pyrophosphated (IPP) by a decarboxylation reaction of the mevalonate-5-pyrophosphate decarboxylase (MVD). The isopentenyl pyrophosphate isomerase converts isopentenyl pyrophosphate into its isomeric form of dimethylallyl pyrophosphate (DMAPP). IPP and DMAPP are isoprenoid precursors and are used for the synthesis of geranyl-pyrophosphate (GPP) and further converted to farnesyl pyrophosphate (FPP) by farnesyl diphosphate synthase (FPPS).
FPP is the metabolic branching point. It serves as substrate of the geranylgeranyl pyrophosphate synthase (GGPPS), which catalyses the downstream extension of FPP (C-15) to geranylgeranyl pyrophosphate (GGPP, C-20) by condensation of FPP and another IPP molecule. FPP and GGPP are essential for prenylation, a post-translational modification of proteins. It is estimated that approximately 2% of the mammalian proteome is prenylated (Nguyen *et al.* 2009). Most prenylated proteins are members of signal transduction cascades. The most prominent ones are GTP-binding proteins (G-proteins) (Yamane *et al.* 1990) including members of the Ras superfamily (Hancock *et al.* 1989). Covalent attachment of the FPP or GGPP lipid tail to a highly conserved cysteine residue at the CAAX box at the C-terminus of G-proteins confers membrane localisation, mediates protein-protein interactions and plays a crucial role in controlling intracellular trafficking. These post-translational modifications are

essential for the function of the proteins and activating mutations in some G-proteins can cause cancer.
Additionally, FPP can be further elongated with additional IPP moieties in multiple condensation reactions. Dolichol is derived from 18-20 IPP molecules and plays an important role in the N-glycosylation of nascent polypeptides in the ER (Carlberg *et al.* 1996). Deregulated protein N-glycosylation is associated with tumour formation, proliferation and metastasis.
Isoprenoids are also used for the synthesis of Co-enzyme Q10 (CoQ10). CoQ10 is located to the inner membrane of the mitochondria anchored by the hydrophobic isoprenoid chain. The ubiquinone group transfers electrons from complex I or II to complex III of the electron transport chain and therefor is crucial for ATP production in cells. The central role of CoQ10 in cellular metabolism is shown by the severe pathological outcomes of a deficiency in CoQ10 biosynthetic pathway: Particularly brain, muscle and kidney tissues are affected by CoQ10 deficiency because of their high-energy demands. Patients show ataxia, neurological manifestations as well as renal dysfunction or hypertrophic cardiomyopathy (Salviati *et al.* 1993).
FPP also serves as a substrate for the farnesyl-diphosphate farnesyltransferase 1 (FDFT1) which is the first specific enzyme in the cholesterol biosynthesis. FDFT1 catalyses the dimerization of two molecules of FPP in a two-step reaction to form squalene. In the next step, squalene monooxygenase (SQLE) oxidises squalene to squalene epoxide and the oxidosqualene cyclase lanosterol synthase, encoded by the LSS gene, cyclizes squalene to form lanosterol. Finally, either the Bloch pathway or the Kandutsch-Russel pathway in 19 steps to cholesterol converts lanosterol. Cholesterol is an essential element of membranes and increased cholesterol biosynthesis contributes to tumour cell proliferation. Cholesterol also serves as a precursor of downstream products, such as steroid hormones and oxysterols, which drive cancer initiation and progression.

1.3 Sterol regulatory binding proteins (SREBPs) – Master Regulators of *de novo* fatty acid synthesis and cholesterogenesis

Sterol regulatory element binding-proteins (SREBPs) are a family of transcription factors, which regulate metabolic processes, specifically the *de novo* fatty acid synthesis as well as the mevalonate pathway and downstream cholesterogenesis. SREBPs transcriptionally activate a cascade of enzymes involved in the synthesis of fatty acids (FAs), TAGs, phospholipids and cholesterol.

1.3.1 Isoform-specific roles and tissue distribution of SREBPs

The mammalian genome encodes three isoforms of SREBPs: SREBP1a, SREBP1c and SREBP2. While SREBP2 is encoded by the *SREBF2* gene at chromosome 22q13, the isoforms 1a and 1c are derived from the single *SREBF1* gene at chromosome 17p11.2 (Hua *et al.* 1995). The SREBP1 isoforms 1a and 1c result from

alternative transcription start sites and alternative splicing of exon 1 and exons 18 and 19, respectively.
SREBP-1c is the predominant isoform expressed in most tissues of mice and humans. Especially, high levels of SREBP1c isoform were found in the liver, adrenal gland and white adipose tissue while isoform 1a is highly expressed in cell lines and tissues with a high capacity for cell proliferation, such as spleen and intestine. Hereby, the SREBP1 and SREBP2 transcripts are controlled independently by regulatory regions of organ-specific and metabolic factors (Shimomura *et al.* 1997).
SREBP1 and SREBP2 display overlapping specificities in transactivating the expression of their respective target genes due to the shared sequence identity of approximately 47% and high structural similarity (Miserez *et al.* 1997). However, several studies showed preferences of either SREBP1a/1c or SREBP2 towards the transcriptional activation of specific target genes. While overexpression studies of SREBP1a revealed increases in the expression of genes involved in fatty acid and cholesterol synthesis (Horton *et al.* 2003), overexpression of SREBP1c demonstrate a selective induction of lipogenic genes (Shimano *et al.* 1997) and increased SREBP2 levels causes preferential induction of genes involved in cholesterol biosynthesis (Horton *et al.* 1998, Horton *et al.* 2003).

1.3.2 SREBP protein structure and sterol-dependent processing

SREBPs are basic-helix-loop-helix zipper (bHLH-zip) transcription factors and are synthesized as approx. 1150 amino acid proteins. SREBP1 and SREBP2 share a similar protein structure and contain three major domains (Figure 1-4): The N-terminal region of about 500 bp contains the transactivation (TA) domain, a serine- and proline-rich region as well as the bHLH-zip structure. Following, the proteins show two hydrophobic transmembrane spanning segments connected by a short loop and the C-terminal regulatory domain (Miserez *et al.* 1997). SREBPs are synthesized as approximately 125 kDa precursors, which are integrated through the transmembrane domains to membranes of the nuclear envelope and the ER (Wang *et al.* 1994) (Figure 1-4). The N- and the C-termini of the proteins are exposed to the cytosol while the hydrophilic loop between the transmembrane domains protrudes into the ER lumen. This protein orientation follows the hairpin model for SREBPs that was postulated by Goldstein and Brown (Wang *et al.* 1994, Hua *et al.* 1995).

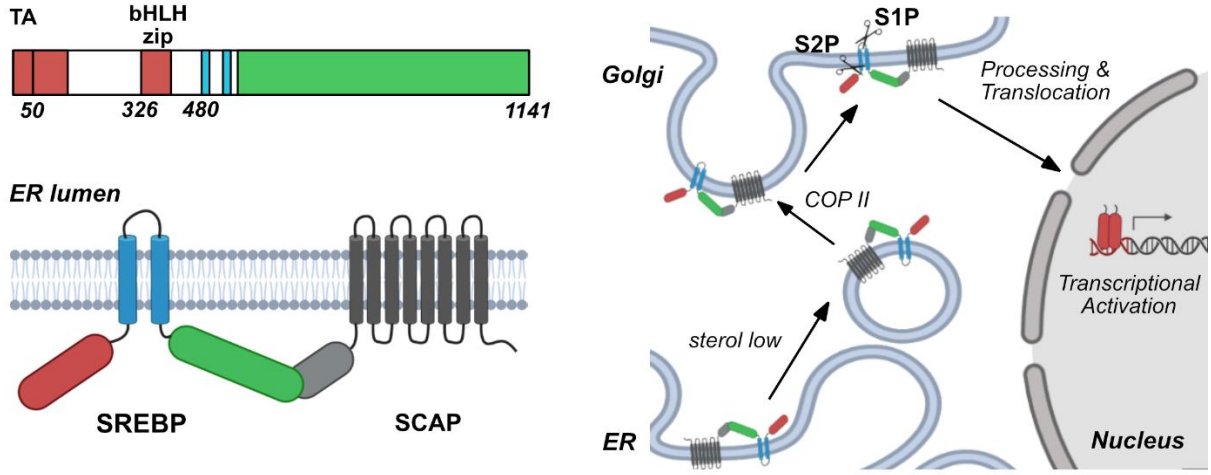

Figure 1-4: SREBP inactive precursors are integrated into the ER until low sterol levels are censored and SREBPs are processed to release the N-terminal active transcription factor.

SREBP domain structure is divided to N-terminal transcriptional domains, two transmembrane segments and a C-terminal regulatory domain. Via the transmembrane domains, SREBP precursors are integrated into the ER membrane and the regulatory domain is bound by SCAP and remains inactive. Upon low intracellular sterol levels, SCAP recruits SREBP via COPII-mediated vesicle transport to the Golgi apparatus where it is cleaved within the luminal loop and the first transmembrane domain by S1P and S2P, respectively. The released N-terminal domain is translocated to the nucleus, binds to promoter sequences and initiates transcription of SREBP target genes.

In sterol-depleted cells, the SREBP precursor is cleaved proteolytically to release the N-terminal fragment that migrates on SDS-PAGE as a cluster of bands with apparent molecular weight in the range of 60-70 kDa (Wang *et al.* 1994). This mechanism is controlled by the SREBP cleavage-activating protein (SCAP) which functions as a sterol sensor (Wang *et al.* 1994, Nohturfft *et al.* 1998). SCAP is a membrane protein with multiple membrane-spanning segments which is integrated into the ER membrane and nuclear envelope. The C-terminal WD40 domain of SCAP forms a complex with the C-terminal regulatory domain of SREBPs (Sakai *et al.* 1997). The SCAP/SREBP complex moves from the ER to the Golgi in a sterol-sensitive fashion (Nohturfft *et al.* 1999). While SCAP recycles to the ER, SREBPs are processed by two sequential cleavages (Sakai *et al.* 1996): The first proteolytic cleavage is catalysed by the site-1 protease (S1P) whose active form resides in the Golgi (Espenshade *et al.* 1999). While the first hydrolyses of a peptide bond occurs within the luminal loop between the two transmembrane domains of SREBPs, the second-site cleavage occurs within the first transmembrane domain by site-2 protease (S2P) (Duncan *et al.* 1997, Duncan *et al.* 1998). After cleavage the C-terminal fragment remains attached to membranes as an integral protein (Hua *et al.* 1995) while the N-terminal mature SREBP (mSREBP) is translocated to the nucleus (Figure 1-4).

In sterol-overloaded cells, the SCAP/SREBP complex remains in the ER. Increased cholesterol abundance favours a SCAP confirmation that binds to the products of the insulin-induced genes (INSIGs), another group of transmembrane proteins and the SCAP/SREBP complex cannot leave the ER (Yabe *et al.* 2002, Yang *et al.* 2002).

A second processing mechanism is dependent on phosphatidylcholine (PC) levels in the cells. Decreased PC levels in the Golgi membrane cause the translocation of S1P

and S2P from the Golgi to the ER to cleave the SREBP precursor and eventually lead to the release of the active transcription factor (Walker *et al.* 2011).
Both modes of regulation establish a feedback loop by coupling SREBP processing and therefore its activation directly to the lipid content of intracellular membranes.

1.3.3 Cooperation with other transcription factors and activation of gene expression

The transcriptional activation mediated by SREBPs was first observed at the promoter region of the low-density lipoprotein (LDL) receptor gene. LDL receptor mediates endocytic uptake of cholesterol-carrying lipoproteins and controls intracellular sterol levels. If cellular sterol stores are depleted, gene transcription of the LDL receptor gets activated: Already more than 30 years ago Goldstein and Brown showed that conserved Repeats 1-3 in the 5'-flanking region of the LDL receptor gene are necessary for the sterol-dependent regulation of gene transcription (Sudhof *et al.* 1987). While Repeat 1 and 3 were matched to the binding site of the Sp1 transcription factor, the designated Repeat 2 decamer sequence (5'-ATCACCCCAC-3') was named sterol regulatory element 1 (SRE-1) and SREBPs were identified as transcription factors recognizing this DNA sequence (Briggs *et al.* 1993).
In the following years, SREBPs were shown to bind alternative SRE recognitions sequences (SRE-2: 5'-ATCACCGTAC-3' and SRE-3: 5'-CTCACACGAG-3') and high binding specificity to the E-box consensus motif (5'-ATCACGTGA-3') (Smith *et al.* 1988, Kim *et al.* 1995, Ericsson *et al.* 1996). Due to the high sequence identity of 71% in the bHLH-zip domain of SREBP1 and SREBP2, both proteins showed similar binding affinities to SRE-1 and comparable transcriptional activation capacity of target genes (Hua *et al.* 1993). Further, co-transfection of low amounts of pSREBP-la and pSREBP-2 into cells stimulated transcription of promoters containing SRE-1 in an additive fashion (Hua *et al.* 1993).
The cooperative DNA-binding of SREBP1 and the transcription factor Sp1 was also first observed in the promoter region of the LDL receptor gene (Briggs *et al.* 1993, Sanchez *et al.* 1995). Sp1 sites were found in several viral and cellular promoters and many promoters with Sp1 sites, so-called GC-boxes, contain other elements that specify the regulated gene expression, here the SRE. Therefore, Sp1 provides basal level of gene activation at the LDL receptor promoter but Sp1 binding is significantly enhanced by SREBP (Sanchez *et al.* 1995).
The cooperative effect of SREBP and the ubiquitous nuclear transcription factor Y (NF-Y) was observed in the farnesyl diphosphate synthase promoter (Ericsson *et al.* 1996): NF-Y binds as an isomeric heterotrimer to the inverted CCAAT (ATTGG) box that is located 20 bp upstream of an SRE at the promoter of *FPPS*. Eventually, NF-Y binding stimulates the binding of mature SREBP1 to the SRE significantly by about 20-fold. In contrast, when NF-Y was not bound at the promoter, SREBP1 was only bound poorly. Similar NF-Y and Sp1 binding motifs were found at the promoter regions of various other SREBP target genes (Guan *et al.* 1995, Jackson *et al.* 1995, Nagai *et al.* 2002, Reed *et al.* 2008).

More recently, a cooperation of SREBPs and the MYC oncogene in regulating enzymes involved in FA synthesis, mevalonate synthesis and cholesterogenesis was shown in cancer mouse models and in esophageal squamous cell carcinoma cell lines (Gouw *et al.* 2019, Zhong *et al.* 2019). Beside the cooperation of SREBPs and MYC, SREBP1 was further found to cooperate with the transcription factors tumour protein p63 (TP63) and Kruppel like factor 5 (KLF5) specifically in squamous cell carcinoma (SCC) to activate cancer-associated signalling pathways (Li *et al.* 2021).

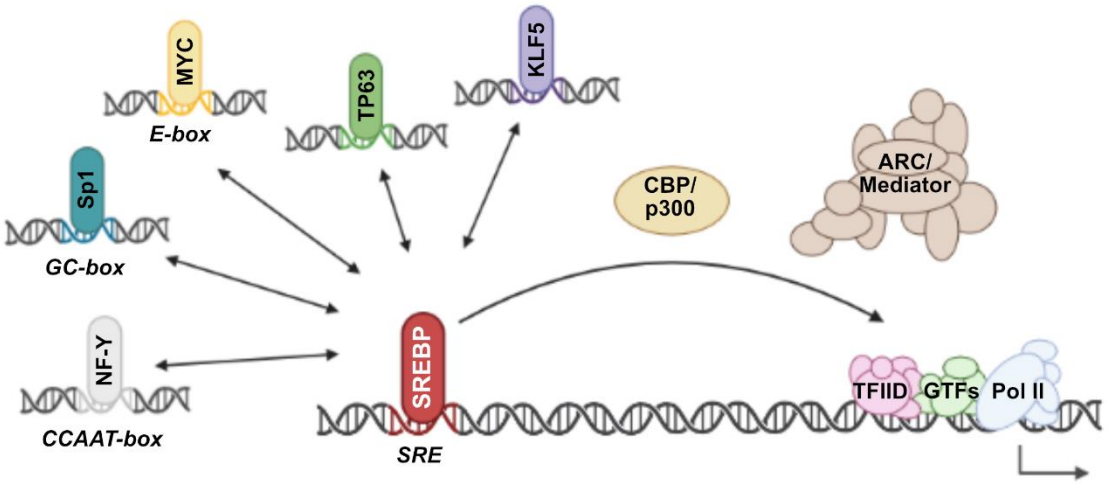

Figure 1-5: SREBPs cooperate with various transcription factors, which facilitate DNA-binding and recruitment of co-activators to the transcription start site for the formation of the preinitiation complex.

Binding motifs of various transcription factors are found in the proximity of SRE and positive cooperative effects of SREBP binding and transcriptional activation was shown for Sp1, NF-Y, MYC, TP63 and KLF5. SREBP mediates the recruitment of co-activators like CBP/p300 and ARC/Mediator subunit 105 via interaction of the TAD with the KIX domains. Eventually, these co-activators facilitate TFIID binding and recruitment of general transcription factors (GTFs) as well as Pol II for the formation of the preinitiation complex for gene transcription.

Once bound to the SRE in the promoter sequence of target genes, SREBPs associate through their N-terminal domain with various transcriptional co-activators including CREB-binding protein (CBP)/p300 and activator-recruited co-factor (ARC)/Mediator (Oliner *et al.* 1996, Naar *et al.* 1998, Naar *et al.* 1999): the SREBP activation domain thereby binds the KIX domain of CBP/p300 and ARC105, a subunit of the ARC/Mediator complex (Yang *et al.* 2006). The recruitment of ARC/Mediator complex mediates the binding of general transcription factors (GTFs). CBP/p300 additionally harbours a histone acetyltransferase (HAT) activity that mediates the opening of the chromatin structure at the promoter site and results in accessible binding of the GTFs. Once the basal transcription machinery including RNA-Polymerase II is bound at the transcriptional start site (preinitiation complex), gene transcription can be initiated.

1.3.4 Post-translational regulation of SREBP activity and stability

SREBPs are transcription factors whose stability and activity is highly regulated at different levels. The active form of SREBPs, the mature transcription factor (mSREBP), shows a much more rapid protein turnover compared to the precursor

form, the full-length protein (Wang *et al.* 1994). To regulate the activity of mSREBPs, the transcription factors are subject to post-translational modifications:
Post-translational regulation of SREBP1 and SREBP2 activity was shown by the phosphorylation at Ser117 and Ser432/Ser455 by the MAP kinases Erk1/2, respectively (Kotzka *et al.* 2000, Roth *et al.* 2000, Kotzka *et al.* 2004). Hereby, insulin stimulates the MAP kinase pathway and results in the phosphorylation of SREBPs, which enhances their transactivation capacity.
First evidence for the regulation of the stability of SREBPs by the ubiquitin-proteasome system was suggested by the observation of a rapid decrease in mSREBPs after cycloheximide treatment (Hirano *et al.* 2001). Many transcription factors, especially those involved in controlling cell growth and proliferation, are unstable proteins and modifications at the transactivation domain (TAD) play a crucial role in this process. Indeed, it was shown that a functional TAD and DNA-binding domain are required for ubiquitination and proteasomal degradation of SREBPs (Sundqvist *et al.* 2003). Sequence alignments of TADs of proteolytically regulated transcription factors revealed a common motif, named after the F box protein Fbw7 (also known as hCdc4) which mediates the recognition of phosphorylated substrates: the Cdc4 phosphodegron (CPD) motif. The regulation of the CPD-containing transcription factors follows a concerted mode of proteolysis: In the first step, the proteins are phosphorylated at specific residues within the CPD motif sequence. In a second step, the transcription factor is recognized the SCF-Fbw7 ubiquitin ligase for ubiquitination and thirdly the E3 ligase mediates the attachment of ubiquitin chains, which subsequentially targets the transcription factor for degradation. The phosphorylation sites within the CPD for SREBP1 were determined to be T426/S430 and for SREBP2 to be S432/S436 and the respective kinase was identified as glycogen synthase kinase 3 (GSK3) (Sundqvist *et al.* 2005).
Similar to the ubiquitination mechanism, SREBPs can be modified by sumoylation (Hirano *et al.* 2003). However, the attachment of a small ubiquitin-related modifier 1 (SUMO-1) at lysine residues negatively regulates the transactivation function of SREBPs but does not influence the stability of the protein. So far, no competition of ubiquitination and sumoylation for SREBP lysine residues could be observed (Hirano *et al.* 2003).
However, the interaction of SREBPs with the transcriptional activator p300 results in acetylation of a lysine residue in the DNA binding domain of the transcription factors. Since this lysine residue was previously identified as ubiquitination site, acetylation thus stabilises SREBPs by preventing ubiquitination (Giandomenico *et al.* 2003).

1.4 Regulation of SREBP-driven metabolic pathways in squamous cancer

Squamous cell carcinomas (SCC) comprise a number of different cancer types that arise from squamous cells and include some forms of skin cancer, thyroid cancer, esophageal cancer, vaginal cancer and lung cancer.

Despite sharing the same cell of origin, the development, the symptoms, the prognosis and the response to cancer treatment are different in the SCCs of the affected tissues. SCCs show a high degree of cellular heterogeneity with cell populations at various stages of differentiation and this makes them particularly difficult to target with monotherapeutic approaches. Understanding the crosstalk between oncogenic pathways is thus of major importance for developing new and targeted therapeutic approaches for this heterogeneous cancer entity.

1.4.1 Mutations in signalling pathways upstream of SREBP determine metabolic features in squamous lung cancer

Lung cancer is the second most common cancer worldwide and contributes 12.2% to the total number of new cases diagnosed in 2020. In men, lung cancer is even the most common cancer (15.4% of all cancer cases) (World Cancer Research Fund International: www.wcrf.org). The largest subgroup with 80-85% of lung cancer are non-small lung cancers (NSLCs) which are further subdivided into the two major subgroups: SCC and adenocarcinomas (ADCs). SCC accounts for 25-30% of all lung cancers and the five-year overall survival rates of advanced lung cancer patients (stage 4) is less than 5% (Office for National Statistics, Cancer survival by stage at diagnosis for England, 2019 – Cancer Research UK).
A direct comparison of SCC and ADC human lung tumours revealed elevated glucose transporter GLUT1 levels and subsequential increased glucose uptake in SCC (Goodwin *et al.* 2017). Targeted inhibition of glucose uptake showed that SCC cells rely on glucose to maintain metabolic pathways and cell proliferation. Glucose is converted to pyruvate and afterwards via the TCA cycle to citrate and further to acetyl-CoA. Acetyl-CoA is a central player of multiple metabolic pathways and can be used for the *de novo* fatty acid synthesis. Many cancer cells rely on lipids and other macromolecules as building blocks for cell growth and proliferation. Indeed, inhibition of acetyl-CoA carboxylase (ACC), which catalyses the conversion of acetyl-CoA to malonyl-CoA, the first step in fatty acid synthesis, supresses tumour growths in NSLC (Svensson *et al.* 2016). Statins, inhibitors of the rate-limiting enzyme HMGCR of the mevalonate pathway, show anti-tumour effects in some lung cancers with a specific genetic mutations: Patients harbouring mutations in the tyrosine kinase domain of the epidermal growths factor (*EGFR*) gene and treated with a EGFR tyrosine kinase inhibitor (EGFR-TKI) benefit from statin use and showed an increased overall survival (Hung *et al.* 2017). Moreover, about half of all lung cancer cases harbour mutations in the *p53* gene and statin treatment of patients with mutant *p53* lung cancer reduced their 5-year mortality (Chou *et al.* 2019). Additionally, HMGCS1 is often altered in lung cancer and nearly exclusively show amplifications in copy number alterations (Cbioportal, TCGA PanCancer Atlas, SCC: 10%; ADC: 7% (Cancer Genome Atlas Research *et al.* 2013)) which suggests, that high levels of HMGCS1 are beneficial for tumorigenesis of lung cancer cells.
Mutational analysis and analyses of copy number alterations revealed, that one of the most common affected genes in squamous lung cancer patients is *PIK3CA*

(Cbioportal, TCGA Nature 2012, 47% (Cancer Genome Atlas Research 2012)). *PIK3CA* encodes the gene for the catalytic subunit p110α of PI3K and the PI3K-AKT pathway plays a central role in the survival and proliferation of various cancers. Activating mutations in the hotspot region of *PIK3CA* lead to constitutive signalling and aberrant activation of the pathway. PI3K-mediated activation of AKT regulates SREBP activity on two levels: Firstly, SREBP activity is increased via mTORC1 (Porstmann *et al.* 2008) and, secondly, mSREBP stability is enhanced by the inactivation of GSK3 (Sundqvist *et al.* 2005). Hence, AKT-mediated phosphorylation of GSK3 inhibits the phosphorylation of target proteins like SREBPs and subsequentially results in the stabilisation of transcription factors regulated by GSK3-dependent mechanisms (see also 1.4.2.).
The tumour suppressor gene *TP53* is mutated in 84% of SCC patient samples mutated (Cancer Genome Atlas Research *et al.* 2013). Missense mutations in the gene locus of *TP53* are a common alteration in cancer, impair the DNA binding of the transcription factor, and prevent cell cycle arrest, apoptosis and DNA repair. Mutant p53 accumulates in cancer cells and promotes carcinogenesis through dominant-negative and gain-of-function activities. Mutant p53 was shown to directly bind to SREBP2 and enhance gene expression of enzymes of the mevalonate pathway (Freed-Pastor *et al.* 2012). In turn, wild type p53 represses the mevalonate pathway through inhibition of SREBP2 maturation and statin treatment restricts tumour initiation in the p53 loss situation (Moon *et al.* 2019, Kaymak *et al.* 2020).
Taken together, there is emerging evidence that SREBP-driven metabolic pathways could play a role in lung cancer, particularly SCC, and that lung cancer cells could be sensitive towards inhibition of *de novo* fatty acid synthesis and the mevalonate pathway regarding uncontrolled proliferation and tumour growth.

1.4.2 The role of Fbw7-USP28 targeting oncogenic transcription factors in SCC

The ubiquitin-mediated degradation of short-lived transcriptional regulators affects various cellular processes. The substrate recognizing F-box protein of the SCF complex Fbw7 has been shown to mediate the ubiquitin-dependent proteolysis of several oncoproteins, including cyclin E1, c-Myc, c-Jun, Notch and SREBPs (1.3.4).
The Fbw7 gene locus encodes three transcripts (α, β and γ) that are produced by alternative splicing and differ only in their first exon. All three isoforms share the same domain structure and are, in principle, functionally identical. However, *cis*-acting signals in the isoform-specific first exon determine the sub-cellular localisation of the different isoforms: While Fbw7α resides in the nucleoplasm and Fbw7γ in the nucleolus, Fbw7β is found in the cytoplasm. Here, the focus is mostly on the α-isoform which specifically regulates transcription factors and plays an important role in tumorigenesis (Welcker *et al.* 2008).
The mode of action by which the E3 ligase recognises its substrates is dependent on prior phosphorylation of amino acids within a conserved phospho-epitope, the CPD motif (Nash *et al.* 2001). The phospho-degron binding pocket of Fbw7 is defined by the eight-bladed barrel-shaped β-propeller structure of the WD40 repeats, which

mediates protein-protein interaction only if the substrate proteins are phosphorylated. GSK3 phosphorylates the central serine or threonine of the CPD motif for priming of the transcription factors, e.g. c-Myc or SREBPs (Welcker *et al.* 2004, Sundqvist *et al.* 2005). This priming phosphorylation leads to the formation of another binding site and the subsequent second phosphorylation of the residue in the -4 position. The attachment of phospho-groups at both positions is required for Fbw7-binding. If these specific phosphorylation sites are substituted by non-phosphorylatable residues, Fbw7 is not recognising its substrate proteins anymore. The kinase GSK3 therefore plays a pivotal role in Fbw7 substrate recognition and is inactivated by phosphorylation by AKT downstream of the PI3K-AKT-pathway (see 1.4.1.).

Fbw7 mutations are common in human cancers and the chromosomal region of the gene locus is often deleted (Knuutila *et al.* 1999, Strohmaier *et al.* 2001, Spruck *et al.* 2002). Fbw7 was found to be mutated in 6% of SCC patients, and most of these events being deep deletions or missense mutations (Cbioportal, TCGA PanCancer Atlas (Cancer Genome Atlas Research *et al.* 2013)).

The deubiquitinase USP28 antagonises the ubiquitination of substrate proteins by Fbw7 by deubiquitination and subsequent stabilisation due to removing the signal for proteasomal degradation. USP28 was first discovered as a USP25 homologue and the two proteins show high sequence identity of more than 50% (Valero *et al.* 2001). While USP25 is mostly found in the cytoplasm and the ER (Bosch-Comas *et al.* 2006, Blount *et al.* 2012), USP28 is located to the nucleus where it stabilises transcription factors, most likely at or close to the promoter sites of their target genes (Popov *et al.* 2007).

High USP28 levels promote proliferation and tumorigenesis in NSCLC and correlate with poor prognosis of the patients. *Vice versa*, a reduction in USP28 level induces apoptosis of lung cancer cells (Zhang *et al.* 2015). USP28 was shown to be required for the induction and maintenance of lung SCC and its expression strongly correlates with common driver mutations, e.g. activating mutations in PI3K components (Prieto-Garcia *et al.* 2022). Additionally, USP28 drives malignant transformation by regulating the stability of SCC-relevant oncogenes like the squamous tumour marker ΔNP63 (Prieto-Garcia *et al.* 2020).

1.5 Aim of the thesis

In this thesis, it was hypothesised that USP28 could regulate the stability of SREBPs by antagonising their Fbw7-mediated ubiquitination and subsequent proteasomal degradation. Thus, the cellular localisation and protein-protein interaction as well as the mode of regulation of the two proteins will be investigated. Based on the distinct regulatory mechanism postulated for E3-DUB pairs, it will also be analysed whether the proposed regulation of SREBPs by USP28 is dependent or independent of SCF-Fbw7.

Further, the consequences of this regulatory axis on the metabolism of cancer cells and the effects on cell proliferation will be investigated. Since metabolic *de novo* synthesis pathways regulated by SREBPs are enhanced when exogenous lipid provision is limited, the effect on cell growth by USP28 inhibition will be monitored under normal and lipid-deprived conditions. Additionally, the metabolic outcome of USP28 depletion on cancer cell proliferation is to be analysed in different cell lines, including a squamous cell line lacking Fbw7 expression. Detailed proteomics, metabolomics and transcriptomics will be performed to unravel cellular changes upon USP28 inhibition.

Statins block cholesterogenesis by inhibiting the rate-limiting enzyme of the mevalonate pathway and statin treatment has shown anti-tumour effects and reduced tumour initiation in several experimental models. It was also shown that SCC are highly dependent on glucose metabolism and *de novo* metabolite synthesis. In this thesis, a potential synergistic effect by a “two-hit” strategy combining USP28 inhibition with statin treatment in SCC cells will also be investigated. For this strategy, a commercially available dual USP25/USP28 inhibitor will be tested in combination with statins and the effects of the combinatorial treatment on the SREBP-mediated metabolic pathways will be analysed.

Lastly, the effects of blocking the USP28-SREBP2 axis in squamous lung cancer will be elucidated. The expression levels of SREBP2 in SCC cell lines and patient data will be determined. Using a squamous lung cancer mouse model, the effects of knockout of Usp28 on protein levels of Srebp1 and 2 and their target genes will be investigated. To show the contribution of Srebps and their regulated metabolic pathways to the squamous lung cancer type, Srebp1 and Srebp2 will be specifically knocked out via a CRSIPR/Cas system *in vivo*. Tumour burden and markers for the different lung cancer subtypes will be analysed.

In summary, to elucidate the mechanism of regulation of SREBPs by USP28 and to unravel their effects on squamous tumour formation is the central aim of this thesis. A better understanding of this process is crucial to find therapeutic potential for a combinatorial treatment of SCC patients.

2 Materials

2.1 Cell lines

2.1.1 Human cell lines

Cell lines were validated using STR analysis and routinely tested for mycoplasma contamination. All cell lines were free of mycoplasma contamination.

Table 1: *Human cell lines of different origin were obtained from collaborating laboratories and institutes.*

Cell line	Culture Media	Origin	Source
HEK 293T	DMEM	Embryonic kidney	AG Eilers
HEK 293T AAV pro	DMEM	Embryonic kidney	ATCC
U2OS	DMEM	Osteosarcoma	AG Eilers
A431	DMEM	Epidermoid carcinoma (Squamous)	AG Diefenbacher
Hela	DMEM	Cervical cancer (Adenocarcinoma)	AG Eilers
Caski	RPMI 1640	Cervical cancer (Squamous)	AG Diefenbacher
PANC-1	DMEM	Pancreatic cancer (Adenocarcinoma)	AG Diefenbacher
BxPC3	RPMI	Pancreatic cancer (Adenocarcinoma)	AG Diefenbacher
SW480	DMEM	Colon Cancer	London Research Institute
LS174T	DMEM	Colon Cancer	AG Eilers
HCT116	DMEM	Colon Cancer	London Research Institute
HT-29	DMEM	Colon Cancer	London Research Institute

H520	RPMI 1640	Lung cancer (Squamous)	AG Diefenbacher
H522	RPMI 1640	Lung cancer (Adenocarcinoma)	AG Diefenbacher
H727	RPMI 1640	Lung cancer (Adenocarcinoma)	AG Diefenbacher
A549	RPMI 1640	Lung cancer (Adenocarcinoma)	London Research Institute
H1299	RPMI 1640	Lung cancer (large cell carcinoma)	AG Diefenbacher
EKVX	RPMI 1640	Lung cancer (Adenocarcinoma)	London Research Institute
LUDLU-1	RPMI 1640	Lung cancer (Squamous)	London Research Institute
Calu-1	RPMI 1640	Lung cancer (Squamous)	Francis Crick Institute
H2170	RPMI 1640	Lung cancer (Squamous)	London Research Institute

2.1.2 Mouse cell lines

Mouse cell lines were positively tested for mycoplasma contamination.

Table 2: *Mouse cell lines with specific mutational background were generated by Oliver Hartmann, AG Diefenbacher (Hartmann et al. 2021) and cultured in DMEM medium.*

Cell line	Genotype	Source
KP	$KRas^{G12D}$, $p53^{-/-}$	AG Diefenbacher
KPL	$KRas^{G12D}$, $p53^{-/-}$, $Lkb1^{-/-}$	AG Diefenbacher

2.2 Bacteria strains

- DH5α competent *E.coli* for (sub)cloning and plasmid amplification

Genotype: F^- Φ80*lac*ZΔM15 Δ(*lac*ZYA-*arg*F) U169 *rec*A1 *end*A1 *hsd*R17(r_k^-, m_k^+) *pho*A *sup*E44 *thi*-1 *gyr*A96 *rel*A1 λ^-

- XL-1 blue competent *E.coli* for (sub)cloning and plasmid amplification

Genotype: endA1 gyrA96(nal^R) thi-1 recA1 relA1 lac glnV44 F'[::Tn10 $proAB^+$ $lacI^q$ Δ(lacZ)M15] hsdR17(r_K^- m_K^+)

2.3 Culture media and supplements

2.3.1 Cell culture media

Glucose-free medium (Sigma D5030) was reconstituted with ddH_2O and supplemented with sodium bicarbonate. The pH was adjusted to 7.25 and the medium was sterile-filtered (0.2 µM).

Table 3: *Cell culture medium and composition.*

Medium	Source	Application	Supplements
DMEM	Sigma (D6546)	Maintenance	10 % FBS 2 mM Glutamine 1% Penicillin/Streptomycin
Transfection DMEM	Sigma (D6546)	Transfection	1 % FBS 2 mM Glutamine
RPMI	Sigma	Maintenance	10% FBS 2 mM Glutamine 1% Penicillin/Streptomycin
DMEM (w/o glucose)	Sigma (D5030)	Metabolic labelling	3.7 g/L sodium bicarbonate 1 mM Sodium pyruvate 10% FBS 2 mM Glutamine 1% Penicillin/Streptomycin
OptiMEM	Gibco	Transfection	-
Freezing medium	-	Cell line storage	80% FBS 20% DMSO

2.3.2 Antibiotics

All antibiotics were obtained from Roth and reconstituted in either ddH_2O or ethanol. Water-based stock solutions were sterile-filtered (0.2 µm) before use.

	Solvent	Final concentration
Puromycin	H_2O	1 µg/mL
G418	H_2O	800 µg/mL
Doxycycline	EtOH	1 µg/mL

2.4 Bacterial Medium and Supplements

2.4.1 Culture media

All components were obtained from Roth.

Luria-Bertani (LB) liquid medium	1% (w/v) Tryptone 0.5% (w/v) Yeast extract 1% (w/v) NaCl After dissolving of reagents pH was adjusted to 7.0 and media was sterilized by autoclaving
LB agar	LB liquid medium (unsterile) 1.5% (w/v) Agar-Agar After medium was sterilized by autoclaving it was cooled down to 50°C, antibiotics were added and medium was poured in 10 cm petri dishes

2.4.2 Antibiotics

All antibiotics were obtained from Roth and reconstituted in either ddH_2O or ethanol. Water-based stock solutions were sterile-filtered (0.2 µm) before use.

	Solvent	**Final concentration**
Ampicillin	H_2O	100 µg/mL
Kanamycin	H_2O	30 µg/mL
Chloramphenicol	EtOH	25 µg/mL

2.5 Chemicals and Reagents

Chemicals and reagents were dissolved and stored regarding recommended by supplier.

Table 4: *All reagents and chemicals were dissolved in recommended solvent and stored either at -20°C or at 4°C.*

Name	**Supplier**	**Stock concentration**
5-Fluorouracil	Calbiochem (343922)	200 mM in DMSO
AM580	Cayman (15261)	20 mM in DMSO
AZ-1	SelleckChem (S8904)	50 mM in DMSO
Betulin	Sigma (B9757)	13.55 mM in H_2O
Cholesterol	Sigma (C4951)	12.93 mM in H_2O

Cisplatin	Sigma (232120)	200 mM in DMSO
Coenzyme Q10	Sigma (C9538)	10 mM in DMF
D-Glucose (U-^{13}C6, 99%)	Cambridge Isotope Laboratories, Inc.)	1 M in H_2O
EmbryoMax Nucleosides (100x)	Merck (ES-008-D)	3 mM C, G, A, U 1 mM T
Geranylgeranyl pyrophosphate ammonium salt	Sigma (G6025)	2.22 mM in MeOH:NH_4OH (7:3)
Hoechst 33258	Thermo Scientific (33342)	5 mg/mL
(R)-Mevalonic acid lithium salt	Sigma (50838)	500 mM in H_2O
MG-132	Sigma (474790)	20 mM in DMSO
Simvastatin	Sigma (S6196)	10 M in DMSO

2.6 Solutions and Buffers

All solutions and buffers were prepared using MilliQ water (ddH_2O) and stored at RT unless otherwise indicated.
All chemicals were purchased from Sigma and Roth.

2.6.1 Cloning

Deoxynucleotide triphosphates (dNTPs)	10 mM of each dNTP in ddH_2O Stored at -20°C
DNA loading buffer (6x)	10 mM EDTA, pH 8.0 0.2% (w/v) Orange G 40% (w/v) sucrose Sterile-filtered and stored at -20°C

2.6.2 Cell transfection and infection

PBS (1X)	137 mM NaCl 2.7 mM KCl 10 mM Na_2HPO_4 1.8 mM KH_2PO_4 Sterilized by autoclaving

Polyethylenimine (PEI), branched	Diluted in H_2O to stock solution 1 µg/µL Sterile-filtered and stored at -20°C
Polybrene stock solution	4 mg/mL stock solution 200 mg Polybrene dissolved in 10 mL H_2O Sterile-filtered and stored at -20°C

2.6.3 Cell Lysis

RIPA cell lysis buffer	150 mM NaCl 50 mM Tris (pH 8.0) 1 % (v/v) NP-40 0.5 % (w/v) sodium deoxycholate 0.1 % (w/v) SDS 5 X stock solution was stored at -20 °C
Fractionation Buffer (Abcam)	20 mM HEPES (pH 7.4) 10 mM KCl 2 mM $MgCl_2$ 1 mM EDTA (pH 7.4) 1 mM EGTA
Nuclear Lysis Buffer (Abcam)	0.1 % SDS in TBS
HR Lysis Buffer	50 mM Tris-HCl pH 7.4 5 mM $MgCl_2$ 250 mM sucrose 0.1 % (w/v) NP-40 Sterile-filtered

2.6.4 SDS-PAGE and Western Blot

Ammonium persulfate (APS) (10%)	10% (w/v) APS Aliquots stored at -20°C
SDS separating gel buffer	1.5 M Tris 0.4% (w/v) SDS pH 8.8
SDS stacking gel buffer	0.5 M Tris 0.4% (w/v) SDS pH 6.8

SDS running buffer	25 mM Tris 0.1% (w/v) SDS 192 mM Glycin
Transfer buffer	25 mM Tris 192 mM Glycin 15% (v/v) ethanol
TBS	20 mM Tris 150 mM NaCl pH 7.6
TBS-T	20 mM Tris 150 mM NaCl 0.1% (v/v) Tween pH 7.6

Additionally, the following SDS sample buffers and blocking solutions were used:

Protein Sample Loading Buffer (4X)	LI-COR
SDS Sample Buffer (Fluorescent compatible, 4X)	Life Technologies (Invitrogen)
Intercept® Blocking Buffer	LI-COR
Blocker™ FL Fluorescent Blocking Buffer (10X)	Thermo Scientific

2.6.5 Cell fixation and staining

Crystal violet solution	0.1 % (w/v) crystal violet 20 % (v/v) ethanol
Paraformaldehyde (PFA)	3.7 % Paraformaldehyde in PBS Stored at 4 °C
Triton X-100	0.2 % Triton X-100 in PBS

Additionally, the following reagents were used for PLA Assay with the Duolink® System:

Duolink® In-situ Detection Reagent Orange	Sigma
Duolink® In-situ Wash Buffers, Fluorescence	Sigma
Duolink® In-situ Mounting medium with DAPI	Sigma

2.7 Standards, Enzymes and Kits

2.7.1 Standards

DNA marker	Gene Ruler 1 kb Plus DNA Ladder (Thermo Scientific)
Protein Marker	PageRuler Prestained Protein Ladder (Thermo Scientific)

2.7.2 Enzymes

All common restriction enzymes used for cloning were purchased from New England Biolabs (NEB).

Alkaline Phosphatase, Calf Intestinal (CIP)	NEB
DNase I (RNase-free)	Promega
M-MLV Reverse Transcriptase	Promega
Phusion HF DNA Polymerase	NEB
Q5® High-Fidelity DNA Polymerase	NEB
SYBR Green qPCR Master Mix	Thermo Scientific
T4 DNA Ligase	NEB
T7 Endonuclease I (T7E1)	NEB

2.7.3 Kits

Preparation of plasmid DNA	PureYield™ Plasmid Miniprep System (Promega) PureLink™ HiPure Plasmid Maxiprep Kit (Invitrogen)
Gel extraction	Monarch® DNA Gel Extraction Kit (NEB)
PCR Clean-up	Monarch® PCR & DNA Cleanup Kit (NEB)
SDS Gele Casting	TGX Stain-free FastCast Acrylamide Kit (Bio-Rad)
Subcellular Fractionation	Subcellular Protein Fractionation Kit for Cultured cells (Thermo Scientific) NE-PER™ Nuclear And Cytoplasmic Extraction Reagents (Thermo Scientific)
Measuring protein concentration	Pierce™ BCA Protein Assay Kit (Thermo Scientific)
Measuring RNA concentration	Qubit™ RNA HS Assay Kit (Invitrogen)
Proximity Ligation Assay	Duolink ® In situ Proximity Ligation Assay (Sigma)

2.8 Nucleic Acids

2.8.1 Oligopeptides

2.8.1.1 Primers for cloning

Table 5: *Oligo sequences used for cloning plasmid constructs.*

Name	Sequence
mirE_XhoI_fwd	TACAATACTCGAGAAGGTATATTGCTGTTGACAGTGAGCG
mirE_EcoRI_rwd	TTAGATGAATTCTAGCCCCTTGAAGTCCGAGGCAGTAGGCA
mSREBP2_BamHI_HA fwd	CGCGGATCCACCATGTACCCATACGATGTTCCAG
mSREBP2_XhoI_rwd	CCGCTCGAGTCACAGAAGAATCCGTGAGCGG
SREBP2 SDM CPD fwd	CAGCCGCTGACTCAGGGTCCCAGGCTGGCTTCTCTCC
SREBP2 SDM CPD rwd	GGGGGGCCATCAGAAGGACATTCTGATTAAAGTCCTCGATCTTCAG
KpnI-sgRNA fwd	GGTACCGGTCTTGAAAGGAGT
HindIII-sgRNA rwd	AAGCTTACACAAAAAACCAACACACAG

2.8.1.2 shRNAs

Table 6: *Human shRNA sequences cloned into pLT3-GEPIR.*

Name	Sequence
shRenilla	TGCTGTTGACAGTGAGCGCAGGAATTATAATGCTTATCTATAGTGAAGCCACAGATGTATAGATAAGCATTATAATTCCTATGCCTACTGCCTCGGA
shUSP28 #1	TGCTGTTGACAGTGAGCGCACAAGAGATTAGAAATATAAATAGTGAAGCCACAGATGTATTTATATTTCTAATCTCTTGTATGCCTACTGCCTCGGA
shUSP28 #2	TGCTGTTGACAGTGAGCGATACAAGAGATTAGAAATATAATAGTGAAGCCACAGATGTATTATATTTCTAATCTCTTGTAGTGCCTACTGCCTCGGA
shUSP28 #3	TGCTGTTGACAGTGAGCGCCCAGATGACATGAATATGGAATAGTGAAGCCACAGATGTATTCCATATTCATGTCATCTGGATGCCTACTGCCTCGGA
shUSP28 #4	TGCTGTTGACAGTGAGCGCGAACAGCTACTAGTTATTTTATAGTGAAGCCACAGATGTATAAAATAACTAGTAGCTGTTCATGCCTACTGCCTCGGA
shSREBF2 #1	TGCTGTTGACAGTGAGCGCTCTGTATATATTTAAACCTAATAGTGAAGCCACAGATGTATTAGGTTTAAATATATACAGATTGCCTACTGCCTCGGA

shSREBF2 #2	TGCTGTTGACAGTGAGCGAAAGGCCATTGATTACATCAAATA GTGAAGCCACAGATGTATTTGATGTAATCAATGGCCTTCTGC CTACTGCCTCGGA
shSREBF2 #3	TGCTGTTGACAGTGAGCGAGCATATCTGTATATATTTAAATA GTGAAGCCACAGATGTATTTAAATATATACAGATATGCCTGC CTACTGCCTCGGA
shSREBF1 #1	TGCTGTTGACAGTGAGCGCAGGTACACAACTTTTAACTTATA GTGAAGCCACAGATGTATAAGTTAAAAGTTGTGTACCTTTGC CTACTGCCTCGGA
shSREBF1 #2	TGCTGTTGACAGTGAGCGCAAACATCTTTTAGAAACAAAATA GTGAAGCCACAGATGTATTTTGTTTCTAAAAGATGTTTATGC CTACTGCCTCGGA
shSREBF1 #3	TGCTGTTGACAGTGAGCGCGTACAGAGAATTAAAAATGAATA GTGAAGCCACAGATGTATTCATTTTTAATTCTCTGTACATGC CTACTGCCTCGGA
shΔNP63 #1	TGCTGTTGACAGTGAGCGCCCAGATCTTTCAGAAATATAATA GTGAAGCCACAGATGTATTATATTTCTGAAAGATCTGGATGC CTACTGCCTCGGA
shΔNP63 #2	TGCTGTTGACAGTGAGCGCCAGCAGCATTGATCAATCTTATA GTGAAGCCACAGATGTATAAGATTGATCAATGCTGCTGTTGC CTACTGCCTCGGA
shΔNP63 #3	TGCTGTTGACAGTGAGCGCATGTGGGATATTGAATGTTAATA GTGAAGCCACAGATGTATTAACATTCAATATCCCACATATGC CTACTGCCTCGGA

2.8.1.3 sgRNAs

Table 7: *sgRNA sequences targeting gene of interest for CRISPR/Cas9 Knockout.*

Name	**Sequence**
sgCtrl (human)	CGAGGTATTCGGCTCCGCG
sgUSP28_1 (human)	GAGTTGATGGTTGGCCAGTT
sgUSP28_2 (human)	ACCCCAATCCCAATGACTGG
sgSREBF2_A (human)	AGCCGGGCGATGGACGACAG
sgSREBF2_B (human)	TGGGAGACATCGACGGTGAG
sgSrebf2_A (mouse)	CTTCAGCGTGGTCAACACAA
sgSrebf2_B (mouse)	AGCGACCGTCTGTACCGTGG
sgSrebf1_A (mouse)	AATGCCCCAGCCGAAAAGCG
sgSrebf1_B (mouse)	CAGCATAGGGGGCGTCAAAC

2.8.1.4 qPCR Primers

Table 8: *Primer for amplification in quantitative PCR (qPCR).*

Name	Sequence
USP28 human fwd	GGAACAGCAGCAAGATGTGA
USP28 human rwd	GGCCGAAGGTCTCATTGTTA
SREBF2 human fwd	GAAAGGCGGACAACCCATAAT
SREBF2 human rwd	AGAACGCCAGACTTGTGCATC
HMGCR human fwd	GTTCGGTGGCCTCTAGTGAG
HMGCR human rwd	GCATTCGAAAAAGTCTTGACAAC
Actin human fwd	GCCTCGCCTTTGCCGAT
Actin human rwd	CGCGGCGATATCATCATCC

2.9 Plasmids

Table 9: *Plasmids used for transient and stable transfection or infection, respectively.*

Name	Source
pTK-HSV-SREBP2	Addgene
pcDNA3 Empty	Addgene
pcDNA3-myc-mSREBP1	(Sundqvist *et al.* 2003)
pcDNA3-myc-mSREBP1 CPD mutant	(Sundqvist *et al.* 2003)
pcDNA3-HA-mSREBP2	C. Maier
pcDNA3-HA-mSREBP2 CPD mutant	C. Maier
pcDNA3-HA-cMyc	(Popov *et al.* 2007)
pcDNA3-HA-USP28	(Popov *et al.* 2007)
pcDNA3-HA-USP28 C171A	(Popov *et al.* 2007)
pcDNA3-FLAG-Fbw7	(Popov *et al.* 2007)
pSico USP28 WT	AG Diefenbacher
pSico USP28 C171A	AG Diefenbacher
pPAX2	Addgene
pMD2G	Addgene
pInducer20-USP28	C. Schülein-Völk (AG Eilers)
pLT3-GEPIR shRenilla	(Fellmann *et al.* 2013)
pLT3-GEPIR shUSP28 #1-#4	C. Maier
pLT3-GEPIR shSREBF2 #1-#3	C. Maier
pLT3-GEPIR shSREBF1 #1-#3	C. Maier
pLT3-GEPIR shTP63 #1-#3	C. Maier
pLenti CRISPR v2 sgSREBF2 (human)	C. Maier
pLKO sgSREBF2 (human)	C. Maier
pX458 sgUSP28	B. Krenz (AG Eilers)
pLenti CRISPR v2 sgSREBF2 (mouse)	C. Maier
pLenti CRISPR v2 sgSREBF1 (mouse)	C. Maier
KPL (AAV backbone)	O. Hartmann (AG Diefenbacher)
KPL sgSREBF2 (mouse)	C. Maier
pHelper/ ΔF6	Addgene

pRCDJ	Addgene

2.10 Antibodies

2.10.1 Primary Antibodies

Table 10: *Primary antibodies used for Immunoblotting, Immunofluorescence including Proximity Ligation Assay and Immunohistochemistry.*

Target Protein	Supplier	Species	Concentration
ACSS2	Cell Signaling (3658)	rabbit	1:1000
Actin	Sigma (A3854)	mouse	1:20000
AKT	Cell Signaling (9272)	rabbit	1:500 or 1:1000
c-Myc (Y69)	Abcam (ab32072)	rabbit	1:1000
Calreticulin	Stressgen (SPA-600)	rabbit	1:1000
FDFT1	Sigma (HPA008874)	rabbit	1:1000
FLAG tag (DYKDDDDK)	Cell Signaling (2368)	rabbit	1:500
GAPDH	Abcam (9482)	mouse	1:1000
GSK3 alpha/beta	Calbiochem (368662)	mouse	1:1000
HA tag (HA.11)	Covance (MMS-101P)	mouse	1:1000
Histone H2B	EMD Millipore (07-371)	rabbit	1:500
HMGCS1	Abcam (ab155787)	rabbit	1:1000
Phospho-AKT (Ser473)	Cell Signaling (9271)	rabbit	1:500
Phospho-GSK3 alpha/beta (Ser21/9)	Cell Signaling (9331)	rabbit	1:500
SCD-1	Sigma (HPA012107)	rabbit	1:1000
SREBP1	Proteintech (14088-1-AP)	rabbit	1:500
SREBP1 (2A4)	Active Motif (39939)	mouse	1:500
SREBP2	R&D Systems (AF7119)	goat	1:500 (2 mg/mL)
SREBP2	R&D Systems (MAB7119)	mouse	IHC (human tissue)
SREBP2	Sigma (HPA031963)	rabbit	IHC (mouse tissue)
Tubulin alpha/beta	Cell Signaling (2148)	rabbit	1:1000
Ubiquitinated proteins (FK2)	EMD Millipore (04-263)	mouse	1:1000
USP25	Sigma (HPA018297)	rabbit	1:1000
USP28	Sigma (HPA006778)	rabbit	1:1000
Vinculin (hVIN-1)	Sigma (V9131)	mouse	1:5000

2.10.2 Secondary Antibodies

Table 11: *Secondary antibodies used for immunoblotting and Immunofluorescence approaches.*

Target Antibody	Supplier	Concentration
Alexa488 anti-mouse	Invitrogen (A11001)	1:2000
Alexa488 anti-goat	Invitrogen (A32814)	1:2000
Alexa555 anti-rabbit	Invitrogen (A21428)	1:2000

Alexa633 anti-rabbit	Invitrogen (A21071)	1:2000
DyLight800 anti-goat	Invitrogen (SA5-10084)	1:2500
HRP-coupled anti-mouse	GE Healthcare (NA931V)	1:10000
IRDye® 800CW anti-mouse	LI-COR (926-32212)	1:1000
IRDye® 800CW anti-rabbit	LI-COR (926-32213)	1:1000
IRDye® 680RD anti-mouse	LI-COR (926-68072)	1:1000
IRDye® 680RD anti-rabbit	LI-COR (926-68073)	1:1000
StarBright Blue520 anti-mouse	Bio-Rad (12005866)	1:5000
StarBright Blue520 anti-rabbit	Bio-Rad (12005869)	1:5000
StarBright Blue700 anti-mouse	Bio-Rad (12004158)	1:5000
StarBright Blue700 anti-rabbit	Bio-Rad (12004161)	1:5000

Table 12: *In-situ PLA probes used for Proximity Ligation Assays.*

Name	**Source**
Duolink® In-situ PLA® Probe Anti-Rabbit Minus	Sigma
Duolink® In-situ PLA® Probe Anti-Goat Plus	Sigma

2.11 Consumables

General consumables were purchased from Eppendorf, Greiner, Nunc, Sarstedt and VWR, including cell cultures dishes and plates, reaction tubes, cryotubes and pipettes. For Immunofluorescence analysis cells were seeded in µ-Slide 18 Well – Flat ibidi slides or in CellCarrier-384 Ultra plates from Perkin Elmer (Operetta measurements). For Western Blot transfer the Immobilon-FL PVDF membrane (pore size 0.45 µm) from Millipore and the Whatman® Gel Blotting Paper (Grade GB003) from Merck was used.

2.12 Equipment

Automated electrophoresis	Experion Automated Electrophoresis System (Bio-Rad)
Cell counter	CASY TTC-2FB-1123 (Schärfe System)
Cell culture incubator	Heracell (Kendro)
	170-300P (Galaxy)
Centrifuges	Avanti J-26 XP (Backman Coulter)
	Eppendorf 5415 D/R (Eppendorf)
	Eppendorf 5810 R (Eppendorf)
	Galaxy MiniStar (VWR)
	Multifuge 1S-R (Heraeus)
Heating blocks	Thermomixer® comfort (Eppendorf)

High Content Imaging System	Operetta (Perkin Elmer)
Hypoxia Chamber	RF 230V Hypoxia Workstation (Whitley)
Immunoblot transfer chambers	Mini Transblot (Bio-Rad)
	Criterion Blotter (Bio-Rad)
Mass Spectrometry	Q-Exactive mass spectrometer
Microscopes	Axiovert 25 (Zeiss)
	FSX100 microscopy system (Olympus)
	TCS SP8 (Leica)
PCR Thermo Cycler	C1000 Touch Thermal Cycler (Bio-Rad)
Photometer	Multiscan Ascent (Thermo Labsystems)
Plate Reader	Biotek Synergie H1 (Biotek)
Quantitative RT-PCR	StepOne plus (Applied Biosystems)
SDS PAGE System	Mini Protean 3 Cell (Bio-Rad)
Ultra Sonifier	Bioruptor® (Diagenode)
Western Blot Detection Systems	Odyssey® DLx (LI-COR)
	Chemidoc MP Imaging System (Bio-Rad)

2.13 Software and Online Programs

Affinity Designer1.8.3	Serif
BEG (VIB/ UGent)	bioinformatics.psb.ugent.be
Biorender	BioRender.com
ChemDoodle	iChemLabs
CHOPCHOP	(Labun *et al.* 2019)
EndNote X9 (Bld 15659)	Clarivate Analytics
Fiji (ImageJ)	(Schindelin *et al.* 2012)
GEPIA 2	Zhang Lab (Tang *et al.* 2019)
Image Lab 6.0.1.	Bio-Rad Laboratories, Inc.
Image Studio Lite Version 5.2.5	LI-COR Biosciences, Inc.
NEBaseChanger	New England Biolabs
NEB Tm calculator	New England Biolabs
PANTHER 17.0	Panther Classification System - pantherdb.org/
Primer3	National Center for Biotechnology Information (NCBI)

Prism 9 9.2.0.	GraphPad Software, LCC.
QuPath 0.2.3	(Bankhead *et al.* 2017)
Serial Cloner 2.6.1.	Serial Basics Software
splashRNA	Memorial Sloan-Kettering Cancer Center
UCSC Genome Browser	(Kent *et al.* 2002)

3 Methods

3.1 Molecular biology methods

3.1.1 Transformation of chemically competent bacteria

Chemically competent bacteria were thawed on ice and mixed with plasmid DNA in a ratio <10% (v/v). The bacteria were incubated on ice for 30 min, followed by a heat shock for 30 sec at 42°C. The reaction was cooled down on ice for 2 min and afterwards 1 mL of pre-warmed LB medium was added. The bacteria were incubated for 20 min at 37°C on a shaker. For inoculating overnight cultures, bacteria suspension was directly added to prewarmed LB medium containing appropriate antibiotic. For single clone growing, the bacteria were carefully centrifuged at 0.8 x g and up to 1 mL supernatant was discarded. Bacteria pellet was resuspended in residual LB medium and plated on pre-warmed LB agar plates containing appropriate antibiotic for selection. LB agar plates were incubates at 37°C for <18 h.

3.1.2 Preparation of plasmid DNA from bacteria

Bacteria overnight cultures were centrifuged at 4000 rpm for 20 min at RT. Supernatant was discarded and bacteria pellet was resuspended in lysis buffer. After incubation on ice, pre-cooled neutralization buffer was added and suspension was centrifuged at maximum speed. Supernatant was transferred to column and either centrifuged or passed through by gravity. Column was washed twice with wash buffer and endotoxins were removed. DNA was eluted in appropriate volume of pre-warmed ddH_2O in two steps. Concentration was determined and DNA was stored at -20°C.
For overnight cultures up to 2 mL, the PureYield™ Plasmid Miniprep System from Promega was used. For DNA preparation of 500 mL bacterial cultures, the PureLink™ HiPure Plasmid Maxiprep Kit (Invitrogen) was used.

3.1.3 Restriction digest

Restriction endonucleases from New England Biolabs (NEB) were used following the manufacturer's protocol. Enzyme amount and buffer conditions were adjusted to the desired purpose.
If not stated otherwise, reaction for restriction digest was set up as follows:
1 µg Plasmid DNA
2 µL Reaction Buffer (10X)
10 U Restriction enzyme (double digest 10 U of each)
Up to 20 µL with ddH_2O

3.1.4 Oligo Annealing

sgRNA sequences were designed using CHOPCHOP and UCSC Genome Browser. Synthesis of oligonucleotides were performed by Sigma with standard conditions.

Each oligo was used as 1 µL of a 100 µM stock solution in a reaction approach containing T4 Ligation Buffer (10X) and T4 PNK in a total reaction volume of 10 µL. Phosphorylation was performed at 37°C for 30 min. Annealing reaction was heated up to 95°C for 5 min and then ramped down to 25°C at <5°C/min. Annealed oligos were diluted 1:100 and either used directly for setting up a ligation reaction or stored at -20°C.

3.1.5 Polymerase chain reaction (PCR)

Primers for PCR approaches were designed using Serial Cloner. Mutagenesis Primer were proposed using NEBase Changer. Custom oligonucleotides were purchased by Sigma or Primer for qPCR were partially used from QIAGEN (QuantiTect Primer).

3.1.5.1 DNA amplification

For DNA amplification, either the Q5 Polymerase or the Phusion Polymerase (both NEB) was used following the manufacturer's protocol. Amount of template DNA was chosen regarding concentration and type of DNA (plasmid-DNA or genomic DNA). Optimal buffer conditions, HF or GC buffer for Phusion Polymerase or additional Enhancer for PCRs using Q5-Polymerase, were determined beforehand.
Reaction buffers were used in a final concentration of 1X. Final concentration for primer was calculated to be 500 µM each and dNTPs were used in a concentration of 200 µM. Reaction volume was either 20 µL or 50 µL dependent on further proceeding. Reaction was incubated in a Thermo Cycler using a protocol recommended by the manufacturer. Individual annealing temperatures of primer pairs were predicted by NEB Tm Calculator.

3.1.5.2 Site-directed Mutagenesis

PCR amplification was performed using Q5-Polymerase and 1 ng of plasmid DNA in a 10 µL reaction volume. PCR without primers were run as a digestion control. The annealing temperature of the mutagenesis primers were calculated by Tm calculator from NEB. For the KLD step, CutSmart Buffer (1X final), 1 µL T4 PNK and DpnI (all NEB) was added and filled up to 19 µL final volume. Reaction was incubated for 2 h at 37°C and enzymes were inactivated by heating up to 80°C for 20 min. After cooling down 1 µL T4 Ligase (NEB) was added and reaction was incubated overnight at 4°C. Next day bacteria were transfected with DNA and positive clones were selected by respective antibiotics (see 3.1.1).

3.1.5.3 Quantitative real-time PCR (qPCR)

Synthesized cDNA from 3.1.11 was diluted regarding the amount and quality of RNA used as template. For a standard set-up, 4 µL cDNA in a dilution of 1:10 to 1:5 was mixed with 5 µL SYBRGreen Mix (2X) from Thermo Scientific and forward and reverse

primer were added in a final concentration of 250 nM or QuantiTect primers (10X) were diluted in the reaction set-up to 1X.
The quantitative PCR was performed in the StepOne Plus machine using the fast template for amplification. Melting curves always showed one specific peak for amplification product and Ct values were analysed in duplicates or triplicates. Thresholds were adjusted manually and β-Actin was used as housekeeping gene for normalisation. Ct values were analysed using the ΔΔCt method and fold change relative to control was calculated.

3.1.6 Gel electrophoretic separation of DNA fragments

Agarose gels were prepared according to the expected size of PCR products or DNA fragments in a concentration range of 0.5% up to 2% agarose. Appropriate amount of agarose was dissolved in TAE buffer and boiled till completely dissolved. Agarose was briefly cooled down, 0.4 µg/mL ethidium bromide was added and solution was poured into gel chamber with combs. Once completely cooled down, samples were prepared with loading buffer and samples together with standard DNA ladder was loaded into the wells. Separation was performed at 110 V for individual time according to percentage of agarose. DNA fragments were visualized on a UV transilluminator.

3.1.7 Extraction and purification of DNA fragments and PCR products

DNA fragments separated by electrophoresis were cut out of agarose gel and extracted with the gel extraction kit from New England Biolabs (Monarch® DNA Gel Extraction Kit) following manufacturer's protocol.
PCR products not separated by electrophoresis were cleaned up using the Monarch® PCR & DNA Cleanup Kit.
In both cases, DNA was eluted with pre-warmed elution buffer in two steps with appropriate volume. DNA concentration was determined and DNA was stored at -20°C until further use.

3.1.8 T7E1 Assay

Extracted genomic DNA was used as a template to amplify respective genomic areas and analyse them according CRISPR/Cas9 induced double strand breaks. Primer for this PCR were designed with Primer3 and bind the DNA 500-750 bp upstream and downstream of the gRNA target site. For amplification of this sequence a PCR, using Q5-Polymerase was set-up in a 50 µL volume following manufacturer's protocol using 100 ng of genomic DNA from extraction. PCR products were separated by agarose gel electrophoresis (1.5% agarose gel) and respective bands were extracted and purified using Monarch® DNA Gel Extraction Kit. DNA concentration was determined by Nanodrop measurement and 200 ng PCR Product of knockout cell lines were mixed each with 200 ng PCR product of parental control in a total volume of 19 µL containing 1X NEBuffer 2. Reactions were set up in duplicates since one was serving as a -T7E1 control. The denaturation and renaturation step was performed as follow: Reactions

were incubated at 95°C for 5 min. Afterwards temperature was reduced to 85°C by -2°C/min. Further reduction in temperature till reaching 25°C were performed by 0,1°C/sec. Afterwards either 1 µL of the T7E1 enzyme (NEB) or water (restriction control) was added and incubated 30 min at 37°C. Reaction was stopped by adding DNA Loading Buffer and restriction analysis was monitored by separation via analytical gel electrophoresis.

3.1.9 Nucleic acid quantification

3.1.9.1 Nanodrop

DNA and RNA concentration of samples was determined with the Nanodrop 1000 measuring the absorbance at 260 nm, 280 nm and 230 nm. For DNA samples, the purity was verified by an A_{260}/A_{280} ratio around 1.8 while for RNA measurements the purity of the samples was shown in an A_{260}/A_{280} ratio greater than 2. Before measurements, residual solvent like ethanol was diminished by heating samples to 70°C.

3.1.9.2 RNA measurement by Qubit™

RNA concentration of samples prepared for RNA sequencing were measured using the Qubit™ RNA high sensitivity (HS) Assay Kit from Invitrogen following the manufacturer's protocol. Samples were diluted 1:400 to be in the concentration range of the standards and measured in duplicates (results 5-10 ng/µL).

3.1.10 Nucleic acid isolation

3.1.10.1 RNA isolation using TriFAST™

Total RNA was isolated with peqGold TriFast™ (VWR). Cells plated on tissue culture dishes were directly lysed by adding 500 µL to 1 mL TriFAST regarding cell number. Cells were incubated with TriFAST for 5 min and homogenized by pipetting up and down. Lysates were transferred and RNA was extracted by adding chloroform. After centrifugation (10 min, 16,100 x g) upper aqueous phase was mixed with one volume isopropanol to precipitate RNA. Precipitation took place >30 min until overnight at 4°C. Precipitated RNA was collected by centrifugation 16,100 x g for 15 min at 4°C. Supernatant was discarded and RNA pellet was washed twice with 70% ethanol. Air-dried pellet was dissolved in appropriate volume of ddH_2O and concentration was determined. Until further use, RNA was stored at -80°C.

3.1.10.2 RNA isolation using RNeasy® Plus Mini Kit

RNA used for RNA-Sequencing was isolated according to manufacturer's protocol using RNeasy® Plus Mini Kit from Qiagen. Instead of adding 2-Mercaptoethanol to RLT Plus buffer, dithiothreitol (DTT) was added and cells were directly lysed in the

vessel. For disruption of cell membrane, a 23G needle was used and lysate was passed through eight times. All optional steps were performed.

3.1.10.3 DNA isolation using Roti®Phenol

Cell pellet was resuspended in R3 buffer of HiPure Plasmid Maxiprep Kit (see 2.7.3) containing RNaseA. Additionally, SDS was added in a final concentration of 0.5 % (v/v) and incubated 5 min at RT. DNA was sheared using a Bioruptor® and isolated by phenol-chloroform extraction: Sheared DNA was mixed with phenol-chloroform-isoamylalcohol (25:24:1) in a ratio of 1:1 and centrifuged at 13.000 rpm at RT for 15 min. Clear upper phase was extracted again like described above. DNA containing upper phase was mixed with 0.1 volume 3M sodium acetate and 1 volume isopropanol. Precipitation was performed for > 45 min at -20°C or overnight at 4°C. Precipitated DNA was collected by centrifugation (30 min at 13.000 rpm, 4°C) and pellet was washed twice with 70% EtOH. DNA pellet was air-dried and dissolved in an appropriate volume of ddH_2O. To remove residual EtOH, DNA solution was heated up to 70°C and incubated for 10 min. DNA concentration was determined and DNA was stored at -20°C until further use.

3.1.11 cDNA synthesis

To perform quantitative RT-PCR (qPCR) isolated RNA was transcribed into complementary DNA (cDNA). Therefore, 0.5 µg-2 µg RNA was digested with DNase I and subsequently reverse transcribed using the M-MLV reverse transcriptase (both from Promega). In the first step, RNA was diluted in a total volume of 7 µL and mixed with 2.25 µL hexanucleotide random primers (0.5 µg/µL) from Roche, 1 µL dNTPs (10 mM) from Invitrogen and 1 µL DNase I in a total volume of 12.5 µL containing 1X DNase Buffer. DNA digest was performed at 37°C for 15 min and Endonuclease was heat-inactivated by incubation at 70°C for 15 min. When reactions were cooled down 1 µL M-MLV and 0.1 µL RNase inhibitor Ribolok (Invitrogen) was added and volume was adjusted with M-MLV buffer (5X) and ddH_2O to 20 µL. Reverse transcription was pre-heated at 25°C for 10 min and reaction was performed at 42°C for 50 min. M-MLV was inactivated by incubating reactions for 15 min at 70°C. cDNA was either directly used for qPCR or stored at -20°C.

3.1.12 RNA Next Generation Sequencing (RNASeq)

Inducible knockdown cells were kept under doxycycline treatment for the indicated time. RNA was extracted using the RNeasy® Plus Mini Kit from Qiagen (3.1.10.2) and RNA concentration was determined by Qubit™ RNA high sensitivity (HS) Assay Kit (3.1.9.2). Quality of samples were checked and RNA was measured by the Genomics and Proteomics Core Facility of the DKFZ Heidelberg. Data was analysed by Dr. Felix Christian Eduard Vogel (Maier *et al.* 2023).

3.2 Cell biology methods

3.2.1 Cultivation of cell lines

Human cell lines (2.1.1) where either obtained by the London Research and Francis Crick Institute or a courtesy of the Department for Biochemistry and Molecular Biology at the Biocenter in Würzburg (AG Eilers, AG Diefenbacher). Mouse cell lines (2.1.2) were generated from mice with specific mutational background by Oliver Hartmann, Group of Markus E. Diefenbacher (Hartmann *et al.* 2021). Cells were grown in indicated culture medium (2.1 & 2.3.1) supplemented with 10% fetal calf serum (FCS, Sigma) and 1X Penicillin/Streptomycin (Sigma) in a cell incubator at 37°C in 5% CO_2.

3.2.1.1 Cell passaging

Cells were passaged regularly every two to three days and confluency was kept below 90 %. For splitting the cells, medium was removed, cells were washed with PBS and detached from dish using trypsin-EDTA. Once cells were completely detached, trypsin was inactivated by adding fresh medium in a ratio of at least 5:1. Cells were resuspended and a fraction of cell suspension was plated on a new cell culture dish with fresh medium. For changing the medium or refresh treatments, medium was removed, cells were once washed with PBS and fresh medium or medium containing inhibitor was added.

3.2.1.2 Cell freezing

For long-term storage, cells were frozen in freezing medium (2.3.1) at -80°C and liquid nitrogen. For this attempt, cells were trypsinated and subsequently resuspended in culture medium. Suspension was centrifuged for 5 min at 500 x g at RT and cell pellet was resuspended in appropriate amount of freezing medium. Cell suspension was transferred to cryotubes and slowly frozen using a Mr. Frosty container placed at -80°C overnight. Cryotubes were afterwards transferred into liquid nitrogen for storage.

3.2.1.3 Cell thawing

Cells frozen in cryotubes were thawed in a 37°C water bath. Immediately, cells were carefully resuspended in freezing medium and directly placed into cell culture dish with pre-warmed culture medium. After cells settled, the medium was changed to remove the DMSO present in freezing medium. Sensitive cells were resuspended in culture medium and centrifuged 5 min at 500 x g at RT. Supernatant containing DMSO was removed and cell pellet was resuspended in fresh media. Cells were placed in cell culture dish. Before performing experiments, cells were cultivated for at least three to five days.

3.2.1.4 Cell cultivation as spheroids

For the cultivation of cells in spheroid culture, cells were trypsinized to detach from cell culture dish. Cells were counted and for each spheroid 10 000 cells in a total volume of 200 µL medium were seeded in individual wells of a 96-well ultralow attachment plate (Corning). Spheroid formation was initiated by centrifugation at 850 x g for 10 min. Spheroids were grown in a cell incubator at 37°C in 5% CO_2 and medium was changed twice a week by removing 100 µL and adding same volume of fresh medium. After one to two weeks, when spheroids reached a certain size, cells were harvested by pooling individual spheroids, washing with PBS and lysis in RIPA buffer (see 3.3.1).

3.2.1.5 Cell starvation treatments

To cultivate cells under full serum (FS) and low serum (LS) conditions, cells were seeded a day before and next day media was removed, cells were washed once with PBS and respective media containing either 10 % FCS or 1 % FCS was added.
For starving cells under acidic conditions, pH of medium was adjusted with HCl to 6.8. Cells were seeded the day before and next day cells were washed with PBS and media pH 6.8 or normal medium (pH 7.4) was added.
Cells cultivated in hypoxic conditions were incubated in a Don Whitley Hypoxia Workstation in 0.5 % O_2 and 5 % CO_2 at 37°C. Dishes were wrapped in aluminium foil to prevent evaporation of medium.

3.2.2 Cell transfection and infection

3.2.2.1 Transfection by Polyethylenimine (PEI)

For stability assays and lentiviral production cells were transfected using Polyethylenimine (PEI). Calculated amount of Plasmid-DNA was prepared in OptiMEM. Separately, PEI was mixed with OptiMEM in a ratio of 1:2 of DNA:PEI. Both solutions were incubated for 5 min at RT and afterwards mixed and incubated for 20 min at RT. Meanwhile cells were washed once with PBS and medium was changed to transfection medium. DNA-PEI solution was added dropwise to the cells and incubated at least 6 h up to 24 h.

3.2.2.2 Transfection by Lipofectamine

Stability Assays were performed by transfecting cells using Lipofectamine 2000. Amount of plasmid DNA, Lipofectamine and OptiMEM were used according manufacture's protocol. Cells were seeded one day before transfection and confluency was <80%. After washing the cells with PBS, transfection medium and transfection solution was added dropwise. Medium was changed to normal culture medium after 6 h.

3.2.2.3 Production of lentiviruses

For the production of lentiviral particles, HEK293T cells were transfected according to 3.2.2.1. Cells were counted the day before and 5 Mio cells were seeded per 10 cm dish. Next morning, DNA solution was prepared in OptiMEM: 12 µg plasmid DNA, 2.8 µg pPAX2 and 1.4 µg pMD2G packaging plasmids in 700 µL OptiMEM. For each transfection 30 µL PEI was diluted in 700 µL OptiMEM. After 5 min incubation at RT PEI solution was dropped to DNA solution, mixed and incubated for 20 min at RT. Meanwhile cells were washed with PBS and medium was changed to transfection medium. DNA-PEI solution was added dropwise and cells were transferred to biosafety level 2 (BSL-2) incubator.

3.2.2.4 Cell infection with lentiviruses

HEK293T cells were transfected described in 3.2.2.3. After 24 h, medium was changed to normal culture medium. Virus was harvested 48 h and 72 h after transfection by filtering the medium to a 0.45 µM filter and directly adding to the target cells. Target cells were seeded a day before infection to reach a confluency of 80-90 % at point of infection. Cells were washed once with PBS and filtered medium containing lentiviral particles were mixed 1:1 with fresh medium and added directly to cells. To increase infection efficiency, polybrene was added in a final concentration of 4 µg/mL. Earliest 24 h after last infection positively infected cells were selected by adding appropriate antibiotics or by FACS-sorting.

3.2.3 Cell quantification

3.2.3.1 Crystal violet staining

For proliferation and growth assays, cells were seeded in the same cell number and cultivated for the indicated period of time under indicated conditions. Afterwards cells were fixed with 3.7 % Paraformaldehyde (PFA) in PBS and incubated for 10 min. Fixed cells were washed once with PBS and incubated with crystal violet solution for >30 min at RT. Crystal violet solution was discarded and cells were washed with water. Dried plates were scanned and signal intensity was quantified by de-staining cells with 10 % acetic acid. Absorbance was measured with a microplate reader at a wavelength of 550 nm.

3.2.3.2 Growth curve by cell counting

For determination of a growth curve, cell lines were seeded using same cell number in triplicates. After indicated time points cells were detached and counted automated using a CASY cell counter. Procedure was repeated for every time point. Cells were not re-seeded.

3.2.3.3 Cell number by nuclei staining (Operetta)

To determine cell numbers, cells were seeded as duplicates in a 384-well plate (PhenoPlate, Perkin Elmer). Next day, cells were treated with individual inhibitor and incubated for indicated time. Cells were fixed with ice-cold methanol (MeOH) for 5 min at RT. MeOH was removed and cells were washed once with PBS. After removal of PBS, cells were stained by adding 2.5 µg/mL Hoechst 33342 in PBS for 10 min at RT in the dark. Cells were washed twice with PBS and number of nuclei was measured by Operetta High Content Analysis System (Perkin Elmer). In total, 15 individual pictures of each well were measured and analysed.

3.2.4 Immunofluorescence

For immunofluorescence staining, cells were grown in ibidi slides. Next day cells were washed once with PBS and afterwards fixed with 3.7 % PFA in PBS. After incubation for 10 min at RT, PFA was removed and cells were washed with PBS. For permeabilization, 0.2 % Triton X-100 in PBS was added for 10 min at RT. Cells were washed with PBS and subsequentially blocked with 3 % BSA in PBS for 30 min at RT. Primary antibodies were diluted in 1% BSA in PBS and cells were incubated with antibody dilution overnight at 4 °C. Cells were washed twice with PBS and incubated with fluorescently labelled secondary antibody dilution for 1 h at RT in the dark. Finally, cells were washed three times with PBS and mounted with mounting medium already containing DAPI. Slides were stored at 4 °C for up to three days. For long-term storage, ibidi slides were frozen at -20 °C.
Concentration of primary antibodies was experimentally determined (1:100 – 1:50), Alexa fluorophores were used in a concentration of 1:200. Quantification of signal intensities was performed with ImageJ software by Elias Einig (AG Popov).

3.2.5 Proximity Ligation Assay (PLA)

Cells used for proximity ligation assay (PLA) were grown in ibidi slides. Fixation and permeabilization were performed like described in 3.2.4. For blocking with Duolink Blocking Solution (Sigma), manufacturer's protocol was followed. Concentration of primary antibodies was determined as 1:100 in Duolink Antibody Diluent (Sigma) in a pilot experiment and incubation time was determined as 2 h at RT on a shaker. PLA probes were diluted like recommended by supplier and incubated for 1 h at 37 °C. Ligation was performed in Duolink Ligation Buffer with ligase 1:40 (both Sigma) for 30 min at 37 °C. During the amplification step, slide was protected from light and amplification buffer and polymerase (both from Sigma) was used. Amplification was incubated for 100 min at 37 °C. After final wash slide was mounted with in situ Mounting Medium (Sigma) containing DAPI and sealed.
Signals were detected using a confocal Leica SP8 microscope and slides were stored at 4°C for short-term and frozen at -20 °C for log-term storage. Quantification of signal was performed using Fiji software.

3.3 Biochemical methods

3.3.1 Preparation of whole cell protein extracts

For the preparation of whole cell extracts cells were washed once with PBS and scraped in an appropriate amount of ice-cold PBS. Cell suspension was collected in a tube and centrifuged at 800 x g for 5 min at 4 °C. PBS was discarded and cell pellet was resuspended in RIPA lysis buffer where Protease Inhibitor cocktail (cOmplete™, Roche) and phosphatase inhibitors (cocktail 2 and 3, Sigma) were added. Lysis was performed for >30 min on ice. Cell lysates were cleared by centrifugation (16 100 x g, 10 min, 4 °C). Either protein concentration was directly determined (3.3.6) and samples were diluted in SDS sample buffer or stored at -80 °C.

3.3.2 Cell Fractionation

3.3.2.1 Subcellular Extraction Kits

For the fractionation of cells either the NE-PER™ Nuclear And Cytoplasmic Extraction Reagents or the Subcellular Protein Fractionation Kit for Cultured Cells (both from Thermo Scientific) was used following manufacturer's protocol. All buffer volumes were adjusted to pellet size (100 µL U2OS, 50 µL A431). Lysates were either adjusted by extraction volume or protein concentration were determined by BCA Assay (3.3.6) and diluted with SDS sample buffer. Lysates were stored at -80 °C.

3.3.2.2 Subcellular fractionation (Abcam protocol)

The following protocol is based on a public available fractionation protocol from Abcam:
Cells were scraped in an appropriate amount of fractionation buffer and incubated for 25 min on ice. Cell suspension was 30 times passed through a 27-gauge needle until cells were completely lysed. Cell suspension was incubated another 20 min on ice and fractionation was performed by centrifugation (720 x g, 5 min, 4 °C). Cytoplasmic fraction was transferred to a fresh tube and lysate was cleared (16 100 x g, 2x 10 min, 4 °C). Nuclear pellet was washed twice with fractionation buffer and passed through a 25-gauge needle 10 times. Suspension was centrifuged at 720 x g for 10 min at 4 °C and supernatant was discarded. Pellet containing nuclei was resuspended in one pellet volume TBS with 0.1 % SDS. Shearing of DNA was performed by passing suspension through a 22-gauge needle 8 times. Lysate was cleared by centrifugation (16 100 x g, 2x 5 min, 4 °C). Cytoplasmic and nuclear fraction were adjusted to extraction volume and diluted in SDS samples buffer. Lysates were stored at -80 °C.

3.3.3 Immunoprecipitation

For endogenous co-immunoprecipitation, cells were harvested by scraping and washed with PBS. The chemical crosslinker Dithiobis[succinimidylpropionate] (DSP)

was added in a final concentration of 0.8 mM in PBS. Cells were resuspended in PBS containing DSP and incubated for 30 min with rotation. To enrich SREBP2 levels cells were fractionated described in 3.3.2.2 and only fraction containing membrane and nuclear proteins were further processed: The protein concentration of the SREBP2-enriched fraction was determined by BCA (3.3.6) and either 5 µg of the anti-SREBP2 or 5 µg IgG goat was added. Input samples of 10 % were taken and directly mixed with SDS loading buffer. The volume was adjusted with PBS supplemented with protease inhibitors to 500 µL and incubated overnight at 4 °C with rotation. Next day, immunoprecipitation was performed using Dynabeads™ Protein A/G Magnetic Beads (Invitrogen) in a ratio of 1:1 with recommended total amount of 1.5 mg per sample. Beads were equilibrated in PBS, added to lysates and coupling was incubated for >2h at 4 °C. Separation was performed using a magnetic rack and beads were washed three times á 10 min with PBS + 0.02% Tween. To elute proteins and antibodies from beads, SDS loading buffer was added and beads were cooked for 5 min at 95 °C. Pulldown samples were directly loaded together with input samples on SDS gels.

3.3.4 Ubiquitination Assays

For *in cellulo* ubiquitination assay, cells were transfected with indicated DNA amounts of overexpression plasmids (pcDNA3, pSico; Table 9) in 6-well plates using either Lipofectamine or PEI transfection (see 3.2.2.1 and 3.2.2.2). Six hours prior harvest, MG-132 in a final concentration of 20 µM was added and cells were harvested 24 h post transfection by trypsination and washed with PBS.
For Ni-NTA pulldown, cell pellet was resuspended in 100 µL PBS and 10% (v/v) was taken as input control. 1 mL lysis buffer (8 M urea + 10 mM imidazole in PBS) was added and lysis was performed for 15 min at RT by end-to-end rotation. Cell debris was separated by centrifugation (16100 x g, 10 min, RT) and clear supernatant was added to pre-washed magnetic Dynabeads™ His-tag beads (Invitrogen). Protein suspension was incubated with beads overnight at RT by end-to-end rotation. Next day, beads were separated by using a magnetic rack and washed twice with PBS. Elution of bound proteins were performed by adding 50 µL 1X SDS sample buffer supplemented with 10% (v/v) β-mercaptoethanol.
For pulldown of HA-tagged mSREBP2, cell pellet was resuspended in 100 µL RIPA lysis buffer (supplemented with protease- and phosphatase inhibitors as well as 20 µM MG-132) and incubated for 1 h on ice. Cell suspension was cleared by centrifugation (16100 x g, 10 min, 4 °C) and 10% (v/v) input sample was taken. For HA-pulldown, supernatant was added to pre-washed Pierce™ Anti-HA Magnetic beads (Thermo Scientific). Volume was adjusted by adding 900 µL PBS supplemented with protease- and phosphatase inhibitors as well as 20 µM MG-132. Pulldown was performed overnight at 4 °C by end-to-end rotation. Next day, beads were separated by using a magnetic rack and washed twice with PBS. Elution of bound proteins were performed by adding 50 µL 1X SDS sample buffer supplemented with 10% (v/v) β-mercaptoethanol.

Input and pulldown samples were separated by SDS PAGE (3.3.7) and ubiquitinated proteins were analysed by immunoblot (3.3.8).

3.3.5 DUB Activity Assay (Warhead Assay)

AZ-1 treated cells were washed and trypsinated to detach from the plate. Cells were resuspended in DMEM and pelleted. Pellet was washed with PBS and cells were resuspended in HR lysis buffer supplemented with 1 mM DTT and protease inhibitors. Samples were kept on ice for 1.5 h. Additionally, cells were sonicated in an ultrasonic bath. Lysates were cleared by centrifugation (14 000 x g, 15 min, 4 °C) and protein concentration was determined by BCA Assay 3.3.6. In a total volume of 10 µL. 50 µg total soluble protein (TSP) was diluted in HR lysis buffer and either 2 µL HA-Ub-VME (25 µM, Enzo) or HR lysis was added and incubated at 37 °C for 30 min. Samples were mixed with SDS loading buffer and analysed by immunoblot.

3.3.6 Bicinchoninic Acid (BCA) Assay

Protein concentration in lysates was determined by the use of the bicinchoninic acid (BCA) assay. Reagents were supplied by Thermo Scientific and procedure was performed following manufacturer's instructions. Standards were diluted like described in the protocol and stored at -20 °C. Volumes were adjusted to 5 µL each standard and sample mixed with 100 µL working reagent (ratio 50:1, reagent A:B). Samples were pipetted in duplicates and incubated for 30 min at 37 °C. Absorption was measured with a microplate reader at a wavelength of 562 nm. Standard curve was calculated using absorbance of BSA standard solutions and protein concentration was calculated. Lysates were adjusted to same protein amount and diluted with SDS sample buffer. Prepared western blot samples were stored at -20 °C.

3.3.7 SDS Polyacrylamide gel electrophoresis (SDS PAGE)

For casting SDS gels either buffers listed in 2.6.4 or for quantification and normalisation to total protein the TGX Stain-free FastCast Acrylamide Kit (Bio-Rad) were used. Lysates mixed with SDS sample buffer were boiled 5 min at 95 °C and equal volume with adjusted protein concentration (20 – 50 µg TSP) were loaded into the pockets. For molecular weight comparison, the pre-stained PageRuler Protein Ladder (Thermo Scientific) was loaded next to the samples. The separation of proteins by size was performed in SDS-PAGE chambers (Bio-Rad) filled with SDS running buffer at constant current of 30 mA per gel.

3.3.8 Immunoblot

After protein separation by SDS-PAGE, proteins were transferred onto fluorescence compatible PVDF membrane (Merck). For this purpose, the membrane was activated in methanol for >30 sec and afterwards equilibrated in transfer buffer. Sponges and whatman paper were also soaked in transfer buffer. For the assembly of the western

blot sandwich, the membrane was placed onto the gel and afterwards flanked by two sheets of whatman paper each side. One sponge on either side was added and all together inserted into the cassette. The cassette was placed into the tank that was filled with transfer buffer. Transfer was performed at RT for 90 min and constant voltage of 75 V.
The membrane was briefly washed in ddH_2O and incubated with blocking solution > 20 min at RT or overnight at 4°C. Incubation with primary antibodies took place overnight at 4 °C. For housekeeping genes like Actin and Vinculin incubation time was shortened to >1h at RT. After washing three times for 5 min with TBS-T fluorescent secondary antibodies were added and incubated for > 1h at RT protected from light. Membrane was finally washed three times á 10 min with TBS-T and fluorescent signals were detected with fluorescence compatible membrane scanner (LI-COR, Bio-Rad) and analysed with the respective software (Image Studio Lite, Image Lab).

3.4 Metabolic Assays

3.4.1 Liquid Chromatography Mass Spectrometry (LC-MS) of metabolites

Cells were seeded in the same cell number and cultivated under indicated conditions. Before harvesting cells were washed with ice-cold 154 mM ammonium acetate and plates were snap frozen in liquid nitrogen.
Extraction and measurement of metabolites was performed by Dr. Lisa Schlicker, Core Facility of Metabolomics at the DKFZ Heidelberg (Maier *et al.* 2023).

3.4.2 Stable Isotope Labelling

For labelling experiments, cells were seeded in the same cell number. Inducible knockdown cell lines were pre-treated with doxycycline, counted, and re-seeded after 72 h. Next day medium was changed to DMEM w/o glucose and either 25 mM ^{13}C-glucose or unlabelled glucose (control) was added. Cells were cultivated for additional 24 h.
Cells were washed and frozen like earlier described (3.4.1).
Extraction and measurement of metabolites was performed by Dr. Lisa Schlicker, Core Facility of Metabolomics at the DKFZ Heidelberg (Maier *et al.* 2023).

3.5 Generation SREBP2 KO Mice

3.5.1 Cloning of KPL sgSREBF2

To approach double sgRNA system, two sgRNAs were cloned into KPL AAV backbone (Hartmann *et al.* 2021) using cloning primers with overhangs for KpnI, HindIII and EcoRI. PCR amplification was performed using Phusion polymerase and PCR products were cleaned-up (Monarch® DNA Gel Extraction Kit, NEB). DNA concentration was determined by Nanodrop measurement and restriction digest of PCR products and vector backbone was set up. Restricted DNA fragments were

purified (Monarch® PCR & DNA Cleanup Kit, NEB) and vector was cleaned-up by agarose gel electrophoresis. Ligation took place overnight at 4 °C and bacteria was transformed. To check successful insertion, colony PCR was set up and plasmid DNA of positive clones was extracted and proofed by Sanger sequencing.

3.5.2 Production of AAV

Four 15 cm dishes with HEK293T cells were transfected with 20 µg pHelper/ ΔF6, 10 µg pRCDJ and 10 µg of KPL sgSREBF2 per dish. The ratio of DNA:PEI was 1:2 and transfection was performed described in 3.2.2.1. Transfection medium was replaced 24 h post transfection to DMEM + 2% FCS and incubated for 72 h. AAV containing supernatant was collected, NaCl was added in a final concentration of 0.5 M and incubated for 1 h on a shaker. Medium was supplemented with Chloroform in a final concentration of 10 % (v/v) and again incubated for 30 min with rotation. Afterwards, suspension was centrifuged for 30 min at 4000 rpm at 4 °C and aqueous phase was collected. For precipitation of AAV 10 % (v/v) PEG8000 was added and incubated overnight at 4 °C.
Precipitated AAV was collected by centrifugation (30 min, 4000 rpm, 4 °C) and pellet was dissolved in PBS supplemented with Protease inhibitor. DNase I and RNase A was added and digestion took place for 2 h at 37 °C. Chloroform was added in a 1:1 ratio and phases were separated by centrifugation (11 000 rpm, 5 min, 4 °C). Water phase was transferred and extraction step was repeated. Aqueous phase was stored at 4 °C until titre of AAV was determined.
AAV titre was determined using a protocol publicly available from the addgene website. The protocol is based on qRT-PCR using primers targeting AAV2 ITR first described in (Aurnhammer *et al.* 2012). qPCR was performed as described in 3.1.5.3 and titre was calculated based on the standard curve.
AAV was either directly used for intratracheal intubation of mice or stored at -80 °C.

3.5.3 Immunohistochemistry (IHC) staining

Mouse intubation as well as coordination of *in vivo* experiment was performed and monitored by Oliver Hartmann, AG Diefenbacher, Biocenter University of Würzburg. After termination of mouse experiment, lung samples were embedded in paraffin and sectioned using a microtome (Leica).
Before staining, slides were de-paraffinized and rehydrated using the as follow: 3 × 5 min in xylene, 2 × 2 min in EtOH (100%), 2 min in EtOH (95%), 2 min in EtOH (80%), 2 × 2 min in EtOH (70%), 2 min in EtOH (50%) and 2 min in H_2O. Epitope retrieval was performed using 10 mM sodium citrate buffer (pH 6.0). Slides were washed with H_2O and cells were permeabilized with TBS-T for 10 min at RT. Afterwards slides were blocked in TBS + 1% BSA for 30 min at RT. Primary antibodies (anti-USP28 (Sigma, HPA006778), anti-HMGCS1 (Abcam, ab155787), anti-SREBF2 (R&D, MAB7119)) were diluted 1:100 in blocking solution and incubated overnight at 4 °C. Slides were washed the next day three times with TBS and incubated with

respective secondary antibody for >1 h at RT. After three washing steps slides were stained using DAB reagent (Vector Lacs) and reaction was stopped by washing with TBS. Counter-staining of nuclei with Haematoxylin and Eosin was performed. Slides were mounted and covered up by a coverslip on top. IHC slides were recorded using Panoramic DESK scanner and analysed using CaseViewer software (3DHISTECH). Quantification of the tumour area and number of tumours were performed using the software QuPath.

3.6 Statistical Analysis

Data was visualized using GraphPad Prism software. Data points are presented as mean or median values of technical triplicates unless otherwise indicated. Error bars represent standard error of the mean (SEM) unless otherwise indicated. Experiments were usually performed in biological duplicates of individual experiments and if possible, with technical triplicates. Significance was calculated using a two-tailed unpaired student t-test if not otherwise indicated in the figure legend. P-values smaller than 0.05 were considered to be statistically significant.

4 Results

Altered metabolism is a hallmark of cancer and therefore metabolic pathways need to be tightly regulated. The *de novo* lipid and cholesterol synthesis are under the control of the master transcription factor family of sterol regulatory element-binding proteins (SREBPs). SREBPs are regulated at various levels. In the focus of this work is the regulation of SREBPs by the ubiquitin system at the post-translational level. The E3 ligase Fbw7 was identified to regulate the stability of SREBPs. Furthermore, Fbw7 shows specificity to other transcription factors like c-Myc, Jun or Notch1. These transcription factors are not only characterized by the presence of a cdc4-phosphodegron motif but were also found to be deubiquitinated by the deubiquitinase USP28.

4.1 USP28 co-localises and interacts with SREBPs

4.1.1 Localisation of SREBPs and USP28 in cells

To investigate a potential regulation of SREBPs by USP28, the locations of both proteins were analysed and the interaction of USP28 with SREBPs was investigated. It is known that SREBP precursors (flSREBPs) are integral to the ER membrane but are proteolytically cleaved in the Golgi system upon activation by different stimuli. After processing, the N-terminal part of SREBPs is translocated to the nucleus to activate expression of target genes. The subcellular localisation of USP28 was reported as being nuclear. It is known that the ubiquitination of SREBPs take place directly on the DNA, most likely at the promoter site (Sundqvist *et al.* 2003, Punga *et al.* 2006). To elucidate if the active transcription factors mSREBP1 and mSREBP2 are co-localised with USP28 in the nucleus, immunofluorescence staining in U2OS cells was performed (Figure 4-1).

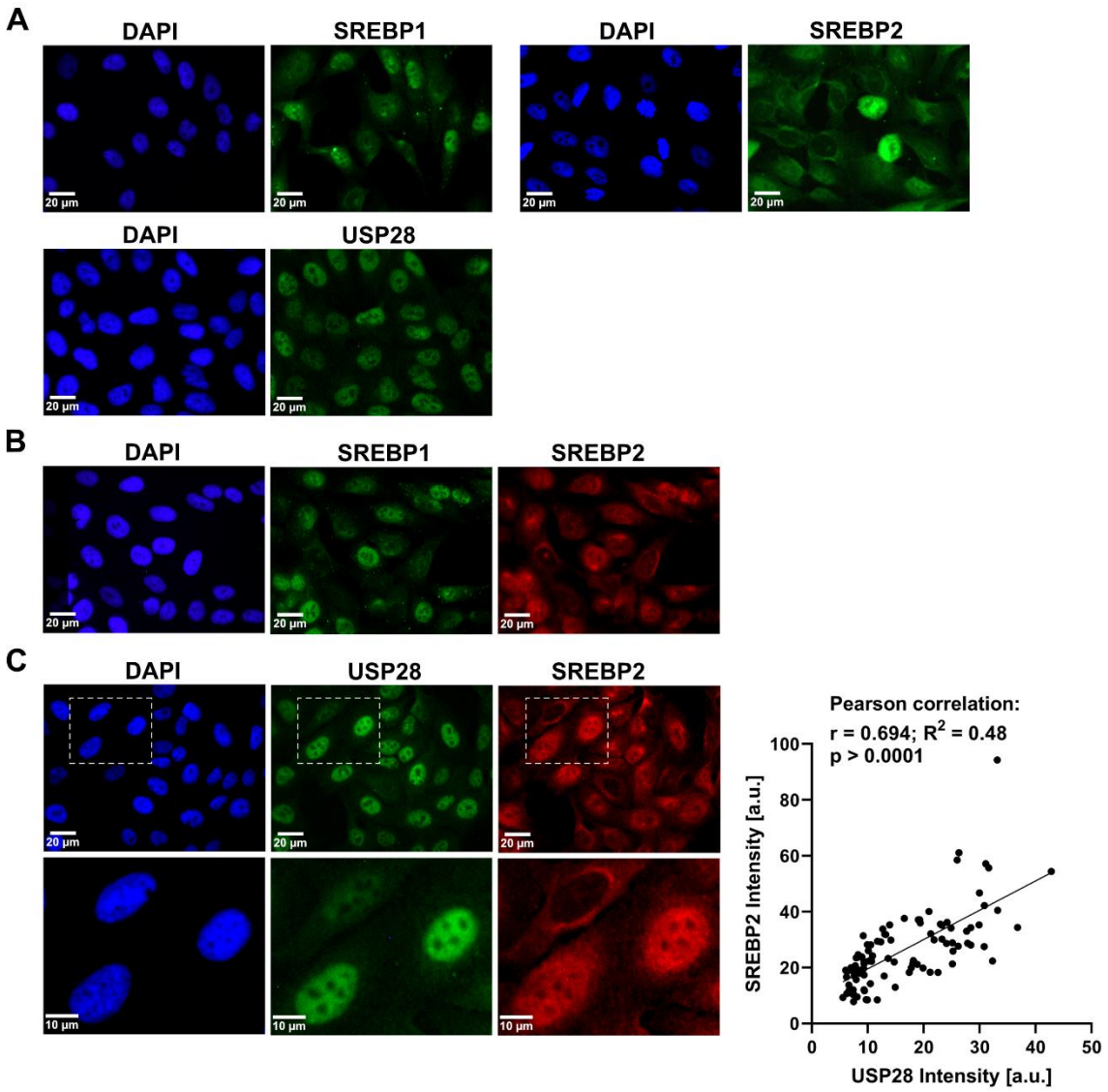

Figure 4-1: SREBPs and USP28 are co-localised in the nucleus of U2OS cells.

A. *Individual immunofluorescence staining of SREBP1, SREBP2 and USP28 (green). DNA detection by DAPI shows respective nuclear staining (blue).* ***B.*** *Co-immunofluorescence staining of SREBP1 (green) and SREBP2 (red) and DNA (blue).* ***C.*** *Co-immunofluorescence staining of USP28 (green) and SREBP2 (red) with corresponding DAPI staining of cell nuclei. Lower part shows enlarged section of individual cells. IF co-staining of USP28 and SREBP2 was quantified using the ImageJ software and Pearson correlation analysis was performed. Correlation analysis was calculated by Elias Einig, AG Popov.*

Individual immunostainings for SREBP1, SREBP2 and USP28 showed fluorescence signals in the nucleus. SREBP1 staining revealed strong signal in the nucleus and perinuclear area of most cells: In contrast, SREBP2 also showed nuclear staining but was mainly localised to the perinuclear area, most likely the ER, in some cells. Furthermore, cells with condensed chromatin during mitosis showed high intensity for nuclear SREBP2 staining. USP28 positivity was exclusively found in the nucleus (Figure 4-1 **A**).

Co-staining of SREBP1 and SREBP2 showed the same tendency of signal intensities: cells with high nuclear staining of SREBP1 also showed strong nuclear signal for

SREBP2. While SREBP1 localisation was mainly restricted to the nucleus, SREBP2 staining again revealed signals also in the perinuclear area. Both SREBP antibodies bind to a peptide sequence in the N-terminus of SREBPs, recognizing therefore flSREBP as well as mSREBP. It can be assumed that perinuclear staining refers to flSREBP while nuclear staining elucidates mSREBP (Figure 4-1 **B**).
Simultaneous cellular localisation of SREBP2 and USP28 support the observations and showed a strong correlation in nuclear staining. Cells with high levels of USP28 in the nucleus showed also high nuclear staining for SREBP2. In contrast, cells with medium or low nuclear USP28 intensity revealed also low nuclear staining for SREBP2 while the perinuclear staining remained unaffected (Figure 4-1 **C**).
These observations showed a nuclear localisation for SREBPs and USP28 and a strong correlation of nuclear SREBP2 and USP28.

To confirm the observations of the nuclear localisation of SREBPs and USP28 in the nucleus further, cellular fractionation experiments were performed (Figure 4-2). Lysates from two cancer cell lines, namely U2OS and A431, were separated into cytoplasmic and nuclear fractions and proteins were analysed by immunoblot.

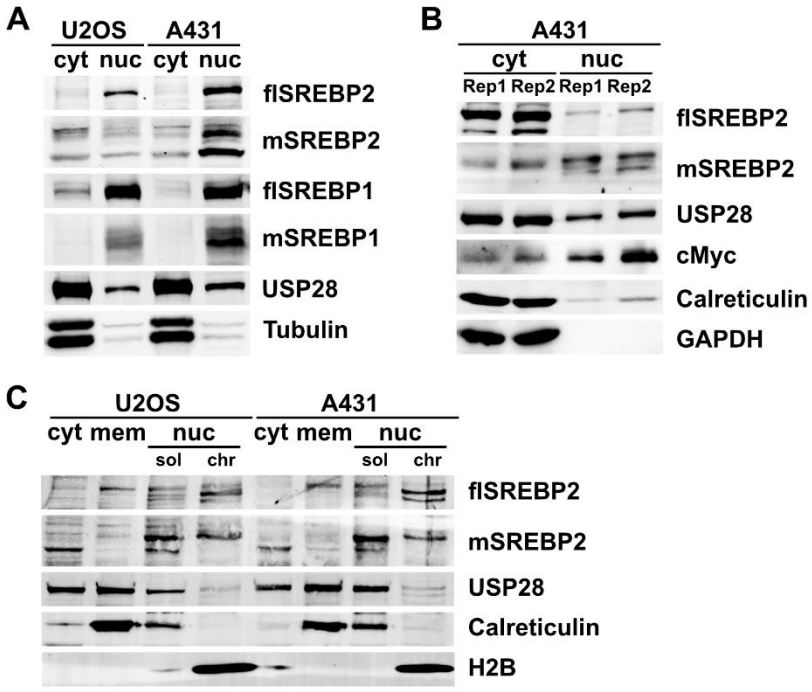

Figure 4-2: mSREBP2 and USP28 are co-localised to the soluble nuclear fraction of U2OS and A431 cells.

A. *Cellular fractionation of U2OS and A431 cells in cytoplasmic (cyt) and nuclear (nuc) fraction using a high salt concertation lysis buffer (3.3.2.2). SREBPs and USP28 levels were detected by Western Blotting. Tubulin serves as cytoplasmic protein marker. Fractions were adjusted to same volume.* ***B.*** *Cellular fractionation of A431 cell lysates using a fractionation kit (3.3.2.1) and detection of SREBP2 and USP28 in two individual replicates (Rep1, Rep2). C-Myc (nucleus), Calreticulin (ER membrane) and GAPDH (cytoplasm) were used as markers for respective cell compartments. Fractions were adjusted to equal volume. Experiment was performed by Celine Reifenberg, AG Schulze* ***C.*** *U2OS and A431 cell lysates were fractionated into cytoplasmic, membrane-bound (mem) and soluble (sol) nuclear and chromatin-bound nuclear (chr) fraction. Protein amount of the fractions were determined, and equal concentrations were separated by SDS-PAGE. SREBP2 and USP28 as well as the compartment markers Calreticulin and Histone 2B (H2B, chromatin-bound) were detected by immunoblot.*

Mature SREBPs were found in the nuclear fraction as well as the flSREBPs, meaning that the nuclear fraction also contains some membrane-bound proteins, while the cytoplasmic fraction seems to be devoid of ER-membrane bound proteins. Unexpectedly, USP28 was found mainly in the cytoplasmic lysate corresponding to the cytoplasmic marker Tubulin (Figure 4-2 **A**).
Separation of cell lysates into cytoplasmic and nuclear proteins was repeated using commercially available fractionation reagents and calreticulin as a marker for the cytoplasmic membrane fraction was included. Membrane-bound proteins were localised to the cytoplasmic fraction, while mSREBP2 was detected in the nucleus. Detection of mSREBPs in western blot reveals two to three closely migrating bands, due to multiple post-translational modifications (Wang *et al.* 1994). As a positive control, c-Myc was detected. Again, USP28 was readily detected in the nuclear fraction, with a substantial proportion also in the cytoplasm (Figure 4-2 **B**).
To further separate cytoplasmic proteins into membrane-bound and soluble fractions and nuclear proteins into soluble chromatin-bound fraction, U2OS and A431 cells were fractionated using a fractionation kit. As a marker for chromatin-bound proteins, histone 2B was detected. Full length SREBP2 was found in membrane-bound as well as soluble nuclear fraction. This was mirrored by the localisation of the ER-membrane protein Calreticulin, suggesting some level of contamination of the soluble nuclear fraction with ER-membrane. Lower molecular bands, potentially representing unspecific signal, were detected in the chromatin-bound fraction. Mature SREBP2 was strongly observed in the soluble nuclear lysate and to a low proportion also in the chromatin bound fraction. USP28 was detected in three subcellular compartments: in the cytoplasm, in the membrane-bound and in the soluble nuclear fraction, but was absent from the chromatin-bound nuclear fraction (Figure 4-2 **C**).
Taken together, the fractionation analysis supported the localisation of flSREBPs as membrane-spanning proteins in the ER and showed the active mSREBPs in the nucleus. USP28 localisation was found in cytoplasm as well as in cytoplasmic membrane and nuclear fractions.

4.1.2 USP28 interacts with SREBP2

For a potential regulation of SREBPs and USP28, it was investigated if and where the proteins are interacting. In previous studies the post-translational regulation of SREBP1 was analysed using myc-tagged overexpression constructs for mature SREBP1 with amino acid sequence 1 to 490 (Sundqvist *et al.* 2003). SREBPs were also shown to be phosphorylated at the cdc4-phosphodegron (CPD) motif (Sundqvist *et al.* 2005). Previous studies also showed that these phosphorylations were essential for Fbw7-mediated binding of the SCF complex and therefor for the ubiquitination and subsequent proteasomal degradation of SREBPs (Nash *et al.* 2001). Mutation of these residues, T426 & S430 in SREBP1 and S432 & S436 in SREBP2, respectively, showed a stabilisation of protein levels due to abolishing proteasomal degradation (Sundqvist *et al.* 2005). The mSREBP2 overexpression constructs were cloned based on pTK-HSV-flSREBP2 using a two-step PCR, introducing first an N-terminal HA tag

and a stop codon following amino acid 484. In the second PCR step, restriction sites for ligation with expression vector were introduced and ligation of restricted plasmid and PCR product was performed. The sequence of human mSREBP2 1-484 was successfully inserted in the pcDNA3 expression vector and the CPDmut SREBP2 plasmid was generated by site-directed mutagenesis (3.1.5.2).
To monitor exogenously expressed SREBPs, U2OS cells were transiently transfected. U2OS cells stably deleted in USP28 by CRISPR/Cas9 technology were a gift from Bastian Krenz, AG Eilers.
Interaction studies were performed in U2OS WT and U2OS USP28 KO cell lines using tagged overexpressed proteins. Additionally, endogenous co-immunoprecipitation was performed in the A431 cell line (Figure 4-3).

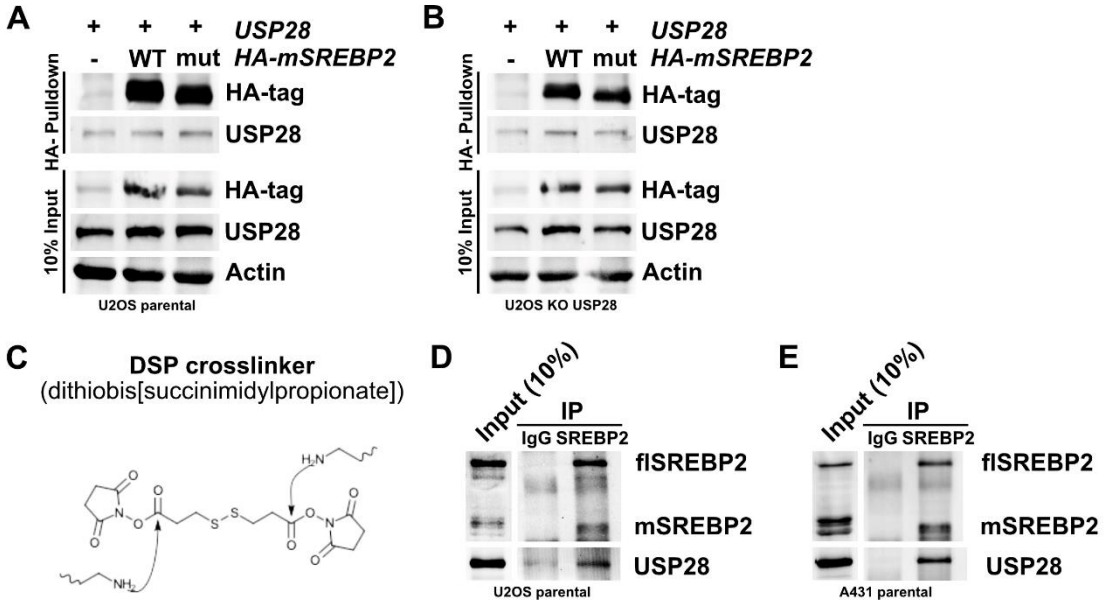

Figure 4-3: Co-Immunoprecipitation in U2OS and A431 cells reveals interaction of USP28 and SREBP2.

A. *U2OS parental and U2OS KO USP28* ***B.*** *Cells exogenously expressing HA-mSREBP2 and USP28 were used to perform HA-tag pulldown and analysed by immunoblot. mSREBP2 was monitored via HA-tag and protein levels in lysates were detected in 10% input. Actin served as loading control.* ***C.*** *Schematic representation of DSP crosslinker reacting with amino groups of proteins to form stable protein-protein interactions. Endogenous IP of SREBP2 in U2OS parental* ***D.*** *and A431 parental E. cells using DSP crosslinker. Cells were treated with 20 µM MG-132 for 6h prior to lysis. SREBP2 and USP28 levels in lysates (10% Input) and Pulldown (SREBP2 IP) were detected by immunoblot. Goat IgG was used as pulldown control.*

To conduct interaction studies of USP28 and SREBP2, U2OS cells were transiently transfected with overexpression constructs for wild type and CPDmut mSREBP2 together with untagged USP28 (pSico USP28, AG Diefenbacher). Co-immunoprecipitation was performed using HA-tag pre-coupled magnetic beads and input and pulldown samples were analysed by immunoblot. USP28 could be detected in immunoprecipitates of wild type and CPDmut SREBP2 but also independent of HA-SREBP2 expression (Figure 4-3 **A**, **B**), suggesting unspecific binding to the immunoglobulin.
For endogenous co-immunoprecipitation, conditions were optimized: In addition to U2OS cells, also A431 cells were used, which display high levels of SREBP2 and

USP28 (compare Figure 4-2). Cells were treated with the proteasome inhibitor MG-132 to increase stability of SREBP2 and support interaction of USP28 and SREBP2. Additionally, cells were incubated with DSP crosslinker (Figure 4-3 **C**) which reacts with amino groups of interacting proteins resulting in stable intermolecular crosslinking. Further, fractionation of cells was performed prior to immunoprecipitation similar to Figure 4-2 **A**. Pulldown was performed using anti-SREBP2 and analysed by immunoblot. USP28 was readily co-precipitated with SREBP2 in both cell lines, indicating an interaction of the two proteins. Using this approach, it cannot be discriminated whether USP28 interacts with flSREBP2 or mSREBP2 and this needs to be further investigated.

To proof the hypothesis that USP28 and SREBP2 are interacting in the nucleus, possibly bound to chromatin at the promoter sites of target genes, a proximity ligation assay (PLA) was performed (Figure 4-4).
U2OS cells were incubated with primary antibodies for either SREBP2 or USP28 and both. Cells without primary antibody incubation were used as control. Secondary antibody probes were incubated and DNA-tags were ligated, amplificated and the resulting signals developed. Cells were monitored with a confocal microscope.

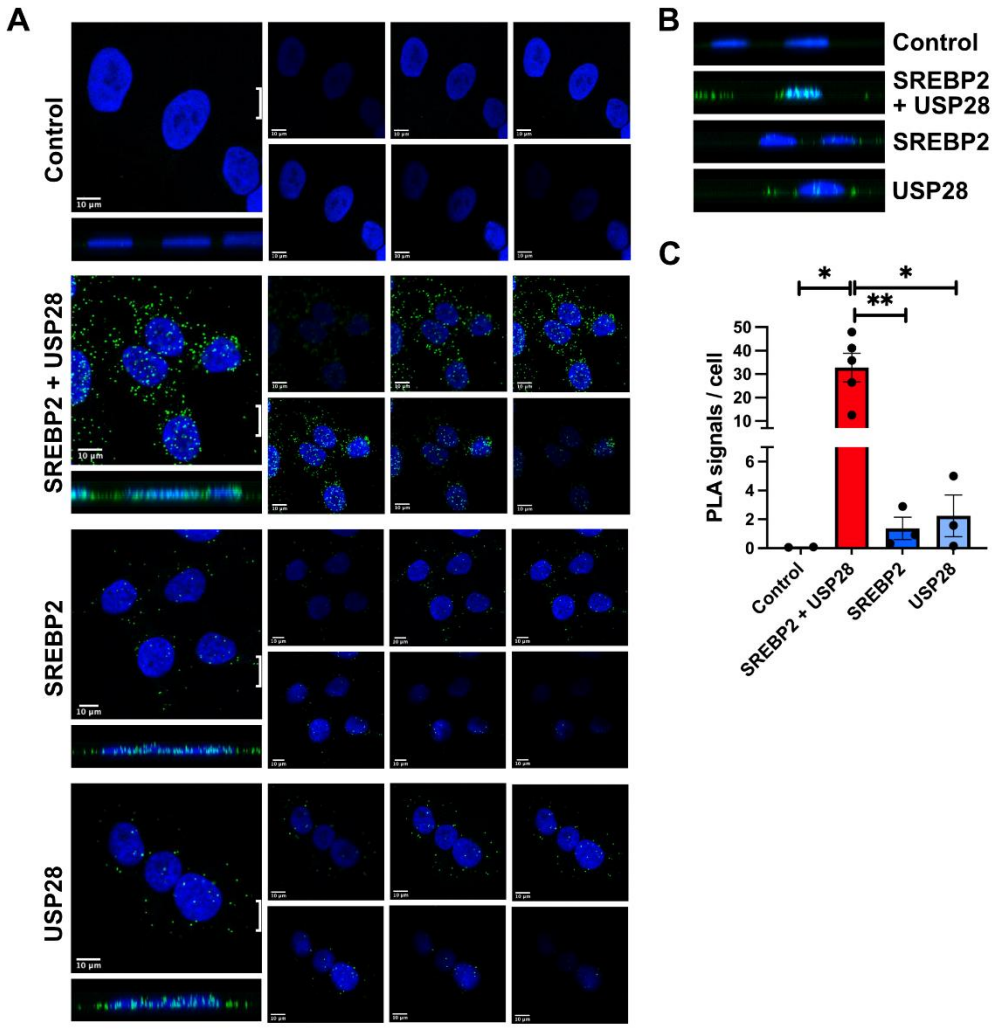

Figure 4-4: SREBP2 and USP28 are in close proximity in U2OS cells.

***A**. Nuclear DAPI staining (blue) and PLA signals (green dots) in control cells (primary antibodies only), SREBP2 and USP28 immunostaining individually, USP28, and SREBP2 co-staining (SREBP2 + USP28). Overview pictures of exemplarily section, z-stack sequential pictures (z = 1 µM) (right) and interpolated 3D projection (bottom) are shown for each condition. **B.** Interpolated 3D projection of samples in A. indicated area. **C.** Quantification of PLA signals with a threshold of >0.5 pixel^2 per cell. Data are presented as mean ± SEM of at least two individual pictures and n > 42 total cell number analysed per condition. *, P < 0.05; **, P < 0.01, unpaired two-tailed Student t test.*

Positive PLA signals (shown as green dots) and DAPI staining (blue) were detected in z-stack mode and interpolated in 3D (Figure 4-4 **A**). In the control cells, only a few background signals could be detected. Cells either incubated with anti-SREBP2 or anti-USP28 alone showed only some positive signals while in cells incubated with both primary antibodies a great number of signals were observed. Signals were distributed throughout the cells, with signals detected in the nucleus and also in the perinuclear region.

To further investigate the location of the proximity signals, the image section marked with a white bracket in Figure 4-4 A was interpolated in 3D. Signals could be observed in the nucleus as well as perinuclear and cytoplasmic area. Quantification of positive signals (Figure 4-4 C) showed a significant increase of PLA signals per cell compared to controls.

Thus, the PLA assay revealed close proximity (< 40 nm) of USP28 and SREBP2 in cells, in the nucleus as well as in perinuclear and cytoplasmic region.

4.2 USP28 regulates SREBP protein levels

So far, it was shown that USP28 and SREBP2 were found in the nucleus and membrane-bound fractions. Further it was shown that USP28 interacts with SREBP2 and both proteins are located in close proximity in cell nucleus, perinuclear region and cytoplasm.
To prove that USP28 indeed influences SREBP2 protein levels stability assays were performed.

4.2.1 Overexpression of USP28 stabilises mSREBP levels even when the CPD is mutated

Ubiquitination and deubiquitination of proteins are post-translational modifications, which can regulate the stability of proteins. While the attachment of K48-linked polyubiquitin chains leads preferentially to the degradation of a protein by the 26S proteasome, the deubiquitination mechanism preserves proteins from proteasomal degradation. It was previously shown that Fbw7 regulates SREBP stability by K48-linked ubiquitination. The deubiquitinase USP28 was reported to be a counteracting DUB for E3-ligase Fbw7, regulating the stability of various Fbw7 target proteins. Among these target proteins and beside SREBPs, multiple additional cancer-related transcription factors were found to be regulated by USP28. The most prominent target protein of the E3-ligase-DUB pair is the oncogene c-Myc (Popov *et al.* 2007): It was shown that overexpression of Fbw7 decreased c-Myc levels and *vice versa,* that overexpression of USP28 results in stabilised c-Myc protein levels.
The key step in the mechanism of deubiquitination by USPs is the hydrolysis of the amide bonds between the ubiquitin and the substrate protein. This reaction is catalysed by the catalytic triad in the active centre of USPs. If the cysteine (C) in this triad is replaced by an alanine (A), the USP is catalytically inactive and therefore unable to remove ubiquitin moieties from target proteins. For USP28, the catalytic cysteine was identified at the position 171 (Valero *et al.* 2001, Zhang *et al.* 2006). Subsequentially, the catalytic inactive version of USP28 is C171A.
To monitor how SREBP protein levels are changing in presence of either overexpressed USP28WT and USP28 C171A or Fbw7, transfection assays with myc-tagged mSREBP1, HA-tagged mSREBP2 and the known substrate HA-c-Myc as a control were performed (Figure 4-5). The mSREBP1 WT and CPD-mutated (CPDmut) expression constructs were kindly provided by the Ericsson Lab (Sundqvist *et al.* 2003) while the HA-tagged c-Myc, USP28 WT and C171A as well as Flag-tagged Fbw7 constructs were a courtesy of Nikita Popov (Popov *et al.* 2007).

Figure 4-5: USP28 specifically stabilises mSREBPs in transfected U2OS and HEK293T cells.

A. *Optimising conditions of transfection assay using HA-tagged c-Myc. Different amounts of USP28 DNA (+ = 2 µg plasmid DNA and ++ = 4 ug plasmid DNA) and Fbw7 (+ = 3 µg plasmid DNA) were co-transfected with HA-tagged c-Myc (0.5 µg DNA) and protein levels were detected via immunoblot.* ***B.*** *Transfection assay of c-Myc and mSREBPs co-transfecting USP28 wild type (WT) and catalytically inactive USP28 mutant (CA) (4 µg plasmid DNA, respectively). Protein levels were monitored via immunoblot. Actin served as loading control. CA = USP28 C171A. Experiments were performed in U2OS (A and B, left and middle panel) and HEK293T cells (B, right panel). One representative experiment of two is shown.*

U2OS cells were transfected with HA-tagged c-Myc together with either USP28 WT or CA mutant, or Flag-tagged Fbw7. Protein levels of c-Myc were analysed by immunoblot. In presence of wild type USP28 the band for c-Myc was increased which was not the case for the co-transfection with catalytically inactive USP28 (CA). In presence of Fbw7 stability of c-Myc was decreased (Figure 4-5 **A**).
Using the determined conditions, transfection assays were performed with myc-tagged mSREBP1 and HA-tagged mSREBP2 and compared to the results of c-Myc. mSREBP1 and mSREBP2 showed the same increase in protein levels as c-Myc in the presence of wild-type USP28 (WT). This stabilising effect was not observable after co-transfecting catalytically inactive USP28 (CA) (Figure 4-5 **B**).

The regulation of target proteins by Fbw7 and USP28 is rather complex, since it was shown that USP28 not only regulates the stability of target proteins by removing ubiquitin chains but also controls the stability of Fbw7 by deubiquitination in a tissue-specific manner (Schulein-Volk *et al.* 2014). Additionally, Fbw7 is also known to regulate its own stability (auto-ubiquitination) (summarized in Taranets *et al.* (2015)). Further, it was published that USP28 binds c-Myc via Fbw7 (Popov *et al.* 2007).

To investigate if the stabilising effect of USP28 on mSREBPs is dependent on the complex regulatory mechanisms involving Fbw7, mSREBP CPD mutants were used (Figure 4-6).

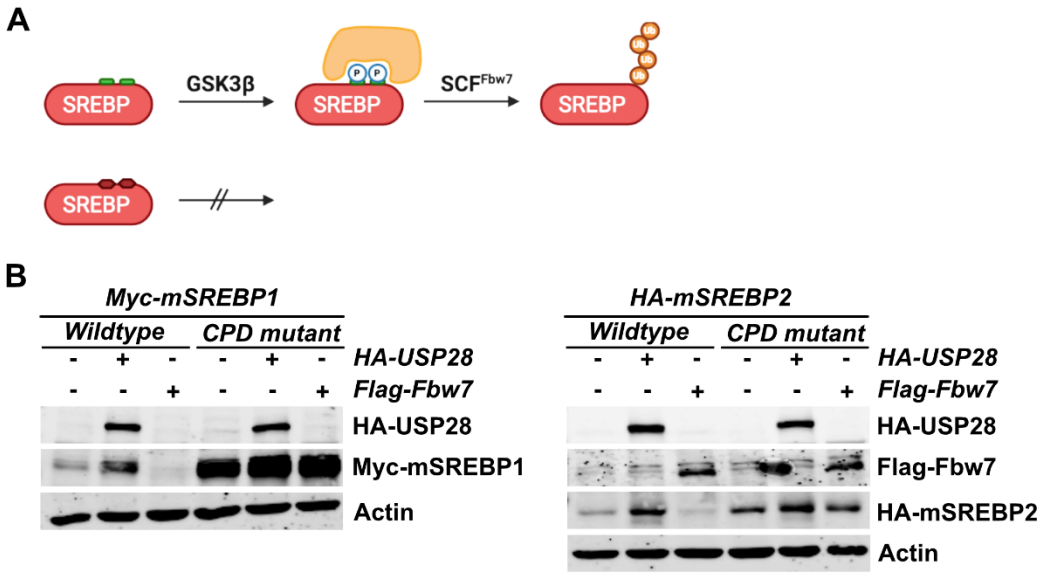

Figure 4-6: mSREBP stabilisation by USP28 is independent of the CPD.

A. *Schematic illustration of SREBP phosphorylation of the CPD (green) by GSK3β and subsequent FBW7 binding, which leads to SREBP ubiquitination. Deletion of the CPD abolishes phosphorylation and prevents ubiquitination by SCF-Fbw7.* ***B.*** *Transfection assay of wild type and CPD mutant mSREBPs in the presence of overexpressed USP28 or Fbw7. mSREBP and USP28 or Fbw7 protein levels were monitored by immunoblot. Actin served as loading control. Transfected plasmid DNA: mSREBPs (Wild type or CPD mutant) = 0.5 µg; USP28 = 4 µg; Fbw7 = 3 µg. CPD = Cdc4-phosphodegron.*

Fbw7 recognizes phosphorylations in the CPD motif introduced by GSK3β, which mediates the binding of the substrate and facilitates its ubiquitination. Mutation of the phosphorylation sites abolish Fbw7-binding (Figure 4-6 **A**).
U2OS cells were co-transfected with either wild type (WT) or CPD mutated (mut) mSREBP1 or mSREBP2 (Figure 4-6 **B**, left and right panels, respectively) together with USP28 or Fbw7. On the immunoblot, it was again observable that for both wild-type mSREBPs protein levels were increased in the presence of USP28 and decreased after co-transfection of Fbw7. For expression of the CPDmut SREBPs higher protein levels could be detected compared to WT (compare lanes 1 and 4). The stabilising effect of mSREBPs by USP28 was also observed for the CPD mutants (compare lanes 4 and 5), albeit to a lower extent, while Fbw7 overexpression had no effect on CPDmut mSREBP levels (compare lanes 4 and 6). This effect was more prominent for mSREBP2 compared to mSREBP1.
In conclusion, the stabilising effect of USP28 on mSREBP1 and mSREBP2 is mostly independent of the presence of the CPD with only a minor contribution by Fbw7 binding and regulation.

To assess if USP28 overexpression also effects endogenous mSREBP2 levels, cell lines with an inducible system to modulate USP28 expression were generated. The plasmid construct pINDUCER20-hUSP28 was kindly provided by Christina Schülein-Völk, AG Eilers. U2OS cells with stably integrated doxycycline-inducible expression cassette of human USP28 were generated by virus-mediated gene transfer.

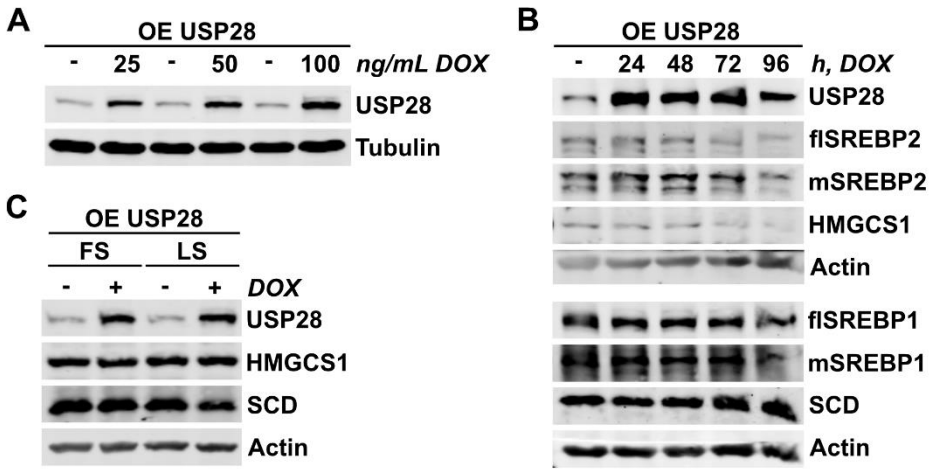

Figure 4-7: Inducible overexpression of exogenous USP28 does not affect SREBPs and their target gene protein levels in U2OS cells.

A. *Titration of Doxycycline concentration. U2OS cells with an inducible USP28 overexpression system were treated with indicated concentration of Doxycycline (DOX) for 24 h. Cells were harvested and USP28 protein levels were monitored via immunoblot.* ***B.*** *Inducible USP28 overexpressing U2OS cells were treated with 100 ng/mL DOX for the indicated times. SREBPs and target gene protein levels were monitored by immunoblotting. Actin was used as loading control.* ***C.*** *U2OS cells with inducible USP28 expression system were cultivated under FS and LS conditions for 72 h. 24 h prior to harvest USP28 expression was induced by adding DOX at a final concentration of 100 ng/mL. Protein levels of USP28 and SREBP target genes were analysed by immunoblot. Actin was detected as loading control. DOX = Doxycycline. OE = Overexpression. FS = Full Serum (10% FCS). LS = Low Serum (1% FCS).*

Based on the reported doxycycline (DOX) concentration (Meerbrey *et al.* 2011) the optimal DOX concentration for the generated cell line was determined (Figure 4-7 **A**). The titration for 24 h showed elevated levels of USP28 already at low concentrations. For further optimisation of the conditions, the concentration of 100 ng/mL was chosen and cells were treated with DOX for 24 up to 96 h (Figure 4-7 **B**). USP28 as well as SREBP1/2 and their target genes HMGCS1 and SCD, respectively, were monitored by immunoblot. mSREBP1 and mSREBP2 levels were only slightly increased upon overexpression of USP28. No effect on the protein levels of SREBP target genes was observable.

SREBPs are regulating *de novo* biosynthetic pathways, being activated under sterol-deprived conditions. It was previously shown that under low serum conditions (1% FCS) SREBP target gene expression is induced (Lewis *et al.* 2015). To analyse if the overexpression of USP28 shows effects of SREBP targets under serum-deprived conditions, cells were cultivated under FS (full serum, 10% FCS) and LS (low serum, 1% FCS) conditions and USP28 expression was induced by doxycycline treatment (Figure 4-7 **C**). This experiment showed that serum withdrawal does not have any effects on protein levels of SREBP targets in U2OS cells (compare lanes 2 and 4). Further, USP28 overexpression did not affect protein levels of HMGCS1 or SCD, neither under FS nor under LS conditions.

Taken together, the inducible overexpression of USP28 only showed mild effects on mSREBP levels and did not affect protein levels of main target genes. It is possible that U2OS cells already express saturating amounts of USP28, thereby limiting the effect of overexpression

4.2.2 USP28 stabilises SREBP through deubiquitination

The regulation of SREBPs takes place at multiple levels: transcriptional, precursor processing and by modulating the stability and activity of the active transcription factors through post-translational mechanisms. The proteolytic processing of the precursor is mainly controlled through a sterol-sensing mechanism that controls the translocation of full-length SREBPs from the ER to the Golgi (Nohturfft *et al.* 1999). It should be noted that SREBPs also regulate their transcription: SRE motifs were found in the promoter sequences of the *SREBF1* and *SREBF2* genes, and it was shown that SREBPs are able to regulate their transcription by a feed-forward loop (Sato *et al.* 1996).
Using transfection assays with exogenous overexpression constructs uncouples the stabilising effects on mSREBPs by USP28 shown in Figure 4-5 and Figure 4-6 from this feed-forward loop since the expression constructs were driven by the CMV promoter. This excludes transcriptional regulation, for example through stabilisation of other transcription factors, as potential mechanism.
Additionally, the hypothesis that the regulation of SREBPs by USP28 occurs post-translationally was supported by stability experiments using the translation inhibitor cycloheximide (CHX) (Figure 4-8).

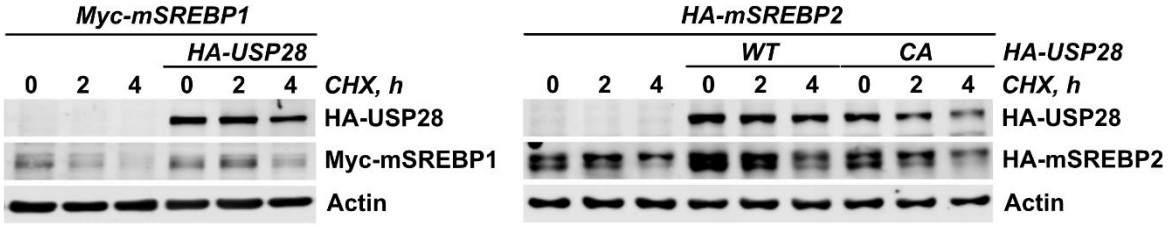

Figure 4-8: USP28 stabilises mSREBPs at a post-translational level.

U2OS cell were transfected with mSREBP and USP28 overexpression plasmids. 48 h after transfection cell were treated with the protein translation inhibitor CHX at a final concentration of 50 µg/mL for the indicated time. SREBP and USP28 protein levels were analysed by immunoblot and actin was detected as loading control. Transfected Plasmid DNA: mSREBPs = 0.5 µg; USP28 = 4 µg. CA = USP28 C171A. CHX = Cycloheximide.

The effect of addition of CHX to U2OS cells transfected with mSREBPs and USP28 on the levels of mSREBP was monitored by immunoblot. The steady-state levels of mSREBP1 clearly showed increased stability in the presence of co-transfected USP28. The same effect was observed for mSREBP2 in presence of USP28 WT compared to control or the catalytically inactive USP28 CA mutant.
Additionally, the stability of USP28 CA was reduced compared to USP28 WT. This observation supports a possible auto-deubiquitination mechanism of USP28, which was described for the close homologue USP25 (Denuc *et al.* 2009). This observation could already be detected in Figure 4-5.

To confirm that the stabilisation of mSREBPs by USP28 results from a direct deubiquitination mechanism, ubiquitinated mSREBPs were monitored by immunoblot (Figure 4-9).

Ubiquitinated proteins are detected as an ubiquitin smear, resulting from a higher molecular mass than the target protein. This is a consequence of the attachment of different numbers of ubiquitin moieties.

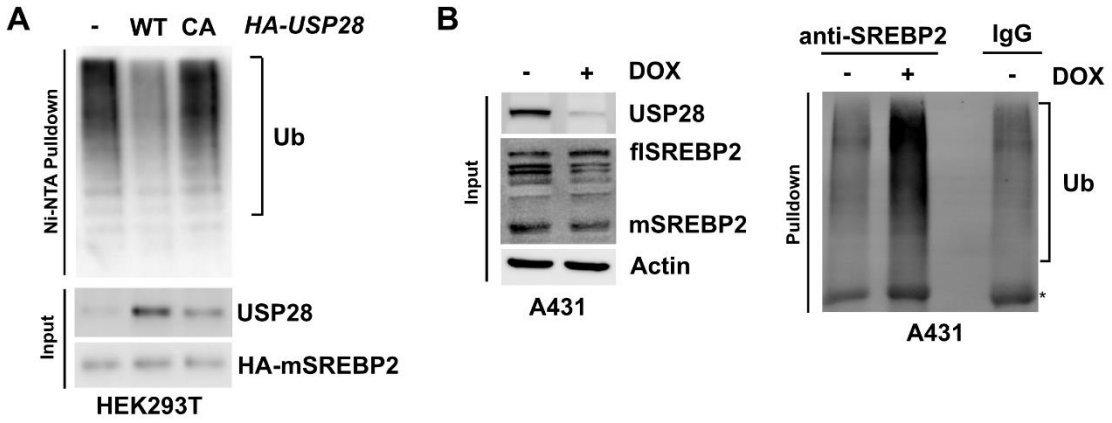

Figure 4-9: mSREBP2 shows reduced ubiquitination pattern in the presence of USP28.

A. *HEK293T cells were transfected with HA-tagged mSREBP2 together with His-Ubiquitin and either USP28 WT or C171A overexpression plasmids. Cells were lysed and a Ni-NTA pulldown was performed. Ubiquitinated proteins were analysed by immunoblot (Ub). Overexpressed USP28 and mSREBP2 was confirmed by immunoblotting in the input. Ni-NTA pulldown assay was performed by Nikita Popov, University Tübingen (Maier et al. 2023)* ***B.*** *A431 cells expressing doxycycline-inducible shUSP28 (#2, 4.4.3.1) were treated with 1 µg/mL DOX or solvent (EtOH) for 96 h. Proteasome inhibitor MG-132 in a final concentration of 20 µM was added for the last 6 h. Cell lysates were subjected to immunoprecipitation using SREBP2 antibody or IgG control. Precipitates were analysed by immunoblotting with ubiquitin K48-specific antibody. Efficient silencing of USP28 and respective flSREBP2 and mSREBP2 levels were confirmed by immunoblotting in the input. Actin was detected as loading control. Pulldown experiment was performed by Kamal Al-Shami, AG Schulze (Maier et al. 2023). CA = USP28 C171A.*

HEK293T cells were transfected with mSREBP2 constructs (Figure 4-9 **A**) together with an expression construct for His-tagged ubiquitin and constructs expressing USP28 WT or the CA mutant. Ubiquitinated proteins were pulled down using Ni-NTA beads and detected with K48-specific anti-ubiquitin antibodies. This data was kindly provided by Nikita Popov, University Tübingen (Maier *et al.* 2023). In the presence of USP28 WT, a reduction in the ubiquitin smear was observable. This reduction in ubiquitinated species was not detectable when overexpressing the catalytically inactive mutant (CA). In conclusion, the overexpression of USP28 reduced the amount of K48-linked ubiquitinated species.

In another attempt, A431 cells expressing a dox-inducible shRNA targeting USP28 mRNA (shUSP28 #2, compare 4.4.3.1) were analysed for ubiquitination pattern of endogenous SREBP2 (Figure 4-9 **B**): Knockdown of USP28 was induced by adding doxycycline or ethanol (control) and cells were treated with proteasome inhibitor for the last 6 h. Lysates were used to perform SREBP2 pulldown and ubiquitinated proteins were detected by ubiquitin-immunoblotting. This experiment was performed by Kamal Al-Shami (AG Schulze) and data was kindly provided (Maier *et al.* 2023). In the absence of USP28 an increase in ubiquitinated species in the SREBP2-pulldown was detected, suggesting that in the absence of USP28 ubiquitinated SREBP2 is accumulating when proteasomal degradation is inhibited.

The CHX and ubiquitination assays revealed that USP28 is stabilising SREBP2 protein levels through post-translational deubiquitination.

4.3 Reduction or deletion of USP28 lead to reduced SREBP2 levels

USP28 is involved in multiple cancer-related pathways whereby regulating the homeostasis of oncogenic transcription factors and counteracting their degradation by Fbw7. Among the target proteins are transcription factors involved in proliferation as well as cell cycle control and DNA repair mechanisms. USP28 therefore plays an important role in increased carcinogenesis and proliferation as well as overcoming apoptosis (Wang *et al.* 2018).
Lately, recent studies showed reduced tumour growth upon loss of USP28 (Prieto-Garcia *et al.* 2020). Of great interest is the question if and how the regulatory axis of USP28-SREBPs is contributing therein.

4.3.1 Knockout of USP28 in U2OS cells reduces SREBP2 stability and target gene expression but does not affect cell viability

The CRSIPR/Cas9 technology enable sequence-specific double strand breaks resulting in a knockout of the protein of interest. U2OS USP28 knockout cell lines were generated by Bastian Krenz (AG Eilers) and kindly provided for further analysis (Figure 4-10).

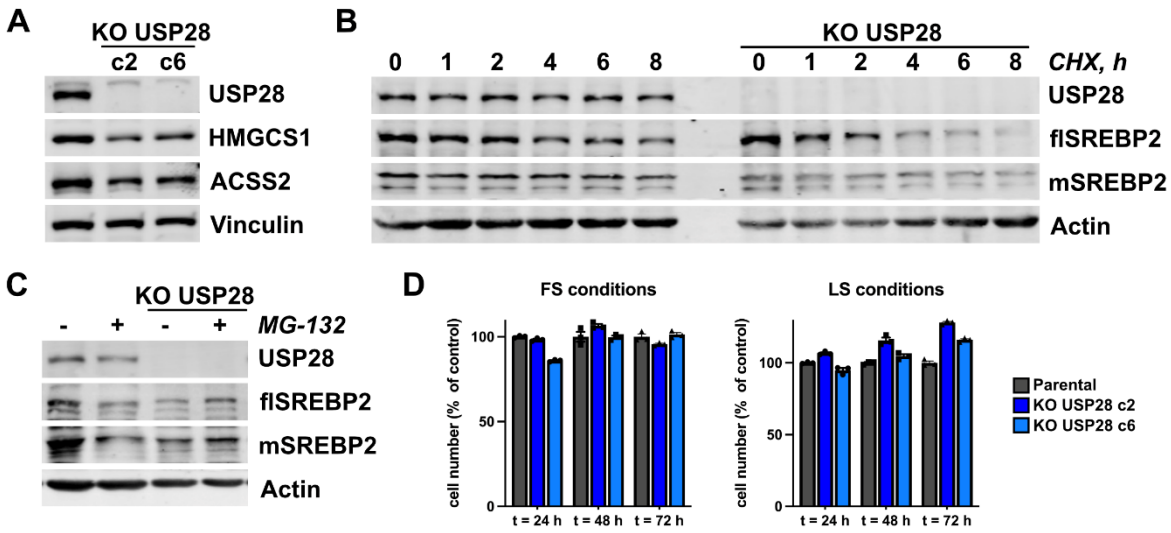

Figure 4-10: KO of USP28 in U2OS cells results in reduced mSREBP2 protein stability and target gene expression but does not affect cell viability under stress conditions.

A. *Western Blot analysis of USP28 KO cell lines compared to parental U2OS cell lines. USP28 and SREBP target genes were monitored by immunoblot. Vinculin was used as loading control. B. CHX time course experiment of endogenous SREBP2 protein level. U2OS parental and KO USP28 c2 cells were treated with 50 µg/mL of the translation inhibitor CHX for indicated time. Cells were harvested after maximum of 8 h of treatment and USP28 and SREBP2 protein levels were visualized by immunoblot. Actin as a house keeping protein was used for loading control. C. Rescue attempt with the proteasome inhibitor MG-132. U2OS parental and USP28 KO c2 cells were treated with a final concentration of 50 µg/mL CHX for 6 h and 25 µM MG-132 for 4h where indicated. USP28 and SREBP2 protein levels were monitored by immunoblot and Actin was used as loading control. D. U2OS parental*

and USP28 KO c2 and c6 cell lines were cultivated under FS and LS conditions for indicated time. Bar graph shows intensity of crystal violet staining of fixed cells normalised to parental control. Data are presented as mean ± SEM. KO = Knockout. CHX = Cycloheximide. FS = Full Serum (10% FCS). LS = Low Serum (1% FCS).

USP28 knockout (KO) cell lines (USP28 KO c2 and c6) showed reduced protein levels of the SREBP target genes HMGCS1 and ACSS2 on immunoblot (Figure 4-10 **A**). Further, it was observed, that the stability of flSREBP2 as well as mSREBP2 was reduced in USP28 KO cells compared to the control cell line in a CHX treatment experiment (Figure 4-10 **B**). Here, it cannot be distinguished whether the reduced abundance of flSREBP2 results from increased degradation or increased processing to maintain mSREBP2 levels. Comparing steady-state levels of mSREBP2 at time point zero, it was observed that mSREBP2 levels were reduced in the USP28 KO cell line (Figure 4-10 **B**, lane 1 and 8).
To confirm that the regulation of SREBP2 by USP28 is mediated by the 26S proteasome, control and USP28 knockout cells were treated with the proteasomal inhibitor MG-132 (Figure 4-10 **C**). The reduced steady-state SREBP2 levels in USP28 KO cell line compared to control cell line could to some extend be rescued by the inhibition of the proteasome showed by the increase in band intensity of SREBP2 in lane 4 compared to lane 3. However, the limited quality of the immunoblot makes the correct interpretation of this result complicated.
Additionally, the proliferation of the USP28 KO cell lines compared to control cell lines was investigated (Figure 4-10 **D**). Cells were seeded in the same cell number and grown for one to three days under normal and serum-deprived conditions. Cells were stained by crystal violet and staining was quantified. Neither under full serum nor under low serum conditions the USP28 KO cells showed reduced proliferation compared to WT.
Taken together, SREBP2 and target gene protein levels were reduced in USP28 KO cells. This results from decreased stability mediated by proteasomal degradation. The KO of USP28 does not affect cell proliferation under normal but also not under lipid-deprived conditions.

4.3.2 Inducible Knockdown of USP28 results in reduced mSREBP2 level and target gene expression

A stable knockout of a specific protein could force cells to compensate and accommodate to the new situation. To monitor the effects of acute loss of USP28 in cancer cells, U2OS cells with inducible expression of shRNAs (Fellmann *et al.* 2013) targeting USP28 were generated. Cells expressing a non-targeting sequence (shRenilla) were included as control.
shUSP28 sequences (#1-#4) were designed using the splashRNA software (http://splashrna.mskcc.org/). Afterwards restriction sites were introduced by PCR amplification and ligated with linearized backbone. Sequences were verified by Sanger sequencing.
Plasmids containing shRNAs were stably integrated in U2OS cells by virus-mediated gene transfer and positive cells were selected for puromycin resistance. USP28

knockdown cell lines were analysed regarding the effect of decreased USP28 on SREBP levels and their target genes by immunoblot (Figure 4-11).

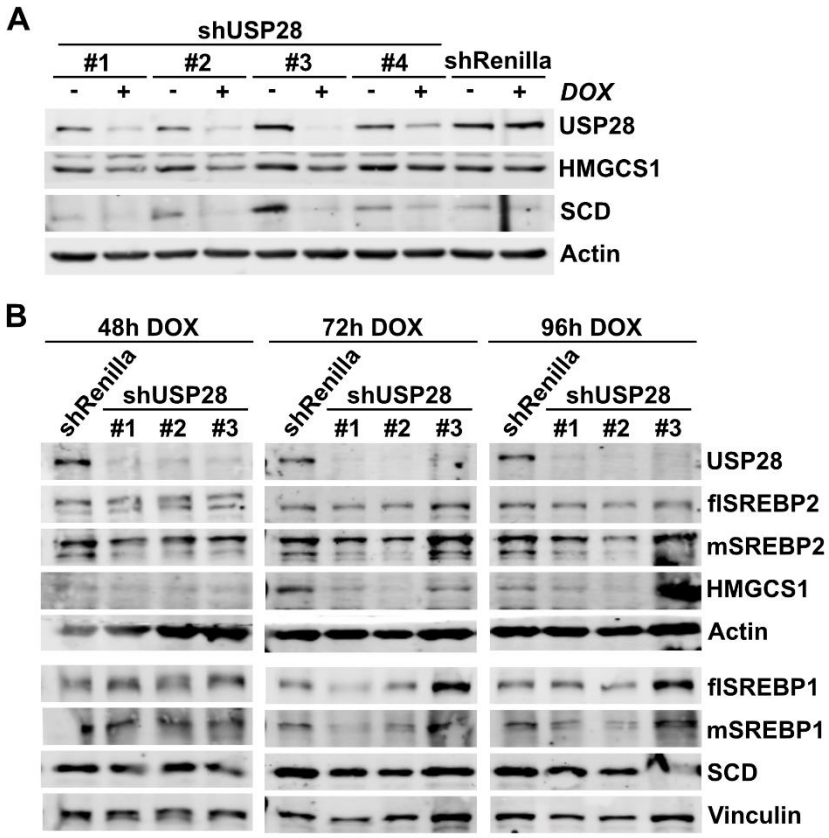

Figure 4-11: Inducible Knockdown of USP28 in U2OS cells reduces SREBP levels and expression of downstream targets.

A. *U2OS shUSP28 #1-#4 cell lines and shRenilla control cell line were generated and treated with 1 µg/mL DOX for 72 h. Knockdown efficiency was analysed by immunoblotting. HMGCS1 and SCD were monitored as representative SREBP2 and SREBP1 target genes, respectively. Actin was detected as loading control.* ***B.*** *Time course experiment to determine optimal USP28 knockdown conditions. U2OS shRenilla and USP28 Knockdown #1-#3 cell lines were treated with 1 µg/mL DOX for indicated time. SREBP and target gene protein levels were detected by immunoblot. Actin and Vinculin served as loading controls. DOX = Doxycycline.*

To verify the USP28 knockdown efficiency, USP28 knockdown cell lines were treated for three days either with DOX or with ethanol as solvent control. Protein levels of USP28 as well as the SREBP1 and SREBP2 target genes SCD and HMGCS1, respectively, were detected by immunoblot (Figure 4-11 **A**). All four knockdown cell lines showed strong reduction of USP28 upon DOX treatment. In addition, SCD and HMGCS1 levels were decreased. DOX treatment of the control cell line shRenilla did not affect protein levels of USP28 or SREBP target genes.

To investigate the effects of USP28 knockdown on SREBP1 and SREBP2 levels, knockdown cell lines were treated with DOX for 48, 72 or 96 hours and protein levels were analysed by immunoblot (Figure 4-11 **B**). The strong knockdown efficiency of sequences #1 and #2 was confirmed and reduced levels of SREBP1 and SREBP2 and respective target genes were observed.

Since the strongest knockdown was achieved by sequences #1 and #2, these cell lines were used for further experiments. The optimal conditions for induction of the USP28 knockdown was determined by DOX treatment for at least 72 h.

4.3.3 Knockdown of USP28 reduces stability of SREBP2

To confirm that the reduction in SREBP protein levels in the USP28 knockdown results from a post-translational mechanism and does not take place at transcriptional level, cycloheximide time-course experiments were performed (Figure 4-12).

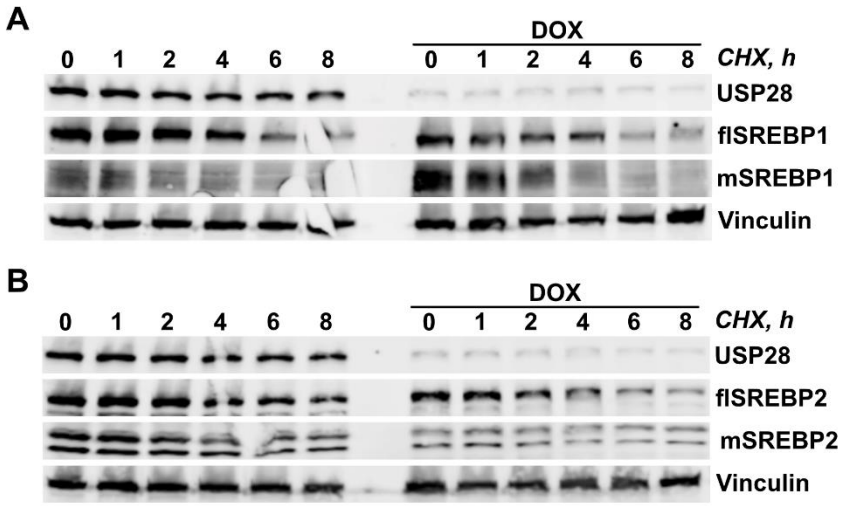

Figure 4-12: Induced Knockdown of USP28 reduces SREBP2 stability.

*CHX time course experiment to analyse the stability of endogenous SREBP1 (**A**.) and SREBP2 (**B**.) over time in presence and absence of endogenous USP28. U2OS shUSP28 cell lines were cultivated with 1 µg/mL DOX or solvent (EtOH), respectively, for 72 h. CHX was added in a final concentration of 50 µg/mL to DOX-treated and untreated cells for the indicated times. USP28 and SREBP protein levels were monitored by immunoblot. Vinculin was used as loading control. DOX = Doxycycline. CHX = Cycloheximide.*

The shUSP28 #2 cell line was treated with DOX for 72 h and for the last eight hours, cycloheximide was added. Endogenous protein levels of either SREBP1 or SREBP2 (Figure 4-12 **A** and **B**, respectively) were monitored by immunoblot. The absence of USP28 in the DOX treated cells was verified. While the stability of SREBP1 was only mildly affected by the absence of USP28, a clear reduction of flSREBP2 in absence of USP28 was observed. Levels of mature SREBP2 was only mildly affected.
Similar to the results shown in Figure 4-10 **B**, it cannot be discriminated if the stable mSREBP2 levels over time are conditioned by a low rate of turnover or the increased processing of the SREBP2 precursor.

4.3.4 USP28 Knockdown does not reduce cell viability in lipid-deprived conditions

SREBPs are master regulators of *de novo* fatty acid and cholesterol biosynthesis pathways and are upregulated upon lack of exogenous lipid supply to maintain intracellular metabolite levels.

To investigate whether under lipid-deprived conditions the knockdown of USP28 sensitize SREBP-driven pathways and affects cell viability, shUSP28 cell lines were cultivated under full serum (10% FCS) and low serum (1% FCS) conditions and USP28 knockdown was subsequently induced by doxycycline treatment (Figure 4-13).

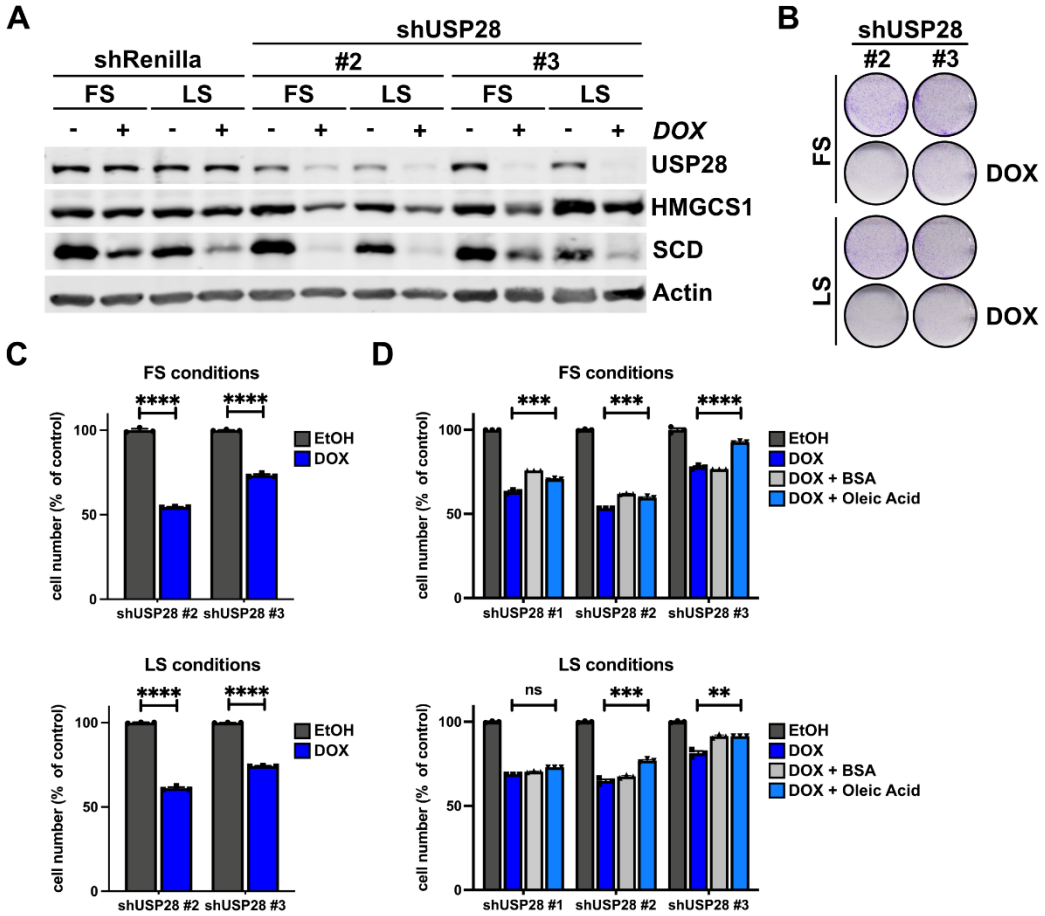

Figure 4-13: Inducible Knockdown of USP28 affects cell viability and proliferation.

A. *U2OS inducible shUSP28 cell lines and shRenilla control cell line were cultivated under FS and LS conditions for 24 h and USP28 Knockdown was induced priory to this by adding DOX in a final concentration of 0.5 µg/mL for 96 h. USP28 levels as well as those of the SREBP target genes HMGCS1 and SCD were monitored by immunoblot. Actin was detected as loading control.* ***B.*** *U2OS shUSP28 cell lines were cultivated for 24 h in FS or LS conditions and knockdown was induced by the addition of 0.5 µg/mL DOX for 96 h beforehand. Cell number was determined by cell fixation and subsequent crystal violet staining.* ***C.*** *Bar graph shows intensity of crystal violet staining of fixed cells in* ***B.*** *normalised to solvent control.* ***D.*** *shUSP28 cell lines were pre-treated with 0.5 µg/mL DOX for 72 h. FS and LS treatment was started and after 24 h BSA or BSA-coupled oleic acid was added. Cells were fixed and stained with crystal violet after an additional 24 h. Data are presented as mean ± SEM. ns = not significant; **, P < 0.01; ***, P < 0.001; ****, P < 0.0001, unpaired two-tailed Student t test. DOX = Doxycycline. FS = Full Serum (10% FCS). LS = Low Serum (1% FCS). BSA = Bovine Serum Albumin.*

USP28 knockdown cell lines were induced, cultivated under FS and LS conditions and protein levels of a representative SREBP2 target gene, HMGCS1, as well as a representative SREBP1 target gene, SCD, were monitored by immunoblot (Figure 4-13 **A**). While in the shRenilla control cell line the HMGCS1 protein levels were not affected, a strong reduction in band intensity was observed upon induction with doxycycline in both shUSP28 cell lines. For the SREBP1 target gene SCD already a

reduction in band intensity in the control cell line under DOX treatment was observed, indicating an effect caused by doxycycline rather than USP28 knockdown in these cells. In general, the U2OS cell line did not show an induction of SREBP target gene expression by LS treatment in the chosen conditions and no additional reduction of SREBP2 target gene levels were obtained by cultivating the cells under LS conditions.

Loss of USP28 resulted a reduction of cell viability and growth in previous studies. Such an effect was not observed in the USP28 KO cell lines used here (compare Figure 4-10 **D**). To investigate if the proliferation of U2OS cells was reduced upon acute downregulation of USP28, the shUSP28 cell lines were induced with doxycycline and cultivated under FS and LS conditions. Cell number was detected by crystal violet staining and subsequent quantification of staining intensity (Figure 4-13 **B** and **C**). The knockdown of USP28 resulted in decreased cell viability under FS conditions. No additional effect on cell viability was observed under LS conditions.
The SREBP1 target gene SCD catalyses the rate-limiting step in the formation of monounsaturated fatty acids (MUFAs), mainly oleate. It was previously shown that reduced levels of SREBPs induce ER stress and increase apoptosis (Griffiths *et al.* 2013). This effect could be blocked by addition of exogenous lipids, specifically oleic acid. For cellular uptake, oleic acid is coupled to BSA.
The rescue experiment in Figure 4-13 **D** confirms a reduction in cell number upon knockdown of USP28 under FS and LS conditions. The supply of oleic acid showed only mild effects in restoring cell viability (DOX + oleic acid). Further, the control group (DOX + BSA) already showed slight beneficial effects on cell viability, independent of oleic acid.

In conclusion, the genetic loss or reduction of USP28 levels using gene silencing in cancer cells strongly decreased SREBP2 and target gene protein levels but only showed mild effects on SREBP1 and its downstream targets. The regulation of SREBP2 by USP28 happens at post-transcriptional level, most likely by deubiquitination. Downregulation of USP28 by RNAi resulted in reduced cell viability under normal and lipid-deprived conditions and could not be rescued by restoring fatty acid availability. Limitation of exogenous lipid supply had no additional effect on the cell viability upon knockdown of USP28.

4.4 Manipulation of endogenous USP28 level results in deregulated mevalonate pathway

The previous experiments showed a regulation of SREBP2 by USP28. SREBP2 is the master regulator of *de novo* cholesterol biosynthesis via the mevalonate pathway. Nearly all of the enzymes involved in this pathway are under the transcriptional control of mSREBP2. Additionally, the intermediate metabolite farnesyl pyrophosphate (FPP) in the mevalonate pathway feeds into various other synthesis processes. Beside the production of the isoprenoid tail of co-enzyme Q10, which plays an important role in the respiratory chain and is involved in pyrimidine synthesis, FPP is used for farnesylation of proteins.
To explore how USP28 influences these cellular processes, pathway analysis and metabolite trafficking analysis was performed.

4.4.1 Knockout of USP28 results in reduced cholesterol levels

In Figure 4-10 the knockout of USP28 in U2OS cells revealed reduced mSREBP2 and HMGCS1 level, its main target gene. Additional key enzymes involved in the mevalonate pathway and cholesterol synthesis whose expression is also controlled by SREBP2 are HMGCR and FDFT1. While HMGCS1 and HMGCR catalyse steps in the upper mevalonate pathway, converting acetoacetyl-CoA to mevalonic acid, the FDFT1 enzyme acts downstream of the branching point of FPP being involved in the synthesis of cholesterol (Figure 4-14 **A**).
To compare the metabolic changes caused by deletion of USP28 leading to reduced levels of SREBP2 with direct inhibition of the pathway, U2OS cells harbouring a stable knockout of *SREBF2*, the gene coding for SREBP2, were generated by CRISPR/Cas9 technology. Viral expression vectors encoding two guide RNAs targeting exon 2 of the *SREBF2* locus were co-infected with a vector coding Cas9 positively infected cells were selected by resistance to puromycin and FACS-sorted for GFP expression.

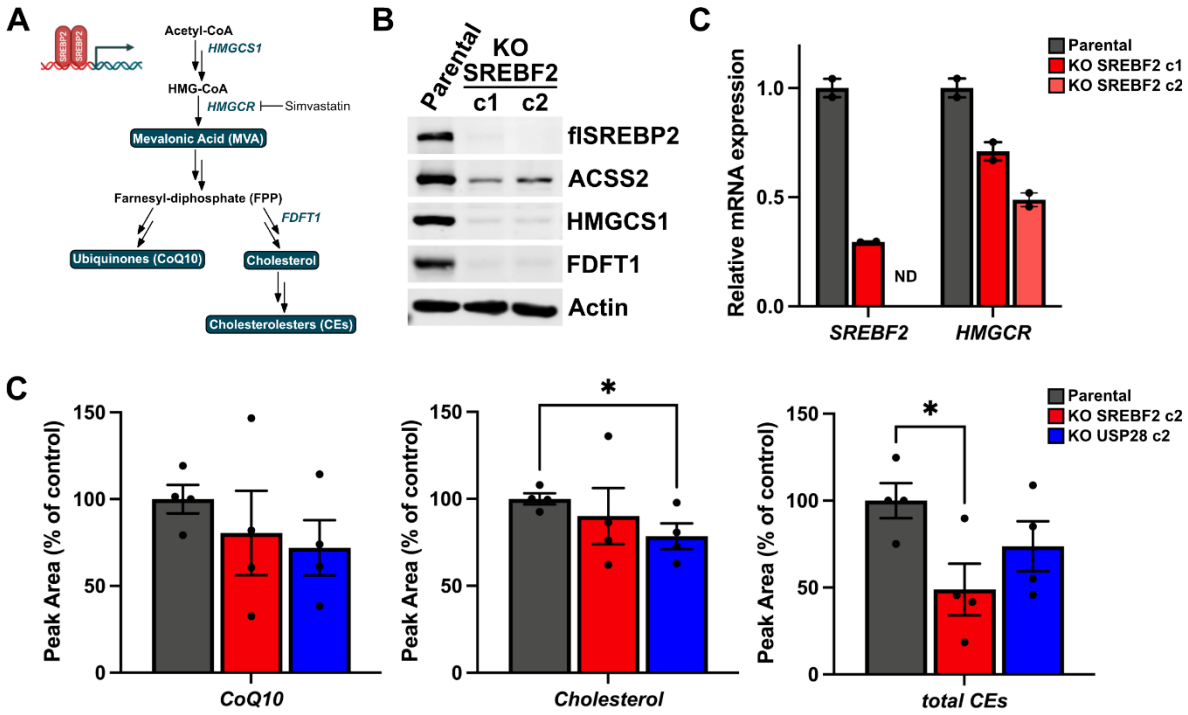

Figure 4-14: SREBF2 knockout in U2OS cells results in decreased SREBP2 target gene expression and knockout of either USP28 or SREBF2 reduces activity of the mevalonate pathway.

A. *Schematic illustration of the mevalonate pathway and the metabolites as either intermediates or products. Selected enzymes catalysing the reactions and being under the transcriptional control of mSREBP2 are shown.* ***B.*** *U2OS cells with knockout (KO) of SREBF2 were generated by CRISPR/Cas9 technology. Protein levels of SREBP2 itself and its target genes ACSS2, HMGCS1 and FDFT1 of single clone cell lines c1 and c2 as well as control cell line (parental) were analysed by immunoblot. Actin is shown as loading control.* ***C.*** *Bar graph showing normalised SREBF2 and HMGCR mRNA expression of SREBF2 KO cell lines c1 and c2 compared to parental control cell line.* ***D.*** *Bar graphs showing normalised levels of co-enzyme Q10 (CoQ10), cholesterol and cholesterol esters (CEs) in SREBF2 c2 and USP28 c2 knockout cell lines with four independent replicates measured by LC-MS (Werner Schmitz, Biocenter Würzburg). Data are presented as mean ± SEM. *, P < 0.05, unpaired two-tailed Student t test. KO = Knockout.*

SREBF2 KO cell lines were generated from selected single clones c1 and c2 and complete loss of *SREBF2* was verified by immunoblot and qPCR analysis. Reported SREBP2 target genes *HMGCR*, *HMGCS1* and *FDFT1* mRNA and protein levels were strongly reduced in the knockout situation. ACSS2 levels, an enzyme that was reported as being regulated by SREBP1 and SREBP2, were also decreased (Figure 4-14 **B** and **C**).

Metabolite levels of U2OS KO *SREBF2* c2 and KO *USP28* c2 were extracted and measured by LC-MS (Werner Schmitz, University of Würzburg). Peak area was normalised to cell number and parental control cell line. In both knockout cell lines, a trend towards decreased levels for co-enzyme Q10 was observable. Further, significantly reduced levels of cholesterol were detected upon KO of USP28. Loss of SREBP2 resulted in reduced cholesterol and significantly reduced levels of cholesterol esters. The results reflect rather mild effects on metabolite levels with high variance.

4.4.2 Reduced USP28 levels lead to downregulation of enzymes involved in Mevalonate Pathway in A431 cells

Recent studies identified the transcription factor ΔNP63 as an USP28 target protein and further focus on the role of USP28 in developing chemo resistance in squamous lung cancer (Prieto-Garcia *et al.* 2020, Prieto-Garcia *et al.* 2021).
In this context, a proteomics dataset comparing control and USP28 knockout cells was generated using the shUSP28 #1 sequence in A431 cells, a human squamous cell line originated from an epidermal carcinoma of the vulva (Prieto-Garcia *et al.* 2021). This dataset was analysed regarding proteins involved in the mevalonate pathway (Figure 4-15).

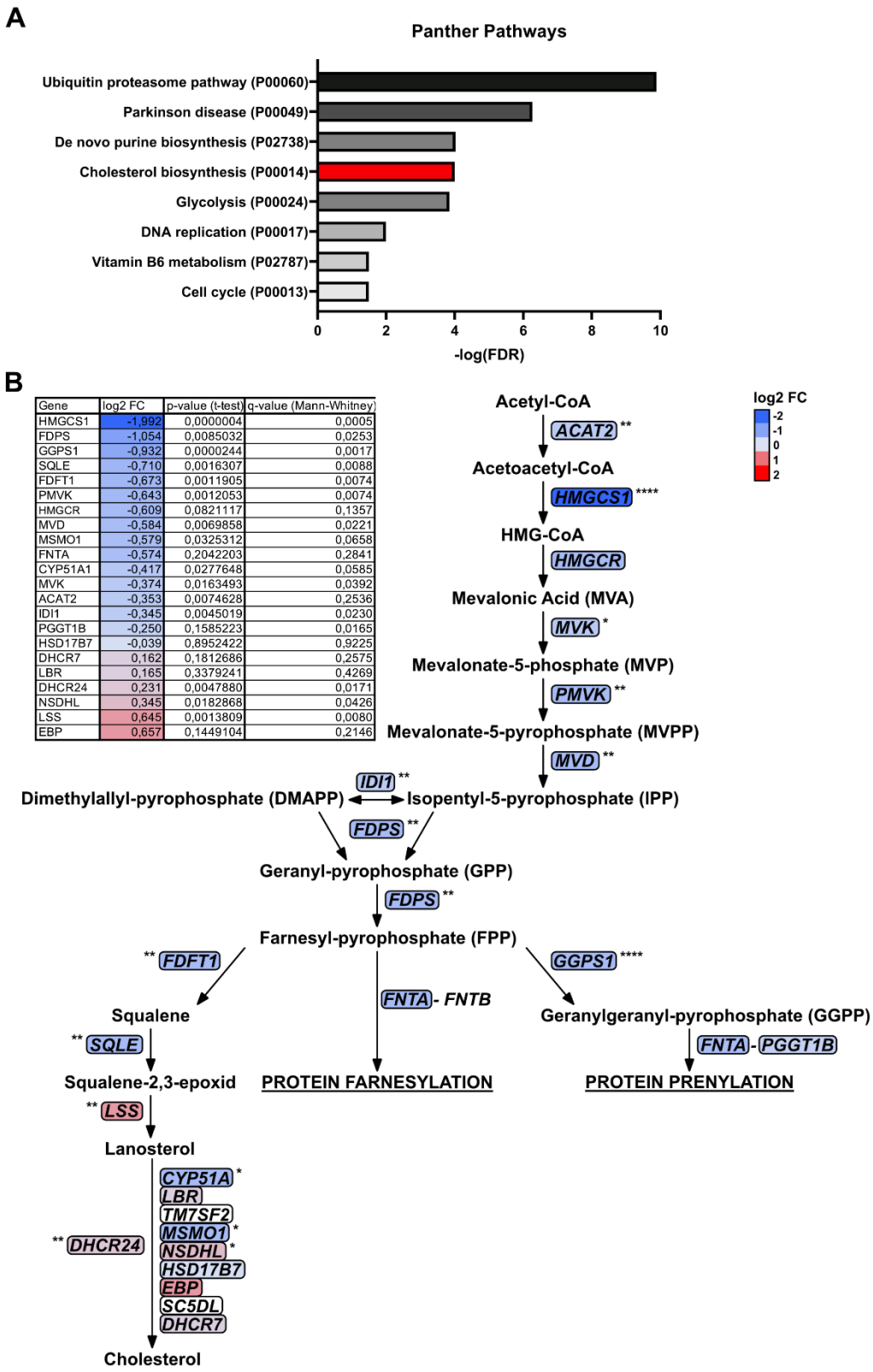

Figure 4-15: Knockdown of USP28 in A431 cells results in downregulation of the cholesterol biosynthesis pathway.

A. *Panther Pathway Analysis of MS dataset upon inducible USP28 knockdown with 1 µg/mL doxycycline treatment for 72 h. All proteins significantly (P < 0.05) downregulated and with a log2-fold change shUSP28/control <1 were used to perform pathway enrichment analysis of GO Panther Pathways using the Panther online tool. Bar graph represents logFDR of top ranked gene sets. Cholesterol biosynthesis pathway is highlighted in red.* ***B.*** *Schematic*

*illustration of the mevalonate pathway. All enzymes represented in proteomics dataset were framed and color-coded by log2FC. Data are represented as mean of triplicates. *, P < 0.05; **, P < 0.01; ****, P < 0.0001, unpaired two-tailed Student t test. FDR = False Discovery Rate. FC = Fold Change.*

The shUSP28 #1 sequence was used by Cristian Pietro-Garcia to generate A431 cell lines harbouring a DOX-inducible knockdown system for USP28. Proteome analysis by mass spectrometry was performed and analysed by the lab of Christian Münch at the University of Frankfurt.
Proteins significantly downregulated in shUSP28 cells and with a log2 fold change greater 1 were used to perform overrepresentation test (Fisher`s exact) with the Panther Online Tool using the PANTHER Pathways datasets. All pathways with a fold enrichment greater than 2.93 were ranked by false discovery rate (1-FDR, with FDR<0.05) (Figure 4-15 **A**). Proteins involved in the cholesterol biosynthesis pathway were significantly downregulated in shUSP28 cells and scored in the pathway analysis with a 12.32 fold enrichment.
The schematic depiction of enzymes of the cholesterol biosynthesis pathway in Figure 4-15 **B** revealed a downregulation of individual enzymes, particularly in the upper mevalonate pathway, mainly catalysing reactions before the branching point of FPP. The lower part of the pathway, which leads to the synthesis of cholesterol, is either unchanged or even slightly upregulated.

Taken together, it can be concluded that loss or downregulation of USP28 results in decreased protein levels of enzymes involved in the mevalonate pathway but only slightly reduces cholesterol and co-enzyme Q10 levels.

4.4.3 Characterisation of the impact of USP28 on the Mevalonate Pathway in squamous A431 cells

Previous studies unravelled the important role of USP28 in squamous cancers (Prieto-Garcia *et al.* 2020, Prieto-Garcia *et al.* 2021). In a squamous cell line, it could be shown that USP28 is regulating the SREBP2 target enzymes involved in the mevalonate pathway (Figure 4-15). To follow up the question how SREBP2 contributes to the squamous phenotype and to elucidate the importance of the USP28-SREBP2 regulatory axis in this system, inducible A431 USP28 knockdown cell lines were generated and further characterised regarding their metabolic features.

4.4.3.1 Generation of inducible SREBF2 and USP28 Knockdown in A431 cells

To characterise squamous A431 cells with inducible knockdown of USP28 and to link the specific phenotypes to a regulation via SREBP2, A431 cell lines were stably infected with virus-based vector expressing shRNAs targeting USP28 and SREBP2. Cells were generated as described before (4.3.2) and expression of USP28, SREBP2 and target genes was analysed (Figure 4-16).

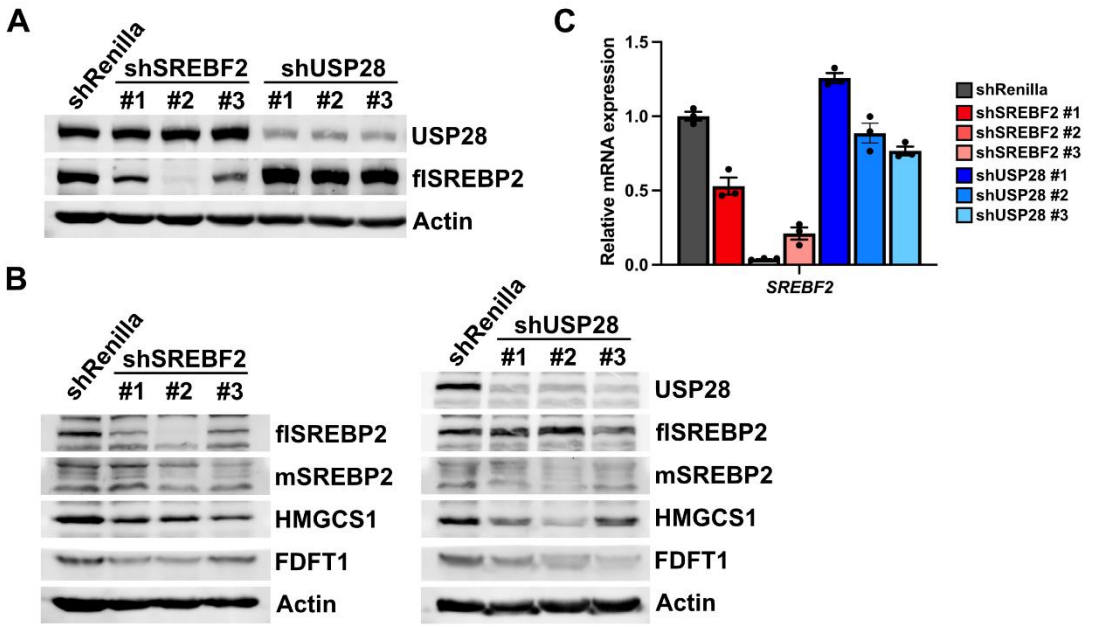

Figure 4-16: Establishing and validation of USP28 and SREBF2 knockdown systems in A431 cells.

A. *A431 inducible shUSP28 and shSREBF2 cell lines and shRenilla control cell lines were treated with 1 µg/mL doxycycline for 72 h and knockdown of USP28 and SREBP2 was monitored by immunoblot using specific anti-SREBP2 and anti-USP28 antibodies. Actin served as loading control.* ***B.*** *Inducible A431 knockdown cell lines shUSP28 #1, #2 and #3, shSREBF2 #1, #2 and #3 and control cell line shRenilla were treated with 1 µg/mL doxycycline for 96 h and USP28 as well as SREBP2 and its target genes HMGCS1 and FDFT1 were detected by western blot using specific antibodies. Actin served as loading control.* ***C.*** *Bar graph showing normalised SREBF2 mRNA expression of shSREBF2 and shUSP28 A431 cell lines compared to shRenilla control cell line upon dox-induced knockdown for 72 h. Experiment was performed in triplicates and data is presented as mean ± SEM.*

The efficiency of *SREBF2* and *USP28* knockdown was verified by immunoblot (Figure 4-16 **A**). For *SREBF2*, a strong reduction in band intensities was observed for all three sequences, while sequence #2 showed the best result. For USP28, the knockdown was equally strong for all sequences which was already observed in the U2OS cell line (Figure 4-11 **A**). Further, it was not observable that knockdown of USP28 has any effects on flSREBP2 levels.

A431 inducible knockdown cell lines were analysed regarding protein levels of SREBP2 and its target genes HMGCS1 and FDFT1. Knockdown of *SREBF2* in A431 cells was most efficient for sequence #2 (Figure 4-16 **B**, left panel). mSREBP2 levels are also reduced but milder than flSREBP2. An explanation for this observation could be that cells compensate by upregulating the processing step from flSREBP2 to mSREBP2. Additionally, SREBP2 target genes HMGCS1 and FDFT1 are reduced at protein level.

The strong knockdown of USP28 by all three sequences reduced mSREBP2 but not flSREBP2 levels, indicating a post-transcriptional regulatory mechanism. Reduction in USP28 levels also resulted in reduced HMGCS1 and FDFT1 protein levels. Sequence #2 obtained the best results (Figure 4-16 **B**, right panel).

In Figure 4-16 **C** relative mRNA levels of SREBF2 in the knockdown cell lines normalised to shRenilla control cell line are displayed upon knockdown of either *USP28* or *SREBF2*. It could be observed that the mRNA levels of SREBF2 are strongly

reduced upon *SREBF2* knockdown but only mildly affected by the knockdown of *USP28*. This supports the hypothesis that the effects of USP28 on SREBP2 level result from a post-transcriptional regulation.

4.4.3.2 Proteasomal degradation inhibitor stabilises mSREBP2 in A431 cells

Betulin is a naturally occurring compound that interacts with SCAP and thereby prevents the proteolytic cleavage of precursor SREBPs. Upon betulin treatment, the SCAP-SREBP complexes remain in the ER (Tang *et al.* 2011). In Figure 4-10 **B** and Figure 4-12 **B** it could not be discriminated if the decrease in flSREBP2 results from enhanced processing. To monitor the steady state levels of mSREBP2 and determine how they are influenced by reduced USP28 levels, control cell lines (shRenilla) as well as USP28 knockdown cell lines (shUSP28 #1 and #2) were treated with betulin either alone or in combination with the 26 S proteasome inhibitor MG-132 (Figure 4-17).

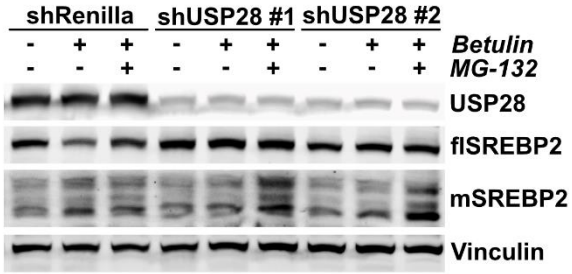

Figure 4-17: Inhibition of proteasomal degradation stabilises ubiquitinated mSREBP2 in absence of USP28.

A413 inducible shUSP28 cell lines as well as shRenilla control cell line were treated with 1 µg/mL DOX for 96 h. During the last 6 h, cells were treated with 10 µM Betulin and 20 µM MG-132 as indicated and protein levels of USP28 and SREBP2 were analysed by immunoblot. Vinculin was detected as loading control.

The addition of betulin to the shRenilla cell line resulted in decreased flSREBP2, which could be restored by additionally treating the cells with the proteasome inhibitor MG-132. This indicates that the precursor SREBP2 is targeted for proteasomal degradation in presence of betulin and levels are restored upon blocking the 26 S proteasome. Unexpectedly, betulin treatment of shRenilla cells resulted in increased mSREBP2 levels and additional MG-132 treatment did not affect mSREBP2 band intensity or band pattern. In the USP28 knockdown situation, betulin alone showed no effect on SREBP2 levels but combinatory treatment with MG-132 showed increased band intensities for mSREBP2 in both USP28 knockdown cell lines. Specifically, a higher molecular band appeared strongly under these conditions, which could refer to ubiquitinated mSREBP2.

4.4.3.3 Serum-deprived conditions do not affect the USP28-SREBP2 regulatory axis in A431 cells

To elucidate if there are additional effects on SREBP2 and downstream target levels by the knockdown of USP28 under serum-deprived conditions, A431 shRNA cell lines

were cultivated under full serum and low serum conditions and protein levels were analysed by immunoblot (Figure 4-18).

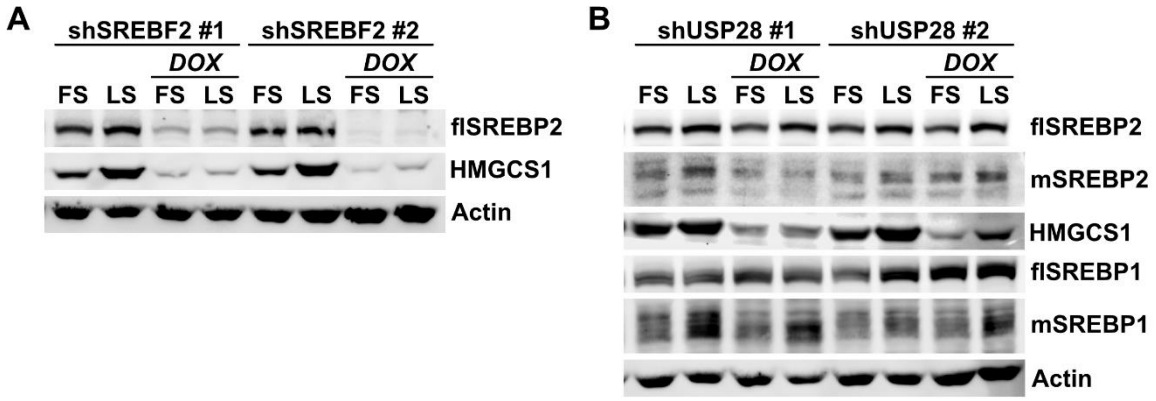

Figure 4-18: Knockdown of USP28 does not show additional effects on SREBP2 levels and downstream targets in serum-deprived conditions.

*A431 inducible knockdown cell lines for SREBF2 (**A**) and USP28 (**B**) were treated with 1 µg/mL doxycycline (DOX) for 96 h. During the last 24 h cells were cultivated in full serum (FS, 10% FCS) or low serum conditions (LS, 1% FCS) as indicated. SREBP and HMGCS1 protein levels were monitored by immunoblot. Actin served as loading control.*

A431 cells cultivated in low serum conditions (LS) showed increased levels of SREBPs and the target gene HMGCS1 compared to normal conditions (FS). This indicated upregulation of enzymes involved in *de novo* metabolite pathways under serum-deprived conditions through intrinsic cellular mechanisms (Figure 4-18 **A**, lane 1/2 and 5/6).

Upon knockdown of *SREBF2,* the protein levels of HMGCS1 decreased drastically. Furthermore, while control cells cultivated under low serum conditions activated intracellular mechanisms to compensate for the deprivation in lipids in their environment which led to an increase of SREBP2 and HMGCS1 protein levels (Figure 4-18 **A**, compare lane 2 and 6), *SREBF2* knockdown cells were not able to initiate this activation to restore the protein levels of HMGCS1 in deprived conditions (Figure 4-18 **A**, lane 4 and 8).

The reduction in USP28 mediated by shRNA also caused reduced levels of mSREBP2 and HMGCS1, while mSREBP1 levels were only mildly affected. The residual mSREBP2 levels after USP28 silencing using sequence #2 were still sufficient to initiate activation of HMGCS1 expression in serum-deprived conditions and restore them to a moderate level (Figure 4-18 **B**, lane 8). The strong reduction of mSREBP2 levels in cells expressing shUSP28 #1 resulted in low levels of HMGCS1 expression even under low serum conditions (Figure 4-18 **B**, lane 4).

In summary, no additional effects on SREBP2 and target gene expression caused by USP28 reduction were observed under serum-deprived conditions.

Since loss or inhibition of USP28 is associated with reduced cell growth and apoptosis (Prieto-Garcia *et al.* 2020), experiments analysing cell viability upon knockdown of USP28 were performed (Figure 4-19).

It was already observed that an induced downregulation of USP28 in U2OS cells affected cell growth and proliferation (compare Figure 4-13).

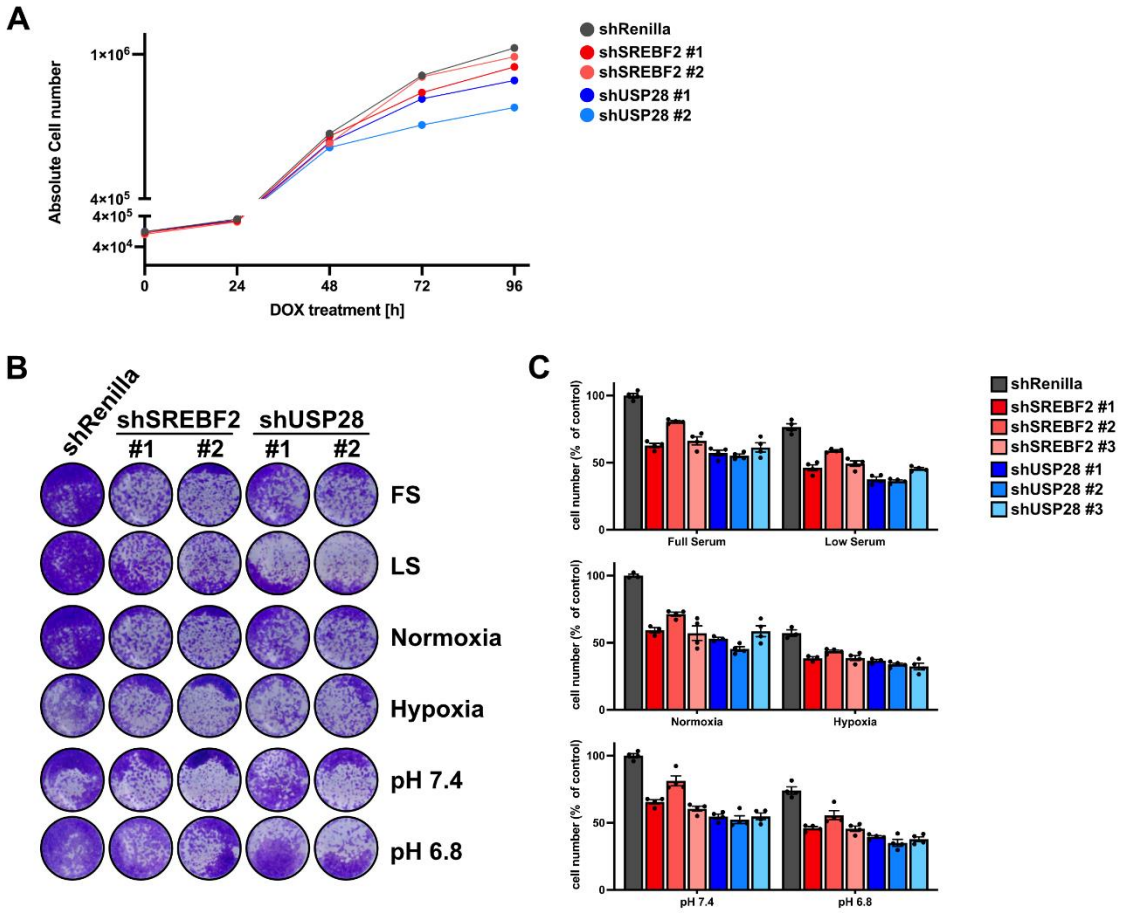

Figure 4-19: Knockdown of USP28 results in reduced cell viability of A431 cells but is not additionally triggered in conditions where SREBP2 was shown to play an essential role.

A. *A431 shUSP28 and shSREBF2 cell lines or controls (shRenilla) were treated for indicated times with 1 µg/mL DOX. Cell number was determined by counting the cells by automated cell counter in triplicates. Graphs show growth curves with absolute cell numbers. Cell numbers are depicted as mean ± SEM.* ***B.*** *A431 shUSP28 and shSREBF2 cell lines were treated together with control cell line (shRenilla) for 96 h with 1 µg/mL DOX. During the last 24 h, cells were cultivated under the indicated conditions. Cell viability was determined by cell fixation and subsequent crystal violet staining. One representative well of triplicates is shown.* ***C.*** *Bar graphs show the quantification of crystal violet staining in (B.). Data are presented as mean ± SEM. DOX = Doxycycline. FS = Full Serum (10% FCS). LS = Low Serum (1% FCS). Normoxia = 20 % O_2. Hypoxia = 0.5 % O_2.*

Proliferation of A431 cells with reduced *SREBF2* or *USP28* levels were monitored by determining cell number over a time period of 96 hours (Figure 4-19 **A**). shUSP28 cells showed a strong reduction of 20-30% in cell number compared to the shRenilla control cell line. Effects on cell number caused by the knockdown of *SREBF2* were less than +/- 10% compared to the control.

Under normal cell culture conditions, many cancer cells do not rely on *de novo* cholesterol synthesis, since cells are supplied by the uptake of essential molecules from the culture medium. Whereas culturing cells in lipid-deprived conditions activates pathways, which are involved in the *de novo* synthesis of these components.

Beside the cultivation in low serum conditions, it was also reported that a hypoxic milieu affects SREBPs and target gene expression (Lewis *et al.* 2015). A study by

Kondo and colleagues revealed that SREBP2 is activated by extracellular acidic pH arising from anaerobic glycolytic excretion of protons and lactate in tumour tissue (Kondo *et al.* 2017). This study analysed the role of transcriptional activation of SREBP2 under low pH, hypoxia and nutrient starvation, thereby mimicking the tumour microenvironment. In this study, it was also shown that knockdown of *SREBF2* is associated with decreased tumour volume in a tumour xenograft model using pancreatic tumour cells (Kondo *et al.* 2017).
To mimic the tumour microenvironment and increase the activity of SREBP2 and target gene expression, A431 cells were cultivated either under full serum or under low serum conditions as well as in normoxia or hypoxia. Additionally, the acidic extracellular pH was mimicked by addition of HCl to the culture medium adjusted to pH 6.8 (Figure 4-19 **B** and **C**). Cell viability was determined by crystal violet staining and quantification of staining intensity. A growth reduction of all knockdown cell lines (shUSP28 and shSREBF2) was already observed under normal culture conditions (FS, normoxia, pH 7.4). An additional reduction of cell number under conditions of serum starvation (LS), hypoxia or acidic milieu (pH 6.8) was not detected.

As serum is a major source of lipids in tissue culture, the usage of low serum conditions has been previously used to achieve lipid deprivation conditions (Griffiths *et al.* 2013, Lewis *et al.* 2015). In addition, several methods to selectively extract lipids to create lipid-reduced serum can be applied. Protocols are based on chemical lipid extraction (Hosios *et al.* 2018) or charcoal dextran stripping of FCS (Brovkovych *et al.* 2019) where not only lipids but also cholesterol levels were strongly reduced.
Lipid-depleted sera based on both above-mentioned methods (kindly provided by Dr. Felix Vogel, AG Schulze) were used to perform viability assays in A431 shRNA cell lines (Figure 4-20). The protocol by Hosios *et al*. is named here and afterwards “Method B” while the method by stripping with charcoal and dextran is entitled as “Method A”.

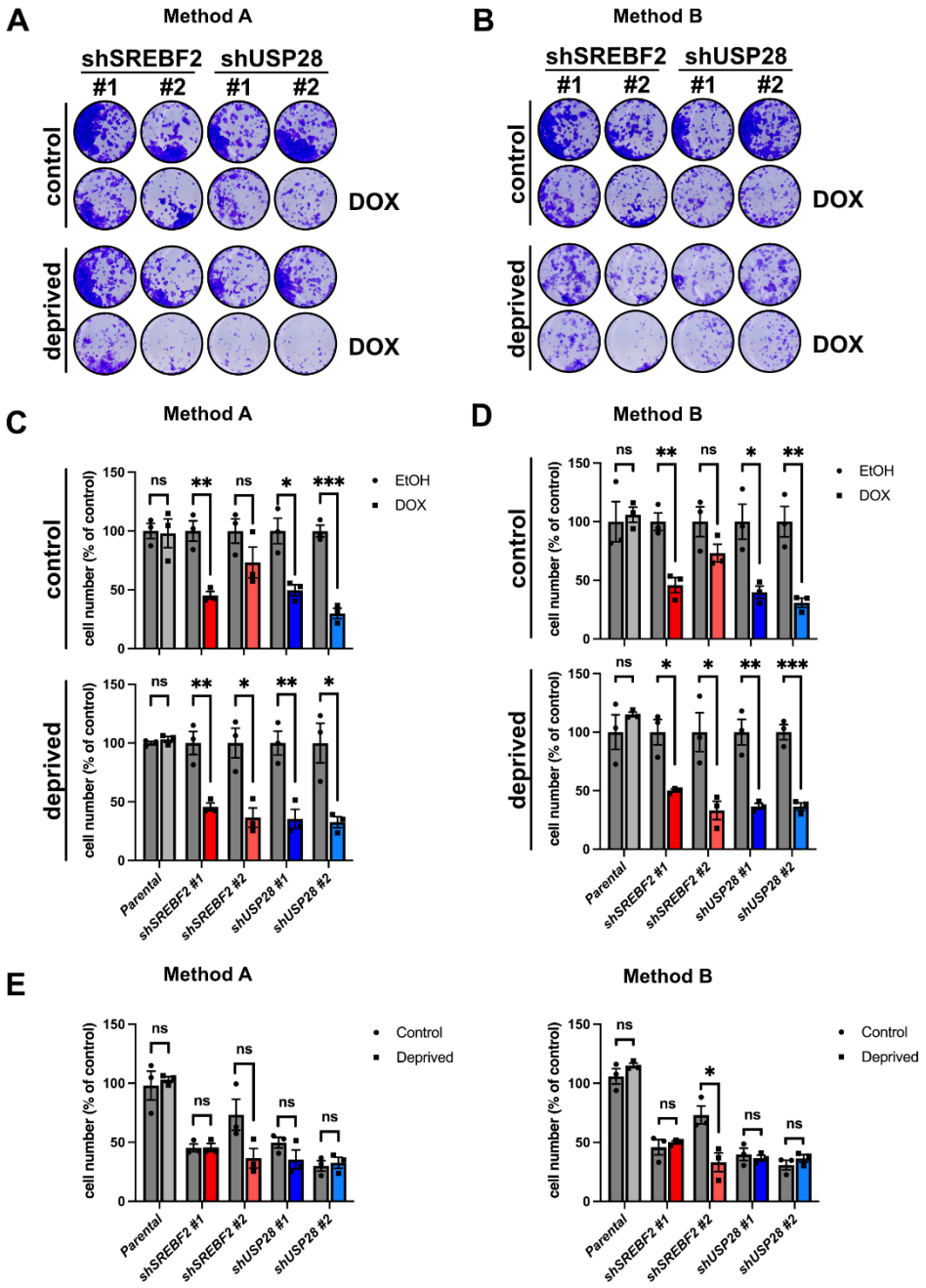

Figure 4-20: Lipid-deprived serum has no effect on cell viability in SREBP2 and USP28 Knockdown cells.

A431 shUSP28 (#1 and #2) and shSREBF2 (#1 and #2) or controls (Parental) cell lines were treated for 96 h with 1 µg/mL DOX or EtOH as solvent control. Cells were either cultivated in medium with Method A ***(A.)*** *or Method B* ***(B.)*** *serum (=deprived) or respective control sera. Cell viability was determined by cell fixation and subsequent crystal violet staining. One representative well of triplicates is shown.* ***C.*** *Bar graphs showing the quantification of crystal violet staining in* ***(A.).*** *Data are normalised to EtOH control and are presented as mean ± SEM.* ***D.*** *Bar graphs showing the quantification of crystal violet staining in (****B.****) of Dox-induced cells normalised to cell number in respective control serum.* ***E.*** *Cell viability measured by crystal violet staining of DOX-treated cell lines under deprived conditions normalised to respective control serum. Data are represented as the mean of triplicates ± SEM. ns = not significant; *, P < 0.05; unpaired two-tailed Student t test DOX = Doxycycline.*

A431 cells showed strong reduction in cell viability upon knockdown of *USP28* or *SREBF2* cultivated with Method A or Method B deprived serum and their respective control serum (Figure 4-20 **A** and **B**). The quantification of the crystal violet staining

revealed a significant reduction upon knockdown of USP28 and SREBP2 in comparison to the ethanol treated control cells, independently of cells cultivated in medium containing control or deprived serum. Only data from shSREBF2 #2 cells in control serum did not reach statistical significance (Figure 4-20 **C** and **D**). No additional negative effect on cell growth was observed in cells cultivated in medium with deprived serum compared to control serum. The quantification of crystal violet staining does not show significant differences in cell viability of DOX-treated cells cultivated in medium supplemented with control or deprived serum (Figure 4-20 **E**).

4.4.3.4 Knockdown of SREBP2 and USP28 reduces cell survival in A431 cells

It was observed that the knockdown of either *USP28* or *SREBF2* reduces cell viability. To analyse this further a colony formation assay, also termed clonogenic assay, was performed (Figure 4-21). A colony formation assay reflects the ability of a single cell to grow into a colony, displaying cell viability and fitness.

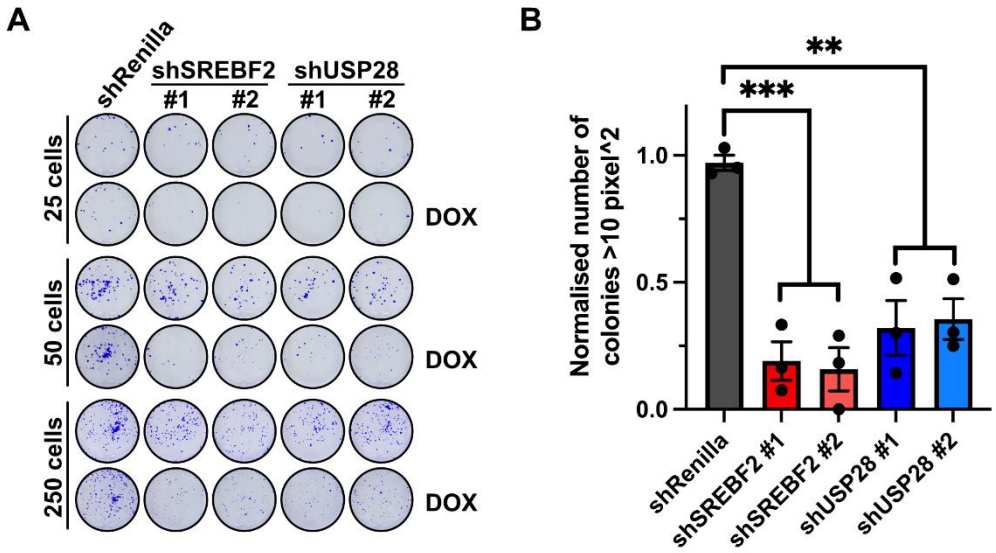

Figure 4-21: Knockdown of SREBP2 and USP28 reduce cell survival in a colony formation assay.

A. *A431 knockdown cell lines shUSP28 (#1 and #2) and shSREBF2 (#1 and #2) and control cell line shRenilla were seeded at the indicated cell numbers and treated for 5 d (250 cells) or 6d (50 cells and 25 cells) with 0.5 µg/mL DOX or EtOH as solvent control. Colony formation was determined by cell fixation and subsequent crystal violet staining.* ***B.*** *Bar graphs showing number of colonies >10 pixel^2 normalised to shRenilla control. Data represents the mean fold change in number of colonies from the three cell numbers ± SEM. **, P < 0.01; ***, P < 0.001; unpaired two-tailed Student t test. DOX = Doxycycline.*

The knockdown of either *SREBF2* or *USP28* resulted in a reduced number of colonies formed from single cells (Figure 4-21 **A**). This was observed after seeing different amounts of cells. Quantification of colony numbers with a threshold of the colony size > 10 pixel^2 revealed significantly reduced number of colonies upon knockdown of *USP28* or *SREBF2* (Figure 4-21 **B**). This result indicates an involvement of USP28 and SREBP2 in pro-survival cellular pathways in A431 cancer cells.

4.4.3.5 *Metabolic analysis of shUSP28 cells revealed reduced metabolic flux in co-enzyme Q10 and de novo pyrimidine synthesis*

Deregulated metabolism is an important feature of malignant transformation and specific metabolic adaptations promote cancer cell survival. Metabolic reprogramming of cancer cells is also regulated by oncogenic transcription factors, some of which were shown to be directly targeted by USP28 for deubiquitination, namely HIF1α (Flugel *et al.* 2012) and c-Myc (Popov *et al.* 2007).
To investigate the metabolic changes in cancer cells upon knockdown of USP28 and the contribution of SREBP2 in this context, A431 knockdown cell lines were analysed by metabolomics (Figure 4-22).

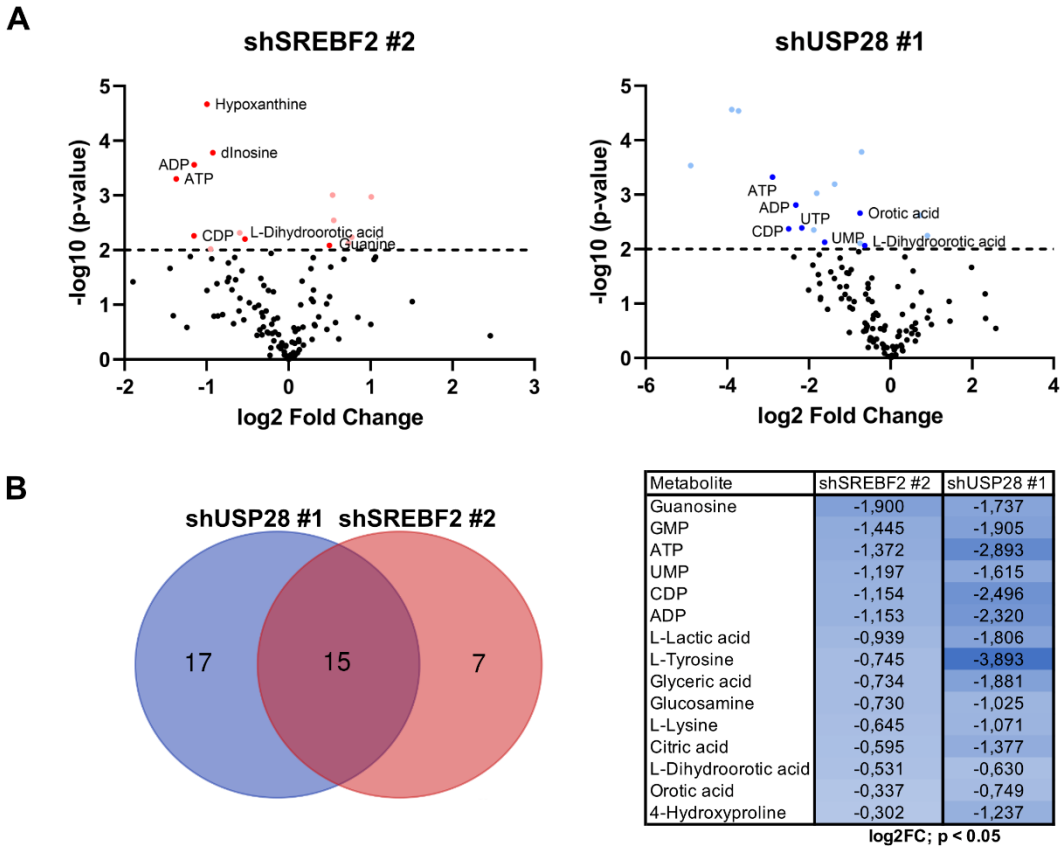

Metabolite	shSREBF2 #2	shUSP28 #1
Guanosine	-1,900	-1,737
GMP	-1,445	-1,905
ATP	-1,372	-2,893
UMP	-1,197	-1,615
CDP	-1,154	-2,496
ADP	-1,153	-2,320
L-Lactic acid	-0,939	-1,806
L-Tyrosine	-0,745	-3,893
Glyceric acid	-0,734	-1,881
Glucosamine	-0,730	-1,025
L-Lysine	-0,645	-1,071
Citric acid	-0,595	-1,377
L-Dihydroorotic acid	-0,531	-0,630
Orotic acid	-0,337	-0,749
4-Hydroxyproline	-0,302	-1,237

log2FC; p < 0.05

Figure 4-22: Knockdown of SREBF2 and USP28 results in a marked decrease of metabolites involved in de novo purine and pyrimidine synthesis.

A431 shSREBF2, shUSP28 and control cell line (shRenilla) were treated with 1 µg/mL DOX for 120 h and polar metabolites were extracted and measured by LC-MS. Peak area was normalised to summed signal and fold change was calculated by normalisation to shRenilla control. ***A.*** *Volcano blots show all metabolites regulated by induced knockdown on SREBF2 (left graph) or USP28 (right graph). Significant metabolites (-log10(p-value) > 2) were highlighted in bright red and bright blue, respectively. Metabolites, which are associated with de novo purine and pyrimidine synthesis, are displayed in red and blue, respectively, and labelled. Dots represent the mean of three replicates.* ***B.*** *Significantly downregulated (p < 0.05) metabolites of shSREBF2 and shUSP28 are shown in a VENN diagram. Log2FC of the overlapping 17 metabolites in both knockdown conditions are listed in table (right). Data represents the mean of three replicates. FC = Fold Change.*

Metabolites extracted from shSREBF2 and shUSP28 A431 cell lines treated with doxycycline for 120 h were analysed by mass spectrometry and metabolite levels were normalised to shRenilla control cell line. Significantly changed metabolites levels upon

knockdown of *USP28* and *SREBF2* are listed in Appendix (8.1). Noticeably, in the *SREBF2* and *USP28* knockdown situation various metabolites involved in *de novo* purine and pyrimidine synthesis were significantly downregulated (Figure 4-22 **A**). The majority of significantly downregulated metabolites in shSREBF2 cells were also found being decreased upon knockdown of USP28 (Figure 4-22 **B**). The overlapping metabolites being significantly downregulated in both knockdown conditions elucidate *de novo* pyrimidine synthesis as a pathway being regulated by USP28, potentially via regulation of SREBP2.

One main outcome of the mevalonate pathway beside cholesterol is the synthesis of isoprenoids. The co-enzyme Q10, or ubiquinone, is a chinone derivate containing lipophilic isoprenoid side chains, polymers containing ten isoprenyl subunits. Ubiquinone functions as an electron acceptor for enzymes located in the inner mitochondrial membrane, most notably complex I and II of the respiratory chain. In addition, in accepts electrons from dihydroorotate dehydrogenase (DHODH), which converts dihydroorotate to orotate. Next, phosphoribose is transferred to orotate and a subsequent carboxylation step results in uridine monophosphate (UMP). UMP is the basis for the synthesis of pyrimidine nucleotides including UTP, CTP and TTP.
The metabolic analysis in Figure 4-22 revealed a regulation of pyrimidine biosynthesis by the USP28-SREBP2 regulatory axis. To further monitor changes in metabolism in A431 knockdown cell lines, metabolic flux analysis with labelled glucose was performed (Figure 4-23).

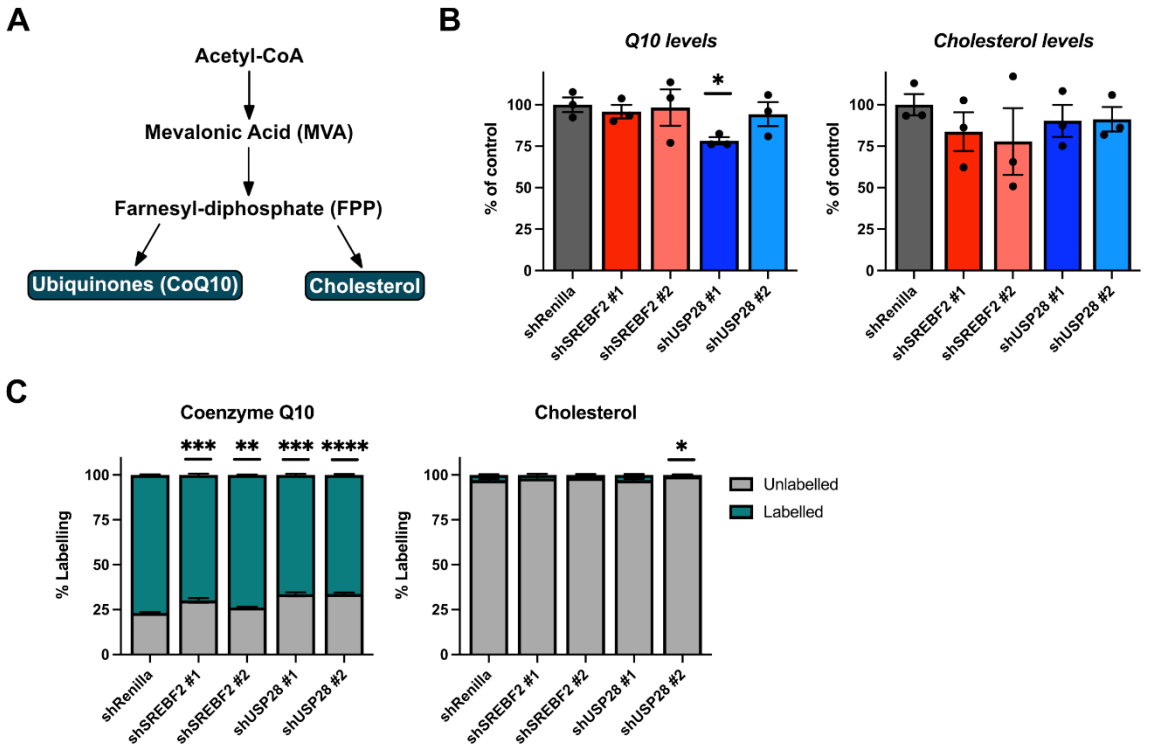

Figure 4-23: A431 cells show high metabolic flux into ubiquinone synthesis which is reduced by knockdown of either SREBF2 or USP28.

A. *Schematic illustration of the mevalonate pathway feeding into the isoprenoid tail containing molecule coenzyme Q10 (CoQ10) and cholesterol biosynthesis.* ***B.*** *Total CoQ10 and cholesterol levels in A431 shSREBF2 (#1 and #2),*

shUSP28 (#1 and #2) cell lines and control shRenilla cell line. Knockdown was induced by 1 µg/mL DOX for 120 h. Metabolites were extracted, analysed by LC-MS and peak area was normalised to internal standard and protein concentration. CoQ10 and cholesterol levels of knockdown cell lines were normalised to shRenilla control. Bar graph shows mean of triplicates ± SEM. ***C.*** *A431 cells with shSREBF2 (#1 and #2), shUSP28 (#1 and #2) and shRenilla cells were treated with 1 µg/mL DOX for 120 h. During the last 48 h cells were cultivated in medium containing a final concentration of 25 mM ^{13}C-labeled glucose. Metabolites were extracted and the fraction of labelled CoQ10 and cholesterol in percent were calculated. Bar graphs show fractions of labelled and unlabelled metabolites as mean ± SEM in triplicates. *, P < 0.05; **, P < 0.01; ***, P < 0.001; ****, P < 0.0001 unpaired two-tailed Student t test.*

To investigate the metabolic flux in A431 cells from glucose into the mevalonate pathway, branching into Co-enzyme Q10 and cholesterol biosynthesis, targeted metabolic analysis of *in cellulo* labelling was performed (Figure 4-23 **A**).
First, metabolites of A431 shSREBF2, shUSP28 and shRenilla cell lines were extracted upon induction of knockdown and total levels of CoQ10 and cholesterol were measured by mass spectrometry. Cholesterol levels were not significantly changed in the knockdown cell lines compared to control. The measurement of CoQ10 levels showed mild but significant reduction in shUSP28 #1 cells. The levels of the other knockdown cell lines were unaffected (Figure 4-23 **B**).
Next, the A431 knockdown cell line panel was treated with doxycycline and cultivated in medium containing ^{13}C-labeled glucose. The analysis of isotopologues of CoQ10 and cholesterol showed a high metabolic flux into the biosynthesis of isoprenoids compared to cholesterol: Up to 80% of the C-atoms were labelled in the CoQ10 while the percentage of labelling in cholesterol reached only up to 3%. The fraction of labelled cholesterol was significantly reduced in shUSP28 #2 cells while the other cell lines also showed reduced labelling but did not reach significance. The percent of labelled CoQ10 was significantly reduced in all knockdown cell lines. The observed reductions in the labelled fractions in SREBP2 and USP28 knockdown cells compared to control were up to 15 % (Figure 4-23 **C**).

In conclusion, the knockdown of either *USP28* or *SREBF2* reduced metabolites which are involved in *de novo* pyrimidine synthesis. Metabolic flux analysis revealed that in A431 cells, CoQ10 is a major output of the mevalonate pathway and that *de novo* biosynthesis of cholesterol occurs only at very low levels. While the overall levels of CoQ10 were not changed upon knockdown of *USP28* and *SREBF2*, the metabolic flux into ubiquinone was significantly decreased in cells with reduced USP28 and SREBP2 levels. Taken together, the metabolic analyses indicated a regulation of the mevalonate pathway and isoprenoid synthesis by USP28 via SREBP2.

4.4.3.6 Genome-wide analysis of transcriptome revealed overlap of pathway regulation downstream of USP28 and SREBP2

Acute reduction in USP28 and SREBP2 levels resulted in decreased cell growth and viability (Figure 4-19 and Figure 4-21). Furthermore, knockdown of either *SREBF2* or *USP28* deregulated the cellular metabolite pool by decreasing the synthesis of CoQ10 (Figure 4-23) and reducing levels of metabolites involved in *de novo* purine and pyrimidine synthesis (Figure 4-22).

In a genome-wide transcriptomics approach of shSREBF2 and shUSP28 cell lines, a pathway analysis of regulated genes was performed (Figure 4-24).

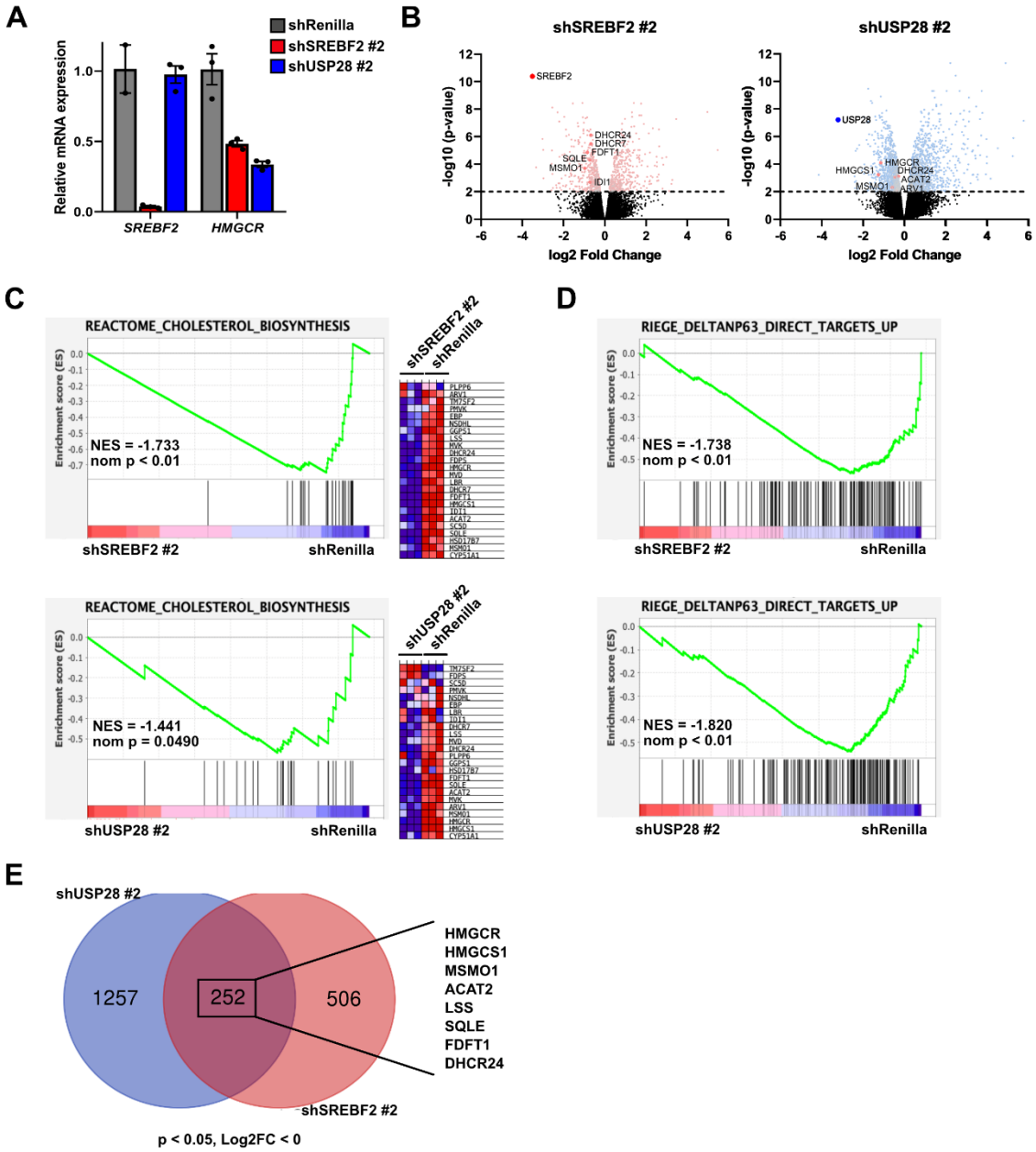

Figure 4-24: Genome-wide transcriptomics approach of shSREBF2 and shUSP28 cells revealed overlap in pathway analysis regarding cholesterol biosynthesis and ΔNP63 target genes.

A431 shSREBF2 #2, shUSP28 #2 and control cell line (shRenilla) were treated with 1 µg/mL DOX for 120 h and total RNA was extracted. ***A.*** *Efficient knockdown of SREBF2 in samples submitted for RNASeq analysis was validated by qPCR analysis. Bar graph shows relative mRNA expression normalised to shRenilla control for SREBF2 and HMGCR RNA transcripts.* ***B.*** *Total isolated RNA was used for library preparation and RNA sequencing (conducted by DKFZ Genomics Core facility). Sequencing data was TMM normalised and p-values and log2FC were calculated. Volcano blots showing total transcripts of shSREBF2 and shUSP28 cell lines, respectively. SREBF2 and USP28 are highlighted in dark red and dark blue, respectively.* ***C.*** *Normalised sequencing data was used to perform gene set enrichment analyses (GSEA) with publicly available data sets (analysis performed by F. Vogel, DKFZ). Graphs show GSEA blots of reactome cholesterol biosynthesis dataset in shSREBF2 (upper panel) and shUSP28 cells (lower panel). Regulation of single genes of the dataset is shown in the heat map beside.* ***D.*** *GSEA of shSREBF2 and shUSP28 cells for Riege* ***Δ****NP63 direct targets up dataset****. E.***

Significantly downregulated (p < 0.05) transcripts of shSREBF2 #2 and shUSP28 #1 are shown in a VENN diagram. Overlapping downregulated SREBP2 target genes listed in table. FC = Fold Change.

To investigate which pathways are affected by the knockdown of *SREBF2* or *USP28,* genome-wide transcriptome analysis was performed in A431 shSREBF2 and shUSP28 cell lines. Total RNA was isolated after five days of doxycycline treatment to induce knockdown and RNA samples were analysed by RT-qPCR to assess *SREBF2* and *HMGCR* mRNA levels (Figure 4-24 **A**). Knockdown of *SREBF2* and *USP28* resulted in a strong decrease of *HMGCR* mRNA, one of the major target genes of SREBP2. The SREBP2 knockdown cell line also showed strong reduction in *SREBF2* transcripts whereas *SREBF2* mRNA levels were not changed upon knockdown of USP28. This result confirms a post-transcriptional regulation of SREBP2 levels by USP28.
Total RNA was used for library preparation and subsequently sequenced by the DKFZ Genomics Core facility. Normalisation and analyses of the sequencing data was obtained by Dr. Felix Vogel, DKFZ.
Normalised read counts were displayed in a volcano plot and SREBP2 and USP28 were highlighted. Efficient knockdown of *SREBF2* and *USP28* was also confirmed by sequencing data, showing that *SREBF2* and *USP28* are strongly downregulated in their respective knockdown cell lines. Additionally, SREBP2 target genes significantly downregulated in the respective knockdown cell line were highlighted in bright red (Figure 4-24 **B**).
Gene set enrichment analyses revealed drastic downregulation of the cholesterol biosynthesis pathway in *SREBF2* and *USP28* knockdown cell lines compared to the shRenilla control cell line. Changes in expression of the single genes of the Reactome Cholesterol Biosynthesis dataset is shown as heat map. Nearly all genes in the dataset were found to be higher expressed in the shRenilla control cell line than in the knockdown cells (Figure 4-24 **C**).
Further, in both knockdown situations the target genes of the transcription factor ΔNP63 were strongly downregulated. ΔNP63 is a marker protein for squamous phenotype and was identified as USP28 target protein (Prieto-Garcia *et al.* 2020). Interestingly, knockdown of SREBF2 also reduced the expression of ΔNP63 target genes (Figure 4-24 **D**).
Significantly, downregulated genes in shUSP28 and shSREBF2 cells showed an overlap of 252 genes. Within this fraction several SREBP2 target genes were identified (Figure 4-24 **E**).

Taken together, the observed results are consistent with a model in which a reduction of USP28 in the squamous A431 cell line affects mSREBP2 levels and decreases the expression of SREBP2 target genes. Moreover, knockdown of *USP28* results in deficiency of cell growth and proliferation. Metabolomics and stable isotope labelling revealed deregulation of intracellular metabolism. In detail, the synthesis of CoQ10 was diminished and the metabolites associated with *de novo* purine and pyrimidine synthesis were reduced. Gene set enrichment analyses showed an overlap of downregulated pathways in *SREBF2* and *USP28* knockdown conditions: Cholesterol

biosynthesis and ΔNP63 target gene datasets were downregulated upon knockdown of *SREBF2* and *USP28*.

4.5 Reduced USP28 levels sensitize cells for statin treatment

Statins are HMG-CoA reductase (HMGCR) inhibitors and are widely used as cholesterol-lowering medications in patients with cardiovascular diseases, since these patients frequently display high cholesterol levels (Maron *et al.* 2000). Statins are competitively inhibiting HMGCR, the rate-limiting enzyme of the mevalonate pathway. The outcome of low intracellular cholesterol levels activates the proteolytic cleavage of flSREBP2 which upregulates the expression of target genes for *de novo* cholesterol biosynthesis and cholesterol uptake via the LDL receptor (LDLR). High LDLR expression in turn increases the uptake of LDL and VLDL extracellularly and *vice versa* reduces LDL concentration in the blood (Maron *et al.* 2000).
For years already, scientists performed studies associating statin treatment with reduced cancer risk in various cancer entities. Namely, it was shown that patients treated with statin had a 26% significant reduction in the risk of developing esophageal cancer (Singh *et al.* 2013). In another study investigating statin treatment in the context of lung cancer, it was shown that statin use for longer than six months was associated with a risk reduction of lung cancer by 55% (Khurana *et al.* 2007).
To further analyse the effects of statin treatment in the absence of USP28, viability assays in the A431 cell lines treated with simvastatin were performed.

4.5.1 USP28 knockdown cells show increased sensitivity to simvastatin treatment

Results obtained so far have shown that the knockdown of USP28 results in decreased levels of SREBP2 and its target genes (Figure 4-16). Consequently, the mevalonate pathway was downregulated (Figure 4-15) as well as the synthesis of Co-enzyme Q10 (Figure 4-23). A deregulation of Co-enzyme Q10 in turn results in the reduction of *de novo* pyrimidine synthesis (Figure 4-22) which is essential for DNA replication and subsequent proliferation of cells. Consequently, the cell viability of USP28 knockdown cancer cell lines was reduced (Figure 4-19 and Figure 4-21).

To further investigate if there is a synergistic effect of knocking down USP28 and additionally blocking the mevalonate pathway by statins, A431 shUSP28 cells or controls were treated with simvastatin and cell viability was monitored (Figure 4-25).

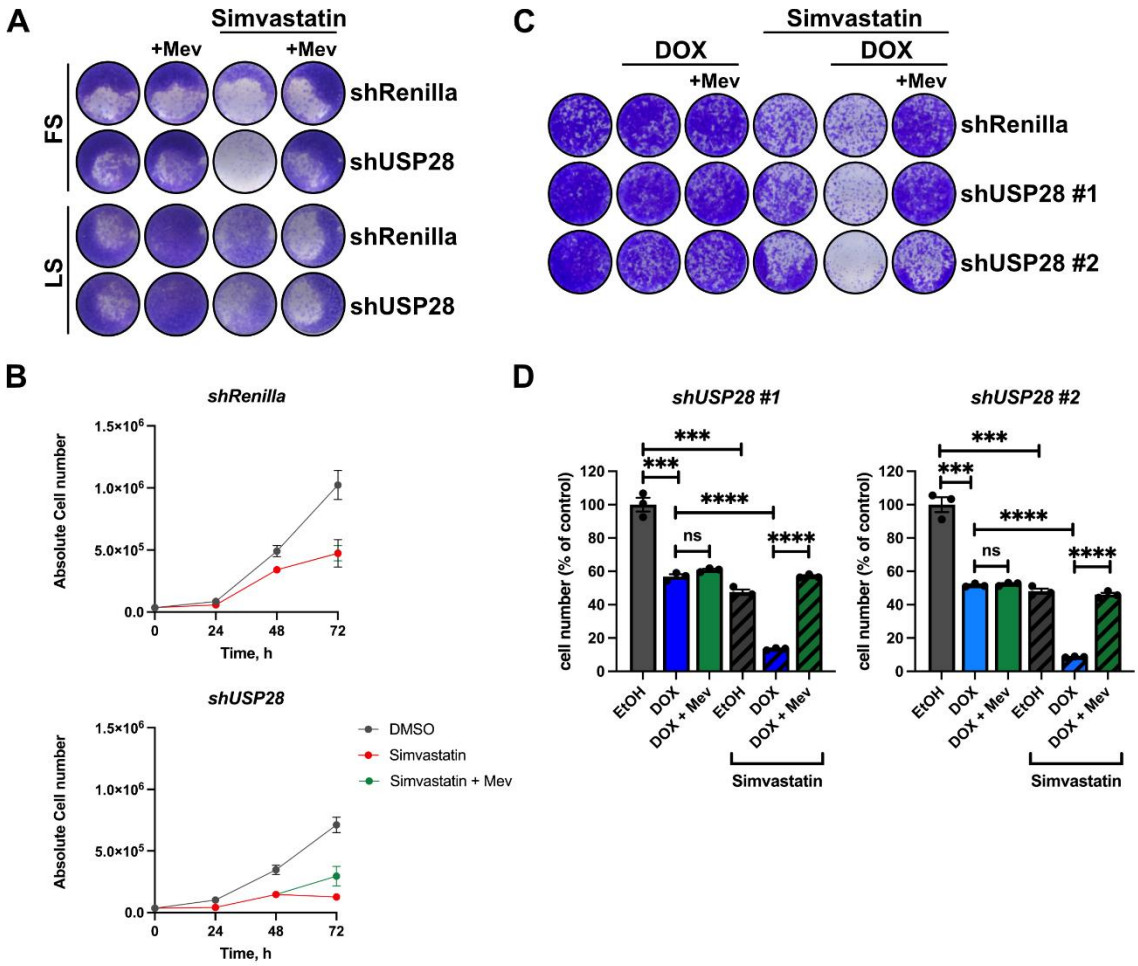

Figure 4-25: Knockdown of USP28 results in reduced cell viability when blocking the mevalonate pathway by Statin.

A. *shRenilla and shUSP28 #1 cell lines were treated with 1µg/mL DOX for 120 h. During the last 24 h, simvastatin at a final concentration of 10 µM and Mevalonic acid (500 µM) were added as indicated and cells were either grown in FS or LS conditions. Cell viability was monitored by crystal violet staining.* ***B.*** *Growth curve of shUSP28 #1 and shRenilla cells. Cells were pre-treated with 1µg/mL DOX for 72 h. Simvastatin was added in a final concentration of 10 µM and cell number was determined by counting cells every 24 h. At time point of 48 h mevalonic acid (500 µM) was added to one group of samples, as indicated. Graphs show mean of triplicates ± SEM.* ***C.*** *Experiment from* ***A.*** *was repeated including shUSP28 #2 cell line and EtOH solvent control. Knockdown via 1 µg/mL DOX was induced simultaneously to adding 10 µM Simvastatin and 100 µM mevalonic acid, as indicated. Cells were incubated for 72 h and cell viability was monitored by crystal violet staining. Figure shows one representative of three replicates. Crystal violet staining intensity was quantified and is displayed for shUSP28 cell lines as bar graph in* ***D.*** *Bar graph represents mean of triplicates ± SEM. ***, P < 0.001; ****, P < 0.0001 unpaired two-tailed Student t test. DOX = Doxycycline. FS = Full Serum (10% FCS). LS = Low Serum (1% FCS).*

Simvastatin treatment of induced USP28 knockdown cell lines showed deficiency in cell viability compared to the shRenilla control cell line. The reduction in cell number could be rescued by addition of mevalonic acid. Simvastatin inhibits the conversion of HMG-CoA to mevalonic acid, catalysed by the SREBP2 target gene HMG-CoA reductase. The enhanced sensitivity of cells with reduced USP28 levels towards simvastatin treatment was not observed under low serum (LS) conditions (Figure 4-25 **A**).

Cell growth of shRenilla and shUSP28 #1 cells was monitored by counting of cell number over time. Knockdown was induced for 72 h, cells were re-seeded and

simvastatin treatment was initiated at time point zero. Cells were counted every 24 h and it could be observed that the knockdown of USP28 already results in a decrease of cell growth compared to control cells (compare grey lines in both graphs) after 24 hours. Simvastatin treatment decreased cell growth in shRenilla cells but the reduction in cell growth in shUSP28 was more severe (compare red lines in both graphs). After 48 h of simvastatin treatment, mevalonic acid was added and no increase in cell number was observed for shRenilla cells (lines overlap) but in USP28 knockdown cells the addition of mevalonic acid partially rescued cell number (green line) (Figure 4-25 **B**).

The experiment in Figure 4-25 **A** was repeated including shUSP28 #2 cell line and EtOH solvent controls. Cells were not pre-treated with DOX, but rather the induction of knockdown, simvastatin treatment and mevalonic acid rescue was induced and started simultaneously. Cells were harvested after 72 h of treatment and stained with crystal violet. USP28 knockdown cell lines showed enhanced sensitivity towards simvastatin treatment, which could be completely rescued by supplementing mevalonic acid. The addition of mevalonic acid could rescue cell number caused by simvastatin treatment but not the reduction in cell viability induced by USP28 knockdown (Figure 4-25 **C** and **D**).

4.5.2 Knockdown of USP28 does not sensitize cells by blocking cholesterol biosynthesis

The intermediate Farnesyl-pyrophosphate (FPP) lies at a branching point in the mevalonate pathway and feeds, among others, into cholesterol biosynthesis and the synthesis of substrates for the prenylation of proteins. To determine if the loss of cholesterol is the crucial circumstance that drives USP28 knockdown cells into reduced cell growth, inhibitor treatments downstream of FPP were performed (Figure 4-26).

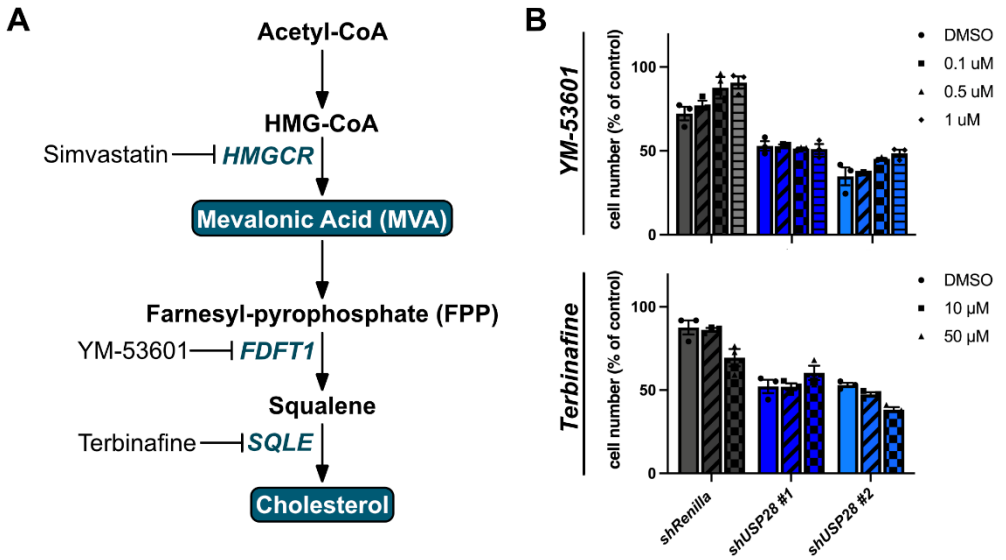

Figure 4-26: Inhibition of the cholesterol synthesis pathway downstream of FPP does not affect additionally cell viability of USP28 knockdown cell lines.

A. *Illustration of the of the mevalonate pathway leading into cholesterol biosynthesis. Key enzymes upstream and downstream of the FPP branching point are indicated with their respective inhibitors.* ***B.*** *Knockdown of USP28 in A431 cells and control cell line shRenilla via 1 µg/mL DOX was induced simultaneously to addition of either YM-53601 or terbinafine in indicated final concentrations. Cells were incubated for 72 h and cell viability was determined by crystal violet staining. Staining intensity was quantified and normalised to respective EtOH control. Data represents mean of triplicates ± SEM****.*

Farnesyl-diphosphate transferase (FDFT1) catalyses a two-step reaction in which two FPP molecules are converted into squalene. This is the first reaction in the synthesis of sterols. The second step in cholesterol biosynthesis is catalysed by squalene monooxygenase, which is the rate-limiting enzyme in this pathway. It oxidizes squalene to 2,3-oxidosqualene that in turn is further modulated in multiple steps to form cholesterol. For both enzymes specific inhibitors are available: YM-53601 and terbinafine, respectively (Figure 4-26 **A**).
The treatment of A431 shRenilla and shUSP28 cell lines with FDFT1 and SQLE inhibitors did not reveal enhanced sensitivity of cell upon knockdown of USP28. Reduced levels of USP28 in general result in decreased cell viability. The additional blocking of the cholesterol biosynthesis in the cells did not add a significant reduction in cell growth (Figure 4-26 **B**). This indicates that cholesterol, as an output of the mevalonate pathway, is not responsible for the enhanced sensitivity of USP28 knockdown cell lines to statin treatment observed previously (Figure 4-25).

4.5.3 Knockdown of USP28 does not sensitize cells by blocking pyrimidine synthesis or DNA replication

Another branch of the mevalonate pathway downstream of FPP is the synthesis of isoprenoid polymers, like ubiquinone. Ubiquinone functions as an electron acceptor for dihydroorotate dehydrogenase (DHODH), an essential enzyme for the generation of pyrimidine nucleotides for DNA and RNA synthesis.
To elucidate if the pyrimidine synthesis and DNA replication are the processes, which mediate the sensitivity to statin treatment in the USP28 knockdown situation, cells were treated with an inhibitor of pyrimidine nucleotide synthesis or DNA damaging agent (Figure 4-27).

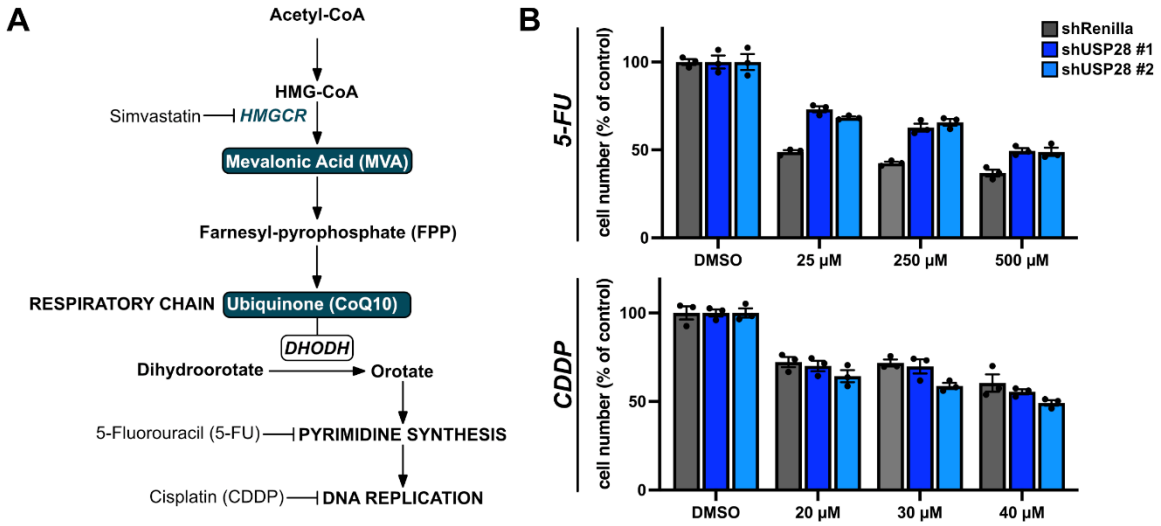

Figure 4-27: A431 cells do not show enhanced sensitivity to inhibition of pyrimidine synthesis or DNA replication in the USP28 knockdown situation.

A. *Illustration of the of the mevalonate pathway branching into pyrimidine synthesis essential for DNA replication. Key processes downstream of FPP branching point are indicated with respective inhibitors.* ***B.*** *USP28 knockdown and control cell line shRenilla were induced by 1 µg/mL DOX for 96 h and afterwards supplemented with either 5-fluorouracil (5-FU) or cisplatin (CDDP) in indicated final concentrations. Cells were incubated for another 48 h and cell viability was determined by crystal violet staining. Staining intensity was quantified and normalised to respective solvent control (DMSO). Data represents mean of triplicates ± SEM.*

The antimetabolite drugs 5-fluorouracil (5-FU) and cisplatin (CDDP) are chemotherapy medication used in various types of cancer. 5-FU is a pyrimidine analogue, which blocks the conversion of dUMP to dTMP by the thymidylate synthase. CDDP interferes with DNA and induces intrastrand crosslinking of guanines. The crosslinking activates DNA repair mechanisms and cells undergo apoptosis if the damage cannot be resolved. As a consequence, 5-FU and CDDP treatment lead to DNA damage and cell death in many cancer cells (Figure 4-27 **A**).

It was therefore investigated whether USP28 knockdown alters 5-FU and CDDP sensitivity of cancer cells. Interestingly, A431 cells showed remarkable resistance toward 5-FU and CDDP treatment. Furthermore, compared to the control cell line, cells with USP28 knockdown showed even slightly more resistance to 5-FU. For the CDDP treatment, no significant differences in cell viability were observed upon knockdown of USP28 (Figure 4-27 **B**).

Collectively, these results show that cells do not show increased sensitivity towards blocking pyrimidine synthesis or inducing DNA damage under constrained mevalonate pathway caused by USP28 depletion.

4.5.4 GGPPi rescues statin sensitivity upon USP28 knockdown revealing geranylation and farnesylation as rate-limiting processes

Prenylation is a post-translational modification, which describes the transfer of either a farnesyl or a geranylgeranyl moiety to a cysteine residue of target proteins. Prenylation of proteins mediates protein-protein and protein-membrane interactions.

Farnesyl pyrophosphate and geranylgeranyl pyrophosphate are both products of the mevalonate pathway.

To elucidate which metabolites and processes mediate the increased sensitivity towards statin treatment of A431 cells in the USP28 knockdown situation, cell viability rescue experiments were performed (Figure 4-28).

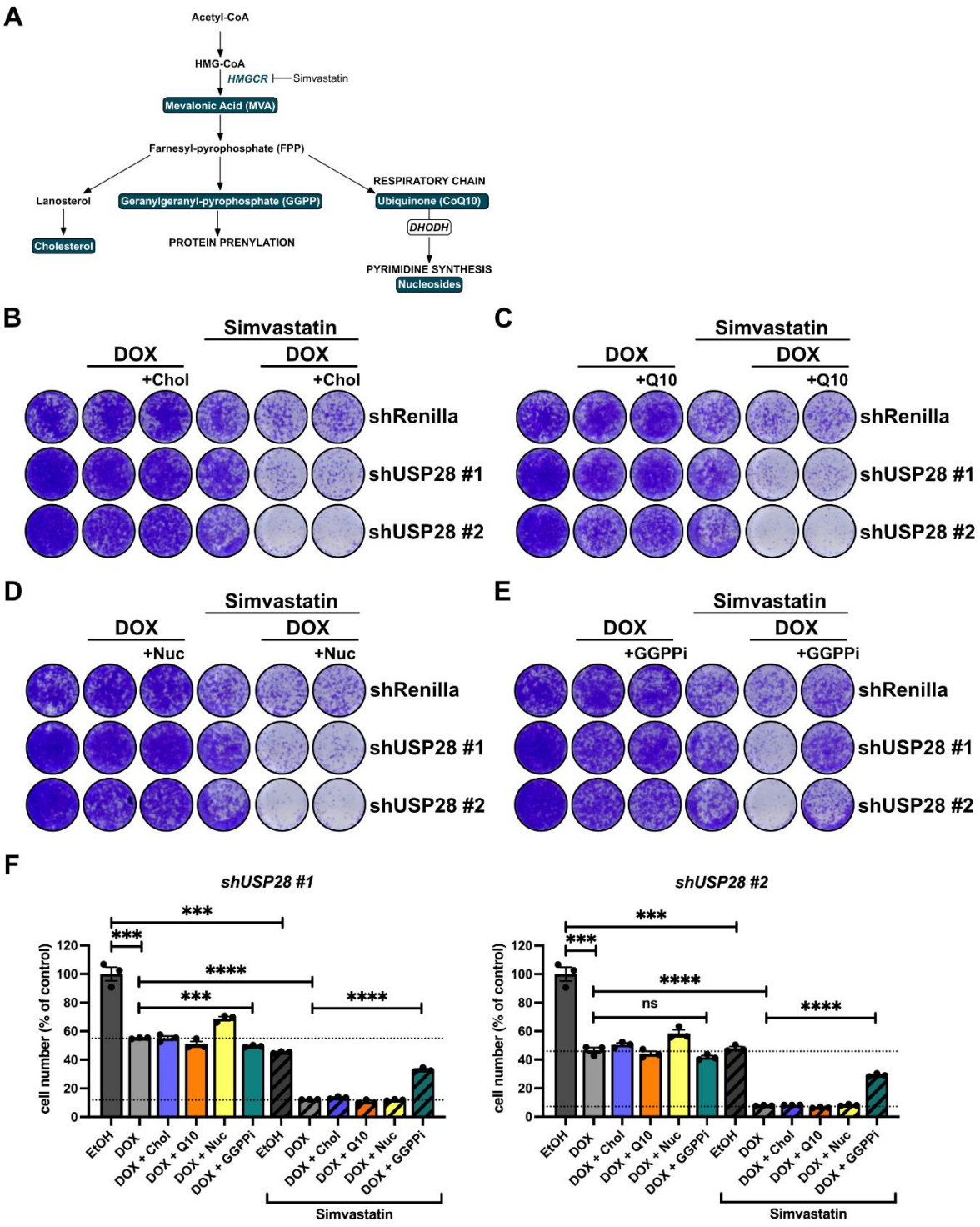

Figure 4-28: The lack in geranylgeranyl pyrophosphate is the critical metabolite, which mediates the enhanced sensitivity of shUSP28 cells toward statin treatment.

A. *Illustration of the of the mevalonate pathway branching into cholesterol biosynthesis, protein prenylation and pyrimidine synthesis essential for DNA replication. Key processes downstream of FPP branching point are*

indicated with respective metabolites. ***B.*** *–* ***E.*** *USP28 knockdown and control cell line shRenilla were induced by 1 µg/mL DOX and supplemented with 10 µM simvastatin and additionally 1 µM cell permeable cholesterol (****B.****), 5 µM CoQ10 (****C.****), 1X Nucleosides (3 µM C, G, A, U; 1 µM T) (****D.****) or 5 µM GGPPi (****E.****). Cells were incubated for 72 h and cell viability was monitored by crystal violet staining. Figure shows one representative of three replicates. Crystal violet staining intensity was quantified and is displayed for shUSP28 cell lines as bar graph in* ***F.*** *Bar graph represents mean of triplicates ± SEM. ns, not significant; ***, P < 0.001; ****, P < 0.0001 unpaired two-tailed Student t test. DOX = Doxycycline. Chol = Cholesterol. Q10 = Co-enzyme Q10. Nuc = Nucleosides. GGPPi = Geranylgeranyl pyrophosphate****.***

A431 USP28 knockdown cells and shRenilla control cell line were induced and treated with simvastatin. As described in Figure 4-25, cells showed enhanced sensitivity to statin treatment upon USP28 knockdown.
To unravel which metabolite or process downstream of the mevalonate pathway causes this phenomenon, cells were supplemented with intermediates or outputs of the mevalonate pathway: FPP is further converted into cholesterol, geranylgeranyl pyrophosphate (GGPPi) and supports via ubiquinone (CoQ10) pyrimidine synthesis (Figure 4-28 **A**).
For the rescue attempts, cells were treated with either cell permeable cholesterol, ubiquinone, nucleosides or GGPPi. Cholesterol as well as adding CoQ10 or nucleosides did not increase cell viability of shUSP28 cells treated with simvastatin (Figure 4-28 **B**, **C**, **D**). Whereas, the addition of GGPPi significantly rescued cell viability of cells lacking in USP28 and treated with simvastatin (Figure 4-28 **E**, **F**). Notably, GGPPi was not able to restore the deficiency of cell growth caused by USP28 knockdown.

In conclusion, USP28 knockdown sensitizes cells to statin treatment. This enhanced sensitivity does not result from the lack of cholesterol or deficiency of pyrimidine synthesis for DNA and RNA synthesis. However, prenylation of proteins seems to be the bottle neck causing the reduced proliferation in statin treated cells lacking in USP28.

4.6 The dual USP25/USP28 inhibitor AZ-1 increases mSREBP2 and target gene levels

Statin treatment is associated with a reduced risk of developing various different cancer types (Khurana *et al.* 2007, Singh *et al.* 2009, Chiu *et al.* 2011, Singh *et al.* 2013). The observation that statin treatment forces cells into cell death or decreases proliferation in a USP28 deficient situation (Figure 4-25) raises the question if it could be exploited for therapeutic intervention in clinical medication of cancer patients.
In 2017, a study of the dual USP25/USP28 inhibitor AZ-1 was performed showing remarkable specificity in blocking enzyme activity of both USPs compared to other members of this class of DUBs. Further, the inhibitor was validated by inducing decreased stability of USP28 target protein c-Myc (Wrigley *et al.* 2017).
To elucidate if a combinatory treatment of statins and USP28 inhibitors might result in reduced cancer cell proliferation and survival, synergy experiments with simvastatin and AZ-1 inhibitor were performed.

4.6.1 Statin and iUSP25/28 treatment did not show deficiency in cell growth or proliferation in A431 spheroid cultures

Culturing cells as spheroids mimic a three-dimensional tumour model, which better comparable to *in vivo* conditions than monolayer cell culture. Spheroids resemble the hypoxic and nutrient-deprived conditions and high lactate concentrations were measured in these cultures confirming the Warburg effect, which explains the altered metabolism of cancer cells towards lactic acid fermentation. Moreover, it was shown that spheroid culture conditions increase mSREBP2 and HMGCS1 levels revealing the dependency on the mevalonate pathway and its associated processes (Kaymak *et al.* 2020).
To study the effects of statin and iUSP25/28 under 3D conditions, A431 cells were grown as spheroids and treated with simvastatin and AZ-1 (Figure 4-29).

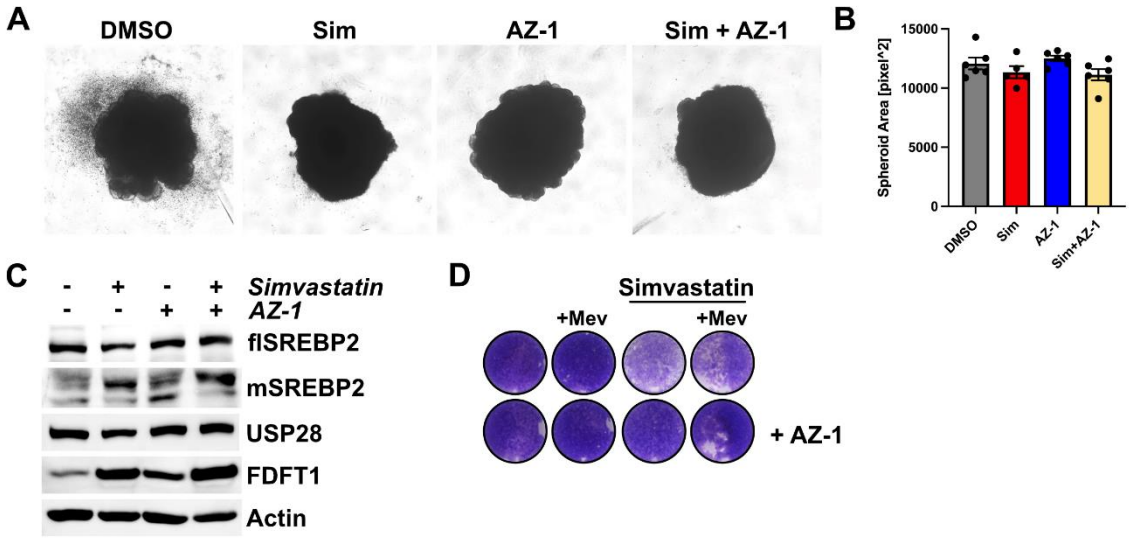

Figure 4-29: Statin or iUSP25/28 treatment did not affect cell growths of A431 spheroids.

A. *A431 cells were seeded as spheroids and cultivated for two weeks under normal conditions. Spheroids were treated with simvastatin or AZ-1 or combinatory treatment (10 µM each). DMSO was added as solvent control. Pictures were taken after 48 h of treatment. Figure represents one replicate out of 5-6 spheroids.* ***B.*** *Area of spheroids was analysed by ImageJ and bar graph shows mean of at least five spheroids per condition ± SEM.* ***C.*** *Spheroids were lysed and pooled and SREBP2 as well as USP28 and FDFT1 were detected by immunoblot. Actin served as loading control.* ***D.*** *A431 cells were grown in monolayer culture and treated with 10 µM simvastatin, 5 µM AZ-1 or a combination of both for 72 h. Mevalonic acid was added in a final concentration of 500 µM during the last 24 hours. Sim = Simvastatin. Mev = Mevalonic acid.*

A431 cells were cultured in 3D and treated with statins, USP25/28 inhibitor (iUSP25/28) or a combination of both. No changes in size of the spheroids were observed, indicating that the inhibitor treatments did not result in decreased cell growth under these conditions (Figure 4-29 **A** and **B**).
Spheroids were pooled and lysed and protein levels of USP28 as well as SREBP2 and target gene FDFT1 were analysed by immunoblot. Simvastatin treatment eventuated in increased mSREBP2 and FDFT1 protein levels, most likely due to inhibition of the negative feedback loop. Unexpectedly, these results were also

obtained by treating the cells with AZ-1. A combination of both inhibitors increased the effect on protein levels even further (Figure 4-29 **C**).
To verify, if the enhanced sensitivity of cells with a knockdown of USP28 to statin treatment, which was observed previously, could also be achieved in cells treated with AZ-1, A431 cells were cultured in monolayer and treated with simvastatin and AZ-1 or a combination of both. AZ-1 treated cells did not show sensitivity to statin treatment. Rather, an enhanced resistance to simvastatin treatment was observed. The addition of mevalonic acid had only a mild effect on cell growth of cells supplemented with simvastatin alone (Figure 4-29 **D**). However, as this experiment was only conducted with a single replicate, additional analysis is needed.

4.6.2 Combinatory treatment of statin and iUSP25/28 affects cell viability in a dose-dependent manner

To further investigate the enhanced cell viability by AZ-1 treatment observed in Figure 4-29 **D**, synergy experiments with increasing concentrations of AZ-1 and simvastatin under normal and serum-deprived conditions were performed in U2OS and A431 cells (Figure 4-30).

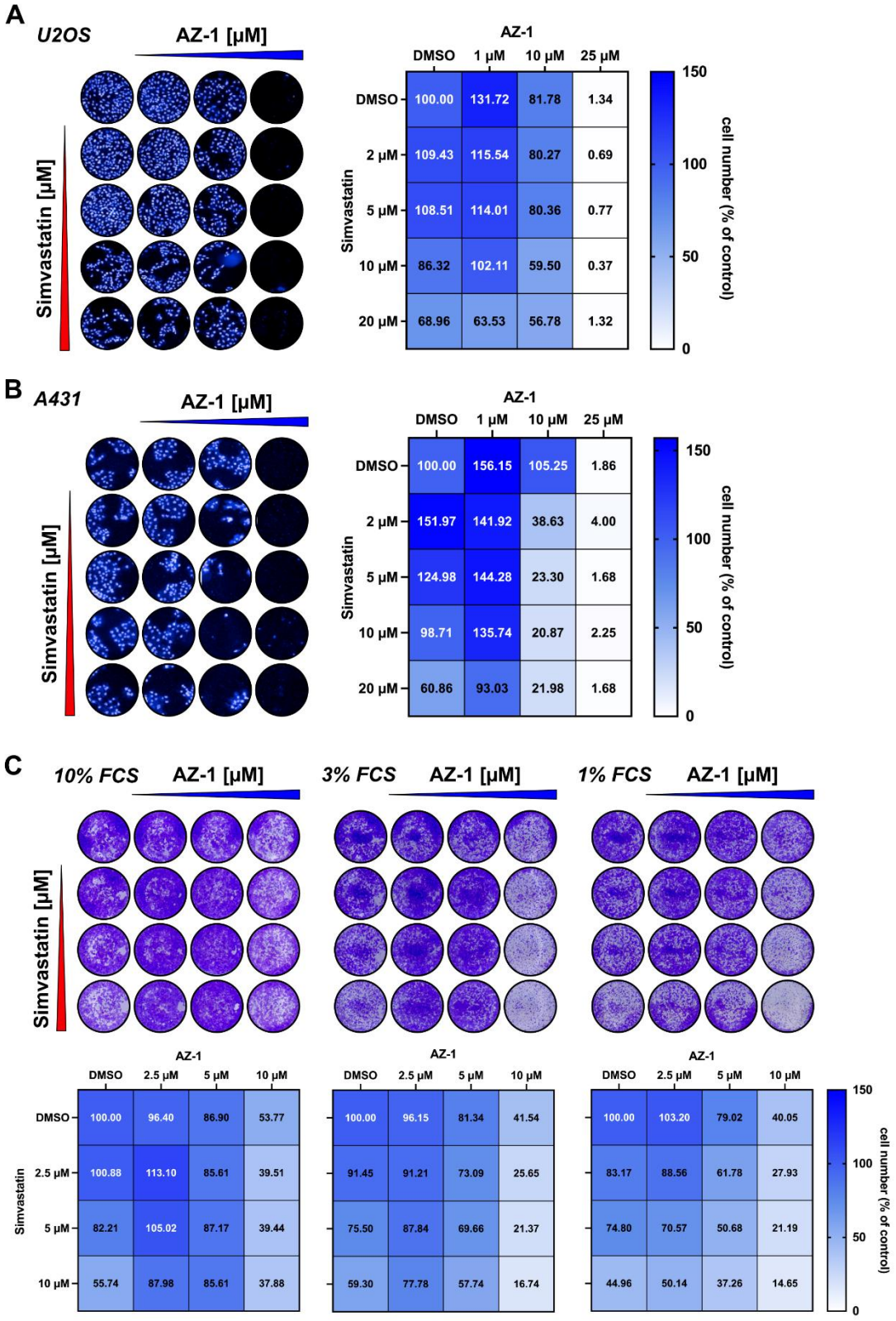

Figure 4-30: Statin and iUSP28 combinatory treatment showed a bi-phasic response in cell growth in U2OS and A431 cells.

A. *U2OS and B. A431 cells were treated with increasing concentrations of AZ-1 (1µM, 10 µM and 25 µM) and Simvastatin (2µM, 5µM, 10 µM and 20µM) as well as a combination of both for 48 h. Cells were fixed and cell nuclei were stained with Hoechst dye. Numbers of nuclei were measured by a high content imaging system. The cell number derived from in total 30 pictures from duplicate samples were normalised to DMSO control and cell*

numbers in % of control are displayed in the right panel. ***C.*** *A431 were treated with increasing concentrations of AZ-1 (2.5µM, 5 µM and 10 µM) and Simvastatin (2.5µM, 5µM and 10 µM) as well as a combination of both for 48 h. Cells were either cultivated in full serum (10% FCS), in medium containing 3 % FCS or in low serum conditions (1% FCS) for 48 h. Cell numbers were monitored by crystal violet staining. Upper panel shows one representative staining of triplicate samples. Staining intensity was quantified and normalised to DMSO control. Mean of cell numbers of triplicates displayed in % of control is shown in lower panels.*

When U2OS and A431 cells were treated with increasing concentrations of AZ-1 in combination with simvastatin, a biphasic response on cell viability was observed: Cells treated with low concentration of AZ-1 first showed an increase in cell viability compared to the lowest AZ-1 concentration used. Selectively, high AZ-1 and simvastatin concentration affected cell viability of the cells. A synergistic effect resulted from an AZ-1 concentration of 10 µM and increasing simvastatin concentrations only (Figure 4-30 **A** and **B**).
To further validate this observation, A431 cells were treated with lower doses of AZ-1 and simvastatin also under serum-deprived conditions of 3% FCS and 1% FCS. The biphasic response in reduced cell viability was again observed in high simvastatin treatment (5 µM and 10 µM) and low AZ-1 concentrations (2.5 µM and 5 µM). For high concentrations of both inhibitors (10 µM each), a synergistic effect was recognized. The cultivation of cells in serum-deprived conditions enhanced this synergistic effect (Figure 4-30 **C**).

4.6.3 AZ-1 treatment results in increased SREBP and target gene levels

To gain insight into the molecular mechanism for the regulation of SREBP2 and target genes, U2OS cells were treated with high and low concentrations of AZ-1 inhibitor. Protein levels were analysed at different time points by immunoblot (Figure 4-31).

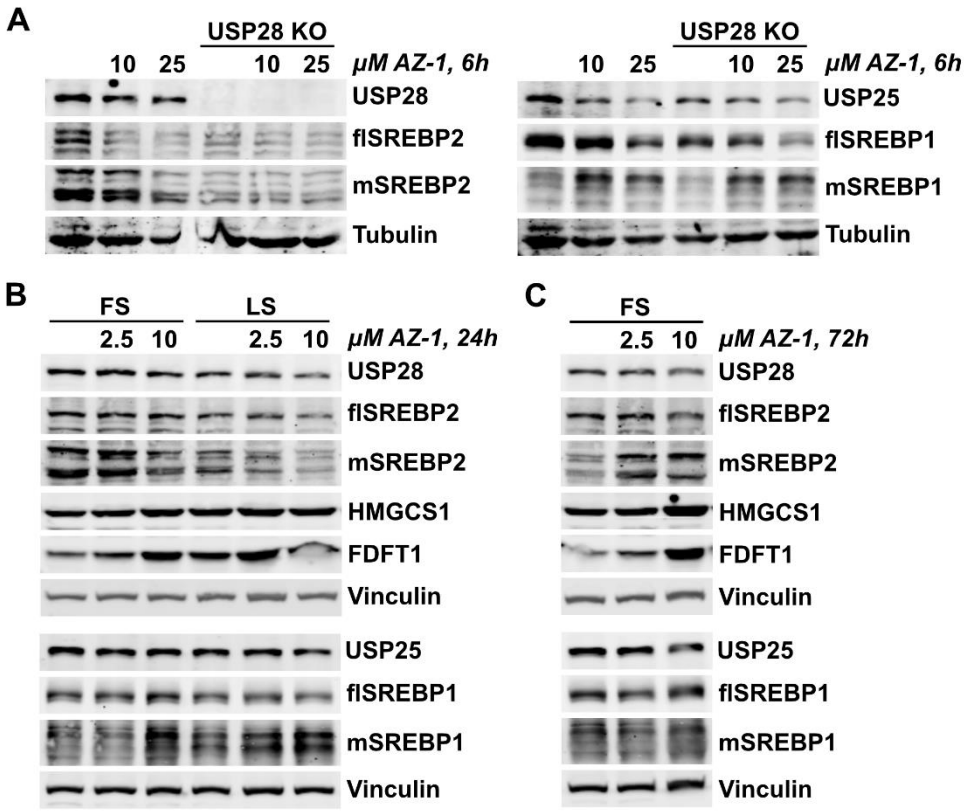

Figure 4-31: Inhibiton of USP28 by AZ-1 in U2OS cells results in deregulated SREBP level in a dose- and time-dependent manner.

A. *U2OS parental and USP28 KO cells were treated with indicated concentrations of AZ-1 for 6h. Protein levels of USP28 and USP25 as well as SREBP1 and SREBP2 were detected by western blot analysis. Tubulin served as loading control.* ***B.-C.*** *U2OS cells were cultivated under FS and LS conditions for 48 h. AZ-1 was added in the inidicated concentrations and cells were incubated for further 24 h (**B.**) or 72 h (**C.**) maintaining the same conditions. Protein levels of USP28 and USP25 as well as SREBP1 and SREBP2 and the target genes HMGCS1 and FDFT1 were detected by western blot analysis. Vinculin served as loading control. FS = Full Serum (10% FCS). LS = Low Serum (1% FCS).*

The immediate effects on protein levels in U2OS cells after 6 hours of AZ-1 treatment were observed by western blot and decreasing overall SREBP2 levels were monitored with increasing inhibitor concentration. This effect was not visible in the USP28 KO situation. The downregulation of flSREBP2 could be explained by reduced transcriptional control via mSREBP2 on its own promoter through the feed-forward loop. High concentration of AZ-1 also led to reduced USP28 levels since it was shown that USP28 deubiquitinates and stabilises itself. Thus, an inhibition results *vice versa* in the destabilisation of the protein. While flSREBP1 also showed reduced band intensities in inhibitor treated cells, the band of the mSREBP1 transcription factor was strongly increased (Figure 4-31 **A**).

The same results for mSREBP1 were obtained at lower concentration but prolonged incubation time under normal and serum-deprived conditions. Whereas mSREBP2 was reduced, flSREBP2 levels were only mildly affected. Unexpectedly, the SREBP2 target gene FDFT1 showed increasing band intensities in inhibitor treatment cells, while HMGCS1 levels were not impacted (Figure 4-31 **B**).

Long term effects with three days of inhibitor treatment revealed increasing protein levels of mSREBP2 and its target genes, indicating, that the regulation of SREBP2 by USP28 inhibition is highly dependent on concentration and duration of treatment (Figure 4-31 **C**).

In summary, AZ-1 increased mSREBP1 level in U2OS cells. Increased mSREBP1 and mSREBP2 levels were also observed in A431 cells treated with increasing concentrations of AZ-1 after 24h and 72 hours of treatment. This increased mSREBP and mSREBP target levels were also detected when cells were cultivated under serum-deprived conditions.

The stability of SREBPs is regulated downstream of the PI3K/Akt pathway (Porstmann *et al.* 2008). The phosphorylation of AKT at T308 and S473 leads its activation, which mediates the phosphorylation of GSK3β at Ser9. The Ser9-phosphorylation of GSK3β inhibits its phosphorylation of primed transcription factors at the CPD and prevents their proteasomal degradation.
Since an increase in cell viability after treating A431 cells with low doses AZ-1 (1 µM) was observed (Figure 4-30), the underlying molecular mechanism was further investigated. The effects of inhibiting USP28 over time on SREBP and target gene expression were monitored by immunoblot. Additionally, the phosphorylation state of AKT and GSK was verified by using phosphor-specific antibodies (Figure 4-32).

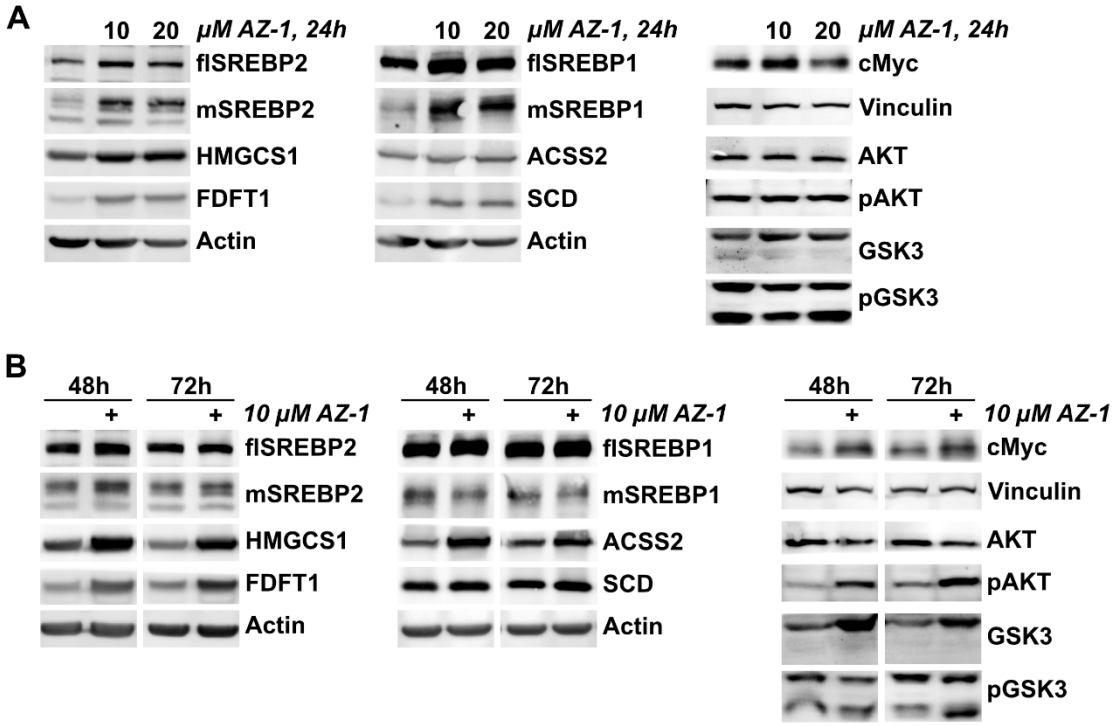

Figure 4-32: Inhibition of USP25/28 by AZ-1 in A431 cells increases SREBP and target gene levels as well as upstream AKT-GSK3 signalling.

A. *A431 cells were treated with indicated concentrations of AZ-1 for 24 h and protein levels of SREBP and its targets (left panel), as well as SREBP1 and its target genes (middle) and expression of c-Myc and the phosphorylation state of AKT (Ser473) and GSK3 α/β (Ser21/9)were monitored by immunoblot. Actin and Vinculin*

served as loading controls. ***B.*** *A431 cells were trated with 10 µM AZ-1 for 48 and 72 h, respectively, and protein levels were detected identical to* ***A.***

Similar to the results displayed in Figure 4-31, A431 cells treated with 10 µM or 20 µM USP25/28 inhibitor AZ-1 showed increased full-length and mature SREBP1 and SREBP2 levels. The downstream upregulation of the targets SCD as well as HMGCS1 and FDFT1, respectively, was also observed. Only ACSS2 levels did not change upon USP25/28 inhibition. To further verify the inhibition of USP28 and the effect on target proteins, c-Myc levels were analysed. As observed for SREBPs, c-Myc levels are increased by USP25/28 inhibition with 10 µM AZ-1. No alteration of the PI3K/Akt pathway, determined by phosphorylation of AKT or GSK3β, under these conditions could be detected (Figure 4-32 **A**).
In this experiment, long-term treatment with iUSP25/28 (48 or 72 hours) induced only slight changes in SREBP level (Figure 4-32 **B**, left and middle panel), whereas SREBP targets as well as c-Myc levels are still induced upon USP25/28 inhibition (Figure 4-32 **B**, right panel). Notably, an activation of the PI3K/Akt pathway by phosphorylation of AKT and GSK3β (lower band) could be detected (Figure 4-32 **B**).

To verify that the upregulation effect of USP25/28 inhibition on SREBP2 targets is mediated by the USP28-SREBP2 axis, iUSP25/28 experiments were performed in A431 shUSP28 and shSREBF2 cell lines (Figure 4-33).

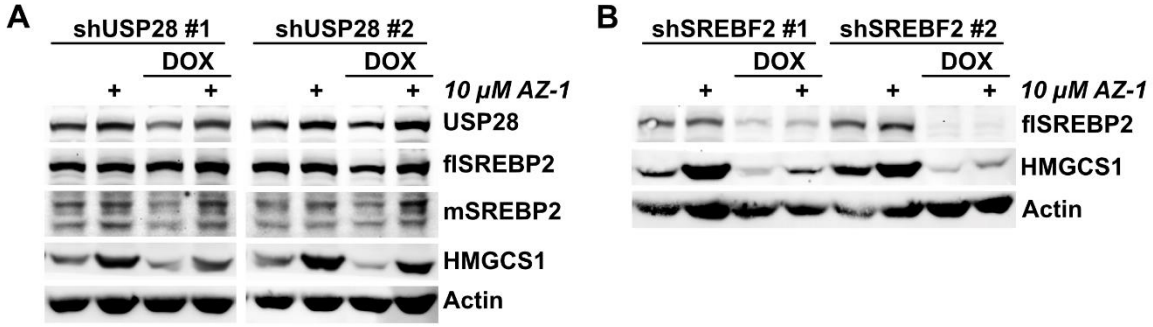

Figure 4-33: iUSP25/28 increases SREBP2 and target gene protein levels also in USP28 and SREBP2 depleted conditions.

*A431 inducible knockdown cell lines for USP28 (****A.****) and SREBF2 (****B.****) were treated with 1 µg/mL doxycycline (DOX) for 96 h. During the last 24 h cells were treated with 10 µM AZ-1 or DMSO as solvent control as indicated. SREBP2 and HMGCS1 protein levels were monitored by immunoblot. Actin served as loading control****.***

The enhancement in band intensity of SREBP2 and HMGCS1 was confirmed in -DOX conditions of shUSP28 cells upon AZ-1 treatment. Knockdown of USP28 by DOX induction revealed only a slight reduction of USP28 levels. Under these conditions, the increase in SREBP2 and HMGCS1 levels upon AZ-1 treatment could still be observed. Notably, a substantial induction of USP28 itself was detected after AZ-1 treatment in the DOX stimulated cells (Figure 4-33 **A**).
HMGCS1 levels upon induction of *SREBF2* knockdown were strongly reduced. Still, AZ-1 treatment resulted in a small increase in HMGCS1 levels also under SREBP2-reduced conditions (Figure 4-33 **B**), indicating that residual amounts of SREBP2 are sufficient for the induction.

4.6.4 AZ-1 treatment mildly affects Co-enzyme Q10 and cholesterol biosynthesis

Inhibition of USP28 with the dual USP25/28 inhibitor AZ-1 revealed synergy with statin treatment in a dose-dependent fashion. Further, the treatment induced SREBP and target gene levels in A431 and U2OS cells.
To further investigate, how the output metabolites of the mevalonate pathway, cholesterol and ubiquinone, are affected by the treatment, LC-MS measurements were performed (Figure 4-34).

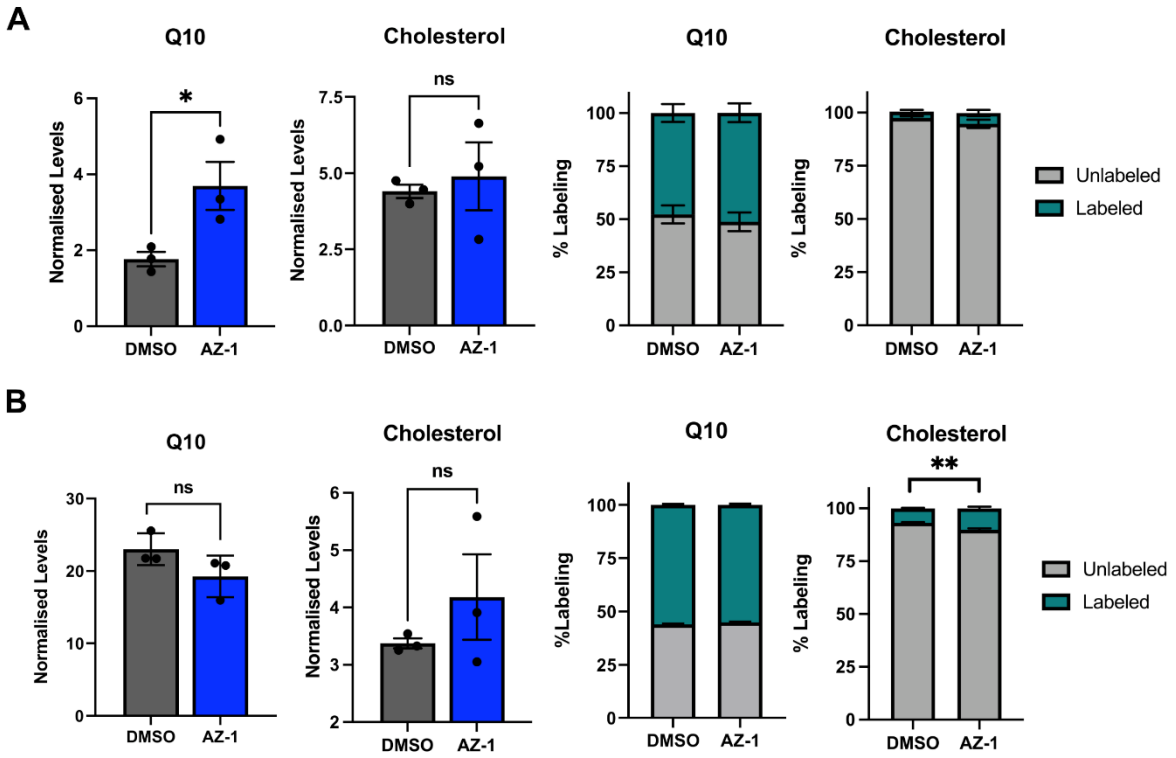

Figure 4-34: Cholesterol and ubiquinone levels show a tendency of increase upon AZ-1 treatment.

*U2OS cells **A.** and A431 cells **B.** were treated with 10 µM AZ-1 for 24 h either in normal conditions or in medium supplemented with 25 mM ^{13}C-glucose. Metabolites were extracted and CoQ10 and cholesterol levels were measured by LC-MS. Peak areas were normalised to cell number or internal standard and protein concentration. Total CoQ10 and cholesterol levels are displayed as mean of triplicates ± SEM. Cells cultivated in medium containing ^{13}C-labeled glucose were lysed and metabolites were extracted. The ratio of labelled Co-enzyme Q10 (CoQ10) and cholesterol was calculated in percent. Bar graphs show fractions of labelled and unlabelled metabolites as mean ± SEM in triplicates. ns = not significant; *, P < 0.05; **, unpaired two-tailed Student t test.*

In U2OS cells, the overall co-enzyme Q10 levels are significantly increased, while cholesterol levels were not changed upon AZ-1 treatment. The flux analysis with ^{13}C-labeled glucose revealed that the inhibitor did not significantly change the biosynthesis of ubiquinone or cholesterol. However, a tendency of a mild increase in labelling pattern was observed (Figure 4-34 **A**).
In contrast, in A431 cells total CoQ10 levels were not affected and cholesterol was somewhat increased but this did not reach significance. The analysis of ^{13}C-glucose labelling confirmed that there are no changes in ubiquinone synthesis but the

synthesis of cholesterol was significantly increased in cells treated with AZ-1 (Figure 4-34 **B**).

4.6.5 Analysis of the activity of USP28 and USP25 upon AZ-1 treatment

USP28 and USP25 show high sequence similarity, rendering the design of specific inhibitors challenging. The small molecule inhibitor AZ-1 engages both DUBs and to verify the inhibition efficiency for USP28 and USP25 under the chosen conditions, a DUB activity assay was performed (Figure 4-35).

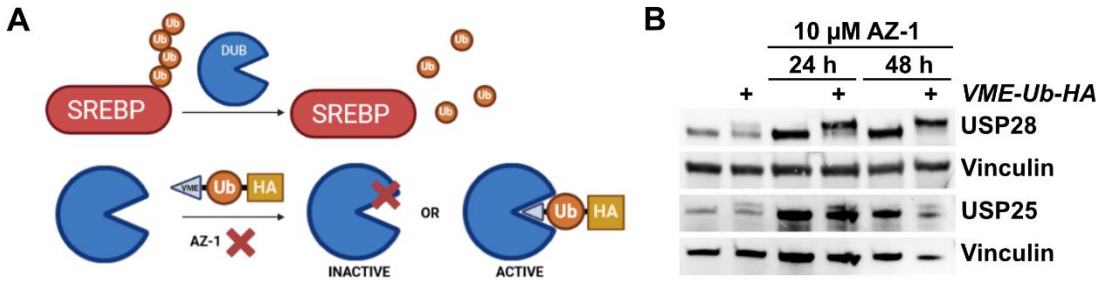

Figure 4-35: DUB acitivity assay with Ub-based DUB probe HA-Ub-VME.

A. *Schematic illustration of the DUB activity assay using an HA-tagged ubiquitin probe. The recognition of the probe by DUBs leads to an irreversible modification of the active site. The thiol-reactive site, here vinyl methyl ester (VME), reacts with the active site cysteine residue forming a covalent bond.* ***B.*** *A431 cells were treated with 10 µM AZ-1 for 24 h or 48 h and cell lysates were incubated with HA-Ub-VME at a final concentration of 2 µM. USP28 and USP25 protein levels were detected in immunoblot, vinculin served as loading control. Mobility shift is indicative of HA-Ub-VME binding****.***

The DUB activity assay is based on the formation of a covalent bond between the catalytic cysteine of USPs and a “suicide probe” mediated by a thiol reactive group, here vinyl methyl ester (VME). The VME is linked to an ubiquitin moiety, which enables the binding, by the DUBs. To detect the active USPs in western blot, the probe contains an additional tag, here HA-tag (Figure 4-35 **A**).
A431 cells treated with AZ-1 for the indicated times were lysed and incubated with the DUB probe. Active USP28 and USP25 were identified on immunoblot by a shift of the band to a higher molecular mass by 10 kDa. In the non-treated control cells, USP28 and USP25 show activity indicated by a double band, where the upper band represented USP28-VME-Ub-HA complexes. Cells treated with AZ-1 showed mainly active USP28 after 24 h and 48 h whereas USP25 only showed weak binding to the probe and was therefore mostly inactive. Notably, the protein concentration was not correctly adjusted, as shown by the loading control vinculin. Still, it is observable that USP28 and USP25 band intensities increased in cells treated with AZ-1. This effect was already observed in Figure 4-33.

4.6.6 USP25 does not directly regulate the active transcription factor mSREBP2

Collectively, the data obtained using the dual USP25/28 inhibitor AZ-1 showed enhanced SREBP2 and target gene levels and conclusively changes in the metabolic pathways in cells. The activity assay showed that under these conditions, the

compound inhibited USP25 rather than USP28. As these two USPs show high sequence identity, to date no specific USP28 inhibitor could be generated.
To analyse, if mSREBP2 could be directly regulated by USP25, the cellular localisation of both proteins was investigated (Figure 4-36).

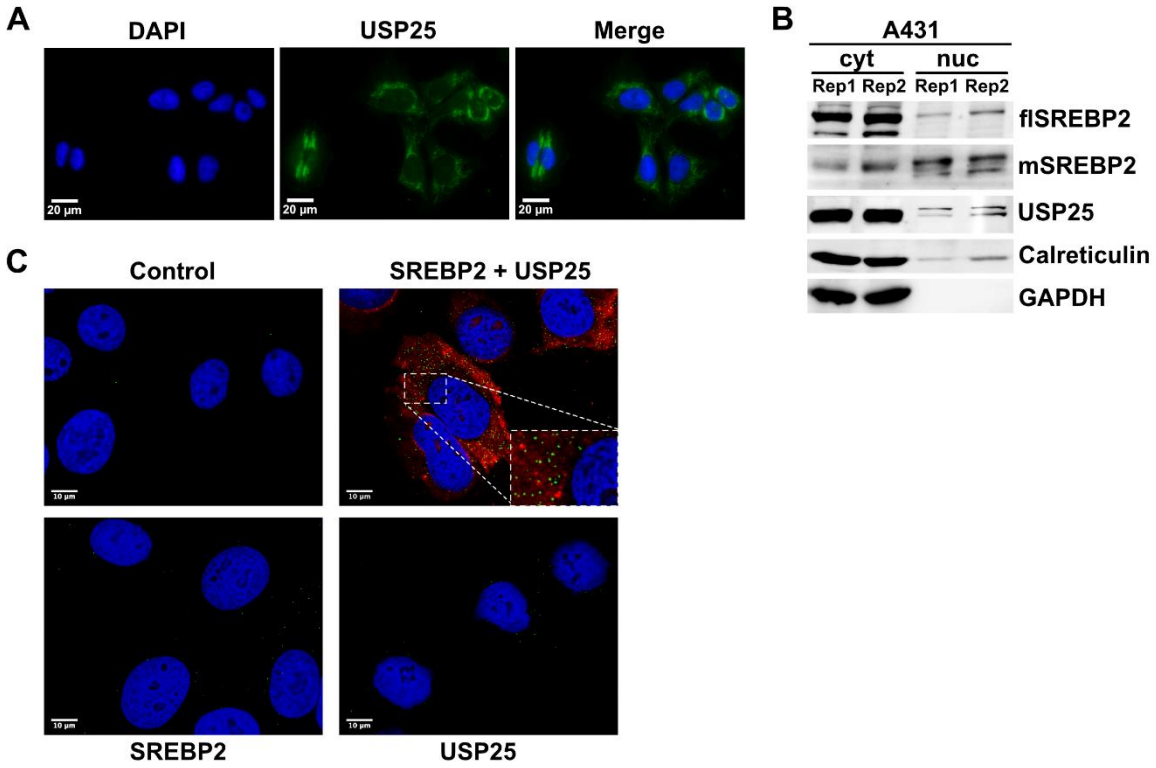

Figure 4-36: USP25 is strictly localised to cytoplasmic and perinuclear area and does not reach the nucleus.

A. *Immunofluorescence staining of USP25 (green) and DNA (blue) in U2OS cells.* ***B.*** *Cellular fractionation of A431 cell lysates and detection of SREBP2 and USP25 in two individual replicates (Rep1, Rep2) by immunoblot. Calreticulin (ER membrane) and GAPDH (cytoplasm) were used as markers for the respective cell compartments.* ***C.*** *Proximity ligation assay in U2OS cells. Nuclear DAPI staining (blue) and PLA signals (green dots) in control cells (primary antibodies only), SREBP2 and USP25 immunostaining individually and USP25 and SREBP2 co-staining (SREBP2 + USP25). GAPDH was additionally stained in red as a cytoplasmic marker.*

The immunofluorescence staining of USP25 revealed strong perinuclear signals, indicating a possible localisation of USP25 at the ER membrane (Figure 4-36 **A**).
Subcellular fractionation of A431 cells detected USP25 in the cytoplasmic and membrane-bound fraction, which is verified by the cytoplasmic marker GAPDH and the ER membrane-bound protein Calreticulin (Figure 4-36 **B**).
A proximity ligation assay showed signals of close proximity of USP25 and SREBP2 (monitored by green dots in Figure 4-36 **C**), while controls only showed occasional signals. The proximity signals were restricted to the perinuclear and cytoplasmic region of the cell and no close proximity within the nucleus was observed (Figure 4-36 **C**).

In conclusion, experiments show that the dual USP25/28 inhibitor AZ-1 affects cell viability in a dose- and time-dependent manner. A synergy of AZ-1 with statin treatment could be observed at high concentration of both inhibitors. Further, the effects of AZ-1 on SREBPs and target genes were distinct in U2OS and A431 cells.

However, both cell lines showed increased SREBP and target gene protein levels when treated with inhibitor for longer than 24 h. At this time point, only slight changes in metabolites synthesized by the mevalonate pathway were observed. The DUB activity assay revealed an inhibition of USP25 rather than USP28 under these conditions. The hypothesis that USP25 could possibly be involved in the regulation of SREBPs was addressed by co-localisation experiments. USP25 strictly localised outside of the nucleus not being in contact with the active transcription factor mSREBP2. Proximity ligation assays showed positive signals in cytoplasm and perinuclear, indicating a possible regulation of the precursor SREBP2 by USP25 at the ER. This hypothesis needs to be further investigated.

4.7 The role of the USP28-SREBP2 regulatory axis in squamous tumours

USP28 was recently shown to play an important role in squamous tumours (Prieto-Garcia *et al.* 2020). Indeed, previous experiments in the squamous A431 cell line showed that cells require USP28 for viability (Figure 4-19). Additionally, the reduction of USP28 levels resulted in altered mevalonate pathway activity (Figure 4-15) and sensitized cells to statin treatment (Figure 4-25 and Figure 4-28). This indicates that the USP28-SREBP2 regulatory axis could be of great importance for cell growth and viability in squamous tumour entities.
In a recent study in esophageal squamous cell carcinoma (ESCC) it was shown that SREBP2 was upregulated and promoted cell viability. Further, a co-operation between c-Myc and SREBP2 was observed in regulating HMGCR, the key enzyme in the mevalonate pathway (Zhong *et al.* 2019).

4.7.1 SREBP2 expression and induction is increased in squamous cancer cell lines

To focus further on the contribution of SREBP2 regulation by USP28 in squamous cancer cell lines, SREBP2 expression, induction and sensitivity to statin treatment was investigated in squamous cancer and adenocarcinoma-derived cell lines from several cancer entities (Figure 4-37).

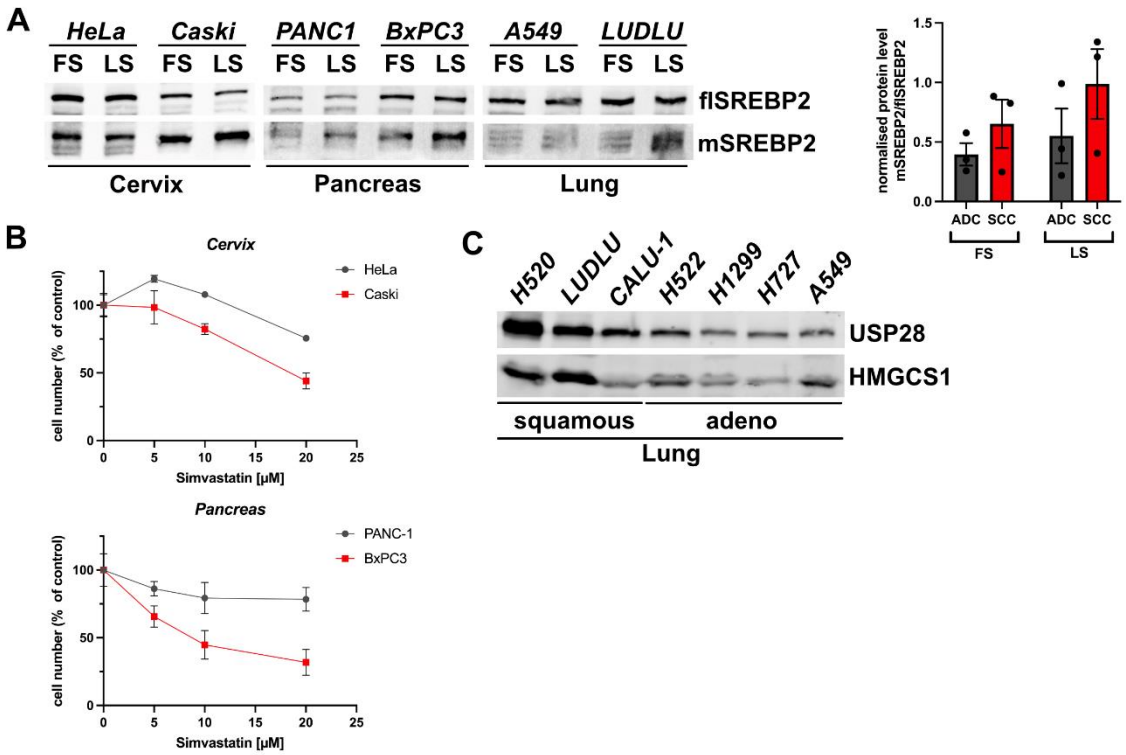

Figure 4-37: Squamous cancer cell lines show high expression of SREBP2 and are sensitive to statin treatment.

A. *Pairs of adenocarcinoma (HeLa, PANC-1, A549) and squamous (Caski, BxPC3, LUDLU) cell lines from cervix, pancreas and lung, respectively, were analysed regarding SREBP2 expression by immunoblot. Cells were cultivated under full serum (FS) or low serum (LS) conditions for 24 h prior lysis. SREBP2 levels were normalised to total protein and graph shows mean ± SEM of mSREBP2/flSREBP2 ratio of adenocarcinoma cell lines (ADC) and squamous cell lines (SCC).* ***B.*** *Squamous (Caski, BxPC3) and adenocarcinoma (HeLa, PANC-1) cell lines were treated with increasing concentrations of simvastatin. Cell viability was determined by crystal violet staining. Bar graph shows crystal violet staining intensity of ADC (grey) and SCC (red) cell lines as mean ± SEM of triplicates for increasing concentrations of simvastatin.* ***C.*** *A panel of lung cancer cell lines were analysed by immunoblot for expression of USP28 and HMGCS1.*

Cell line pairs of adenocarcinomas (ADC) and squamous cell carcinomas (SCC) from different tumour entities were analysed regarding the expression and activation state of SREBP2 in normal and serum-deprived conditions. The cervical squamous cell line Caski showed increased mSREBP2 levels compared the adenocarcinoma cell line HeLa. In both cell lines, an induction of SREBP2 processing in LS conditions was not observed. The pancreatic squamous cell line BxPC3 showed increased overall SREBP2 levels compared to the ADC pendant PANC-1. Increased levels of mSREBP2 under serum-deprived conditions were observed in both cell lines. In the SCC lung cancer cells LUDLU higher mSREBP2 levels were observed compared to the ADC line A549. The induction by LS treatment of the cells was higher in LUDLU compared to A549. Overall, the SCC cell lines showed a tendency towards higher ratio of mSREBP2/flSREBP2 compared to ADC cells (Figure 4-37 **A**).

Comparison of the cervical and pancreatic ADC and SCC pairs regarding their sensitivity to simvastatin treatment showed, that SCC cell lines (Caski and BxPC3; red) were more sensitive than ADC (HeLa, PANC-1; grey) cell lines (Figure 4-37 **B**).

Moreover, the correlation of USP28 and HMGCS1 expression in a panel of lung cancer cell lines was monitored by immunoblot. A positive correlation of the proteins could be detected: Squamous cell lines showed high protein levels of USP28 and HMGCS1, while levels were lower in adenocarcinoma-derived lung cancer cell lines (Figure 4-37 **C**).

4.7.2 SREBP2 and target genes are upregulated in squamous lung cancer and correlate with USP28 expression

Since the importance of USP28 in squamous lung cancer by regulating the transcription factor ΔNp63 was revealed in a recent study by Prieto-Garcia et al. (Prieto-Garcia *et al.* 2020, Prieto-Garcia *et al.* 2021), the contribution of SREBP2 in this context was further investigated.
Expression data from The Cancer Genome Atlas (TCGA) program of the National Cancer Institute was used to analyse expression and correlation of USP28 and SREBP2 in lung SCC and ADC (Figure 4-38).

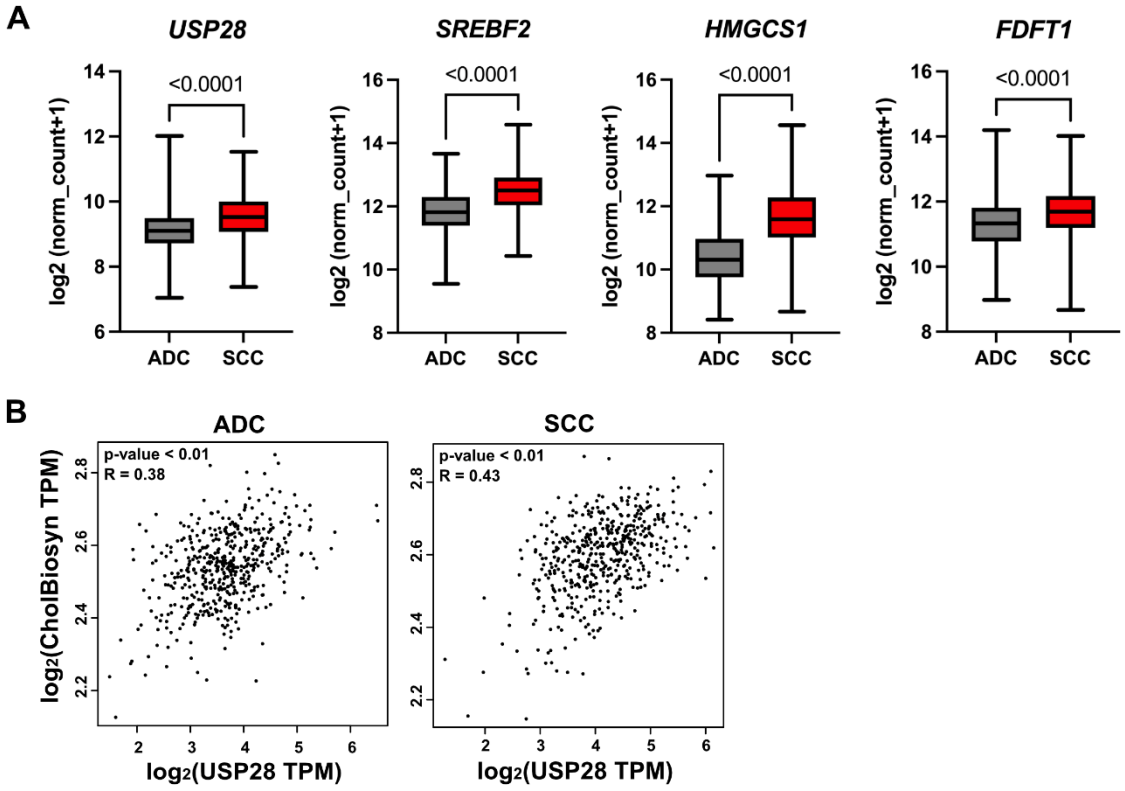

Figure 4-38: USP28 and SREBP2 are upregulated in lung SCC compared to ADC and their expression is correlating in both subtypes.

A. *Graphs showing expression of USP28 and SREBP2 as well as the target genes HMGCS1 and FDFT1 in human lung ADC (706 samples) and SCC (626 samples) datasets of the TCGA (National Cancer Institute). P < 0.0001, unpaired two-tailed Student t test.* ***B.*** *Correlation of USP28 and the Reactome Cholesterol Biosynthesis gene set was calculated by GEPIA2 software. R-value was determined by Pearson correlation. TPM = transcripts per million.*

Expression data for *USP28* as well as *SREBF2* and target genes *HMGCS1* and *FDFT1* was downloaded from TCGS via the UCSC Xena browser. The comparison of human lung ADC samples to SCC samples showed highly significant increased

expression of all genes, thus indicating that lung squamous tumours could be dependent on elevated levels of enzymes involved in the mevalonate pathway (Figure 4-38 **A**).
To investigate a potential correlation of USP28 and expression of genes coding for proteins catalysing reactions within the mevalonate pathway, a correlation analysis of *USP28* expression and the expression of the Reactome Cholesterol Biosynthesis gene set in lung ADC and SCC with the GEPIA2 software was performed. The Pearson correlation index und significance was calculated by the software. In lung ADC and SCC, correlation indices of 0.38 and 0.43, respectively, were observed (Figure 4-38 **B**).

These results supported the hypothesis that the USP28-SREBP2 regulatory axis is important in lung cancer, especially in squamous lung tumours. To gain insights into the role of SREBP2 in lung cancer, squamous and adenocarcinoma cell lines were analysed regarding SREBP2 expression, activity and their sensitivity to inhibition of the mevalonate pathway by statin treatment (Figure 4-39).

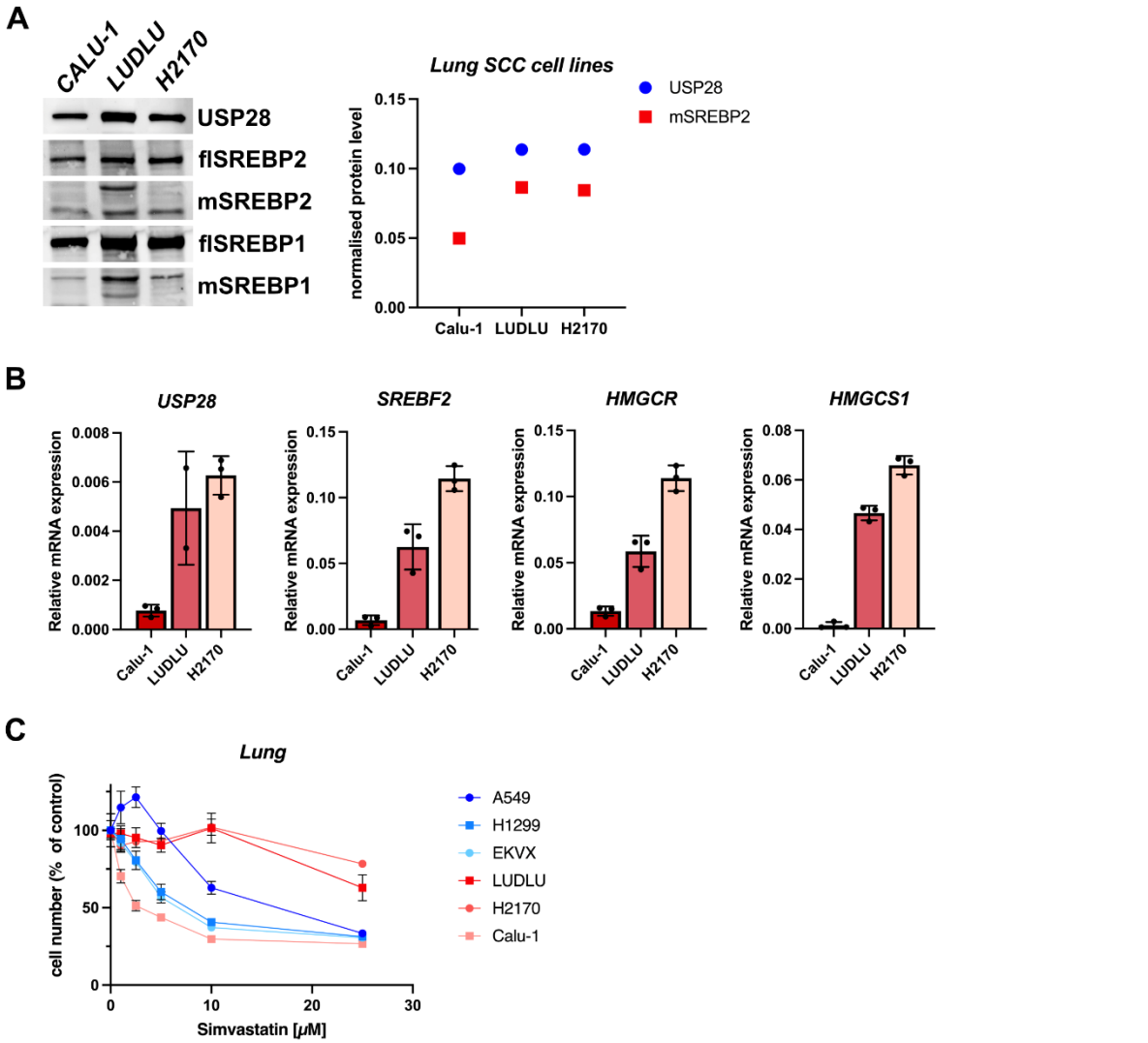

Figure 4-39: High levels of USP28 correlates with SREBP2 levels in lung SCC cell lines and shows decreased sensitivity to statin treatment.

A. *SREBP and USP28 expression in squamous human lung cancer cell lines LUDLU, H2170 and Calu-1 was analysed by immunoblot. Graph shows band intensities of USP28 and mSREBP2 normalised to total protein.* ***B.*** *Quantitative RT-PCR of USP28, SREBF2 and target gene mRNA levels in squamous cell lines from A. . $2^{-\Delta Ct}$ values were calculated and graph represents mean ± SEM of triplicates. C. Adenocarcinoma (A549, H1299, EKVX) and squamous (LUDLU, H2170, Calu-1) lung cancer cell lines were treated with increasing concentrations of simvastatin for 48 h. Cell viability was monitored by crystal violet and staining intensity was measured and normalised to solvent control****.***

The squamous lung cancer cell lines Calu-1, LUDLU and H2170 showed differences in USP28 and SREBP1 and 2 levels. In tendency, USP28 expression correlated with the expression of SREBPs. USP28 and mSREBP2 band intensities were normalised to total protein per lane (determines by in gel staining) and illustrated in a graph, revealing potential co-regulation of both proteins (Figure 4-39 **A**).
mRNA levels of *USP28* and *SREBF2* as well as the target genes *HMGCS1* and *HMGCR* were determined by qPCR analysis. While Calu-1 cells contained only low levels of mRNA for *USP28* and *SREBF2* and target genes, LUDLU and H2170 cells showed higher expression of these genes (Figure 4-39 **B**).
To investigate the sensitivity of lung SCC and ADC cell lines towards statin treatment, cells were incubated with increasing concentrations of simvastatin and cell viability was determined. In the experiment shown in Figure 4-37, SCC cell lines of cervical and pancreatic cancer were more sensitive to statin treatment compared to tissue-matched ADC cell lines. Unexpectedly, lung ADC cell lines showed increased sensitivity to simvastatin compared to SCC LUDLU and H2170 cell lines. Notably, the Calu-1 cell line with comparatively low levels of USP28 and SREBP2 showed increased sensitivity to statin treatment comparable to ADC cell lines (Figure 4-39 **C**). These results also match the previous observation that A431 cells with reduced USP28 levels were more sensitive to simvastatin treatment (Figure 4-25).

4.7.3 SREBP2 and target genes are upregulated in mouse lung cancer *in vivo*

To further investigate the role of the USP28-SREBP2 regulatory axis *in vivo*, mouse lung cancer samples were analysed regarding the expression of USP28 and SREBP2 as well as its target gene HMGCS1.
A virus-based method for implementing mouse lung tumours was established by Hartmann et al. (Hartmann *et al.* 2021). Via the CRISPR/Cas9 technology, an activation mutation of $KRas^{G12D}$ was introduced and an additional loss of *TP53* was targeted. Hereby, $Rosa26^{Cas9\text{-}IRES\text{-}eGFP}$ mice were infected with adeno-associated virus (AAV) encoding single guide RNAs (sgRNAs) targeting *TP53* and *KRas*, while supplying simultaneously a homologous repair construct introducing the $KRas^{G12D}$ mutation.
The liver kinase B1 (Lkb1), also termed serine/threonine kinase 11 (STK11), is an upstream kinase of adenosine monophosphate-activated protein kinase (AMPK). In turn, AMPK regulates the mTOR pathway, which tightly regulates the activity of SREBPs. Lkb1 deficiency is associated with tumour growth in various tumour types and has been observed to accelerate tumour development by inducing metabolic reprogramming (Zhang *et al.* 2021).

Lung tissue of mice infected with either KRas and TP53 construct (KP) or additional sgRNA targeting Lkb1 (KPL) was analysed regarding the expression of HMGCS1 in tumours compared to non-transformed tissue (Figure 4-40).

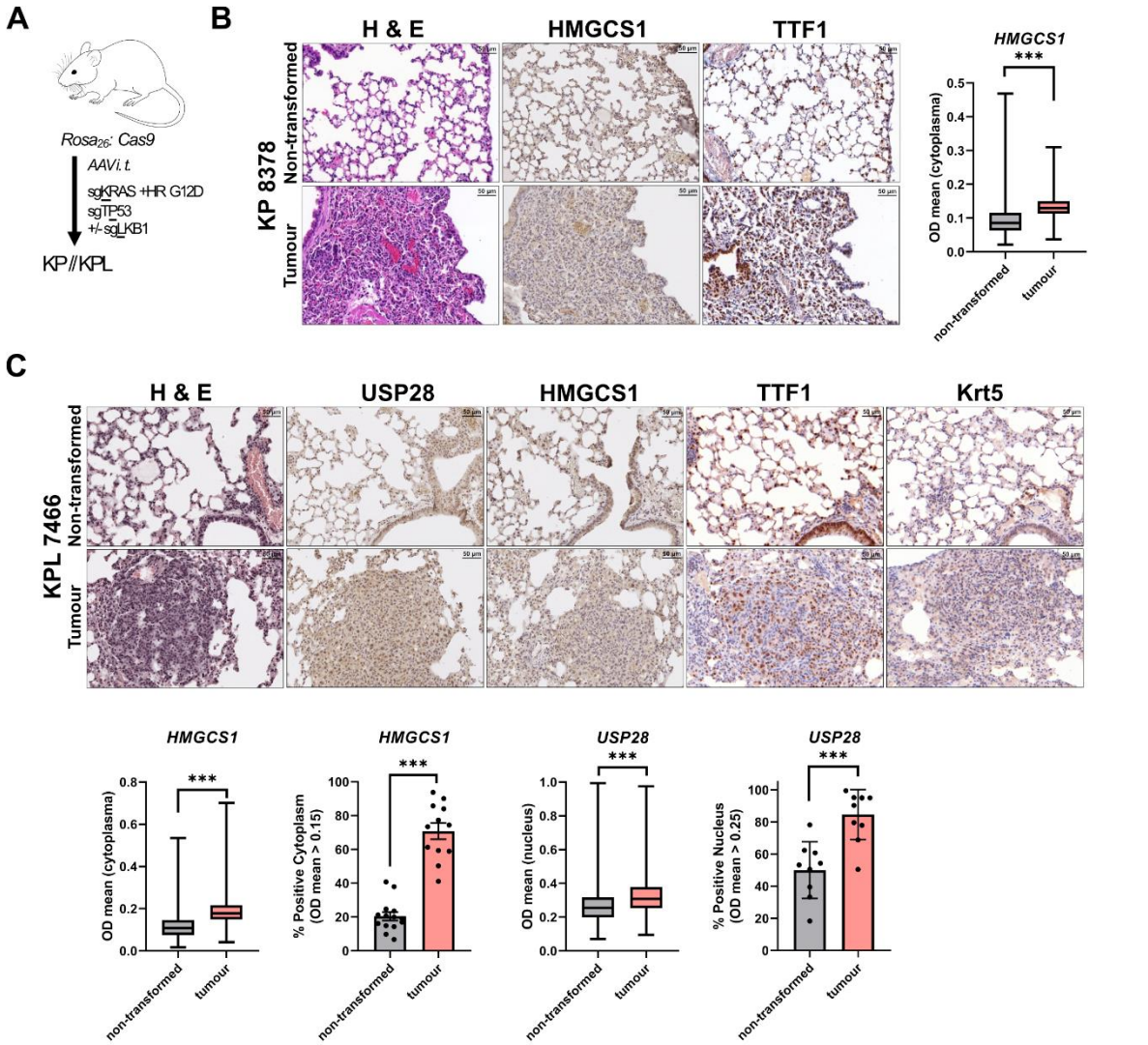

Figure 4-40: Lung tumours of KP and KPL mice showed significantly increased USP28 and HMGCS1 levels compared to non-transformed tissue.

A. *Schematic illustration of the generation of KP and KPL mice. Cas9-expressing mice are intratracheally (i.t.) infected with adeno-associated virus (AAV) containing sgRNAs for KRAS and TP53 (KP) or additionally sgRNAs for LKB1 (KPL).* ***B.*** *Paraffin embedded lung tissue of KP mice was sectioned and stained by immunohistochemistry for haematoxylin and eosin (H&E), HMGCS1 and thyroid transcription factor 1 (TTF1). Upper panel represents representative areas of non-transformed tissue, lower panel shows staining in tumour tissue. Cytoplasmic HMGCS1 staining was quantified using the QuPath software analysing three non-transformed lung tissue areas and three independent tumour areas with a total number of >3800 cells. Quantified staining is shown as OD mean in cytoplasm of non-transformed and tumour tissue as boxplot graph (Min to Max, vertical line indicates mean value and box show 25th to 75th percentile).* ***C.*** *Paraffin-embedded lung tissue of KPL mice was sectioned and stained by immunohistochemistry for haematoxylin and eosin (H&E), USP28 and HMGCS1. Upper panel represents representative areas of non-transformed tissue, lower panel shows staining in tumour tissue. Cytoplasmic HMGCS1 and nuclear USP28 staining was quantified using the QuPath software analysing >9 independent non-transformed lung tissue and tumour areas with >15000 cells, respectively. Quantified staining is shown as OD mean in cytoplasmic HMGCS1 or nuclear USP28 of non-transformed and tumour tissue as boxplot graph (Min to Max, vertical line indicates mean value and box show 25th to 75th percentile). ***, P < 0.001; unpaired two-tailed Student t test. H & E = Haematoxylin and eosin. OD = optical density.*

Mice harbouring a Cas9 expression cassette in the Rosa26 locus constitutively express the DNA endonuclease ubiquitously were used for these experiments. Lung tumour formation was induced by supplying sgRNAs for respective targets via intratracheal (i.t.) AAV delivery. Experiment was terminated 12 weeks post infection or when mice showed symptoms (Figure 4-40 **A**) Tumour induction and histological analyses were conducted in close collaboration with Oliver Hartmann and Markus Diefenbacher, Biocenter Würzburg.
Lungs of KP mice were paraffin-embedded, sectioned and stained for HMGCS1. Haematoxylin and eosin (H & E) staining revealed high tumour content. In a direct comparison of cytosolic HMGCS1 staining intensity in non-transformed and tumour tissue, a significant increase in staining was observed within tumour tissue. Thyroid transcription factor 1 (TTF1) staining was used as a marker to determine tumour subtype. Strong TTF1 staining indicated the development of adenocarcinomas (Figure 4-40 **B**).
It was shown that an additional Lkb1 loss significantly enhances tumour burden and increases tumour cell proliferation when compared to KP mutational background (Hartmann *et al.* 2021). Further, Lkb1 deficiency is associated with metabolic reprogramming, including the upregulation of SREBP activity (Zhang *et al.* 2021).
Staining of tumour and non-transformed tissue for USP28 and HMGCS1 expression in KPL mice revealed significantly higher expression levels in tumour tissue compared to wild type tissue. Thus showing that with the genetic background of KRas, TP53 and Lkb1 mutation, USP28 and SREBP2 expression is highly upregulated in tumours indicating a pivotal role of these factors in tumour development or maintenance (Figure 4-40 **C**).

The detailed analysis of the KPL mouse model revealed both tumour subtypes: adenocarcinomas (ADC) and squamous cell carcinomas (SCC), whereas the KP model exclusively resulted in the development of adenocarcinomas (Prieto-Garcia *et al.* 2020). Since previous data showed a higher expression of *USP28* and *SREBF2* in human SCC tumours (Chapter 4.7.2), the classification of the tumours obtained in the KPL mouse model was further investigated (Figure 4-41).

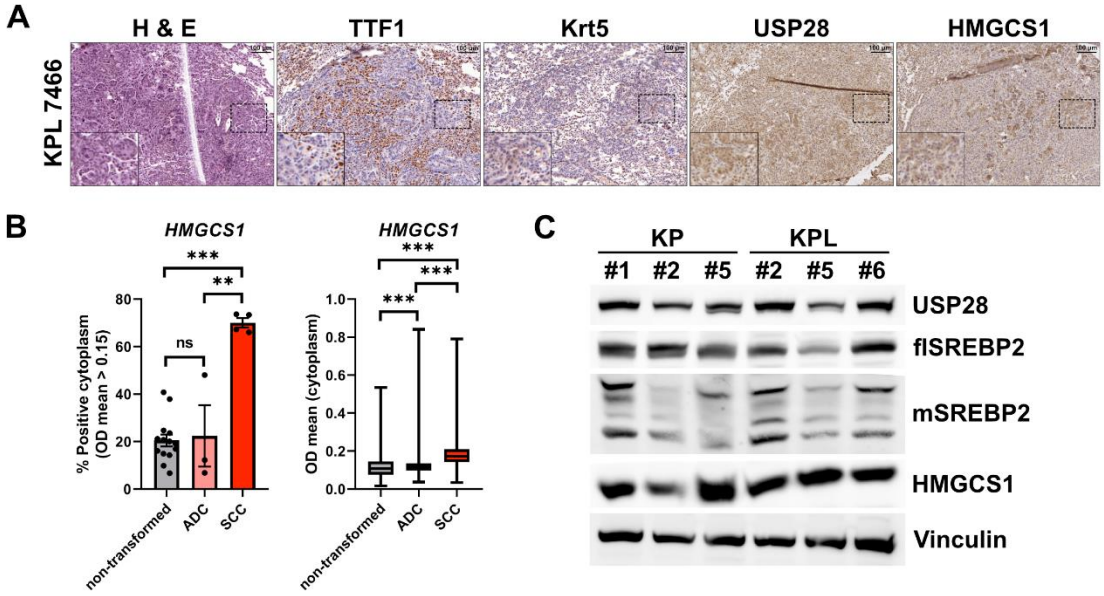

Figure 4-41: Squamous and adenocarcinoma lung cancer tumour regions show differences in HMGCS1 expression in KPL mice.

***A**. Paraffin-embedded lung tissue of KPL mice was sectioned and stained by immunohistochemistry for haematoxylin and eosin (H&E), thyroid transcription factor 1 (TTF1) as marker for adenocarcinomas, Keratin 5 (Krt5) as marker for squamous tumours, USP28 and HMGCS1. Panel represents representative areas of tumour tissue. Enlarged section is shown in lower left corner. **B.** Based on marker staining, prevalently squamous and adenocarcinoma tumour areas were identified in KPL mice. Cytoplasmic HMGCS1 staining was quantified using the QuPath software analysing four squamous areas (SCC), three adenocarcinoma areas (ADC) and 14 non-transformed areas with 11000< cells, respectively. Quantified staining is shown as % positive cells with a threshold of OD mean > 0.15 for cytoplasmic HMGCS1 staining (left graph) and OD mean of cytoplasmic HMGCS1 in non-transformed, ADC and SCC areas as boxplot graph (Min to Max, vertical line indicates mean value and box show 25th to 75th percentile, right graph). **C.** Three individual KP and KPL cell lines, isolated from tumour tissue of KP and KPL mice were analysed by immunoblot for expression of USP28, SREBP2 and HMGCS1. Vinculin is shown as loading control. ns, not significant; **, P< 0.01; ***, P < 0.001; unpaired two-tailed Student t test. H & E = Haematoxylin and eosin. OD = optical density.*

Lung tumour sections of KPL mice were stained with the SCC marker keratin 5 (Krt5) and the ADC marker thyroid transcription factor 1 (TTF1). The marker staining showed squamous areas as well as adenocarcinomas. It was observed that the tumours did not show exclusive positivity for Krt5 or TTF1, but rather a co-existence of cells from both subtypes within each lesion (Figure 4-41 **A**).

Based on the marker staining, ADC and SCC regions were identified and HMGCS1 staining intensity was determined. The quantification of the staining showed significant differences in HMGCS1 expression in the defined SCC compared to ADC regions (Figure 4-41 **B**). While HMGCS1 expression in ADC areas did not differ from the intensity observed in non-transformed tissue, HMGCS1 levels were strongly increased in prevalent SCC areas.

Observing multifold increase in HMGCS1 expression in KPL mice compared to KP mice (Figure 4-40 **B** and **C**), isolated mouse KP and KPL tumour cell lines were analysed by immunoblot for USP28, SREBP2 and HMGCS1. However, cultivated cell lines did not show differences in expression levels of these proteins when comparing KP and KPL background (Figure 4-41 **C**).

In conclusion, *in vivo* data showed elevated expression levels of USP28 and HMGCS1 in lung tumours induced by mutations in KRas, TP53 and Lkb1. The classification into squamous and adenocarcinoma regions in the tumour showed differences in expression of cytoplasmic HMGCS1. Isolated tumour cell lines from KP and KPL mice did not differ distinctly in the expression of either USP28 or SREBP2 and HMGCS1. Cell lines were not classified for SCC or ADC markers.

4.7.4 USP28 KO reduced SREBP2 and HMGCS1 levels in lung tumours in mice

Prieto-Garcia and colleagues used the above-described KPL mouse model and additionally targeted USP28 for knockout in mouse lung tumours (Prieto-Garcia *et al.* 2020). This study revealed that USP28 knockout in this mouse lung cancer model (KPLU) resulted in decreased tumour area per lung area and an overall reduced number of tumours. Further analyses regarding tumour type revealed that loss of USP28 abolished the presence of SCC tumours. Additionally, the survival of KPLU mice was significantly prolonged compared to KPL mice.
To unravel the role of SREBP2 in the context of the lung cancer mouse model in presence and absence of USP28, mouse lung tissue from KPL and KPLU mice was analysed for the expression of SREBP2 and its target genes (Figure 4-42).

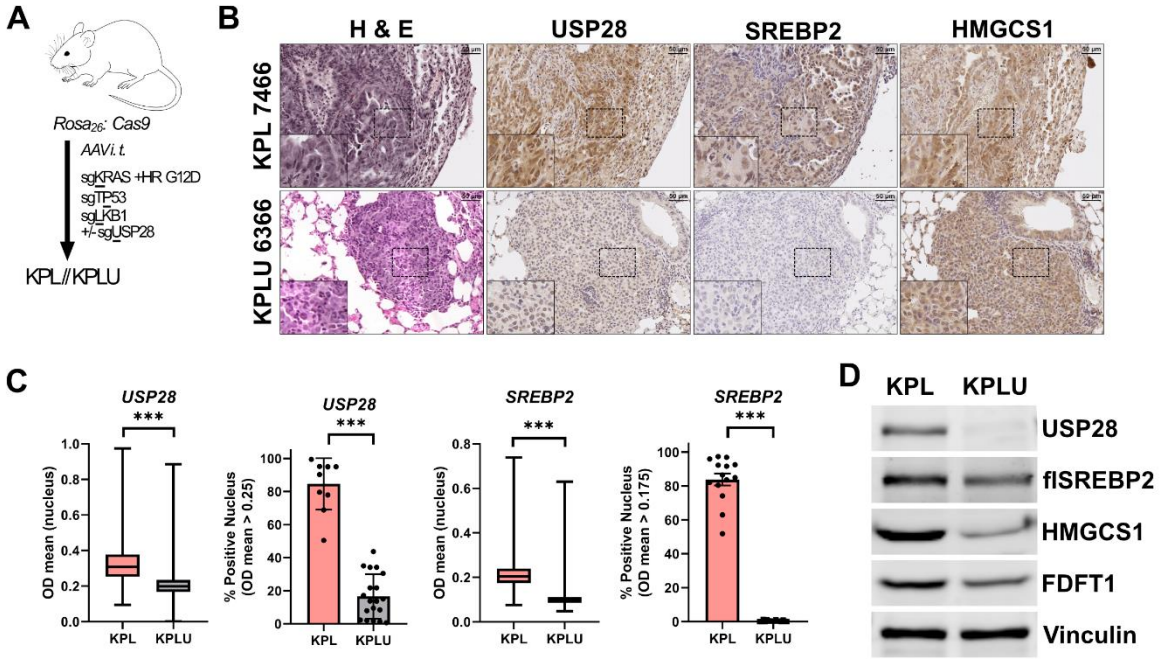

Figure 4-42: Loss of USP28 in vivo results in decreased levels of SREBP2 and its target genes.

A. *Schematic illustration of the generation of KPL and KPLU mice. Cas9-expressing mice are intratracheally (i.t.) infected with adeno-associated virus (AAV) containing sgRNAs for KRAS (together with homologues repair construct KRAS^{G12D}), TP53, Lkb1 (KPL) and additionally sgUSP28 (KPLU).* ***B.*** *Paraffin-embedded lung tissue of KPL and KPLU mice was sectioned and stained by immunohistochemistry for haematoxylin and eosin (H&E), USP28, SREBP2 and HMGCS1. Panel represents representative areas of tumour tissue. Enlarged section are shown in lower left corner.* ***C.*** *Nuclear USP28 and SREBP2 staining was quantified using QuPath software. Graph shows staining intensities for USP28 and SREBP2 as % positive using a threshold of OD mean > 0.25 or OD mean > 0.175, respectively. OD mean of cellular USP28 and SREBP2 is shown as boxplot graph (Min to Max, vertical line indicates mean value and box show 25th to 75th percentile). In total more than 10 tumour areas of KPL and KPLU mice were used with > 17000 cells for each genetic background.* ***D.*** *Tumours of KPL and KPLU mice were*

*lysed and analysed by immunoblot for expression of USP28, SREBP2 and target genes HMGCS1 and FDFT1. Vinculin is shown as loading control. ***, P < 0.001; unpaired two-tailed Student t test. H & E = Haematoxylin and eosin. OD = optical density.*

To confirm that USP28 regulates SREBP2 *in vivo*, lung tumours of KPL and KPLU mice (Figure 4-42 **A**) were stained for USP28, SREBP2 and the downstream target HMGCS1.
As shown before, KPL tumours show high staining intensity of USP28, SREBP2 and HMGCS1 while the knockdown of USP28 in the lung tumours resulted in decreased intensity of SREBP2 and HMGCS1 staining (Figure 4-42 **B**).
Quantification of USP28 and SREBP2 staining revealed strong reduction in nuclear SREBP2 protein levels upon loss of USP28 (Figure 4-42 **C**).
The analysis of protein levels in lysates from macroscopically excised primary lung tumours of KPL and KPLU mice by immunoblot (Figure 4-42 **D**) confirmed the knockout of USP28 and showed reduced levels of flSREBP2 and the downstream target genes HMGCS1 and FDFT1. The reduction in full-length SREBP2 could be a consequence of reduced mSREBP2 levels due to the feedback regulatory loop of SREBPs.

Taken together, SREBP2 and its target genes are highly expressed in squamous lung tumours. This is similar to the results shown before for demonstrating that USP28 is upregulated in squamous lung tumours (Prieto-Garcia *et al.* 2020). The knockout of USP28 *in vivo* resulted in a strong reduction of SREBP2 and its target genes in lung tumour tissue. This finding supports the notion that SREBP2 and the regulation of the mevalonate pathway play an essential role in the development and progression of squamous lung cancer.

4.7.5 Loss of SREBP2 reduces tumour formation and progression *in vivo*

SREBP2 is a master regulator of the mevalonate pathway and controls the cellular metabolite pool for cholesterol biosynthesis, Coenzyme Q10 synthesis and posttranslational modification of proteins by farnesylation and prenylation. Reduced SREBP2 protein levels affected cell growth (Figure 4-19) and the ability to form colonies (Figure 4-21) in squamous cancer cell lines, most likely by a reduction of *de novo* synthesized metabolites (Figure 4-22). High SREBP2 levels were found in human squamous lung cancer tissue (Figure 4-38) and squamous lung cancer cell lines with high SREBP2 expression showed reduced sensitivity towards mevalonate pathway inhibition by simvastatin treatment (Figure 4-39).
To elucidate the role and the contribution of SREBP2 in squamous lung cancer a murine SREBP2 knockout tumour model was established.
For CRISPR/Cas9-mediated knockout of SREBPs in an *in vivo* mouse model, knockout constructs were generated. sgSREBF2 guide RNAs were designed and cloned into the pCRISPRv2 vector containing the Cas9 coding sequence. Positively transfected cells were selected by CRISPRv2-mediated resistance to puromycin. To test the knockout efficiency of the guide RNAs prior to use *in vivo*, AKT or Ras driven

murine hepatocellular carcinoma cell lines (Rudalska *et al.* 2014) (mHCC AKT and mHCC Ras, respectively) were transfected with the knockout constructs, selected for puromycin resistance and analysed for double strand breaks in the *SREBF2* locus by T7E1 assay and for SREBP2 protein levels by immunoblot (Figure 4-43).

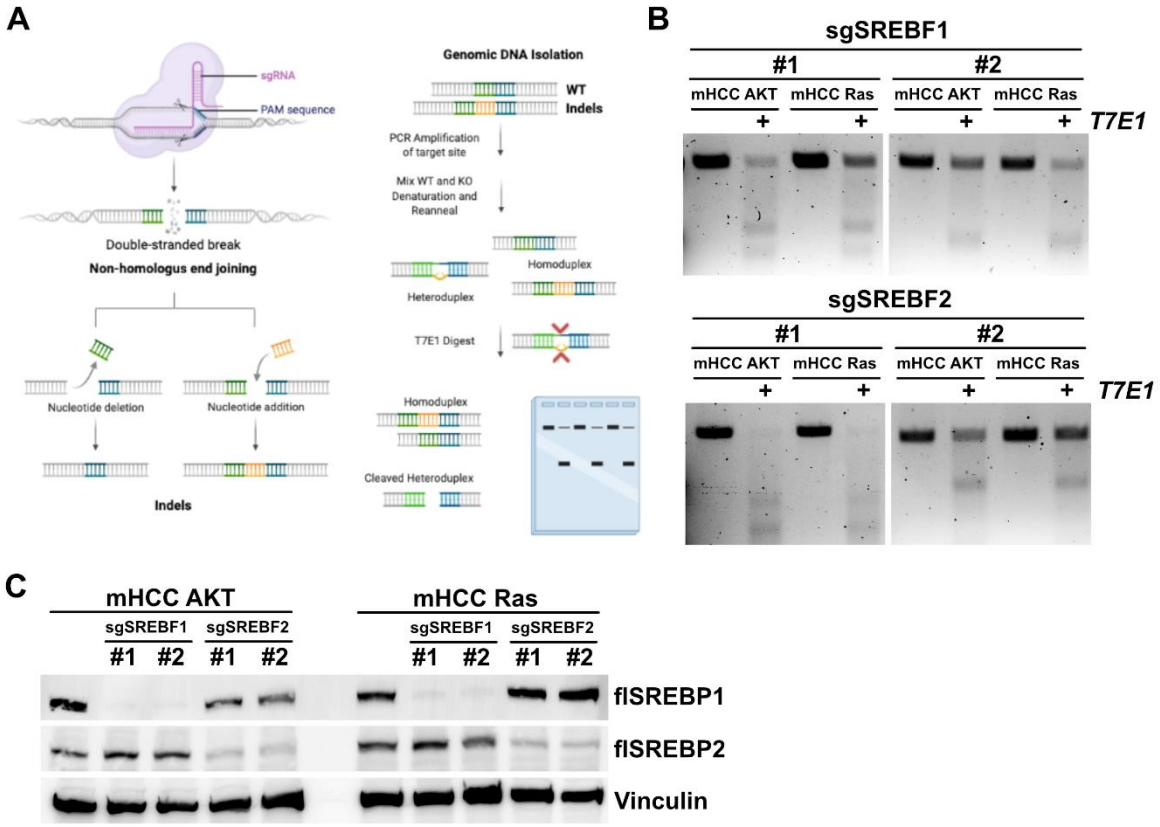

Figure 4-43: Evaluation of CRISPR/Cas9 Knockout constructs targeting SREBF2 in vivo.

A. *Schematic representation of the CRISPR/Cas9 Knockout strategy and T7 Endonuclease 1 (T7E1) assay. Single-stranded guide RNAs (sgRNAs) are used by the endonuclease Cas9 to mediate double strand breaks in the specific gene locus and this results in nucleotide deletions or additions (indels). After genomic DNA isolation, the gene locus is amplified by PCR and DNA of WT and KO cells are mixed. Subsequent denaturation and reannealing forms either homoduplexes or heteroduplexes with nicks. Nicks are recognized by T7E1, which cleaves the heteroduplex, and resulting DNA fragments are analysed on agarose gel.* ***B.*** *Two guide RNAs (#1 and #2) for either SREBF1 or SREBF2, respectively, were cloned into the pLenti-CRISPR v2 expression vector and mouse-derived hepatocellular carcinoma (mHCC) cells with either a mutation in AKT or Ras were infected with viral particles containing guide RNAs and coding sequence of Cas9. Positive transfected cells were selected by puromycin selection. Genomic DNA was extracted and T7E1 assay was performed. Respective size of DNA fragments was visualized on agarose gel. C. mHCC AKT and mHCC Ras SREBF1 and SREBF2 KO cell lines were lysed and proteins were analysed by immunoblot for protein levels of SREBP1 and SREBP2. Vinculin is shown as loading control. PCR = Polymerase Chain Reaction. WT = Wild type. KO = Knockout****.***

mHCC SREBP2 KO cell lines were generated by virus-mediated stable transfection and subsequent selection for plasmid integration in cell pools. To analyse the *SREBF2* gene locus regarding double strand breaks and subsequent insertion or deletion (indels) of base pairs, T7E1 assay was performed (Figure 4-43 **A**). Genomic DNA was isolated from SREBP2 KO, SREBP1 KO and control cells and *SREBF1* and *SREBF2* gene locus was amplified by PCR 300-700 bps upstream and downstream of the respective gRNA target sites. PCR products were purified and WT and KO amplicons

were mixed in a 1:1 ratio. Double strands were denaturated and slowly re-annealed. Heteroduplexes of WT and KO strands formed nicks, which are recognised by T7 Endonuclease 1 and are subsequently cleaved at this site. Either 2x 500 bp or 300 + 700 bp fragments are visualised upon addition of T7E1 on agarose gel (Figure 4-43 **B**). The analysis of the *SREBF1* and *SREBF2* gene locus in SREBP1 and SREBP2 KO mHCC cell lines revealed indels at the sgRNA target sites caused most likely by a double strand break due to the CRISPR/Cas9 KO system.
SREBP1 and SREBP2 protein levels of *SREBF1* KO and *SREBF2* KO mHCC cell lines were analysed by immunoblot. *SREBF1* KO cell lines showed decreased SREBP1 protein levels compared to the control cell line, while SREBP2 levels were not changed. *SREBF2* KO cell lines showed decreased SREBP2 protein levels, while SREBP1 levels stayed stable (Figure 4-43 **C**). Band intensities revealed nearly complete knockout of SREBP1 and efficient knockout of SREBP2 in the generated pooled KO cell lines.

To further investigate the contribution of SREBP2 in the development and progression of squamous lung cancer, $Rosa_{26}$:Cas9 mice were intratracheally infected with adeno-associated virus containing sgRNAs for KRas (together with a repair construct to generate $Kras^{G12D}$), Tp53 and Lkb1 (KPL mice) as described before. For additional knockout of *SREBF2*, the tested sgRNAs #1 and #2 (Figure 4-43) were cloned into the KPL vector system and $Rosa_{26}$:Cas9 mice were intratracheally infected with adeno-associated virus with the same virus titre and under the same conditions (KPLS2 mice). The characteristics of the tumours of KPL and KPLS2 mice were analysed regarding tumour load and tumour subtype (Figure 4-44).

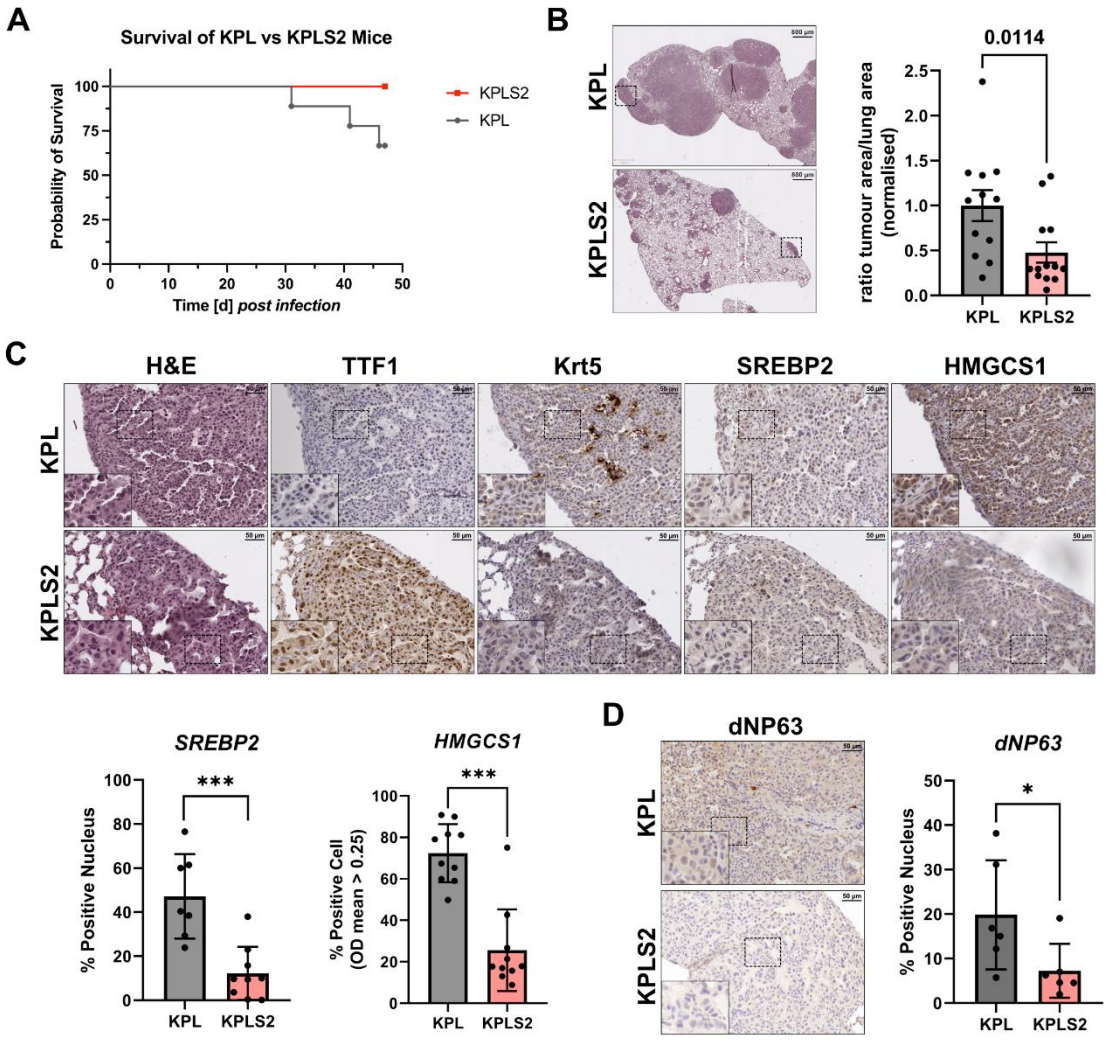

Figure 4-44: Loss of SREBP2 in squamous lung cancer results in reduced tumour load.

A. *Survival curve of KPL and KPLS2 mice. Mice are intratracheally (i.t.) infected with adeno-associated virus (AAV) containing sgRNAs for KRas (together with a repair construct to generate Kras^{G12D}), Tp53, Lkb1 (KPL) or additionally sgSREBF2 (KPLS2). At the indicated days (d) after infection, some KPL mice needed to be sacrificed upon showing symptoms. 47 days post infection, the cohort was terminated.* ***B.*** *Lungs of 12 KPL and 13 KPLS2 mice were analysed regarding tumour load. Quantification shows ratio of tumour area to total lung area in each mouse cohort. C. Indicated area (dashed square in B.) was analysed regarding SREBP2 knockout and subtype of tumours by IHC staining for SREBP2 and its target gene HMGCS1 and the ADC marker TTF1 and the SCC marker Krt5, respectively. H&E staining is also shown. SREBP2 staining of 7 KPL and 9 KPLS2 tumours and HMGCS1 staining of 10 KPL and 10 KPLS2 tumours was quantified and % positive nuclei or cells, respectively, are shown in bar graph.* ***D.*** *Tumours of KPL and KPLS2 mice (6 each) were stained for **Δ**NP63 (dNP63) and bar graph shows quantified IHC staining as % positive nuclei. *, P < 0.05; ***, P < 0.001; unpaired two-tailed Student t test. H & E = Haematoxylin and eosin. OD = optical density**.**

To target SREBP2 for knockdown in a squamous lung cancer mouse model, KPL and KPLS2 mice were generated by an AAV-mediated CRISPR/Cas9 approach as described before (4.7.3). After 31 days, the first KPL mouse showed lung cancer associated symptoms and was sacrificed. At day 41 and 46 post transfection another two KPL mice needed to be sacrificed and the whole cohort was terminated at 47 days post infection (Figure 4-44 **A**).

The lungs of KPL and KPLS2 mice were paraffinized and sectioned. Tissue slices were analysed regarding tumour size by H&E staining. The ratio of tumour area to normal lung area was calculated. Lungs of KPLS2 mice showed significantly lower tumour load compared to lungs of KPL mice (as determined by Mann-Whitney-U-test) (Figure 4-44 **B**).
Tumour tissue from KPL and KPLS2 mice was stained for SREBP2 and its target gene HMGCS1. Both proteins were significantly reduced in SREBP2 KO lung tumours, revealing successful knockout of SREBP2 in tumours of KPLS2 mice (Figure 4-44 **C**). Furthermore, the subtype of the tumours in KPL and KPLS2 mice was analysed by marker staining for SCC and ADC. The staining intensity of the ADC marker TTF1 was increased in the KPLS2 situation compared to KPL tumours. *Vice versa* staining intensity for keratin 5 and ΔNP63, both markers for the squamous subtype of lung cancer, was decreased in tumours from KPLS2 mice compared to KPL tumours (Figure 4-44 **C** and **D**).
In conclusion, SREBP2 KO in lung tumours leads to prolonged survival and reduced tumour load in the lung cancer mouse model. Additionally, residual tumours found in KPLS2 mice map predominantly to the adenocarcinoma rather than squamous subtype.

5 Discussion

The stability of SREBP2, the master regulator of the mevalonate pathway, is regulated at various levels. Beside the transcriptional control and the regulatory mechanism by processing of the precursor to generate the mature form which translocate to the nucleus and acts as active transcription factor, mSREBP2 is also regulated post-translationally by phosphorylation and subsequent ubiquitination. Here it was shown that mSREBP2 could be stabilised through deubiquitination by USP28 to prevent its degradation by the 26S proteasome. USP28 levels influence therefore the stability and activity of mSREBP2 and regulate the expression of target genes involved in the mevalonate pathway. In squamous cancer cells, USP28 levels are upregulated that leads to increased expression of SREBP2 target genes and high metabolic flux into the mevalonate pathway to supply cancer cells with essential metabolites, like cholesterol and ubiquinone as well as prenyl residues for protein prenylation.

5.1 USP28 regulates the mevalonate pathway by stabilising mSREBP2

USP28 regulates the stability of transcription factors by antagonizing E3-mediated K48-linked ubiquitination (Taranets *et al.* 2015) thereby preventing degradation via the UPS. Preferably, USP28 counteracts the ubiquitination of the E3-ligase FBW7, forming a corresponding E3-DUB pair. FBW7-substrate proteins are phosphorylated at the CPD prior to ubiquitination (Welcker *et al.* 2008). The CPD is a highly conserved motif found in various transcription factors, also in SREBPs.

5.1.1 USP28 binds and deubiquitinates mSREBP2

SREBPs were shown to be regulated by FBW7-mediated ubiquitination via phosphorylation of the CPD (Sundqvist *et al.* 2005). In this thesis USP28 was identified to deubiquitinate SREBP2, resulting in increased stability and transcriptional activity.
USP28 and mSREBP2 were co-localised to the nucleus and perinuclear region (Figure 4-1). Interestingly, USP28 was also be localised to the cytoplasm and in membrane-bound fraction when performing cellular fractionation of A431 cancer cells (Figure 4-2), while in immunofluorescence staining signal was exclusively detected in cell nucleus. USP28 was described as nuclear protein (Human Protein Atlas). The accumulation of nuclear signal could negotiate the mild fluorescence signal in cytoplasm explaining this observation by technical limitations. Additionally, in the PLA assay demonstrating close proximity of USP28 and SREBP2, signals were detected in the nucleus as well as the cytoplasm (Figure 4-4) raising the hypothesis that USP28-SREBP2 complexes can be formed in the nucleus and could be exported to the cytoplasm. To proof this hypothesis, further experiments need to be performed.
The binding of USP28 to SREBP2 was shown by co-immunoprecipitation of both proteins (Figure 4-3). A DSP crosslinker was used to stabilise the protein-protein binding and experiment was performed by MG-132 treatment of the cells prior to lysis

to increase ubiquitinated species. It can be assumed that USP28 only binds ubiquitinated SREBP2 via its UBA and UIM domains (Prieto-Garcia *et al.* 2021).
In presence of USP28, the ubiquitination smear on mSREBP2 was decreased while this effect was not observable in the presence of the catalytically active mutant (Figure 4-9). Additionally, in absence of USP28 the ubiquitinated SREBP2 was increased identifying mSREBP2 as a USP28 substrate protein for deubiquitination. These experiments proof that USP28 deubiquitinates SREBP2.

5.1.2 USP28 regulates the mevalonate pathway via SREBP2

SREBP2 is the master transcriptional regulator of enzymes involved in the mevalonate pathway (Brown *et al.* 1997). Knockdown and knockout of USP28 in U2OS cancer cells and A431 cancer cells resulted in reduced levels of the SREBP2 target gene HMGCS1 (Figure 4-10 & Figure 4-11). Proteomic analysis of USP28 knockdown cancer cell lines revealed that the cholesterol biosynthesis pathway is the fourth most downregulated pathway upon loss of USP28 (Figure 4-15). Interestingly, enzymes in the mevalonate pathway were downregulated while levels of enzymes involved in *de novo* cholesterol biosynthesis were either not changed or even upregulated. Transcriptomic analysis of shUSP28 or shSREBF2 cells showed reduction in cholesterol biosynthesis pathway, confirming that a loss of USP28 lead to the reduced transcription of SREBP2 target genes (Figure 4-24).
Analysis of the metabolic flux in the A431 cancer cells revealed a high *de novo* synthesis of ubiquinone while *de novo* synthesis of cholesterol was surprisingly low (Figure 4-23). These results indicate that A431 cells prefer the cholesterol uptake rather than *de novo* synthesis. Further, metabolite measurement in USP28 or SREBP2 knockdown cancer cell lines showed a marked decrease in *de novo* purine and pyrimidine synthesis (Figure 4-22). This finding raises the hypothesis that A431 cells show high metabolic flux into the mevalonate pathway and downstream synthesis of CoQ10 and pyrimidine synthesis but the *de novo* cholesterol synthesis pathway is not upregulated.
It has to be noted that an overexpression of USP28 in U2OS cells showed no effect on SREBP2 levels or target genes (Figure 4-7). An explanation for the missing stabilisation of SREBP2 in presence of overexpressed USP28 could be a technical problem. It is unclear if the exogenously expressed USP28 is able to enter the nucleus binding to mSREBP2 at the promoter site. The plasmid used for transfection did not contain a nuclear import sequence.

5.1.3 Reduction in USP28 affect cell viability and sensitizes cells for simvastatin treatment

USP28 or SREBP2 knockdown cancer cell lines showed impaired cell viability (Figure 4-13 & Figure 4-19 **A** & Figure 4-21). Maintaining high SREBP2 levels in cells was shown to be important in cancer cell under serum-deprived conditions, in hypoxia and

in acidic milieu (Lewis *et al.* 2015, Kondo *et al.* 2017). No additional effect on cell viability has been observed under these conditions (Figure 4-19 **B** & **C** & Figure 4-20). Simvastatin is a commonly used cholesterol-lowering drug which inhibits HMGCR, the key enzyme of the mevalonate pathway (Maron *et al.* 2000). Multiple studies report population-based data where cancer patients simultaneously treated with statins showed beneficial effects on cancer therapy (Khurana *et al.* 2007, Chiu *et al.* 2011, Hung *et al.* 2017, Kang *et al.* 2021). In this thesis, it was shown that cancer cells with reduced USP28 levels are sensitized to statin treatment (Figure 4-25). The cell viability could be restored by supplementing cancer cells with GGPP, indicating an important role of prenylation of proteins in A431 cells. In summary, these results raise the possibility of combinatorial treatment of cancer cells. The therapeutic window still needs to be investigated.

5.1.4 The role of the USP28-MSREBP2 axis in squamous cancer

Previous studies showed an important role of USP28 in squamous lung cancer by regulating the stability of ΔNP63 (Prieto-Garcia *et al.* 2020). High levels of USP28 correlate with poor prognosis of lung cancer patients.
SREBP2 as well as its target genes are upregulated in SCC and showed a correlation to USP28 expression (Figure 4-38). Further, in vivo data showed increased levels of USP28 and SREBP2 in lung cancer tumour tissue (Figure 4-40), especially in squamous lung tumour (Figure 4-41). A knockout of USP28 or SREBP2 reduced tumour burden (Prieto-Garcia *et al.* 2020, Figure 4-44). The remaining tumours upon knockout of SREBP2 showed reduced levels of the squamous tumour marker ΔNP63, raising the possibility that this tumours are of ADC subtype. Further investigations on a double knockout approach to prevent tumorigenesis or a combinatorial treatment of USP28 inhibitors and blocking the mevalonate pathway need to be addressed. Further, ADC cancer cell ines showed increased sensitivty to simvastatin treatment (Figure 4-39).To verify these results, in vivo experiments in an ADC mouse model for simastatin treatement should be performed.

5.2 USP28 regulates the stability of oncogenic transcription factors in squamous cancer cells

The deubiquitinase USP28 is a known regulator of the stability of various oncogenic transcription factors, namely c-Myc, Jun, Notch and ΔNP63 (Popov *et al.* 2007, Diefenbacher *et al.* 2014, Prieto-Garcia *et al.* 2020). USP28 therefore influences pathways, which play pivotal roles in tumour formation and progression. Additionally, mSREBP2 stability was shown to be regulated by USP28 and consequently the deubiquitinase influences the mevalonate pathway and the intracellular metabolite pool.

5.2.1 USP28 does not regulate the stability of SREBP1 and does not alter *de novo* lipid synthesis

USP28 is a known counteracting DUB of the F-box protein Fbw7 in the SCF-complex. Various oncogenic transcription factors are ubiquitinated by SCF-Fbw7 and deubiquitinated by USP28. The master regulator of *de novo* lipid synthesis, SREBP1 was also shown to be regulated by SCF-Fbw7 (Sundqvist *et al.* 2003). It is logical to assume that this dual regulatory mechanism by the E3-DUB pair is also true for SREBP1. Indeed, a stability assay using exogenous overexpressed mSREBP1 and USP28 revealed a stabilisation for wild type USP28 but not for the catalytically inactive USP28^{C171A} mutant (Figure 4-5 & Figure 4-6). However, knockdown of USP28 showed only slight changes in SREBP1 level and its target genes (Figure 4-11 & Figure 4-12). In the squamous A431 cell line, knockdown of USP28 did not reveal a dysregulation of genes involved in the *de novo* lipid synthesis (Figure 5-1).

A

Gene	log2 FC	p-value (t-test)	q-value (Mann-Whitney)
ACACA	-0,649	0,0000004	0,0005
ACLY	-0,324	0,0085032	0,0253
FASN	-0,482	0,0000244	0,0017
SQLE	0,718	0,0016307	0,0088

log2 FC
-2
-1
0
1
2

B

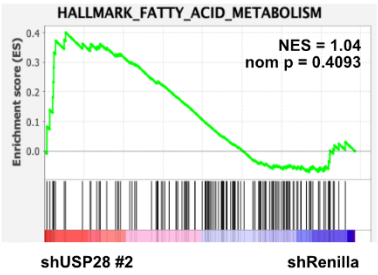

Figure 5-1: USP28 does not regulate SREBP1 target genes in A431 cells.

A. *SREBP1 target genes significantly regulated in proteomic approach (compare Figure 4-15) upon knockdown of USP28 in A431 cells. B. GSEA of Fatty Acid Metabolism Hallmark dataset in transcriptomic analyses (compare Figure 4-24) of shUSP28 A431 cells.*

Neither proteomic nor transcriptomic analyses revealed changes in the *de novo* lipid synthesis genes upon knockdown of USP28. In conclusion, in squamous cancer cells, a regulatory USP28-SREBP1 axis could not be identified, but this cannot be excluded for other systems.

5.2.2 SREBP1 is not compensating for the loss of SREBP2 and *vice versa*

SREBP1 and SREBP2 share high structural similarity and activate the transcription of target genes by binding sequences in the promoter regions (Hua *et al.* 1993, Yokoyama *et al.* 1993). SREBPs are classified as basic helix-loop-helix leucine zipper (bHLH-LZ) transcription factors but unlike other members of this family, SREBPs have a tyrosine residue instead of a well-conserved arginine residue in their basic domain. This substitution allows SREBPs to bind SRE motifs (5'-TCACNCCAC-3') as well as E-boxes (5'-CANNTG-3') (Kim *et al.* 1995).
SREBP1 and SREBP2 show some degree of specificity for the binding to promoter sequences of their respective target genes. Horton and colleagues investigated which target genes are preferentially under the transcriptional control of SREBP1 and SREBP2, respectively (Horton *et al.* 2003). The results of this study show that most

SREBP target genes can be regulated by either SREBP1 or SREBP2, meaning that there is a huge overlap in target specificity between the two proteins (Horton, Shah et al. 2003, Table 1). Only a few genes are regulated exclusively by either SREBP1 or SREBP2 (Horton, Shah et al. 2003, Table 2 and 3). Notably, proteins involved in fatty acid synthesis are upregulated by overexpression of SREBP1 but unchanged in cells with elevated levels of SREBP2. Taken this into account, it can be assumed that a loss of SREBP2 can be partially compensated by SREBP1 and *vice versa*.
The proteomic and transcriptomic analyses revealed that only SREBP2 target genes involved in the mevalonate pathway are affected by manipulation of USP28 (Figure 4-15, Figure 4-24) while genes playing a role in fatty acid synthesis are unchanged (Figure 5-1). Further, loss of SREBP2 does not result in upregulated SREBP1 levels and *vice versa* (Figure 4-43). This leads to the conclusion, that SREBP1 does not play a role in the identified USP28—SREBP2 regulatory axis in squamous cancer cells and cannot compensate the reduction in proteins involved in the mevalonate pathway.

5.2.3 USP28 does not influence c-Myc transcriptional activity in squamous cancer cells

Weak transcription factors often require co-activators, which facilitate the binding of the transcriptional machinery and initiate the transcription process. Consequently, SREBPs associate through their N-terminal domain with various co-activators, e.g. CREB-binding protein (CBP)/p300 (Oliner *et al.* 1996) or the ARC-mediator co-activator complex (Naar *et al.* 1999).
Additionally, SREBPs cooperate with other transcription factors, which bind within the promoter and enhancer regions of SREBP target genes. The LDLR promoter was first investigated regarding the cooperative effect of SREBPs and the transcription factor Sp1 (Dawson *et al.* 1988, Sanchez *et al.* 1995). Whereupon Näär and colleagues developed a model for co-activator requirement for a synergistic activation by SREBP1 and Sp1 on the LDLR promoter (Naar *et al.* 1998). In the promoter sequences of FPP, HMGCS1 and SQLE, key enzymes involved in the mevalonate pathway, binding sites for the NF-Y transcription factor were identified and a cooperative stimulation of transcription activation was shown by SREBP1/2 and NF-Y binding (Jackson *et al.* 1995, Sato *et al.* 1996).
In its role in SKOM-mediated reprogramming of stem cells, Wu *et al.* demonstrate that SREBP1 physically interacts with c-Myc in an *in vitro* Pulldown Assay (Wu *et al.* 2016). However, the formation of SREBP1/c-Myc-heterodimers could not be proven to date. In 2019, it was shown that c-Myc induces SREBP1 expression and thereby regulates fatty acid synthesis and lipogenesis (Gouw *et al.* 2019). Interestingly, both c-Myc and SREBP1 were found to bind to the same DNA molecules within the promoter sequences of the *FASN* gene. In this study, it was also shown that a MYC ON system results in increased transcription of enzymes involved in the mevalonate pathway and cholesterol synthesis but it was not investigated whether c-Myc induces SREBP2 or enhances its transcriptional activity. Additionally, c-Myc is a direct target protein of USP28 (Popov *et al.* 2007). The effects of the loss of USP28 in the squamous cancer

cell line on c-Myc levels revealed that c-Myc does not play a role in the USP28-mediated regulation on SREBP2 and its target genes.

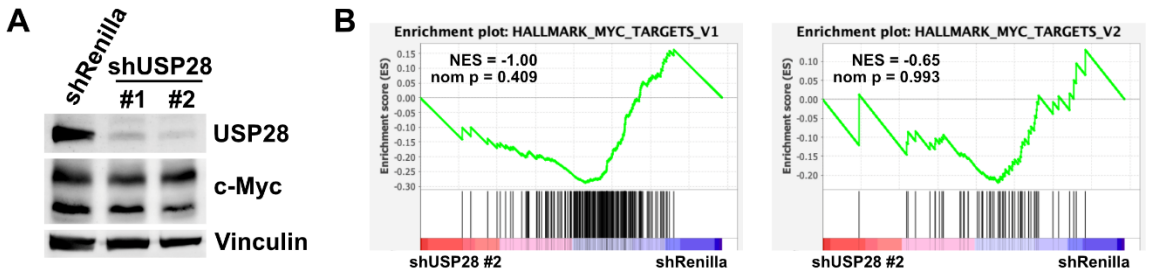

Figure 5-2: Knockdown of USP28 in A431 does not affect c-Myc levels or transcriptional activity.

A. *Western Blot analysis of shUSP28 A431 cells upon 96 h doxycycline-induced knockdown of USP28 cell lines (#1 and #2) and shRenilla control cell line (compare Figure 4-16). Immunoblot shows USP28 and c-Myc protein levels; Vinculin serves as loading control. B. GSEA of Myc targets Hallmark dataset v1 and v2 in transcriptomic analyses (compare Figure 4-24) of shUSP28 A431 cells. V1 = version 1; v2 = version 2.*

Western blot analysis confirmed unchanged protein levels of c-Myc upon knockdown of USP28 (Figure 5-2 **A**). Transcriptomics approach showed that the expression of the Myc hallmark gene sets version 1 (v1, 199 target genes) and version 2 (v2, 58 target genes) (Liberzon *et al.* 2015) was not changed upon knockdown of USP28. In summary, the data confirms that the regulation of c-Myc by USP28 does not play a role in the squamous A431 cell line used in this study. Conclusively, the changes in the expression of mevalonate pathway genes occur by the regulation of SREBP2 by USP28 and not via a cooperative effect involving SREBP2 and c-Myc.

5.2.4 Potential interplay or cooperative effects of SREBP2 and ΔNP63 in squamous cells

The transcription factor ΔNP63 is a master regulator of epithelial cell identity and plays an essential role in the survival of cancer cells from squamous tumour entities in lung, head and neck, oesophagus, cervix and skin cancer. Further it was shown that ΔNP63 is targeted by Fbw7 and USP28 for ubiquitination and deubiquitination and subsequent stabilisation and destabilisation, respectively (Galli *et al.* 2010, Prieto-Garcia *et al.* 2020).

Recently, Li and colleagues showed cooperation between SREBP1 and ΔNP63 and linked this interplay to the regulation of fatty acid metabolism in SCC (Li *et al.* 2021). Since SREBP1 and SREBP2 share high sequence similarity, this SREBP1-ΔNP63 cooperation raises the possibility of a similar interplay between SREBP2 and ΔNP63 in SCC. Based on this, it has to be considered that the deregulation of mevalonate pathway genes upon manipulation of USP28 results partly from changes in the stability of ΔNP63 regulated by USP28 rather than SREBP2.

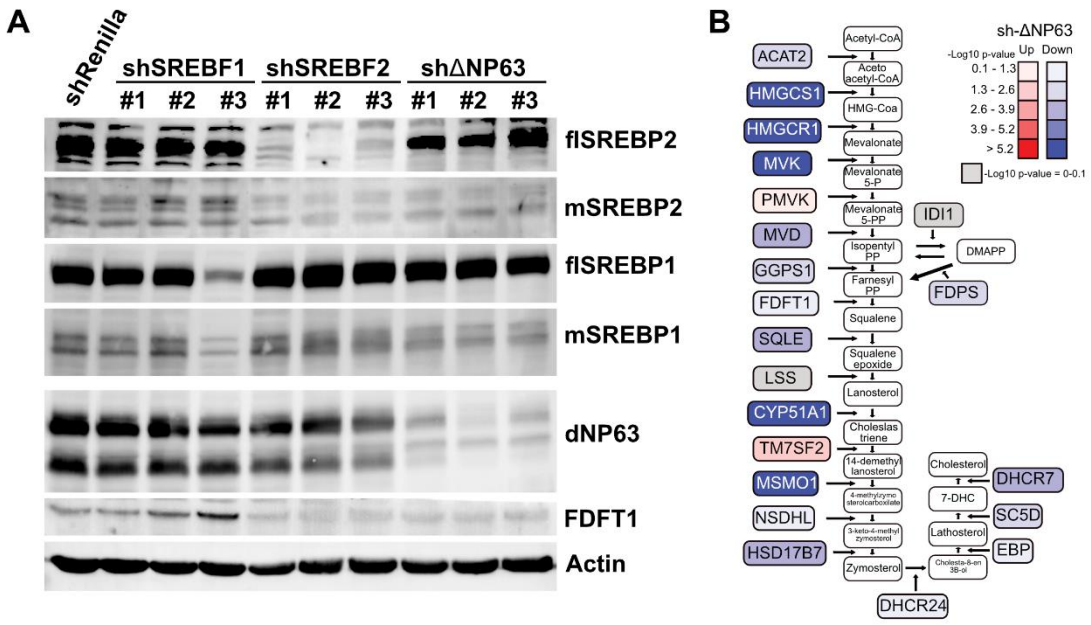

Figure 5-3: Knockdown of ΔNP63 results in decrease of enzymes involved in the mevalonate pathway.

A. *A431 shRenilla control and knockdown cell lines (shSREBF1 #1-#3, shSREBF2 #1-#3 and sh**Δ**NP63 #1-#3) were treated for 96h with doxycycline to induce knockdown and protein levels of SREBP1, SREBP2, **Δ**NP63 and the SREBP2 target gene FDFT1 were analysed by immunoblot. Actin served as loading control.* ***B.*** *RNASeq data of A431 cells with a stable knockdown of **Δ**NP63 (Prieto-Garcia et al. 2020) were analysed regarding the expression of SREBP2 target genes involved in the mevalonate pathway. Data was kindly provided and analysed by Cristian Prieto-Garcia**.***

Pooled A431 knockdown cell lines targeting *SREBF1*, *SREBF2* and Δ*NP63* were generated and analysed by immunoblot. Efficient knockdown of *SREBF1* could only be obtained with sequence #3. In this cell line, no effects on protein levels of SREBP2 or ΔNP63 could be observed. Efficient knockdown of *SREBF2* or Δ*NP63* was observed in all three of the shRNA expressing cell lines. Knockdown of *SREBF2* resulted in a slight decrease in ΔNP63 protein levels, while knockdown of Δ*NP63* reduced mSREBP2 and mSREBP1 levels. While knockdown of *SREBF1* resulted in increased levels of FDFT1 a knockdown of *SREBF2* or Δ*NP63* reduced FDFT1 levels (Figure 5-3 **A**). RNASeq data of A431 cells harbouring a stable knockdown of ΔNP63 (Prieto-Garcia *et al.* 2020) show decreased expression of enzymes involved in the mevalonate pathway (Figure 5-3 **B**).

Additionally, the knockout of *Srebf2* in an *in vivo* lung cancer mouse model showed reduced ΔNP63 levels in the residual tumours compared to lung tumours of control mice (Figure 4-44).

Taken together, it can be concluded that ΔNP63 influences the expression of enzymes involved in the mevalonate pathway. In contrast, knockdown of SREBF2 decreases ΔNP63 target genes (Figure 4-24 **D**). Thus, an interplay between both proteins seems highly likely and their cooperation in transcriptional activation needs to be further investigated.

5.3 The SREBP2-USP28 regulatory axis plays an important role in squamous cancer

Reprogramming of metabolic pathways occurs in a variety of cancers and contributes to rapid tumour growth. The upregulation of aerobic glycolysis includes the generation of either pyruvate, which is converted to lactate, or acetyl-CoA, which is introduced into the TCA cycle. Citrate produced by the TCA cycle can then be exported from the mitochondria and used to produce cytoplasmic acetyl-CoA. Enhanced cytosolic acetyl-CoA can be used to form HMG-CoA and thus to initiate mevalonate synthesis.

5.3.1 Metabolic reprogramming of cancer cells upregulates the metabolite synthesis via the mevalonate pathway

Aberrant lipid metabolism, amino acid metabolism, mitochondrial biogenesis and other cellular metabolism pathways have been associated with metabolic remodelling in cancer: Thereby, activation mutations of oncogenes or inactivation mutations of tumour suppressors are often found to affect the expression or activity of metabolic enzymes. Among the frequent oncogenic mutations, alterations in the PI3K-AKT-mTOR pathway also via loss of PTEN lead to an activation of gene expression of metabolic enzymes, including those regulated by SREBPs. Additionally, in cancer commonly mutated transcription factors like c-Myc and p53 upregulate the transcription of proteins in metabolic synthesis pathways.
SREBP2 is regulated by p53 in different ways. Firstly, wild type p53 can block the post-translational processing of SREBP2 and consequentially downregulate the mevalonate pathway. The gene expression of ATP-binding cassette transporter A1 (ABCA1) is under the control of p53 and binding of p53 to the promoter of ABCA1 induces its expression (Moon *et al.* 2019). ABCA1 is a membrane-associated cholesterol transport protein and bidirectionally regulates the movement of sterols across the plasma membrane and therefore contributes to cellular cholesterol homeostasis (Yamauchi *et al.* 2015). As SREBP2 processing is a cholesterol-sensing process, high levels of ABCA1 decreased SREBP2 maturation (Moon *et al.* 2019). Secondly, SREBP2 levels were found to be increased in colon cancer cells that have lost p53, leading to the activation of the mevalonate pathway (Kaymak *et al.* 2020). This was mediated by inhibition of GSK3-dependent SREBP2 phosphorylation, leading to the stabilisation of the mature protein (Kaymak *et al.* 2020). Thirdly, mutant p53 was shown to directly bind to SREBP2 and enhance expression of mevalonate pathway enzymes (Freed-Pastor *et al.* 2012).
Taken together, the transcription factor p53 is one of the main tumour suppressor genes in cancer and more than half of human tumours exhibit mutations in the TP53 gene. This includes missense, truncation and loss-of-function mutations. Loss of wild-type p53 or expression of mutant p53 results in metabolic reprogramming and enhances the activation of the mevalonate pathway to ensure the cellular supply of metabolites and to drive tumorigenic processes and promote cancer progression.

Hartmann *et al.* used a CRIPSR-Cas9 mouse model where specific oncogenes are knocked out in the lung. Based on the most observed mutations found in patients, the KPL mice harbour mutations of $Kras^{G12D}$ and loss of function mutations of Tp53 and Lkb1 (Hartmann *et al.* 2021). To gain further insights how the mevalonate pathway contributes to tumour transformation, in a Tp53 loss situation or if Tp53 is mutated, tumours and cancer cell lines were analysed regarding expression levels of SREBP2 and its target genes as well as the metabolic outcome.
A direct comparison of protein levels of a key enzyme of the mevalonate pathway, HMGCS1, in non-transformed and tumour tissue in a lung cancer mouse model revealed increased protein levels (Figure 4-40). Metabolic tracing of the ^{13}C-glucose in the p53-mutant squamous cell line A431 revealed that only a small proportion of cholesterol is generated via *de novo* synthesis, but that the mevalonate pathway feeds the synthesis of CoQ10 (Figure 4-23 and Figure 4-34).
The mevalonate pathway provides Co-Q10 to maintain pyrimidine synthesis, especially in p53-deficient cancer cells (Kaymak *et al.* 2020): Co-Q10 functions as an electron acceptor for DHODH, which converts dihydroorotate to orotate. Orotate in turn is converted to UMP and further into UTP and CTP.
Mass spectrometry analysis of targeted metabolites in A431 cancer cells upon knockdown of either SREBP2 or USP28 revealed decreased purine and pyrimidine levels (Figure 4-22). Consequently, a reduction of SREBP2 activity in cancer cells negatively regulates the synthesis of RNA for transcription and DNA for the replication process and affects the cell proliferation and survival (Figure 4-21).
Interestingly, cell viability of squamous A431 cells was decreased upon inhibition of pyrimidine synthesis and DNA replication by 5-fluorouracil and cisplatin, respectively (Figure 4-27). Cisplatin is a common chemotherapy medication used to treat various types of cancer, e.g. cervical cancer, head and neck cancer, esophageal cancer and lung cancer (Dasari *et al.* 2014). Cisplatin interferes with DNA replication, which leads to apoptosis of highly proliferating cells. In contrast, viability of the same cells was not affected by inhibitors of FDFT1 or SQLE, two enzymes in the cholesterol biosynthesis pathway (Figure 4-26). Inhibition of FDFT1 or SQLE affects cholesterol synthesis but does not interfere with CoQ10 production. This confirms that metabolites upstream of FDFT1 are required for the viability of A431 cells.
In summary, metabolic cancer reprogramming upregulates the mevalonate pathway to adjust to the increased need for metabolites. Reduced SREBP2 levels, either through direct depletion or because of USP28 inhibition, lead to a reduction of purines and pyrimidines and affects viability and survival of cancer cells.

5.3.2 The tumour microenvironment influences SREBP2 activation and regulates metabolite synthesis

Pivotal parameters of the tumour microenvironment can play critical roles in the regulation of SREBP2 activation, activity of the mevalonate pathway and cell proliferation of cancer cells.

Under metabolic stress, cancer cells in poorly vascularized solid tumours need to adapt to low-oxygen and reduced nutrient levels. The hypoxia-inducible factor 1α (HIF1α) is activated by hypoxic conditions and promotes glycolysis rather than oxidative phosphorylation and increases the formation of reactive oxygen species (Nagao *et al.* 2019). Hughes and colleagues showed in the yeast *S. pombe* that the SREBP homolog Sre1 is required for cell growth under hypoxic conditions and stimulates the transcription of genes maintaining metabolic flux and the adaptation to hypoxia. Additionally, they could show that sterol depletion activates the cleavage of Sre1 and increases target gene transcription (Hughes *et al.* 2005). Moreover, hypoxic and lipid-deprived conditions were found to increase SREBP1 activity in mammalian cancer cells (Lewis *et al.* 2015), and increased SREBP2 protein stability and mevalonate pathway activity was associated with an 3D-tumorigenic spheroid culturing method mimicking reduced oxygen and nutrient supply, especially in p53-deficient cancer cells (Kaymak *et al.* 2020).
Additionally, due to the Warburg effect, tumour cells increase the rate of glucose uptake and favour fermentation and production of lactate, regardless of the presence of oxygen. Aerobic glycolysis accumulates lactate and facilitates acidosis within the tumour microenvironment (Webb *et al.* 2011). It has been shown that an acidic extracellular pH triggers nuclear translocation of SREBP2, which increases cholesterol biosynthetic gene transcription and promotes cancer progression (Kondo *et al.* 2017). The effect of reduced USP28 or SREBP2 levels on cell viability in squamous A431 cells was only mildly affected by serum starvation or by placing cells in hypoxic or acidic conditions (Figure 4-19 and Figure 4-20). Knockdown of either USP28 or SREBP2 reduced cell growth compared to the controls but did not show an additional negative effect on cell viability under these stress conditions, where the SREBP2 pathway has previously been shown to be essential to maintain metabolic flux and support cancer cell growth.
Hypoxia, nutrient starvation and acidic environment showed increased SREBP2 target gene expression and enhanced mevalonate pathway activity. However, the loss of SREBP2 under these conditions did not reveal additional sensitivity and was not further investigated. It is possible that under hypoxic and acidic conditions cancer cells are able to compensate for the reduced levels of SREBP2 and intracellular metabolites by increased uptake of biomolecules via SREBP2-independent pathways. The insensitivity of the squamous cancer cell line towards SREBP2 knockdown in the lipid-deprived situation further suggests that cell growth is mostly independent on *de novo* synthesis of metabolites in a 2D culture model.

5.3.3 Mutational landscape of squamous cancer cells reveals a complex regulatory network of the mevalonate pathway

Non-small cell lung cancer can be divided into the predominant subtypes of adenocarcinoma and squamous cell carcinoma. These subtypes show distinct histological, molecular and clinical features (Hou *et al.* 2017). The metabolic signatures of ADC and SCC were investigated by Goodwin and colleagues who

identified increased GLUT1 levels and subsequently upregulated glycolytic flux (Goodwin *et al.* 2017). Metabolic reprogramming in SCC and ADC and its effect on the mevalonate pathway, were analysed in human patient derived samples (Figure 4-38, Figure 5-4) and human cancer cell lines (Figure 4-37).

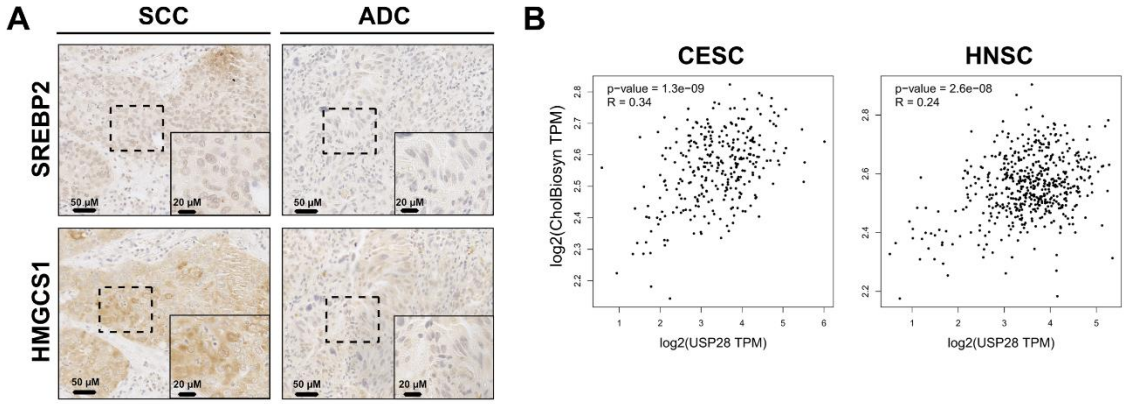

Figure 5-4: SREBP2 and target genes are increased in squamous tumours and correlate with USP28 levels.

A*. Human patient derived adenocarcinoma and squamous samples were immunohistochemically analysed for SREBP2 and HMGCS1 expression. Samples were kindly provided by M. Rosenfeldt (UKW).* ***B.*** *Correlation analysis of expression levels of the gene set of cholesterol biosynthesis and USP28 in human cervical squamous cancer (CESC) and head and neck squamous cancer (HNSC) using the GEPIA2 software.*

Squamous tumour entities show increased SREBP2 and target gene expression, which correlates with USP28 expression not only in lung squamous cancer but also in cervical and head and neck squamous cancer cells (Figure 5-4).

SCCs are histologically characterized by the presence of intercellular bridges, keratinization and squamous pearls composed of keratins. In SCC tumours USP28 is strongly expressed and stabilises the main histological marker used for classifying SCC, the squamous transcription factor ΔNp63 (Conde *et al.* 2010, Prieto-Garcia *et al.* 2020). Inhibition of USP28 reduces tumour growth and increases cell death in a mouse model of lung SCC (Prieto-Garcia *et al.* 2020).

Squamous tumours show a complex genetic landscape of mutations. Among the most common mutations are *TP53* and *MYC*, and the PI3K-AKT signalling pathway is often deregulated due amplification and/or activation mutations in *PIK3CA* (Dotto *et al.* 2016). Enhanced PI3K-AKT signalling results in impaired phosphorylation and therefore ubiquitination of SREBPs (Sundqvist *et al.* 2005). Additionally, AKT activates mTORC1, which results in an accumulation of nuclear SREBP1 and increased transcriptional activity (Porstmann *et al.* 2008, Duvel *et al.* 2010, Peterson *et al.* 2011). Beside the effects of increased signalling, also Fbw7 was found to be commonly deleted tumours (Welcker *et al.* 2008). A loss of Fbw7 function leads to increased stability of SREBPs by diminishing its degradation via the proteasomal system. Further, it was previously shown, that loss of Fbw7 increased SREBP levels and leads to an accumulation of cholesterol and lipids, which in turn activate AKT, resulting in a circular activation loop (Bengoechea-Alonso *et al.* 2022).

In contrast, USP28 was shown to be commonly upregulated in squamous cell lines and tumours (Figure 4-37, Figure 4-38, Figure 4-40) and to be primarily expressed during the early stages of oncogenic transformation (Prieto-Garcia *et al.* 2022).
Liver kinase B1 (LKB1) is an essential enzyme that regulates cellular processes, including cell metabolism. *Lkb1* inactivation is commonly found in human tumours and promotes metabolic reprogramming (Zhang *et al.* 2021). The loss of *Lkb1* plays an important role in the development and progression of squamous lung cancer by elevating ΔNp63 levels (Xu *et al.* 2014, Liu *et al.* 2019). Furthermore, SREBPs are part of the LKB1-AMPK-mTOR signalling pathway (Li *et al.* 2011). Inhibition of LKB1 reduces AMPK activity and increases mTOR signalling which in turn mediates accumulation of active SREBPs (Shaw *et al.* 2005, Porstmann *et al.* 2008).
Lung tumours derived in a sgKRas+HR^{G12D}/sgTP53/sgLKB1 (KPL) mouse model (Hartmann *et al.* 2021) reveal adenocarcinoma as well as squamous cell carcinoma phenotypes. Targeting *KRas* for activation as well as *TP53* and *Lkb1* for deletion reflects a common mutational landscape of lung cancers in patients. Detailed expression analysis of tumour subtypes showed increased levels of HMGCS1 as well as USP28 (Figure 4-41). However, isolated primary cell lines derived from the mouse tumours did not show an increase in SREBP2 levels and activity when comparing KPL to KP. Since KP and KPL cell lines did not show differences in their morphology and the cell lines were not stained for squamous or adenocarcinoma marker proteins, the actual subtype represented by the cells remains undetermined. It cannot be excluded that adenocarcinoma cells overgrew the squamous cell carcinoma cells or that the squamous cells lost their squamous features during cultivation.
Using the same CRISPR/Cas9 mouse model to further target USP28 for knockout (KPLU) revealed decreased levels of SREBP2 and HMGCS1 in lung tumours upon knockout of USP28 (Figure 4-42). Prieto-Garcia *et al.* showed that the USP28 targets c-Jun and c-Myc are not downregulated in tumours of the KPLU mice when compared to KPL (Prieto-Garcia *et al.* 2020). However, loss of USP28 reduced active Notch1, which is also commonly mutated in squamous cancers (Dotto *et al.* 2016) and was previously identified as a USP28 target (Diefenbacher *et al.* 2014).

Taken together, the metabolic reprogramming of squamous cancer cells to upregulate the master transcription factor SREBP2 is either a consequence of mutations in oncogenes and tumour suppressors, leading to a deregulation of cellular signalling pathways and/ or results from altered conditions of the microenvironment. SREBP2 activity is regulated downstream of prominent signalling pathways activated in cancer cells as well as influenced by conditions mainly found in the tumour microenvironment. Furthermore, USP28 is upregulated in squamous cancer, regulating the stability of prominent squamous oncogenic transcription factors like ΔNp63 and Notch1. SREBP2 target genes correlate strongly with USP28 expression in human tumours and are reduced upon knockdown of USP28 in a predominantly squamous lung cancer mouse model. This implicates an essential role of the USP28-SREBP2 axis in squamous cancers and presents possibilities for therapeutic interventions.

5.4 Interrogating the USP28- SREBP2-axis in squamous cancer cells reveals pro-tumorigenic functions

Since the loss of either USP28 or SREBP2 in the squamous lung cancer mouse model resulted in reduced tumour load (Prieto-Garcia *et al.* 2020) (Figure 4-44), it seems likely that the USP28-SREBP2 regulatory axis promotes. Tumorigenesis defines the gain of malignant properties of normal cells and includes metabolic reprogramming (discussed in 5.3.1), uncontrolled proliferation and evasion of the immune system, and ultimately also spreading into other areas of the body.

5.4.1 USP28 and SREBP2 drive cell growth and proliferation in squamous cancer cells

Squamous A431 cells with inducible knockdown systems for either USP28 or SREBP2 revealed impaired cell proliferation (Figure 4-19 & Figure 4-20). The cancer cells tolerated reduced levels of SREBP2 and USP28 for a certain period of time and cell growth was more affected by reduced USP28 levels compared to SREBP2 depletion. The restricted proliferation of the USP28 knockdown cells was not rescued by the addition of mevalonate (Figure 4-25), since USP28 regulates multiple processes which are important for cell proliferation (Wang *et al.* 2018). USP28 regulates the stability of multiple proteins involved in tumorigenesis (5.3.3) and it can by assumed that the cellular effects of several dysregulated USP28 target proteins cause the observed reduction of cell viability.

Interestingly, the inhibition of the mevalonate pathway by statins reduces cell growth in squamous cancer cell lines (Figure 4-25). While this suggests that the mevalonate pathway is indeed essential for the growth of these cells, pleiotropic cholesterol-independent effects of statins have also been described. Besides cellular effects explained by reduced levels of other metabolites of the mevalonate pathway than cholesterol, statins were also found to bind to other proteins not involved in cellular metabolism (Weitz-Schmidt *et al.* 2001, Ahmadi *et al.* 2020). The mechanism by which statins reduce cell growth in squamous cancer cells needs to be further investigated.

Silencing of SREBP2 or USP28 results in a decreased number of colonies in a colony formation assay (Figure 4-21). This assay displays the ability of a single cell to grow into a colony and therefore determines cell vitality. The knockdown of USP28 and SREBP strongly affects the survival of single cells and impairs cell proliferation. Since the knockdown was induced after cells were settled in the plate, the reduced ability of colony formation reflects either increased cell death or impaired cell growth.

5.4.2 Epithelial mesenchymal transition is not promoted by SREBP2 in squamous cancer cells

High colony forming ability is furthermore associated with epithelial mesenchymal transition (EMT) in renal cell carcinoma (Singla *et al.* 2018). EMT is the process whereby cells loose E-cadherin expression and differentiate into mesenchymal cells with stem-like features (Wilson *et al.* 2020). EMT results in reduced cell-cell adhesion

and enhanced migratory potential. The gaining of invasive properties especially plays a pivotal role in cancer metastasis during disease progression (Ribatti *et al.* 2020).
The mevalonate pathway regulates the synthesis of various metabolites and biomolecules. Beside cholesterol and CoQ10, it additionally supplies cells with dolichol and geranylgeranyl diphosphate for N-glycosylation and prenylation, respectively, two essential post-translational modifications of proteins (Figure 1-3).
The inhibition of dolichol synthesis was shown to result in reduced ER-associated protein N-glycosylation and Golgi-associated N-glycan remodelling which consequently decreases EMT and impairs metastasis in highly invasive breast cancer (Yu *et al.* 2021). Further, EMT and invasiveness of breast cancer cells was displayed by receptor tyrosine kinase (RTK)-mediated activation via PI3K/AKT pathway upstream of SREBP activation.
Additionally, geranylgeranyl transferase II (GGTII) prenylates Rab11b that transports Arf6 to the plasma membrane to be activated. Arf6 activation constitutes a pathway promoting invasion and metastasis by downregulating E-cadherin-based cell-cell adhesion and by upregulating recycling of β1-integrins (Hashimoto *et al.* 2016).
Furthermore, mevalonate and cholesterol were reported to activate the estrogen-related receptor α (ERRα) pathway in breast cancer, which enhances the expression of genes associated with metabolic switching, enhanced proliferation, motility and propagation of cancer stem-like cells (CSCs) (Brindisi *et al.* 2020). Additionally, Rho GTPases (RhoA and RhoC) are essential in maintaining stemness of CSCs and both proteins get activated upon prenylation (Molnar *et al.* 2001). CSC are tumour cells displaying high metabolic flexibility, which contributes to the aggressiveness of the cells and promotes resistance to therapies, recurrence, and metastasis (De Francesco *et al.* 2018).
It is noteworthy that in breast cancer, a highly invasive and metastatic kind of cancer, primarily driven by mutations of the *TP53* gene, mutant p53 interacts with SREBP2 to upregulate transcription of enzymes involved in the mevalonate pathway, subsequently enhancing the invasiveness of breast cancer cells (Freed-Pastor *et al.* 2012).
Unexpectedly, the loss of USP28 in breast cancer promotes malignancy, tumour growth and angiogenesis and the expression of USP28 is associated with a better survival of human breast cancer patients (Richter *et al.* 2018). Richter and colleagues reported a distinct morphological change in cells upon knockdown of USP28, which was not observed in the A431 cells used in this thesis.
To better understand the role of the USP28-SREBP2 axis in the context of EMT in squamous tumours, the transcriptomic dataset was analysed regarding the expression of the respective hallmark gene set.

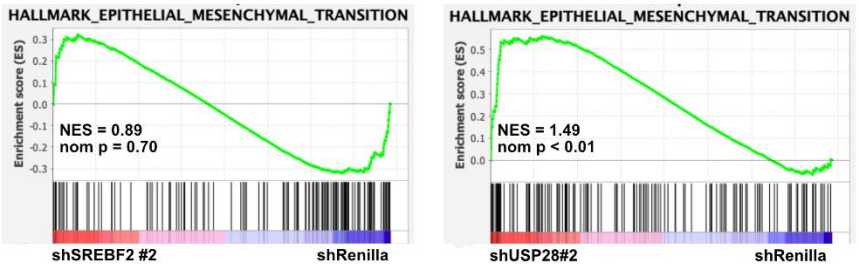

Figure 5-5: Knockdown of SREBP2 or USP28 does not reduce EMT properties of the squamous A431 cell line.

GSEA of Epithelial_Mesenchymal_Transition Hallmark dataset in transcriptomic analyses (compare Figure 4-24) of shSREBP2 and shUSP28 A431 cells.

The analysis of the data generated by the transcriptomic approach revealed that a knockdown of SREBP2 in the squamous A431 cell line did not reduce the EMT signature of the cells. Further, reduced USP28 result in increased expression of genes associated with EMT (Figure 5-5) and supports the findings of Richter *et al.* (Richter *et al.* 2018). The promotion of EMT in squamous cells mediated by USP28 is therefore independent of its regulation of SREBP2 and the mevalonate pathway.

Taken together, these observations suggest that the regulatory axis of USP28 and SREBP2 does not influence the transition from epithelial to mesenchymal phenotype and, consequently, is unlikely to have an effect on invasiveness and metastatic properties in squamous cancer cells. To establish cancer stemness properties and investigate if these are enhanced by USP28 via SREBP2 in squamous cancer cells, further investigations are needed.

5.4.3 Reduced flux in the mevalonate pathway drives pro-inflammatory signatures and potentially supports immunosurveillance

Interferons type I (IFN-I) are cytokines which are central regulators of the host defence system upon infections and are associated with inflammation and the cell-mediated innate and adaptive immune responses (Cheon *et al.* 2023). In the context of cancer, interferons were presented as antitumor cytokines, which facilitate immunosurveillance. It is assumed that highly immunogenic tumour cells induce inflammation and orchestrate the activation of immune cells for clearing by the immune system.

Perturbations in cholesterol biosynthesis can activate IFN signalling: York and colleagues have shown that limiting flux through the cholesterol biosynthesis pathway leads to the activation of a type I IFN response by conformational activation of STING in the ER-membrane of macrophages (York *et al.* 2015). Additionally, inhibition of the mevalonate pathway reduced prenylation of KRas (Shamma *et al.* 2009). Prenylation anchors KRas on the cell membrane, enabling it to initiate downstream signalling and suppression of KRas prenylation by inhibition of the mevalonate pathway provokes

severe ER stress-mediated inflammation with enhanced IFN production (Nam *et al.* 2021).

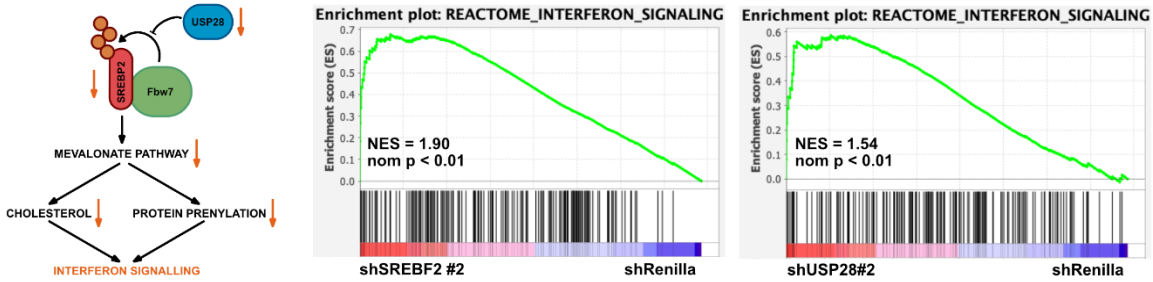

Figure 5-6: Knockdown of USP28 and SREBP2 induces interferon signalling in squamous A431 cells.

Illustration showing the effects of reduced USP28 and SREBP2 levels on the mevalonate pathway and downstream cholesterol synthesis and protein prenylation which results in enhanced interferon signalling. GSEA of interferon signalling REACTOME dataset in transcriptomic analyses (compare Figure 4-24) of shSREBP2 and shUSP28 A431 cells.

Indeed, transcriptional analysis of squamous A431 cells with either reduced SREBP or USP28 levels reveal increased transcriptional activation of genes involved in interferon signalling. This strong induction of pro-inflammatory signatures supports the hypothesis of an important role of this axis in preventing cellular stress responses and limiting the activation of the immune system during tumour surveillance.

Further immunomodulatory properties of blocking the mevalonate pathway have been previously identified: Statin treatment reduces the flux of the mevalonate pathway and decreases protein prenylation. The lack in farnesylation and prenylation, most likely of GTPases of the Ras superfamily, leads to the activation of caspase-1-mediated maturation and secretion of the interleukins IL-1β and IL-18. These interleukins are potent co-stimulatory cytokines for natural killer (NK) cells, special kinds of T cells and innate lymphocytes, which are crucial anti-tumour effector cells (Gruenbacher *et al.* 2010, Nussbaumer *et al.* 2011).
It needs to be noted that in contrast to the reduced flux of the mevalonate pathway, also high levels of its intermediates were shown to activate immune response: The mevalonate pathway is the sole intracellular source of IPP in human cells and increased levels of IPP has been shown to activate T cells that subsequently kill IPP-overexpressing cells (Gober *et al.* 2003, Wang *et al.* 2011).
One promising aspect of these finding is the use of zoledronate, a biphosphonate that inhibits FPPS. Consequently, IPP is accumulated and FPPS inhibition abolishes the downstream cholesterol synthesis and protein prenylation (Figure 1-3). Combinatorial cancer treatments with zoledronate are investigated in clinical trials (Mitri *et al.* 2016, Piperno-Neumann *et al.* 2016).
However, the mechanism by which the mevalonate pathway induces an immune response and supports immunosurveillance, as well as the role of different intermediates of the pathway in influencing pro-inflammatory features and recruit immune cells needs to be further investigated, especially in an immunocompetent *in vivo* model.

Furthermore, it will be interesting to analyse whether a combinatorial treatment using USP28 inhibitors and statins reduce tumour growth and induce anti-tumour immunity.

5.5 Combinatorial treatment targeting the USP28-SREBP2 axis reveal potential therapeutic approaches

The genetic loss of USP28 in the squamous lung cancer mouse model resulted in decreased tumour load (Prieto-Garcia *et al.* 2020). The same result was achieved by genetic deletion of SREBP2 in squamous lung tumours (Figure 4-44).
Investigations of combinatorial treatment of the inhibition of the mevalonate pathway by simvastatin and either shRNA-based reduction of USP28 expression or chemical inhibition using the dual USP25/28 inhibitor AZ-1 revealed a potential therapeutic approach for further studies targeting squamous cancer.

5.5.1 Efficiency of reducing cell proliferation by blocking the mevalonate pathway is dependent on tumour entity and subtype

Various studies in cancer patients with statin treatment demonstrate increased survival and overall better outcome (Ahmadi *et al.* 2020). Especially, patients with squamous subtypes gain from therapeutic treatment including statins, as demonstrated for late state lung or esophageal cancer patients (Lin *et al.* 2016, Nguyen *et al.* 2018).
Fatostatin, a chemical compound distinct from the classical HMGCR inhibitors, was firstly reported to inhibit SREBP function by blocking the binding of SCAP, thereby preventing nuclear translocation of SREBPs (Kamisuki *et al.* 2009). Further studies revealed that fatostatin suppresses cell proliferation and induces apoptosis. Therefore, fatostatin has been used for treating different types of cancer in preclinical models (Li *et al.* 2014, Brovkovych *et al.* 2018, Gao *et al.* 2018).
For specifically blocking the SREBP2-regulated mevalonate pathway, compounds targeting the rate-limiting enzyme HMGCR are preferred. In various cancer types, high cholesterol levels are a risk factor and drive tumour growth (Ding *et al.* 2019). Increased flux into the mevalonate pathway is associated with worse prognosis for patients (Guerra *et al.* 2021). Cancer patients with high cholesterol levels treated with statins targeting HMGCR showed reduced incidence and recurrence in various cancers, including esophageal and lung cancer (Khurana *et al.* 2007, Singh *et al.* 2009, Chiu *et al.* 2011, Singh *et al.* 2013).
Considering the discussed aspects regarding the different tumour subtypes (see 5.3), adenocarcinoma and squamous cell carcinoma cell lines from different tumour entities were treated with simvastatin and cell proliferation was analysed. SREBP2 levels in cell lines of cervix, pancreas and lung cancer were increased in the SCC compared to the ADC subtype and further induced by lipid deprivation (Figure 4-37). However, simvastatin treatment of the same cell lines did not reveal overall differences in sensitivity between the two subtypes (Figure 4-37 & Figure 4-39): While in two of the squamous tumour entities (cervix and pancreas) blocking of the mevalonate pathway

by statins resulted in reduced cell viability and proliferation (Figure 4-37; IC50 = 10-15 µM)), squamous lung cancer cell lines showed a lower sensitivity towards inhibition of HMGCR by statins compared to lung adenocarcinoma cells (Figure 4-39; IC50>25 µM).
Taking into consideration, that diverse tumour entities show highly specific mutational landscapes and metabolic reprogramming, this variance in treatment response could be caused by compensational effects. It is noteworthy, that a switch of tumour cells to alternative metabolic processes was already observed in lung squamous cell carcinoma cell evading the anti-proliferative effect of PI3K and mTOR inhibitors to maintain tumour growth and proliferation (Park *et al.* 2016, Momcilovic *et al.* 2018).
The high flexibility of squamous lung cancer cells to adjust the microenvironmental changes and circumvent the inhibition of pro-proliferative pathways poses a substantial challenge for the development of new therapies for patients in future.

A recent study investigated the metabolism as well as the interaction of the tumour with the microenvironment and immune cells in ADC and SCC in human patients and could find large differences between the subtypes (Leitner *et al.* 2022).
Interestingly, the remaining lung tumours forming in mice upon loss of SREBP2 displayed high levels of the ADC marker TTF1 and a strong decrease in ΔNP63 positivity. This indicates that SREBP2 plays an essential role in the tumour initiation and/or progression of squamous tumours while loss of SREBP2 and the downregulation of the mevalonate pathway is better tolerated in ADC tumours. This further substantiates the conclusion regarding a possible cooperation between SREBP2 and ΔNP63 (discussed in 5.2.4), as ΔNP63 is solely expressed in SCC.
Further, the discrepancy between the results in cell lines and the mouse model regarding the effects of blocking the mevalonate pathway points out that the microenvironment (discussed in 5.3.2) and the interaction of the tumour cells with the immune system (discussed in 5.4.3) could be needed to uncover the pivotal role of the USP28-SREBP2 axis, especially in SCC. The perturbation of SREBP2-mediated metabolic pathways needs to be further investigated in detail in a systemic model.

5.5.2 Targeting USP28 by gene silencing and simultaneous treatment with simvastatin reveals enhanced sensitivity and reduces cell growth and proliferation

SREBP inhibition increases the sensitivity of cancer cell to gefitinib, an EGFR-tyrosine kinase inhibitor (EGFR-TKI) which is a standard therapy in non-small cell lung cancer patients – this observation reveals a potential targeting point for therapeutically intervention (Li *et al.* 2016). Further, the analysis of patient data after combinatorial treatment with statins and EGFR-TKI stated a beneficial outcome for lung cancer patients: Lung cancer patients receiving EGFR-TKI therapy and additionally statin treatment showed significantly reduced risk of death and longer median progression-free and overall survival compared to non-statin treated patients receiving only EGFR-TKI (Hung *et al.* 2017).

Interestingly, the inhibition of USP28 activity in combination with gefitinib reduced USP28 and target protein levels and decreased cell survival and proliferation in oncogene-transformed human tracheal cells (Prieto-Garcia *et al.* 2022). Since USP28 regulates the stability of essential tumour-drivers, like ΔNP63 and SREBP2 in SCC and increases pro-tumorigenic signalling pathways, this finding could enable a targeted therapy for SCC patients.
Following up on the strategy of targeting pro-proliferative pathways in tumours at two essential key proteins, simvastatin treatment showed stronger anti-tumour activity in USP28 silenced cells (Figure 4-25). Indeed, reduced levels of USP28 sensitized squamous A431 cell to simvastatin treatment and decreased cell proliferation and growth. The addition of mevalonate nearly completely eliminated the effect of simvastatin and restored cell viability. The strong synergistic effect between simvastatin and USP28 silencing was further investigated regarding the various branch points of the mevalonate pathway and the essentiality of the synthesized metabolites.
Silencing of USP28 in squamous A431 cell lines revealed reduction in the expression of proteins of the upper mevalonate pathway while the cholesterol synthesis enzymes downstream of FPP showed either no change in gene expression or even displayed elevated levels (Figure 4-15). Additionally, metabolic flux analysis using stable isotope labelled glucose indicated extremely low *de novo* cholesterol synthesis in these cells, while metabolic flux into the synthesis of coenzyme Q10 was nearly 75% (Figure 4-23). The inhibition of FDFT1 or SQLE did not result in increased toxicity in combination with reduced USP28 levels (Figure 4-26) and addition of membrane-permeable cholesterol did not rescue cell viability when USP28-silenced cells were treated with simvastatin (Figure 4-28). In conclusion, blocking cholesterol synthesis is not the main reason for statins causing reduced viability of cells with low USP28 levels.

Since A431 cells showed high activity of *de novo* CoQ10 synthesis (Figure 4-23) and reduced USP28 and SREBP2 levels affected purine and pyrimidine synthesis (Figure 4-22), this pathway was further investigated by blocking pyrimidine synthesis using 5-FU and DNA replication by Cisplatin in the presence or absence of USP28 silencing (Figure 4-27). The results indicated that the inhibition of this downstream process did not reflect the increased sensitivity of USP28 depleted cells towards statins. Neither did the addition of nucleosides in USP28-silenced A431 cells treated with simvastatin restore cell viability (Figure 4-28). Accordingly, it has to be concluded that reduced CoQ10 synthesis and subsequent lower pyrimidine synthesis and DNA replication do not drive cells lacking in USP28 activity into cell death when the mevalonate pathway is blocked by statins.
In colon cancer cells cultured as tumour spheroids, simvastatin treatment exclusively enhanced apoptosis in p53 deficient cells (Kaymak *et al.* 2020). Cell viability upon statin treatment could be rescued by adding mevalonate or the supplementation of either CoQ10 or nucleosides (Kaymak *et al.* 2020). These results demonstrate that the consequences of blocking SREBP2-driven mevalonate pathway in cancer is highly

dependent on tumour entity and mutational landscape of the cells (discussed in 5.5.1 and 5.3.1).

FPP, the central branching point in the mevalonate pathway, can be extended by GGPPS to GGPP by condensation of FPP with another IPP building block. The attachment of isoprenoids (prenylation), like FPP (farnesylation) or geranylgeranyl pyrophosphate (GGPP, geranylation), is a post-translation modification of proteins which determines their activity (Molnar *et al.* 2001). The effect of simvastatin in USP28 depleted cells was blocked by the addition of GGPP (Figure 4-28). Thus, the reduction in isoprenoid building blocks, most likely for the prenylation of pro-tumorigenic proteins, causes diminished cell growth in the absence of USP28 when the metabolic flux of the mevalonate pathway is blocked by simvastatin.

The prenylation of Ras proteins is an obligate process for their biologic activity (Molnar *et al.* 2001). Due to this modification, Ras proteins are trafficked first to the ER membrane where they are further processed and activated and afterwards are anchored to the plasma membrane (or other internal membranes) where they activate downstream signalling pathways.

Besides the farnesylation and geranylation of Ras proteins, proteins of the Ras homolog family (Rho) of GTPases are also regulated via prenylation. Like Ras, prenylation-dependent docking of Rho GTPases to the cell membrane is required for their signalling activity. Activated Rho GTPases regulate multiple pro-tumorigenic cellular processes, like cell cycle progression, proliferation and cell migration (Molnar *et al.* 2001). Hence, inhibition of isoprenoid transferases or depletion of FPP and GGPP was shown to reduce cancer progression and cell migration in cancer cells (Dudakovic *et al.* 2011, Freed-Pastor *et al.* 2012).

Taken together, the results presented in this thesis indicate that USP28 depletion reduced the viability of A431 squamous cancer cells and rendered them highly sensitive to mevalonate pathway inhibition by simvastatin. This effect could be partially rescued by the protein prenylation substrate GGPP, indicating that protein prenylation is the bottleneck process affecting cell proliferation in USP28-depleted SCC cells treated with statins. Prenylation could be required for the activation of Ras and Rho signalling in SCC cells and the mevalonate pathway provides the essential substrates initiating this signalling cascade.

5.5.3 Combinational treatment of USP28 inhibitor and statins reduces cell proliferation in a concentration-dependent manner

SCC show a high degree of cellular heterogeneity, with cells representing different stages of differentiation (Dotto *et al.* 2016). The variety of quiescent, slow-cycling and highly proliferating cells in the population makes it particularly difficult to target this cancer type using a monotherapeutic approach: Elkabets and colleagues showed that single agent inhibition of the PI3K pathway drives squamous head and neck cancer cells and esophageal cancer cells into resistance. SCC cells rapidly escape the antitumor activity of PI3K inhibition and upregulate alternative signalling pathways to maintain mTOR activity and cell proliferation. However, a combined therapy approach using PI3K and EGFR inhibitors reduced cell growth and proliferation (Elkabets *et al.* 2015).

Combination therapy approaches in cancer therapy show the potential to improve treatment response and minimise the development of resistance.

The combinatorial treatment of paclitaxel, a common chemotherapy for patients with cervical cancer, and simvastatin enhances paclitaxel's efficacy by inhibition of protein prenylation in several cancer cell lines (Pan *et al.* 2020). In a prospective cohort study of lung cancer patients, it was shown that metformin, aspirin and statins reduced cancer risk and mortality, while a combined use of all three drugs exhibited an even more prominent protective association with cancer risk and mortality (51% and 58%, respectively) (Kang *et al.* 2021). Another recent study mimicked chemotherapy resistant SCLC in a xenograft model and showed that the metabolic reprogramming is relying on the mevalonate pathway and protein prenylation. Statin treatment of the tumours overcame the chemo resistance and combined statin and chemotherapy treatment resulted in durable response in at least two out of seven patients from a small clinical trial (Guo *et al.* 2022).

The concomitant use of double or triple therapy exploiting the metabolic vulnerabilities in SCC showed favourable effects on squamous cancer (Dotto *et al.* 2016). Hence, the concurrent inhibition of multiple pro-proliferative pathways potentially leads to synergistic anti-tumour effects and reveals potentially effective treatment of chemo resistant SCC.

The concomitant inhibition of USP28 and the mevalonate pathway was achieved by the dual USP25/28 inhibitor AZ-1 in combination with simvastatin. In spheroid culture, neither the inhibition of USP28 or the mevalonate pathway nor a double treatment reduced the size of the spheroids. Unexpectedly, an increased in expression of SREBP2 and its target genes were detected in this system. The before observed effect of simvastatin in cells with reduced USP28 levels on cell growth was not achieved using the dual USP25/28 inhibitor, even more, AZ-1 addition even led to resistance towards simvastatin treatment (Figure 4-29).

Inhibition of HMGCR by simvastatin consequentially depletes the sterol pool in the cell and leads to a feedback activation of SREBP2 cleavage (Longo *et al.* 2019). Nevertheless, the strong increase in SREBP2 and target genes was unexpected, since metabolic flux analysis revealed that cells are mostly independent on *de novo*

cholesterol synthesis and most likely favour cholesterol uptake. It needs to be noted that metabolic tracing was performed in monolayer culture and the reprogramming of the A431 cells in the 3D culture model was not investigated. The differences in culturing the cells could have an influence on cholesterol homeostasis and consequentially on simvastatin treatment.
The increase in SREBP2 and target genes after inhibition of USP25/28 was also unexpected, since a reduction in USP28 results in decreased levels of SREBP2 and enzymes involved in the mevalonate pathway (Figure 4-15 & Figure 4-16).
Further investigations of combinatorial treatment on cell viability revealed a biphasic response: Low concentrations of AZ-1 and simvastatin showed cooperative effects and even increased cell viability compared to single treatment and this response is dependent on the serum-concentration (Figure 4-30). Higher concentrations of inhibitors revealed a synergistic effect and strongly reduced cell viability. The determined EC_{50} values for AZ-1 were found to be in the range of 18-20 µM, at least for colon cancer cell lines (Wrigley *et al.* 2017). Thus, even higher concentrations of AZ-1 need to be tested in combination with simvastatin treatment to validate a positive synergetic effect of the combinatorial treatment and demonstrate anti-proliferative effects.
A genome-wide shRNA screen demonstrated that targeting more than one member of the mevalonate pathway could further sensitize cells to statin treatment: A concerted reduction in the levels of SREBP2, HMGCS1 and GGPPS1 in combination with statins enhanced tumour cell apoptosis (Pandyra *et al.* 2015). Thus, a combinatorial treatment of specific USP28 inhibitors, targeting various prominent oncogenes for degradation, together with inhibitors of additional mevalonate pathway enzymes or enzymes involved in proteins prenylation could disclose a specific and efficient therapeutic strategy to sensitize SCCs to statin treatment.

5.5.4 The dual USP25/USP28 inhibitor AZ-1 influences SREBP-driven metabolic pathways

The small inhibitor AZ-1 is a benzylaminoethanol, which was identified in a high throughput screen to inhibit USP28 with an IC_{50} < 1 µM. AZ-1 showed a marked specificity to bind to USP28 and its close homologue USP25 but does not affect the activity of other DUBs (Wrigley *et al.* 2017).
AZ-1 treated U2OS cells showed decreased mSREBP2 levels, which was dependent on the presence of USP28. Under the same conditions, AZ-1 treatment resulted in increased mSREBP1 levels through a mechanism independent of USP28, hinting on the involvement of other cellular signals or an additional role for USP25. Prolonged AZ-1 treatment with low concentrations eventually also showed increased mSREBP2 levels and enhanced expression of target genes (Figure 4-31).
The same stabilising effect on SREBPs and target genes as well as on the USP28 target protein c-Myc could be observed in squamous A431 cells and further analyses showed the activation of the PI3K/AKT pathway (Figure 4-32).

The time- and concentration-dependent effect of AZ-1 on has already been shown by Wrigley and colleagues: AZ-1 treatment of colon cancer cell lines resulted in a concentration-dependent biphasic increase and subsequent decrease of c-Myc protein levels. A significant reduction of c-Myc was observed with an AZ-1 concentration of 60 µM (Wrigley *et al.* 2017). Furthermore, AZ-1 treatment revealed increased levels of USP28 itself (Figure 4-33), an effect that was also observed in the biochemical analyses of Wrigley *et al*. Since USP28 has been shown to deubiquitinate itself and regulate its stability, this observation was unexpected.

The increasing levels of SREBPs and its target genes observed in absence or at reduced USP28 levels raises the hypothesis that the deubiquitinase USP25 also plays a role in this regulatory network.
USP25 is involved in antiviral immunity as well as processes affected in Alzheimer's disease (Blount *et al.* 2012, Zhong *et al.* 2013). The role of USP25 in cancer is currently under investigation: It was shown that USP25 is often mutated in hepatocellular carcinoma and breast cancer (Deng *et al.* 2007, Fujimoto *et al.* 2012). Further, reduced USP25 levels in NSCLC revealed tumour-suppressive effects, like reduced migration and invasion capacity mediated by overexpression of miR-200c, and USP25 expression correlates with the clinical stage of human patients (Li *et al.* 2014).
To determine to which extent USP28 and USP25 were inhibited by AZ-1, a DUB activity assay was performed: In presence of active deubiquitinases, the DUB probe is bound and activity can be detected by a shift to higher molecular weight on immunoblot. Under the given experimental conditions (10 µM AZ-1 for 24h and 48h), USP28 remained completely active, while USP25 was unable to bind the probe, indicating an inactive state (Figure 4-35). It should be noted that experimental conditions might need to be optimized to confirm this result.
Biochemical analysis of cells treated with the AZ-1 compound detected a reduced activity of USP28 of around 50% and for USP25 approximately 80% in colon cancer cell lines. Additionally, the determined IC_{50} values of the two DUBs under AZ-1 treatment (IC_{50}(USP28) = 0.7 µM and IC_{50}(USP25) = 0.62µM) as well as EC_{50} values (EC_{50}(USP28) = 5.3 µM and EC_{50}(USP25) = 3.3 µM) indicate, that AZ-1 is slightly more potent in inhibition of USP25 (Wrigley *et al.* 2017).
However, Prieto-Garcia and colleagues showed in A431 cells that USP28 activity is already reduced to less than 30% at a concentration of 3 µM of AZ-1 (Prieto-Garcia *et al.* 2020). AZ-1 was described as a reversible inhibitor of USP28 and its dilution completely restores DUB activity (Wrigley *et al.* 2017). During the mild lysis of the cells, the DUB probe was added and then competes with AZ-1 for active DUBs. Dilution during the lysis process could have removed the inhibitor and favoured the probe binding. To avoid artificial dilution effects, the concentration of AZ-1 needs to be kept constant. Additionally, further investigations on the binding and mode of inhibition of USP28 and USP25 by AZ-1 need to be conducted.

Since SREBP1 was upregulated by AZ-1 treatment in the absence of USP28, it cannot be excluded that USP25 also regulates SREBPs in an indirect manner.
USP25 was reported to play a pivotal role in the ER-associated degradation (ERAD) of unfolded or misfolded proteins, revealing its function in preventing neurodegenerative diseases (Blount *et al.* 2012). USP25 localises to the ER and interacts with components of the ERAD machinery (Figure 4-36). Beside an interaction with VCP/p97, USP25 was also found to bind to the E3 ligase HRD1, also known as HMGCR degradation protein 1 (Hampton *et al.* 1996), which protects against ER stress-induced apoptosis by ubiquitination-mediated proteolysis (Kaneko *et al.* 2002, Blount *et al.* 2012). Further, HRD1 was found to be a critical regulator in liver metabolism: HRD1 depletion led to a downregulation of SREBP1 and its target genes, at least partially due to the ENTPD5-AMPK pathway (Wei *et al.* 2018).
USP25 opposes HRD1-mediated ubiquitination and regulates the stability of several ER proteins (Blount *et al.* 2012).

To better understand the role of USP25 in the context of AZ-1 treatment, the significantly downregulated proteins in a proteomic dataset from A431 cells with knockdown of USP28 or after AZ-1 treatment were analysed (Figure 5-7).

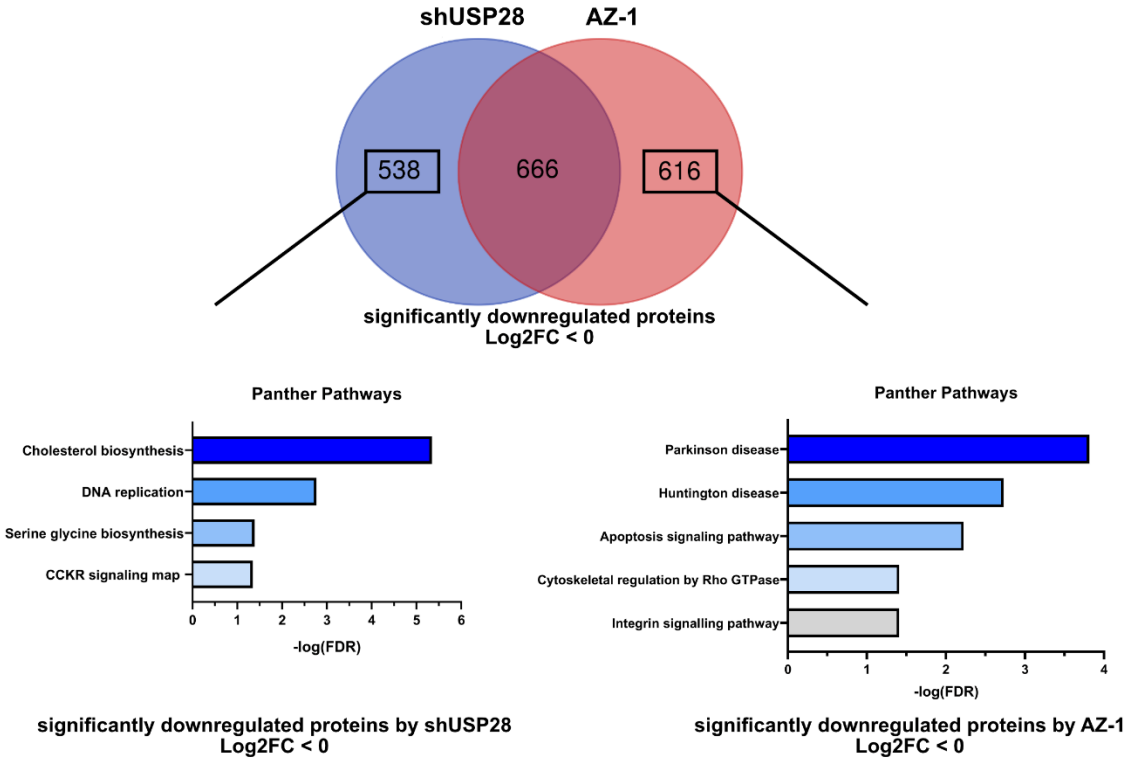

Figure 5-7: Proteomic analysis of AZ-1- and shUSP28-regulated proteins in A431 cells.

VENN diagram showing the significantly downregulated proteins of A431 cells harbouring a knockdown of USP28 (compare Figure 4-15) and downregulated proteins after AZ-1 treatment. This proteomic dataset was kindly provided by Cristian Pietro-Garcia and Markus Diefenbacher (Prieto-Garcia et al. 2021). Knockdown of USP28 and AZ-1 treatment of A431 cells show 666 commonly downregulated proteins, while 538 proteins were identified to be specifically decreased after USP28 knockdown and 616 proteins were affected only by AZ-1 treatment. Specifically regulated proteins were used for pathway analysis and diagrams show –(log)FDR of pathways significantly downregulated by knockdown of USP28 or AZ-1 treatment.

USP28-knockdown or AZ-1 treated A431 cells showed 666 commonly downregulated proteins, 616 proteins specifically downregulated in AZ-1 treated cells and 538 proteins which were reduced only in the knockdown cells. The 616 proteins specifically downregulated in inhibitor treated cells were further analysed regarding the reduction in cellular pathways. Since these proteins were not affected in the knockdown cells, it can be assumed that the effects are caused by USP25. Indeed, the pathway analysis revealed important reduction in the USP25-associated pathways of neurodegenerative diseases.
The main pathway downregulated in the shUSP28 cells but not affected by AZ-1 treatment was determined as cholesterol biosynthesis. Additionally, proteins important in the DNA replication mechanism were found to by solely downregulated in shUSP28 cells but not when cells were treated with AZ-1.
USP28 is known to play an important role in the DNA damage response (DDR) and loss of USP28 was associated with a decrease in proteins involved in DNA replication (Zhang *et al.* 2006, Prieto-Garcia *et al.* 2021): Upon DNA damage or replication stress, USP28 gets phosphorylated which increases its activity and stabilises substrate proteins important for DDR. Reduced USP28 therefore is associated with increased DNA damage and could subsequently block DNA replication in cells.
The fact that proteins involved in the mevalonate pathway and cholesterol biosynthesis are specifically reduced in USP28-knockdown cells but not affected by AZ-1 treatment supports the hypothesis that under the chosen conditions USP25 activity is preferably inhibited by the compound while USP28 is still active, substantiating the result of the DUB activity assay (Figure 4-35). While it cannot be excluded that the inducible knockdown system results in some off-target effects, it seems unlikely that the shRNA-mediated knockdown specifically reduces several enzymes involved in the mevalonate pathway, since these do not show common structural features or chromosomal location.
To unravel the observation that a high number of proteins are downregulated by USP28-knockdown but not targeted by AZ-1, further investigations regarding the specificity of the inhibitor and the knockdown system need to be performed.

As demonstrated by the finding in this thesis, the dual USP25/28 inhibitor AZ-1 poses many challenges in concentration- and time-dependent treatment, which need to be overcome for future therapy in patients. It is necessary to develop compounds that specifically inhibit either USP25 or USP28, since their roles in metabolic pathway regulation are opposing and an anti-tumour effect can only be achieved when USP28 activity is specifically inhibited. Currently, selective USP28 inhibitors are under pre-clinical evaluation, which has shown promising anti-tumour effects in lung squamous tumours and revealed a higher affinity to bind to USP28 than to USP25 when used in low concentrations (Ruiz *et al.* 2021). In future, the therapeutic window for specifically inhibiting either USP25 or USP28 needs to be determined and possible combinatorial treatments have to be developed to increase anti-tumour effects and reduce potential negative side effects for the cancer patients.

6 Concluding Remarks and Future Outlook

Reprogramming cancer metabolism plays an important role in the development and progression of cancer. The regulation of metabolic pathways is often controlled by master transcription factors, which activate the transcription of enzymes, involved in the uptake, the conversion, or *de novo* synthesis of metabolites.
SREBPs are master regulators of fatty acid synthesis as well as the mevalonate pathway and downstream cholesterogenesis. These transcription factors are tightly regulated at different levels. The active mature forms of SREBPs are highly instable and are rapidly degraded by ubiquitin-mediated proteasomal degradation. The work described in this thesis identified USP28 as a deubiquitinating enzyme for mSREBPs by counteracting the respective E3 ligase and removing ubiquitin chains. The removal of the degradation signal results in stabilized mSREBPs, which activate transcription of their target genes.

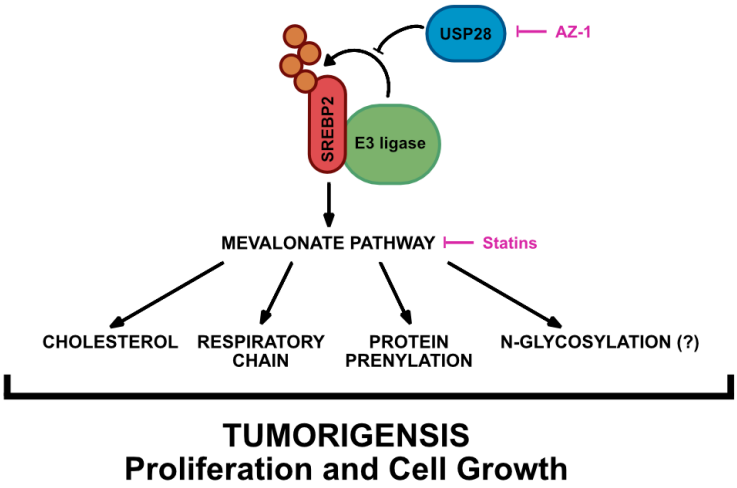

Figure 6-1: USP28 regulating SREBP2 stability and affects the mevalonate pathway and downstream processes.

Furthermore, USP28-SREBP interaction was localised to the nucleus as well as the cytoplasm (Figure 4-4). USP28 is described as a nuclear protein, acting directly on transcription factors bound to DNA on promoter sites. Here, USP28 was found in both nuclear and cytoplasmic compartments and additionally in the membrane-bound fraction (Figure 4-2). The presence of USP28 outside of the nucleus and its functional role in other compartments needs to be further investigated.
Increased USP28 levels stabilised mSREBPs independent of the binding of the E3 ligase Fbw7 (4.2). The binding and deubiquitination of mSREBPs by USP28 has been shown (Figure 4-3 & Figure 4-9).
The resolution of the crystal structure of USP28 revealed that this DUB has a conformation of an active dimer (Gersch *et al.* 2019, Sauer *et al.* 2019). Whether USP28 deubiquitinates its substrates by binding in its the dimeric form, as it was proposed for its counteracting E3 ligase Fbw7 (Welcker *et al.* 2013), needs to be clarified in future.

The respective lysine residues, which serve as ubiquitin attachment sites in SREBPs, were not identified yet. Since post-translational modifications are in concurrence of each other, it would be interesting to further analyse if ubiquitination blocks the respective lysine residues for other PTMs, e.g. acetylation or sumoylation (Hirano *et al.* 2003). SREBPs were shown to be acetylated in their DNA binding domain and this increases their stability, most likely by preventing ubiquitination (Giandomenico *et al.* 2003). To clarify if deubiquitination of SREBPs also releases the respective lysine residues for acetylation and subsequential enhanced transcriptional activity, further experiments are required.

In the absence of USP28, SREBP2 and its target genes were downregulated and cell proliferation was decreased (4.3). To confirm that this cell growth inhibition is mediated by the loss of USP28 deubiquitination activity and consequently reduced stability of SREBP2, experiments with exogenously expressed USP28 and mutant SREBP2, in which either the CPD or the ubiquitinated lysine residue are abolished, need to be performed to monitor if SREBP target gene levels and cell viability can be restored in USP28 knockout cells.

Further, this study also revealed, that reduced USP28 levels decrease expression of SREBP2 target genes in cells and *in vivo* (Figure 4-15, Figure 4-16 & Figure 4-42). Thus, the mevalonate pathway is regulated by USP28 activity also under the metabolic conditions found *in vivo*. Detailed metabolic analysis showed that reduced USP28 and SREBP2 levels led to a reduction in the synthesis of coenzyme Q10 and metabolites involved in the *de novo* purine and pyrimidine synthesis (Figure 4-22 & Figure 4-23). Squamous A431 cells indicated a high flux of glucose-derived carbons into the mevalonate pathway, but *de novo* cholesterol synthesis was unexpectedly low. This observation raises the hypothesis that the cells prefer the uptake of cholesterol. This hypothesis needs to be proven by determining the proteins responsible for metabolite uptake. Since additional serum deprivation or other conditions where SREBP2 and the activation of the mevalonate pathway were reported to be essential did not result in decreased cell viability (Figure 4-19 & Figure 4-20), further metabolic profiling is needed to characterize altered metabolic flux as well as changes in the *de novo* synthesis of metabolites as a consequence of reduced USP28 and SREBP2 levels.

USP28 was shown to play an essential role in the development and progression of squamous lung tumours by regulating oncogenes, like ΔNp63 or Notch1 (Prieto-Garcia *et al.* 2020). In the current study the contribution of the USP28-SREBP2 regulatory axis in squamous cancer, especially lung SCC, was investigated: In a lung cancer mouse model of SCC, increased levels of USP28 and the SREBP2 target gene HMGCS1 were detected. Furthermore, knockout of SREBP2 in lung tumours reduced tumour load and increased animal survival (Figure 4-40 & Figure 4-44). This provides proofs for the essentiality of SREBP2 and increased mevalonate pathway activity to initiate tumorigenesis and tumour growth in SCC.

Interestingly, high levels of USP28, SREBP2, HMGCS1 and FDFT1 are associated with the squamous phenotype of lung cancer in mice and humans (Figure 4-41 & Figure 4-38). Loss of SREBP2 in lung cancer showed a marked reduction of ΔNp63 expression in the residual tumours (Figure 4-44), indicating that SREBP2 and the

mevalonate pathway are specifically essential to maintain the squamous phenotype. This observation is also supported by transcriptomic analysis, indicating downregulation of ΔNp63 target genes when USP28 or SREBP2 are targeted by knockdown in squamous A431 cells (Figure 4-24).

Since it was shown that SREBP1 cooperates with ΔNp63 to increase target gene transcription in squamous cancers (Li *et al.* 2021), a similar mode of regulation for SREBP2 and ΔNp63 seems likely. To unravel the interplay between SREBP2 and ΔNp63 in the context of SCC, further studies evaluating chromatin binding and transcriptional activity of the two proteins need to be conducted.

The pivotal role of the USP28-SREBP2 regulatory axis in SCC raises the possibility for therapeutic intervention in SCC patients. For this purpose, SCC cells with reduced USP28 levels were treated with simvastatin, which inhibits the rate-limiting enzyme of the mevalonate pathway. Analysis of cell viability showed that the loss of USP28 sensitizes the cancer cells to simvastatin treatment (Figure 4-25), and this was likely due to reduced protein prenylation (Figure 4-28) rather than reduced cholesterol or CoQ10 synthesis (Figure 4-26 & Figure 4-27). The production of dolichol by the mevalonate pathway and its role in N-glycosylation of proteins was not investigated in this study, and conclusions about this branch of the mevalonate pathway and how it could affect cell viability and proliferation also in the context of therapeutic intervention in SCC require further experiments.

The therapeutic treatment of SCC patients is highly challenging due to the specific features of squamous cancers. Combinatorial approaches targeting at least two pro-proliferative signalling pathways in SCC cells showed first promising effects by reducing tumour growth. Especially, simvastatin use has been already associated with beneficial outcomes for patients. The simultaneous treatment of SCC cells with increasing concentrations of simvastatin and the dual USP25/28 inhibitor AZ-1 showed synergistic effects in reducing cell growth and viability at high concentrations (Figure 4-30). Interestingly, the combination of both inhibitors revealed pro-proliferative effect at lower concentrations and a marked resistance to simvastatin treatment (Figure 4-29 & Figure 4-30). Further analysis showed that AZ-1 upregulates SREBPs and target genes and activates the PI3K-AKT pathway in a dose- and time-dependent manner (Figure 4-32). One explanation could be an alternative regulation of SREBPs by USP25 (discussed in 5.5.4). To exploit the observed synergistic effect for therapeutically use, the therapeutic window needs to be stringently determined and AZ-1 inhibitor should be further characterized regarding its effects on other metabolic pathways or pro-survival processes in cancer cells. The development of an inhibitor specifically targeting USP28 and not affecting its close homolog USP25 is challenging due to high sequence similarity of both proteins.

However, a combinatorial treatment of two or even more inhibitors specifically interfering with USP28 in combination with blocking the mevalonate pathway and additional downstream processes may reveal promising therapeutic intervention strategies for SCC patients.

7 Bibliography

Ahmadi, M., S. Amiri, S. Pecic, F. Machaj, J. Rosik, M. J. Los, . . . S. Ghavami (2020). "**Pleiotropic effects of statins: A focus on cancer**." Biochim Biophys Acta Mol Basis Dis 1866(12): 165968.

Amerik, A. Y. and M. Hochstrasser (2004). "**Mechanism and function of deubiquitinating enzymes**." Biochim Biophys Acta 1695(1-3): 189-207.

Aurnhammer, C., M. Haase, N. Muether, M. Hausl, C. Rauschhuber, I. Huber, . . . A. Baiker (2012). "**Universal real-time PCR for the detection and quantification of adeno-associated virus serotype 2-derived inverted terminal repeat sequences**." Hum Gene Ther Methods 23(1): 18-28.

Bankhead, P., M. B. Loughrey, J. A. Fernandez, Y. Dombrowski, D. G. McArt, P. D. Dunne, . . . P. W. Hamilton (2017). "**QuPath: Open source software for digital pathology image analysis**." Sci Rep 7(1): 16878.

Bengoechea-Alonso, M. T., A. Aldaalis and J. Ericsson (2022). "**Loss of the Fbw7 tumor suppressor rewires cholesterol metabolism in cancer cells leading to activation of the PI3K-AKT signalling axis**." Front Oncol 12: 990672.

Blount, J. R., A. A. Burr, A. Denuc, G. Marfany and S. V. Todi (2012). "**Ubiquitin-specific protease 25 functions in Endoplasmic Reticulum-associated degradation**." PLoS One 7(5): e36542.

Bosch-Comas, A., K. Lindsten, R. Gonzalez-Duarte, M. G. Masucci and G. Marfany (2006). "**The ubiquitin-specific protease USP25 interacts with three sarcomeric proteins**." Cell Mol Life Sci 63(6): 723-734.

Briggs, M. R., C. Yokoyama, X. Wang, M. S. Brown and J. L. Goldstein (1993). "**Nuclear protein that binds sterol regulatory element of low density lipoprotein receptor promoter. I. Identification of the protein and delineation of its target nucleotide sequence**." J Biol Chem 268(19): 14490-14496.

Brindisi, M., M. Fiorillo, L. Frattaruolo, F. Sotgia, M. P. Lisanti and A. R. Cappello (2020). "**Cholesterol and Mevalonate: Two Metabolites Involved in Breast Cancer Progression and Drug Resistance through the ERRalpha Pathway**." Cells 9(8).

Brovkovych, V., A. Aldrich, N. Li, G. E. Atilla-Gokcumen and J. Frasor (2019). "**Removal of Serum Lipids and Lipid-Derived Metabolites to Investigate Breast Cancer Cell Biology**." Proteomics 19(18): e1800370.

Brovkovych, V., Y. Izhar, J. M. Danes, O. Dubrovskyi, I. T. Sakallioglu, L. M. Morrow, . . . J. Frasor (2018). "**Fatostatin induces pro- and anti-apoptotic lipid accumulation in breast cancer**." Oncogenesis 7(8): 66.

Brown, M. S. and J. L. Goldstein (1997). "**The SREBP pathway: regulation of cholesterol metabolism by proteolysis of a membrane-bound transcription factor**." Cell 89(3): 331-340.

Cancer Genome Atlas Research, N. (2012). "**Comprehensive genomic characterization of squamous cell lung cancers**." Nature 489(7417): 519-525.

Cancer Genome Atlas Research, N., J. N. Weinstein, E. A. Collisson, G. B. Mills, K. R. Shaw, B. A. Ozenberger, . . . J. M. Stuart (2013). "**The Cancer Genome Atlas Pan-Cancer analysis project**." Nat Genet 45(10): 1113-1120.

Carlberg, M., A. Dricu, H. Blegen, M. Wang, M. Hjertman, P. Zickert, . . . O. Larsson (1996). "**Mevalonic acid is limiting for N-linked glycosylation and translocation of the insulin-like growth factor-1 receptor to the cell surface. Evidence for a new link between 3-hydroxy-3-methylglutaryl-coenzyme a reductase and cell growth**." J Biol Chem 271(29): 17453-17462.

Cheon, H., Y. Wang, S. M. Wightman, M. W. Jackson and G. R. Stark (2023). "**How cancer cells make and respond to interferon-I**." Trends Cancer 9(1): 83-92.

Chiu, H. F., S. C. Ho, C. C. Chen and C. Y. Yang (2011). "**Statin use and the risk of liver cancer: a population-based case-control study**." Am J Gastroenterol 106(5): 894-898.

Chou, C. W., C. H. Lin, T. H. Hsiao, C. C. Lo, C. Y. Hsieh, C. C. Huang and Y. P. Sher (2019). "**Therapeutic effects of statins against lung adenocarcinoma via p53 mutant-mediated apoptosis**." Sci Rep 9(1): 20403.

Conde, E., B. Angulo, P. Redondo, O. Toldos, E. Garcia-Garcia, A. Suarez-Gauthier, . . . F. Lopez-Rios (2010). "**The use of P63 immunohistochemistry for the identification of squamous cell carcinoma of the lung**." PLoS One 5(8): e12209.

Dang, F., L. Nie and W. Wei (2021). "**Ubiquitin signaling in cell cycle control and tumorigenesis**." Cell Death Differ 28(2): 427-438.

Dasari, S. and P. B. Tchounwou (2014). "**Cisplatin in cancer therapy: molecular mechanisms of action**." Eur J Pharmacol 740: 364-378.

Dawson, P. A., S. L. Hofmann, D. R. van der Westhuyzen, T. C. Sudhof, M. S. Brown and J. L. Goldstein (1988). "**Sterol-dependent repression of low density lipoprotein receptor promoter mediated by 16-base pair sequence adjacent to binding site for transcription factor Sp1**." J Biol Chem 263(7): 3372-3379.

De Francesco, E. M., F. Sotgia and M. P. Lisanti (2018). "**Cancer stem cells (CSCs): metabolic strategies for their identification and eradication**." Biochem J 475(9): 1611-1634.

Deng, S., H. Zhou, R. Xiong, Y. Lu, D. Yan, T. Xing, . . . H. Yang (2007). "**Over-expression of genes and proteins of ubiquitin specific peptidases (USPs) and**

proteasome subunits (PSs) in breast cancer tissue observed by the methods of RFDD-PCR and proteomics." Breast Cancer Res Treat 104(1): 21-30.

Denuc, A., A. Bosch-Comas, R. Gonzalez-Duarte and G. Marfany (2009). "**The UBA-UIM domains of the USP25 regulate the enzyme ubiquitination state and modulate substrate recognition**." PLoS One 4(5): e5571.

Deveraux, Q., V. Ustrell, C. Pickart and M. Rechsteiner (1994). "**A 26 S protease subunit that binds ubiquitin conjugates**." J Biol Chem 269(10): 7059-7061.

Diefenbacher, M. E., N. Popov, S. M. Blake, C. Schulein-Volk, E. Nye, B. Spencer-Dene, . . . A. Behrens (2014). "**The deubiquitinase USP28 controls intestinal homeostasis and promotes colorectal cancer**." J Clin Invest 124(8): 3407-3418.

Ding, X., W. Zhang, S. Li and H. Yang (2019). "**The role of cholesterol metabolism in cancer**." Am J Cancer Res 9(2): 219-227.

Dotto, G. P. and A. K. Rustgi (2016). "**Squamous Cell Cancers: A Unified Perspective on Biology and Genetics**." Cancer Cell 29(5): 622-637.

Dudakovic, A., H. Tong and R. J. Hohl (2011). "**Geranylgeranyl diphosphate depletion inhibits breast cancer cell migration**." Invest New Drugs 29(5): 912-920.

Duncan, E. A., M. S. Brown, J. L. Goldstein and J. Sakai (1997). "**Cleavage site for sterol-regulated protease localized to a leu-Ser bond in the lumenal loop of sterol regulatory element-binding protein-2**." J Biol Chem 272(19): 12778-12785.

Duncan, E. A., U. P. Dave, J. Sakai, J. L. Goldstein and M. S. Brown (1998). "**Second-site cleavage in sterol regulatory element-binding protein occurs at transmembrane junction as determined by cysteine panning**." J Biol Chem 273(28): 17801-17809.

Duvel, K., J. L. Yecies, S. Menon, P. Raman, A. I. Lipovsky, A. L. Souza, . . . B. D. Manning (2010). "**Activation of a metabolic gene regulatory network downstream of mTOR complex 1**." Mol Cell 39(2): 171-183.

Elkabets, M., E. Pazarentzos, D. Juric, Q. Sheng, R. A. Pelossof, S. Brook, . . . J. Baselga (2015). "**AXL mediates resistance to PI3Kalpha inhibition by activating the EGFR/PKC/mTOR axis in head and neck and esophageal squamous cell carcinomas**." Cancer Cell 27(4): 533-546.

Elsasser, S. and D. Finley (2005). "**Delivery of ubiquitinated substrates to protein-unfolding machines**." Nat Cell Biol 7(8): 742-749.

Ericsson, J., S. M. Jackson and P. A. Edwards (1996). "**Synergistic binding of sterol regulatory element-binding protein and NF-Y to the farnesyl diphosphate synthase promoter is critical for sterol-regulated expression of the gene**." J Biol Chem 271(40): 24359-24364.

Ericsson, J., S. M. Jackson, B. C. Lee and P. A. Edwards (1996). "**Sterol regulatory element binding protein binds to a cis element in the promoter of the farnesyl diphosphate synthase gene**." Proc Natl Acad Sci U S A 93(2): 945-950.

Espenshade, P. J., D. Cheng, J. L. Goldstein and M. S. Brown (1999). "**Autocatalytic processing of site-1 protease removes propeptide and permits cleavage of sterol regulatory element-binding proteins**." J Biol Chem 274(32): 22795-22804.

Fellmann, C., T. Hoffmann, V. Sridhar, B. Hopfgartner, M. Muhar, M. Roth, . . . J. Zuber (2013). "**An optimized microRNA backbone for effective single-copy RNAi**." Cell Rep 5(6): 1704-1713.

Flugel, D., A. Gorlach and T. Kietzmann (2012). "**GSK-3beta regulates cell growth, migration, and angiogenesis via Fbw7 and USP28-dependent degradation of HIF-1alpha**." Blood 119(5): 1292-1301.

Freed-Pastor, W. A., H. Mizuno, X. Zhao, A. Langerod, S. H. Moon, R. Rodriguez-Barrueco, . . . C. Prives (2012). "**Mutant p53 disrupts mammary tissue architecture via the mevalonate pathway**." Cell 148(1-2): 244-258.

Fujimoto, A., Y. Totoki, T. Abe, K. A. Boroevich, F. Hosoda, H. H. Nguyen, . . . H. Nakagawa (2012). "**Whole-genome sequencing of liver cancers identifies etiological influences on mutation patterns and recurrent mutations in chromatin regulators**." Nat Genet 44(7): 760-764.

Galli, F., M. Rossi, Y. D'Alessandra, M. De Simone, T. Lopardo, Y. Haupt, . . . L. Guerrini (2010). "**MDM2 and Fbw7 cooperate to induce p63 protein degradation following DNA damage and cell differentiation**." J Cell Sci 123(Pt 14): 2423-2433.

Gao, S., Z. Shi, X. Li, W. Li, Y. Wang, Z. Liu and J. Jiang (2018). "**Fatostatin suppresses growth and enhances apoptosis by blocking SREBP-regulated metabolic pathways in endometrial carcinoma**." Oncol Rep 39(4): 1919-1929.

Geng, F., S. Wenzel and W. P. Tansey (2012). "**Ubiquitin and proteasomes in transcription**." Annu Rev Biochem 81: 177-201.

Gersch, M., J. L. Wagstaff, A. V. Toms, B. Graves, S. M. V. Freund and D. Komander (2019). "**Distinct USP25 and USP28 Oligomerization States Regulate Deubiquitinating Activity**." Mol Cell 74(3): 436-451 e437.

Giandomenico, V., M. Simonsson, E. Gronroos and J. Ericsson (2003). "**Coactivator-dependent acetylation stabilizes members of the SREBP family of transcription factors**." Mol Cell Biol 23(7): 2587-2599.

Gober, H. J., M. Kistowska, L. Angman, P. Jeno, L. Mori and G. De Libero (2003). "**Human T cell receptor gammadelta cells recognize endogenous mevalonate metabolites in tumor cells**." J Exp Med 197(2): 163-168.

Goodwin, J., M. L. Neugent, S. Y. Lee, J. H. Choe, H. Choi, D. M. R. Jenkins, . . . J. W. Kim (2017). "**The distinct metabolic phenotype of lung squamous cell carcinoma defines selective vulnerability to glycolytic inhibition**." Nat Commun 8: 15503.

Gouw, A. M., K. Margulis, N. S. Liu, S. J. Raman, A. Mancuso, G. G. Toal, . . . D. W. Felsher (2019). "**The MYC Oncogene Cooperates with Sterol-Regulated Element-Binding Protein to Regulate Lipogenesis Essential for Neoplastic Growth**." Cell Metab 30(3): 556-572 e555.

Griffiths, B., C. A. Lewis, K. Bensaad, S. Ros, Q. Zhang, E. C. Ferber, . . . A. Schulze (2013). "**Sterol regulatory element binding protein-dependent regulation of lipid synthesis supports cell survival and tumor growth**." Cancer Metab 1(1): 3.

Gruenbacher, G., H. Gander, O. Nussbaumer, W. Nussbaumer, A. Rahm and M. Thurnher (2010). "**IL-2 costimulation enables statin-mediated activation of human NK cells, preferentially through a mechanism involving CD56+ dendritic cells**." Cancer Res 70(23): 9611-9620.

Guan, G., G. Jiang, R. L. Koch and I. Shechter (1995). "**Molecular cloning and functional analysis of the promoter of the human squalene synthase gene**." J Biol Chem 270(37): 21958-21965.

Guerra, B., C. Recio, H. Aranda-Tavio, M. Guerra-Rodriguez, J. M. Garcia-Castellano and L. Fernandez-Perez (2021). "**The Mevalonate Pathway, a Metabolic Target in Cancer Therapy**." Front Oncol 11: 626971.

Guo, C., R. Wan, Y. He, S. H. Lin, J. Cao, Y. Qiu, . . . H. Ji (2022). "**Therapeutic targeting of the mevalonate-geranylgeranyl diphosphate pathway with statins overcomes chemotherapy resistance in small cell lung cancer**." Nat Cancer 3(5): 614-628.

Hampton, R. Y., R. G. Gardner and J. Rine (1996). "**Role of 26S proteasome and HRD genes in the degradation of 3-hydroxy-3-methylglutaryl-CoA reductase, an integral endoplasmic reticulum membrane protein**." Mol Biol Cell 7(12): 2029-2044.

Hanahan, D. and R. A. Weinberg (2011). "**Hallmarks of cancer: the next generation**." Cell 144(5): 646-674.

Hancock, J. F., A. I. Magee, J. E. Childs and C. J. Marshall (1989). "**All ras proteins are polyisoprenylated but only some are palmitoylated**." Cell 57(7): 1167-1177.

Hartmann, O., M. Reissland, C. R. Maier, T. Fischer, C. Prieto-Garcia, A. Baluapuri, . . . M. E. Diefenbacher (2021). "**Implementation of CRISPR/Cas9 Genome Editing to Generate Murine Lung Cancer Models That Depict the Mutational Landscape of Human Disease**." Front Cell Dev Biol 9: 641618.

Hashimoto, A., T. Oikawa, S. Hashimoto, H. Sugino, A. Yoshikawa, Y. Otsuka, . . . H. Sabe (2016). "**P53- and mevalonate pathway-driven malignancies require Arf6 for metastasis and drug resistance**." J Cell Biol 213(1): 81-95.

Hirano, Y., S. Murata, K. Tanaka, M. Shimizu and R. Sato (2003). "**Sterol regulatory element-binding proteins are negatively regulated through SUMO-1 modification independent of the ubiquitin/26 S proteasome pathway**." J Biol Chem 278(19): 16809-16819.

Hirano, Y., M. Yoshida, M. Shimizu and R. Sato (2001). "**Direct demonstration of rapid degradation of nuclear sterol regulatory element-binding proteins by the ubiquitin-proteasome pathway**." J Biol Chem 276(39): 36431-36437.

Horton, J. D., N. A. Shah, J. A. Warrington, N. N. Anderson, S. W. Park, M. S. Brown and J. L. Goldstein (2003). "**Combined analysis of oligonucleotide microarray data from transgenic and knockout mice identifies direct SREBP target genes**." Proc Natl Acad Sci U S A 100(21): 12027-12032.

Horton, J. D., I. Shimomura, M. S. Brown, R. E. Hammer, J. L. Goldstein and H. Shimano (1998). "**Activation of cholesterol synthesis in preference to fatty acid synthesis in liver and adipose tissue of transgenic mice overproducing sterol regulatory element-binding protein-2**." J Clin Invest 101(11): 2331-2339.

Hosios, A. M., Z. Li, E. C. Lien and M. V. G. Heiden (2018). "**Preparation of Lipid-Stripped Serum for the Study of Lipid Metabolism in Cell Culture**." Bio Protoc 8(11): e2876.

Hou, S., S. Zhou, Z. Qin, L. Yang, X. Han, S. Yao and H. Ji (2017). "**Evidence, Mechanism, and Clinical Relevance of the Transdifferentiation from Lung Adenocarcinoma to Squamous Cell Carcinoma**." Am J Pathol 187(5): 954-962.

Hua, X., J. Sakai, Y. K. Ho, J. L. Goldstein and M. S. Brown (1995). "**Hairpin orientation of sterol regulatory element-binding protein-2 in cell membranes as determined by protease protection**." J Biol Chem 270(49): 29422-29427.

Hua, X., J. Wu, J. L. Goldstein, M. S. Brown and H. H. Hobbs (1995). "**Structure of the human gene encoding sterol regulatory element binding protein-1 (SREBF1) and localization of SREBF1 and SREBF2 to chromosomes 17p11.2 and 22q13**." Genomics 25(3): 667-673.

Hua, X., C. Yokoyama, J. Wu, M. R. Briggs, M. S. Brown, J. L. Goldstein and X. Wang (1993). "**SREBP-2, a second basic-helix-loop-helix-leucine zipper protein that stimulates transcription by binding to a sterol regulatory element**." Proc Natl Acad Sci U S A 90(24): 11603-11607.

Hughes, A. L., B. L. Todd and P. J. Espenshade (2005). "**SREBP pathway responds to sterols and functions as an oxygen sensor in fission yeast**." Cell 120(6): 831-842.

Hung, M. S., I. C. Chen, C. P. Lee, R. J. Huang, P. C. Chen, Y. H. Tsai and Y. H. Yang (2017). "**Statin improves survival in patients with EGFR-TKI lung cancer: A nationwide population-based study**." PLoS One 12(2): e0171137.

Jackson, S. M., J. Ericsson, T. F. Osborne and P. A. Edwards (1995). "**NF-Y has a novel role in sterol-dependent transcription of two cholesterogenic genes**." J Biol Chem 270(37): 21445-21448.

Kamisuki, S., Q. Mao, L. Abu-Elheiga, Z. Gu, A. Kugimiya, Y. Kwon, . . . M. Uesugi (2009). "**A small molecule that blocks fat synthesis by inhibiting the activation of SREBP**." Chem Biol 16(8): 882-892.

Kaneko, M., M. Ishiguro, Y. Niinuma, M. Uesugi and Y. Nomura (2002). "**Human HRD1 protects against ER stress-induced apoptosis through ER-associated degradation**." FEBS Lett 532(1-2): 147-152.

Kang, J., S. M. Jeong, D. W. Shin, M. Cho, J. H. Cho and J. Kim (2021). "**The Associations of Aspirin, Statins, and Metformin With Lung Cancer Risk and Related Mortality: A Time-Dependent Analysis of Population-Based Nationally Representative Data**." J Thorac Oncol 16(1): 76-88.

Kaymak, I., C. R. Maier, W. Schmitz, A. D. Campbell, B. Dankworth, C. P. Ade, . . . A. Schulze (2020). "**Mevalonate Pathway Provides Ubiquinone to Maintain Pyrimidine Synthesis and Survival in p53-Deficient Cancer Cells Exposed to Metabolic Stress**." Cancer Res 80(2): 189-203.

Kent, W. J., C. W. Sugnet, T. S. Furey, K. M. Roskin, T. H. Pringle, A. M. Zahler and D. Haussler (2002). "**The human genome browser at UCSC**." Genome Res 12(6): 996-1006.

Khurana, V., H. R. Bejjanki, G. Caldito and M. W. Owens (2007). "**Statins reduce the risk of lung cancer in humans: a large case-control study of US veterans**." Chest 131(5): 1282-1288.

Kim, J. B., G. D. Spotts, Y. D. Halvorsen, H. M. Shih, T. Ellenberger, H. C. Towle and B. M. Spiegelman (1995). "**Dual DNA binding specificity of ADD1/SREBP1 controlled by a single amino acid in the basic helix-loop-helix domain**." Mol Cell Biol 15(5): 2582-2588.

Knuutila, S., Y. Aalto, K. Autio, A. M. Bjorkqvist, W. El-Rifai, S. Hemmer, . . . Y. Zhu (1999). "**DNA copy number losses in human neoplasms**." Am J Pathol 155(3): 683-694.

Komander, D. and M. Rape (2012). "**The ubiquitin code**." Annu Rev Biochem 81: 203-229.

Kondo, A., S. Yamamoto, R. Nakaki, T. Shimamura, T. Hamakubo, J. Sakai, . . . T. Osawa (2017). "**Extracellular Acidic pH Activates the Sterol Regulatory Element-Binding Protein 2 to Promote Tumor Progression**." Cell Rep 18(9): 2228-2242.

Kotzka, J., S. Lehr, G. Roth, H. Avci, B. Knebel and D. Muller-Wieland (2004). "**Insulin-activated Erk-mitogen-activated protein kinases phosphorylate sterol regulatory element-binding Protein-2 at serine residues 432 and 455 in vivo**." J Biol Chem 279(21): 22404-22411.

Kotzka, J., D. Muller-Wieland, G. Roth, L. Kremer, M. Munck, S. Schurmann, . . . W. Krone (2000). "**Sterol regulatory element binding proteins (SREBP)-1a and SREBP-2 are linked to the MAP-kinase cascade**." J Lipid Res 41(1): 99-108.

Labun, K., T. G. Montague, M. Krause, Y. N. Torres Cleuren, H. Tjeldnes and E. Valen (2019). "**CHOPCHOP v3: expanding the CRISPR web toolbox beyond genome editing**." Nucleic Acids Res 47(W1): W171-W174.

Leitner, B. P., K. B. Givechian, S. Ospanova, A. Beisenbayeva, K. Politi and R. J. Perry (2022). "**Multimodal analysis suggests differential immuno-metabolic crosstalk in lung squamous cell carcinoma and adenocarcinoma**." NPJ Precis Oncol 6(1): 8.

Lewis, C. A., C. Brault, B. Peck, K. Bensaad, B. Griffiths, R. Mitter, . . . A. Schulze (2015). "**SREBP maintains lipid biosynthesis and viability of cancer cells under lipid- and oxygen-deprived conditions and defines a gene signature associated with poor survival in glioblastoma multiforme**." Oncogene 34(40): 5128-5140.

Li, J., Q. Tan, M. Yan, L. Liu, H. Lin, F. Zhao, . . . M. Yao (2014). "**miRNA-200c inhibits invasion and metastasis of human non-small cell lung cancer by directly targeting ubiquitin specific peptidase 25**." Mol Cancer 13: 166.

Li, J., H. Yan, L. Zhao, W. Jia, H. Yang, L. Liu, . . . G. Huang (2016). "**Inhibition of SREBP increases gefitinib sensitivity in non-small cell lung cancer cells**." Oncotarget 7(32): 52392-52403.

Li, L. Y., Q. Yang, Y. Y. Jiang, W. Yang, Y. Jiang, X. Li, . . . D. C. Lin (2021). "**Interplay and cooperation between SREBF1 and master transcription factors regulate lipid metabolism and tumor-promoting pathways in squamous cancer**." Nat Commun 12(1): 4362.

Li, M., C. L. Brooks, N. Kon and W. Gu (2004). "**A dynamic role of HAUSP in the p53-Mdm2 pathway**." Mol Cell 13(6): 879-886.

Li, M., D. Chen, A. Shiloh, J. Luo, A. Y. Nikolaev, J. Qin and W. Gu (2002). "**Deubiquitination of p53 by HAUSP is an important pathway for p53 stabilization**." Nature 416(6881): 648-653.

Li, X., Y. T. Chen, P. Hu and W. C. Huang (2014). "**Fatostatin displays high antitumor activity in prostate cancer by blocking SREBP-regulated metabolic pathways and androgen receptor signaling**." Mol Cancer Ther 13(4): 855-866.

Li, Y., S. Xu, M. M. Mihaylova, B. Zheng, X. Hou, B. Jiang, . . . M. Zang (2011). "**AMPK phosphorylates and inhibits SREBP activity to attenuate hepatic**

steatosis and atherosclerosis in diet-induced insulin-resistant mice." Cell Metab 13(4): 376-388.

Liberzon, A., C. Birger, H. Thorvaldsdottir, M. Ghandi, J. P. Mesirov and P. Tamayo (2015). "**The Molecular Signatures Database (MSigDB) hallmark gene set collection**." Cell Syst 1(6): 417-425.

Lin, J. J., N. Ezer, K. Sigel, G. Mhango and J. P. Wisnivesky (2016). "**The effect of statins on survival in patients with stage IV lung cancer**." Lung Cancer 99: 137-142.

Liu, J., T. Wang, C. J. Creighton, S. P. Wu, M. Ray, K. S. Janardhan, . . . F. J. DeMayo (2019). "**JNK(1/2) represses Lkb(1)-deficiency-induced lung squamous cell carcinoma progression**." Nat Commun 10(1): 2148.

Longo, J., P. J. Mullen, R. Yu, J. E. van Leeuwen, M. Masoomian, D. T. S. Woon, . . . L. Z. Penn (2019). "**An actionable sterol-regulated feedback loop modulates statin sensitivity in prostate cancer**." Mol Metab 25: 119-130.

Maier, C. R., O. Hartmann, C. Prieto-Garcia, K. M. Al-Shami, L. Schlicker, F. C. E. Vogel, . . . A. Schulze (2023). "**USP28 controls SREBP2 and the mevalonate pathway to drive tumour growth in squamous cancer**." Cell Death Differ.

Maron, D. J., S. Fazio and M. F. Linton (2000). "**Current perspectives on statins**." Circulation 101(2): 207-213.

Meerbrey, K. L., G. Hu, J. D. Kessler, K. Roarty, M. Z. Li, J. E. Fang, . . . S. J. Elledge (2011). "**The pINDUCER lentiviral toolkit for inducible RNA interference in vitro and in vivo**." Proc Natl Acad Sci U S A 108(9): 3665-3670.

Miserez, A. R., G. Cao, L. C. Probst and H. H. Hobbs (1997). "**Structure of the human gene encoding sterol regulatory element binding protein 2 (SREBF2)**." Genomics 40(1): 31-40.

Mitri, Z., R. Nanda, K. Blackwell, C. M. Costelloe, I. Hood, C. Wei, . . . C. Translational Breast Cancer Research (2016). "**TBCRC-010: Phase I/II Study of Dasatinib in Combination with Zoledronic Acid for the Treatment of Breast Cancer Bone Metastasis**." Clin Cancer Res 22(23): 5706-5712.

Molnar, G., M. C. Dagher, M. Geiszt, J. Settleman and E. Ligeti (2001). "**Role of prenylation in the interaction of Rho-family small GTPases with GTPase activating proteins**." Biochemistry 40(35): 10542-10549.

Momcilovic, M., S. T. Bailey, J. T. Lee, M. C. Fishbein, D. Braas, J. Go, . . . D. B. Shackelford (2018). "**The GSK3 Signaling Axis Regulates Adaptive Glutamine Metabolism in Lung Squamous Cell Carcinoma**." Cancer Cell 33(5): 905-921 e905.

Moon, S. H., C. H. Huang, S. L. Houlihan, K. Regunath, W. A. Freed-Pastor, J. P. t. Morris, . . . C. Prives (2019). "**p53 Represses the Mevalonate Pathway to Mediate Tumor Suppression**." Cell 176(3): 564-580 e519.

Naar, A. M., P. A. Beaurang, K. M. Robinson, J. D. Oliner, D. Avizonis, S. Scheek, . . . R. Tjian (1998). "**Chromatin, TAFs, and a novel multiprotein coactivator are required for synergistic activation by Sp1 and SREBP-1a in vitro**." Genes Dev 12(19): 3020-3031.

Naar, A. M., P. A. Beaurang, S. Zhou, S. Abraham, W. Solomon and R. Tjian (1999). "**Composite co-activator ARC mediates chromatin-directed transcriptional activation**." Nature 398(6730): 828-832.

Nagai, M., J. Sakakibara, Y. Nakamura, F. Gejyo and T. Ono (2002). "**SREBP-2 and NF-Y are involved in the transcriptional regulation of squalene epoxidase**." Biochem Biophys Res Commun 295(1): 74-80.

Nagao, A., M. Kobayashi, S. Koyasu, C. C. T. Chow and H. Harada (2019). "**HIF-1-Dependent Reprogramming of Glucose Metabolic Pathway of Cancer Cells and Its Therapeutic Significance**." Int J Mol Sci 20(2).

Nam, G. H., M. Kwon, H. Jung, E. Ko, S. A. Kim, Y. Choi, . . . I. S. Kim (2021). "**Statin-mediated inhibition of RAS prenylation activates ER stress to enhance the immunogenicity of KRAS mutant cancer**." J Immunother Cancer 9(7).

Nash, P., X. Tang, S. Orlicky, Q. Chen, F. B. Gertler, M. D. Mendenhall, . . . M. Tyers (2001). "**Multisite phosphorylation of a CDK inhibitor sets a threshold for the onset of DNA replication**." Nature 414(6863): 514-521.

Nguyen, T., A. Khan, Y. Liu, H. B. El-Serag and A. P. Thrift (2018). "**The Association Between Statin Use After Diagnosis and Mortality Risk in Patients With Esophageal Cancer: A Retrospective Cohort Study of United States Veterans**." Am J Gastroenterol 113(9): 1310.

Nguyen, U. T., Z. Guo, C. Delon, Y. Wu, C. Deraeve, B. Franzel, . . . K. Alexandrov (2009). "**Analysis of the eukaryotic prenylome by isoprenoid affinity tagging**." Nat Chem Biol 5(4): 227-235.

Nohturfft, A., M. S. Brown and J. L. Goldstein (1998). "**Topology of SREBP cleavage-activating protein, a polytopic membrane protein with a sterol-sensing domain**." J Biol Chem 273(27): 17243-17250.

Nohturfft, A., R. A. DeBose-Boyd, S. Scheek, J. L. Goldstein and M. S. Brown (1999). "**Sterols regulate cycling of SREBP cleavage-activating protein (SCAP) between endoplasmic reticulum and Golgi**." Proc Natl Acad Sci U S A 96(20): 11235-11240.

Nussbaumer, O., G. Gruenbacher, H. Gander and M. Thurnher (2011). "**DC-like cell-dependent activation of human natural killer cells by the bisphosphonate**

zoledronic acid is regulated by gammadelta T lymphocytes." Blood 118(10): 2743-2751.

Oliner, J. D., J. M. Andresen, S. K. Hansen, S. Zhou and R. Tjian (1996). "**SREBP transcriptional activity is mediated through an interaction with the CREB-binding protein**." Genes Dev 10(22): 2903-2911.

Pan, Q., J. Xu and L. Ma (2020). "**Simvastatin enhances chemotherapy in cervical cancer via inhibition of multiple prenylation-dependent GTPases-regulated pathways**." Fundam Clin Pharmacol 34(1): 32-40.

Pandyra, A. A., P. J. Mullen, C. A. Goard, E. Ericson, P. Sharma, M. Kalkat, . . . L. Z. Penn (2015). "**Genome-wide RNAi analysis reveals that simultaneous inhibition of specific mevalonate pathway genes potentiates tumor cell death**." Oncotarget 6(29): 26909-26921.

Park, S., C. Y. Chang, R. Safi, X. Liu, R. Baldi, J. S. Jasper, . . . D. P. McDonnell (2016). "**ERRalpha-Regulated Lactate Metabolism Contributes to Resistance to Targeted Therapies in Breast Cancer**." Cell Rep 15(2): 323-335.

Peterson, T. R., S. S. Sengupta, T. E. Harris, A. E. Carmack, S. A. Kang, E. Balderas, . . . D. M. Sabatini (2011). "**mTOR complex 1 regulates lipin 1 localization to control the SREBP pathway**." Cell 146(3): 408-420.

Pickart, C. M. and M. J. Eddins (2004). "**Ubiquitin: structures, functions, mechanisms**." Biochim Biophys Acta 1695(1-3): 55-72.

Piperno-Neumann, S., M. C. Le Deley, F. Redini, H. Pacquement, P. Marec-Berard, P. Petit, . . . G. French Sarcoma (2016). "**Zoledronate in combination with chemotherapy and surgery to treat osteosarcoma (OS2006): a randomised, multicentre, open-label, phase 3 trial**." Lancet Oncol 17(8): 1070-1080.

Popov, N., M. Wanzel, M. Madiredjo, D. Zhang, R. Beijersbergen, R. Bernards, . . . M. Eilers (2007). "**The ubiquitin-specific protease USP28 is required for MYC stability**." Nat Cell Biol 9(7): 765-774.

Porstmann, T., C. R. Santos, B. Griffiths, M. Cully, M. Wu, S. Leevers, . . . A. Schulze (2008). "**SREBP activity is regulated by mTORC1 and contributes to Akt-dependent cell growth**." Cell Metab 8(3): 224-236.

Prieto-Garcia, C., O. Hartmann, M. Reissland, F. Braun, S. Bozkurt, N. Pahor, . . . M. E. Diefenbacher (2022). "**USP28 enables oncogenic transformation of respiratory cells, and its inhibition potentiates molecular therapy targeting mutant EGFR, BRAF and PI3K**." Mol Oncol 16(17): 3082-3106.

Prieto-Garcia, C., O. Hartmann, M. Reissland, F. Braun, T. Fischer, S. Walz, . . . M. E. Diefenbacher (2020). "**Maintaining protein stability of Np63 via USP28 is required by squamous cancer cells**." EMBO Mol Med 12(4): e11101.

Prieto-Garcia, C., O. Hartmann, M. Reissland, T. Fischer, C. R. Maier, M. Rosenfeldt, . . . M. E. Diefenbacher (2021). "**Inhibition of USP28 overcomes Cisplatin-resistance of squamous tumors by suppression of the Fanconi anemia pathway**." Cell Death Differ.

Prieto-Garcia, C., I. Tomaskovic, V. J. Shah, I. Dikic and M. Diefenbacher (2021). "**USP28: Oncogene or Tumor Suppressor? A Unifying Paradigm for Squamous Cell Carcinoma**." Cells 10(10).

Punga, T., M. T. Bengoechea-Alonso and J. Ericsson (2006). "**Phosphorylation and ubiquitination of the transcription factor sterol regulatory element-binding protein-1 in response to DNA binding**." J Biol Chem 281(35): 25278-25286.

Ravid, T., R. Doolman, R. Avner, D. Harats and J. Roitelman (2000). "**The ubiquitin-proteasome pathway mediates the regulated degradation of mammalian 3-hydroxy-3-methylglutaryl-coenzyme A reductase**." J Biol Chem 275(46): 35840-35847.

Reed, B. D., A. E. Charos, A. M. Szekely, S. M. Weissman and M. Snyder (2008). "**Genome-wide occupancy of SREBP1 and its partners NFY and SP1 reveals novel functional roles and combinatorial regulation of distinct classes of genes**." PLoS Genet 4(7): e1000133.

Ribatti, D., R. Tamma and T. Annese (2020). "**Epithelial-Mesenchymal Transition in Cancer: A Historical Overview**." Transl Oncol 13(6): 100773.

Richter, K., T. Paakkola, D. Mennerich, K. Kubaichuk, A. Konzack, H. Ali-Kippari, . . . T. Kietzmann (2018). "**USP28 Deficiency Promotes Breast and Liver Carcinogenesis as well as Tumor Angiogenesis in a HIF-independent Manner**." Mol Cancer Res 16(6): 1000-1012.

Roth, G., J. Kotzka, L. Kremer, S. Lehr, C. Lohaus, H. E. Meyer, . . . D. Muller-Wieland (2000). "**MAP kinases Erk1/2 phosphorylate sterol regulatory element-binding protein (SREBP)-1a at serine 117 in vitro**." J Biol Chem 275(43): 33302-33307.

Rudalska, R., D. Dauch, T. Longerich, K. McJunkin, T. Wuestefeld, T. W. Kang, . . . L. Zender (2014). "**In vivo RNAi screening identifies a mechanism of sorafenib resistance in liver cancer**." Nat Med 20(10): 1138-1146.

Ruiz, E. J., A. Pinto-Fernandez, A. P. Turnbull, L. Lan, T. M. Charlton, H. C. Scott, . . . A. Behrens (2021). "**USP28 deletion and small-molecule inhibition destabilizes c-MYC and elicits regression of squamous cell lung carcinoma**." Elife 10.

Sakai, J., E. A. Duncan, R. B. Rawson, X. Hua, M. S. Brown and J. L. Goldstein (1996). "**Sterol-regulated release of SREBP-2 from cell membranes requires two sequential cleavages, one within a transmembrane segment**." Cell 85(7): 1037-1046.

Sakai, J., A. Nohturfft, D. Cheng, Y. K. Ho, M. S. Brown and J. L. Goldstein (1997). "**Identification of complexes between the COOH-terminal domains of sterol regulatory element-binding proteins (SREBPs) and SREBP cleavage-activating protein**." J Biol Chem 272(32): 20213-20221.

Salviati, L., E. Trevisson, M. Doimo and P. Navas (1993). Primary Coenzyme Q(10) Deficiency. GeneReviews((R)). M. P. Adam, G. M. Mirzaa, R. A. Pagon, S. E. Wallace, L. J. H. Bean, K. W. Gripp and A. Amemiya. Seattle (WA).

Sanchez, H. B., L. Yieh and T. F. Osborne (1995). "**Cooperation by sterol regulatory element-binding protein and Sp1 in sterol regulation of low density lipoprotein receptor gene**." J Biol Chem 270(3): 1161-1169.

Sato, R., J. Inoue, Y. Kawabe, T. Kodama, T. Takano and M. Maeda (1996). "**Sterol-dependent transcriptional regulation of sterol regulatory element-binding protein-2**." J Biol Chem 271(43): 26461-26464.

Sauer, F., T. Klemm, R. B. Kollampally, I. Tessmer, R. K. Nair, N. Popov and C. Kisker (2019). "**Differential Oligomerization of the Deubiquitinases USP25 and USP28 Regulates Their Activities**." Mol Cell 74(3): 421-435 e410.

Schindelin, J., I. Arganda-Carreras, E. Frise, V. Kaynig, M. Longair, T. Pietzsch, . . . A. Cardona (2012). "**Fiji: an open-source platform for biological-image analysis**." Nat Methods 9(7): 676-682.

Schulein-Volk, C., E. Wolf, J. Zhu, W. Xu, L. Taranets, A. Hellmann, . . . N. Popov (2014). "**Dual regulation of Fbw7 function and oncogenic transformation by Usp28**." Cell Rep 9(3): 1099-1109.

Semenza, G. L., P. H. Roth, H. M. Fang and G. L. Wang (1994). "**Transcriptional regulation of genes encoding glycolytic enzymes by hypoxia-inducible factor 1**." J Biol Chem 269(38): 23757-23763.

Shamma, A., Y. Takegami, T. Miki, S. Kitajima, M. Noda, T. Obara, . . . C. Takahashi (2009). "**Rb Regulates DNA damage response and cellular senescence through E2F-dependent suppression of N-ras isoprenylation**." Cancer Cell 15(4): 255-269.

Shaw, R. J., K. A. Lamia, D. Vasquez, S. H. Koo, N. Bardeesy, R. A. Depinho, . . . L. C. Cantley (2005). "**The kinase LKB1 mediates glucose homeostasis in liver and therapeutic effects of metformin**." Science 310(5754): 1642-1646.

Shim, H., C. Dolde, B. C. Lewis, C. S. Wu, G. Dang, R. A. Jungmann, . . . C. V. Dang (1997). "**c-Myc transactivation of LDH-A: implications for tumor metabolism and growth**." Proc Natl Acad Sci U S A 94(13): 6658-6663.

Shimano, H., J. D. Horton, I. Shimomura, R. E. Hammer, M. S. Brown and J. L. Goldstein (1997). "**Isoform 1c of sterol regulatory element binding protein is less active than isoform 1a in livers of transgenic mice and in cultured cells**." J Clin Invest 99(5): 846-854.

Shimomura, I., H. Shimano, J. D. Horton, J. L. Goldstein and M. S. Brown (1997). "**Differential expression of exons 1a and 1c in mRNAs for sterol regulatory element binding protein-1 in human and mouse organs and cultured cells**." J Clin Invest 99(5): 838-845.

Singh, H., S. M. Mahmud, D. Turner, L. Xue, A. A. Demers and C. N. Bernstein (2009). "**Long-term use of statins and risk of colorectal cancer: a population-based study**." Am J Gastroenterol 104(12): 3015-3023.

Singh, S., A. G. Singh, P. P. Singh, M. H. Murad and P. G. Iyer (2013). "**Statins are associated with reduced risk of esophageal cancer, particularly in patients with Barrett's esophagus: a systematic review and meta-analysis**." Clin Gastroenterol Hepatol 11(6): 620-629.

Singla, M., A. Kumar, A. Bal, S. Sarkar and S. Bhattacharyya (2018). "**Epithelial to mesenchymal transition induces stem cell like phenotype in renal cell carcinoma cells**." Cancer Cell Int 18: 57.

Smith, J. R., T. F. Osborne, M. S. Brown, J. L. Goldstein and G. Gil (1988). "**Multiple sterol regulatory elements in promoter for hamster 3-hydroxy-3-methylglutaryl-coenzyme A synthase**." J Biol Chem 263(34): 18480-18487.

Snyder, N. A. and G. M. Silva (2021). "**Deubiquitinating enzymes (DUBs): Regulation, homeostasis, and oxidative stress response**." J Biol Chem 297(3): 101077.

Spruck, C. H., H. Strohmaier, O. Sangfelt, H. M. Muller, M. Hubalek, E. Muller-Holzner, . . . S. I. Reed (2002). "**hCDC4 gene mutations in endometrial cancer**." Cancer Res 62(16): 4535-4539.

Strohmaier, H., C. H. Spruck, P. Kaiser, K. A. Won, O. Sangfelt and S. I. Reed (2001). "**Human F-box protein hCdc4 targets cyclin E for proteolysis and is mutated in a breast cancer cell line**." Nature 413(6853): 316-322.

Sudhof, T. C., D. R. Van der Westhuyzen, J. L. Goldstein, M. S. Brown and D. W. Russell (1987). "**Three direct repeats and a TATA-like sequence are required for regulated expression of the human low density lipoprotein receptor gene**." J Biol Chem 262(22): 10773-10779.

Sundqvist, A., M. T. Bengoechea-Alonso, X. Ye, V. Lukiyanchuk, J. Jin, J. W. Harper and J. Ericsson (2005). "**Control of lipid metabolism by phosphorylation-dependent degradation of the SREBP family of transcription factors by SCF(Fbw7)**." Cell Metab 1(6): 379-391.

Sundqvist, A. and J. Ericsson (2003). "**Transcription-dependent degradation controls the stability of the SREBP family of transcription factors**." Proc Natl Acad Sci U S A 100(24): 13833-13838.

Svensson, R. U., S. J. Parker, L. J. Eichner, M. J. Kolar, M. Wallace, S. N. Brun, . . . R. J. Shaw (2016). "**Inhibition of acetyl-CoA carboxylase suppresses fatty acid**

synthesis and tumor growth of non-small-cell lung cancer in preclinical models." Nat Med 22(10): 1108-1119.

Swatek, K. N. and D. Komander (2016). "**Ubiquitin modifications**." Cell Res 26(4): 399-422.

Tang, J. J., J. G. Li, W. Qi, W. W. Qiu, P. S. Li, B. L. Li and B. L. Song (2011). "**Inhibition of SREBP by a small molecule, betulin, improves hyperlipidemia and insulin resistance and reduces atherosclerotic plaques**." Cell Metab 13(1): 44-56.

Tang, Z., B. Kang, C. Li, T. Chen and Z. Zhang (2019). "**GEPIA2: an enhanced web server for large-scale expression profiling and interactive analysis**." Nucleic Acids Res 47(W1): W556-W560.

Taranets, L., J. Zhu, W. Xu and N. Popov (2015). "**Fbw7 and Usp28 - enemies and allies**." Mol Cell Oncol 2(3): e995041.

Thrower, J. S., L. Hoffman, M. Rechsteiner and C. M. Pickart (2000). "**Recognition of the polyubiquitin proteolytic signal**." EMBO J 19(1): 94-102.

Valero, R., M. Bayes, M. Francisca Sanchez-Font, O. Gonzalez-Angulo, R. Gonzalez-Duarte and G. Marfany (2001). "**Characterization of alternatively spliced products and tissue-specific isoforms of USP28 and USP25**." Genome Biol 2(10): RESEARCH0043.

Walker, A. K., R. L. Jacobs, J. L. Watts, V. Rottiers, K. Jiang, D. M. Finnegan, . . . A. M. Naar (2011). "**A conserved SREBP-1/phosphatidylcholine feedback circuit regulates lipogenesis in metazoans**." Cell 147(4): 840-852.

Wang, H., G. Sarikonda, K. J. Puan, Y. Tanaka, J. Feng, J. L. Giner, . . . C. T. Morita (2011). "**Indirect stimulation of human Vgamma2Vdelta2 T cells through alterations in isoprenoid metabolism**." J Immunol 187(10): 5099-5113.

Wang, X., Z. Liu, L. Zhang, Z. Yang, X. Chen, J. Luo, . . . X. Guo (2018). "**Targeting deubiquitinase USP28 for cancer therapy**." Cell Death Dis 9(2): 186.

Wang, X., R. Sato, M. S. Brown, X. Hua and J. L. Goldstein (1994). "**SREBP-1, a membrane-bound transcription factor released by sterol-regulated proteolysis**." Cell 77(1): 53-62.

Warburg, O. (1956). "**On the origin of cancer cells**." Science 123(3191): 309-314.

Warburg, O., F. Wind and E. Negelein (1927). "**The Metabolism of Tumors in the Body**." J Gen Physiol 8(6): 519-530.

Webb, B. A., M. Chimenti, M. P. Jacobson and D. L. Barber (2011). "**Dysregulated pH: a perfect storm for cancer progression**." Nat Rev Cancer 11(9): 671-677.

Wei, J., Y. Yuan, L. Chen, Y. Xu, Y. Zhang, Y. Wang, . . . D. Fang (2018). "**ER-associated ubiquitin ligase HRD1 programs liver metabolism by targeting multiple metabolic enzymes**." Nat Commun 9(1): 3659.

Weitz-Schmidt, G., K. Welzenbach, V. Brinkmann, T. Kamata, J. Kallen, C. Bruns, . . . U. Hommel (2001). "**Statins selectively inhibit leukocyte function antigen-1 by binding to a novel regulatory integrin site**." Nat Med 7(6): 687-692.

Welcker, M. and B. E. Clurman (2008). "**FBW7 ubiquitin ligase: a tumour suppressor at the crossroads of cell division, growth and differentiation**." Nat Rev Cancer 8(2): 83-93.

Welcker, M., E. A. Larimore, J. Swanger, M. T. Bengoechea-Alonso, J. E. Grim, J. Ericsson, . . . B. E. Clurman (2013). "**Fbw7 dimerization determines the specificity and robustness of substrate degradation**." Genes Dev 27(23): 2531-2536.

Welcker, M., A. Orian, J. Jin, J. E. Grim, J. W. Harper, R. N. Eisenman and B. E. Clurman (2004). "**The Fbw7 tumor suppressor regulates glycogen synthase kinase 3 phosphorylation-dependent c-Myc protein degradation**." Proc Natl Acad Sci U S A 101(24): 9085-9090.

Wilkinson, K. D. (2009). "**DUBs at a glance**." J Cell Sci 122(Pt 14): 2325-2329.

Wilson, M. M., R. A. Weinberg, J. A. Lees and V. J. Guen (2020). "**Emerging Mechanisms by which EMT Programs Control Stemness**." Trends Cancer 6(9): 775-780.

Wrigley, J. D., G. Gavory, I. Simpson, M. Preston, H. Plant, J. Bradley, . . . D. M. Andrews (2017). "**Identification and Characterization of Dual Inhibitors of the USP25/28 Deubiquitinating Enzyme Subfamily**." ACS Chem Biol 12(12): 3113-3125.

Wu, Y., K. Chen, X. Liu, L. Huang, D. Zhao, L. Li, . . . X. Liu (2016). "**Srebp-1 Interacts with c-Myc to Enhance Somatic Cell Reprogramming**." Stem Cells 34(1): 83-92.

Xu, C., C. M. Fillmore, S. Koyama, H. Wu, Y. Zhao, Z. Chen, . . . K. K. Wong (2014). "**Loss of Lkb1 and Pten leads to lung squamous cell carcinoma with elevated PD-L1 expression**." Cancer Cell 25(5): 590-604.

Yabe, D., M. S. Brown and J. L. Goldstein (2002). "**Insig-2, a second endoplasmic reticulum protein that binds SCAP and blocks export of sterol regulatory element-binding proteins**." Proc Natl Acad Sci U S A 99(20): 12753-12758.

Yamane, H. K., C. C. Farnsworth, H. Y. Xie, W. Howald, B. K. Fung, S. Clarke, . . . J. A. Glomset (1990). "**Brain G protein gamma subunits contain an all-trans-geranylgeranylcysteine methyl ester at their carboxyl termini**." Proc Natl Acad Sci U S A 87(15): 5868-5872.

Yamauchi, Y., N. Iwamoto, M. A. Rogers, S. Abe-Dohmae, T. Fujimoto, C. C. Chang, . . . S. Yokoyama (2015). "**Deficiency in the Lipid Exporter ABCA1 Impairs Retrograde Sterol Movement and Disrupts Sterol Sensing at the Endoplasmic Reticulum**." J Biol Chem 290(39): 23464-23477.

Yang, F., B. W. Vought, J. S. Satterlee, A. K. Walker, Z. Y. Jim Sun, J. L. Watts, . . . A. M. Naar (2006). "**An ARC/Mediator subunit required for SREBP control of cholesterol and lipid homeostasis**." Nature 442(7103): 700-704.

Yang, T., P. J. Espenshade, M. E. Wright, D. Yabe, Y. Gong, R. Aebersold, . . . M. S. Brown (2002). "**Crucial step in cholesterol homeostasis: sterols promote binding of SCAP to INSIG-1, a membrane protein that facilitates retention of SREBPs in ER**." Cell 110(4): 489-500.

Yokoyama, C., X. Wang, M. R. Briggs, A. Admon, J. Wu, X. Hua, . . . M. S. Brown (1993). "**SREBP-1, a basic-helix-loop-helix-leucine zipper protein that controls transcription of the low density lipoprotein receptor gene**." Cell 75(1): 187-197.

York, A. G., K. J. Williams, J. P. Argus, Q. D. Zhou, G. Brar, L. Vergnes, . . . S. J. Bensinger (2015). "**Limiting Cholesterol Biosynthetic Flux Spontaneously Engages Type I IFN Signaling**." Cell 163(7): 1716-1729.

Yu, R., J. Longo, J. E. van Leeuwen, C. Zhang, E. Branchard, M. Elbaz, . . . L. Z. Penn (2021). "**Mevalonate Pathway Inhibition Slows Breast Cancer Metastasis via Reduced N-glycosylation Abundance and Branching**." Cancer Res 81(10): 2625-2635.

Yuan, J., K. Luo, L. Zhang, J. C. Cheville and Z. Lou (2010). "**USP10 regulates p53 localization and stability by deubiquitinating p53**." Cell 140(3): 384-396.

Zhang, D., K. Zaugg, T. W. Mak and S. J. Elledge (2006). "**A role for the deubiquitinating enzyme USP28 in control of the DNA-damage response**." Cell 126(3): 529-542.

Zhang, L., B. Xu, Y. Qiang, H. Huang, C. Wang, D. Li and J. Qian (2015). "**Overexpression of deubiquitinating enzyme USP28 promoted non-small cell lung cancer growth**." J Cell Mol Med 19(4): 799-805.

Zhang, Y., Q. Meng, Q. Sun, Z. X. Xu, H. Zhou and Y. Wang (2021). "**LKB1 deficiency-induced metabolic reprogramming in tumorigenesis and non-neoplastic diseases**." Mol Metab 44: 101131.

Zhong, B., X. Liu, X. Wang, X. Liu, H. Li, B. G. Darnay, . . . C. Dong (2013). "**Ubiquitin-specific protease 25 regulates TLR4-dependent innate immune responses through deubiquitination of the adaptor protein TRAF3**." Sci Signal 6(275): ra35.

Zhong, C., L. Fan, Z. Li, F. Yao and H. Zhao (2019). "**SREBP2 is upregulated in esophageal squamous cell carcinoma and cooperates with cMyc to regulate HMGCR expression**." Mol Med Rep 20(4): 3003-3010.

8 Appendix

8.1 Supplementary Tables

Table 13: Significantly downregulated metabolites in A431 shSREBF2 #2 cells.

Metabolite	Log2FC	-log10(p-value)
Guanosine	-1,8997553	1,41688209
GMP	-1,4452128	1,66380558
ATP	-1,3716537	3,30050273
dGTP	-1,3716537	3,30050273
UMP	-1,1974539	1,8827613
CDP	-1,1540645	2,2603562
ADP	-1,1525294	3,5612311
dGDP	-1,1525294	3,5612311
Hypoxanthine	-0,9959259	4,66791328
D-Erythrose 4-phosphate	-0,9507801	2,01876345
L-Lactic acid	-0,938775	1,83848084
dInosine	-0,9242273	3,78171086
dTTP	-0,8729423	1,3856748
L-Tyrosine	-0,7451536	1,42180223
Glyceric acid	-0,7336314	1,7633259
Glucosamine	-0,7297922	1,49308406
S-Adenosylhomocysteine	-0,6556958	1,86293657
L-Lysine	-0,6452607	1,45779394
Citric acid	-0,5951899	2,31471902
L-Serine	-0,5687666	1,62248272
L-Dihydroorotic acid	-0,5313161	2,2024073
Orotic acid	-0,3373458	1,48320003
4-Hydroxyproline	-0,3022625	1,35104298
Fumaric acid	-0,2136961	1,94127144

Table 14: Significantly downregulated metabolites in A431 shUSP28 #1 cells.

Metabolite	**Log2FC**	**-log10(p-value)**
L-Tryptophan	-4,8960584	3,53628614
L-Tyrosine	-3,893268	4,56584643
Phenylpyruvic acid	-3,7254912	4,54021562
ATP	-2,8930636	3,32270337
dGTP	-2,8930636	3,32270337
CDP	-2,4963298	2,37162129
L-Cystathionine	-2,3698389	1,85737374
ADP	-2,3195032	2,80983645
dGDP	-2,3195032	2,80983645
UTP	-2,1723487	2,39022956
GMP	-1,9052154	1,70798618
Glyceric acid	-1,8813488	2,35064761
L-Lactic acid	-1,8064108	3,02514304
CTP	-1,7672601	1,5313966
NADP	-1,747179	1,89695062
Guanosine	-1,7366555	1,36761864
UMP	-1,6152471	2,12722566
dTMP	-1,4652539	1,58044504
Citric acid	-1,376623	1,46047754
Gluconic acid	-1,3716448	3,1951589
IMP	-1,2405011	1,30587314
4-Hydroxyproline	-1,2365091	1,83543065
Glyceraldehyde-3-phosphate	-1,1923748	1,66319517
S-Adenosylmethionine	-1,0816212	1,31344461
L-Lysine	-1,0707945	1,56480629
Glucosamine	-1,0249101	1,55241207
Glycine	-0,9665678	1,62403587
Citrulline	-0,7830905	1,95256663
Orotic acid	-0,7491909	2,66011945
L-Methionine	-0,745456	2,10669329
L-Valine	-0,7087262	3,78499729
L-Dihydroorotic acid	-0,6296708	2,06478606
Putrescine	-0,5532455	1,36614328
Pantothenic acid	-0,4561966	1,46937787

8.2 List of Figures

8.3 Abbreviations

AAV	Adeno associated virus
ABCA	ATP-binding cassette, subfamily A
ACAT	Acetyl-CoA acetyltransferase
ACC	Acetyl-CoA carboxylase
ACLY	ATP citrate lyase
ACSS2	Acyl-CoA Synthetase Short Chain Family Member 2
ADC	Adenocarcinoma
ALLN	N-acetyl-leucyl-norleucinal
AMPK	Adenosine monophosphate-activated protein kinase
APS	Ammonium persulfate
ARC	Activator-recruited co-factor
ATCC	American Type Culture Collection
BCA	Bicinchoninic Acid
bHLH	Basic helix-loop helix
BSA	Bovine serum albumin
BSL	Biosafety level
CBP	CREB-binding protein
CDDP	Cisplatin
CESC	Cervical squamous cancer
CHX	Cycloheximide
CIP	Calf intestinal phosphatase
CMV	Cytomegalovirus
COP	Coat protein complex
CPD	Cdc4 phosphodegron
CREB	cAMP response element binding protein
CSC	Cancer stem-like cells
CUL	Cullin
DAB	3,3’-diaminobenzidine
DAPI	4’,6-diamidino-2-phenylindole
DDR	DNA damage response
DHODH	Dihydroorotate dehydrogenase
DMAPP	Dimethylallyl pyrophosphate
DMEM	Dulbecco's Modified Eagle's Medium
DMF	Dimethylformamid
DMSO	Dimethylsulfoxid
DNA	Deoxyribonucleic acid
dNTPs	Deoxynucleotides
DOX	Doxycycline
DSP	Dithiobis[succinimidylpropionate]
DTT	Dithiothreitol
DUB	Deubiquitinase
EGFR	Epidermal Growth Factor Receptor
EMT	Epithelial mesenchymal transition
ER	Endoplasmatic Reticulum
ERAD	ER-associated degradation
ESCC	Esophageal squamous cell carcinoma

FASN	Fatty acid synthase
FBS/FCS	Fetal Bovine/Calf Serum
FDFT1	Farnesyl-diphosphate farnesyltransferase 1
FPP	Farnesyl pyrophosphate
FPPS	Farnesyl diphosphate synthase
GAPDH	Glyceraldehyde 3-phosphate dehydrogenase
GFP	Green Fluorescent Protein
GGPP	Geranylgeranyl pyrophosphate
GGPPS	Geranylgeranyl pyrophosphate synthase
GSEA	Gene Set Enrichment Analysis
GSK3	Glycogen synthase kinase 3
GTF	General Transcription Factors
HAT	Histone acetyltransferase
HECT	Homologous to the E6-AP carboxyl terminus
HIF	Hypoxia-inducible factor
HMGCS	HMG-CoA synthase
HMGCR	HMG-CoA reductase
HRD1	HMGCR degradation protein 1
IFN	Interferone
IHC	Immunohistochemistry
INSIG	Insulin-induced gene
IPP	Isopentenyl pyrophosphate
KLF5	Kruppel like factor 5
KO	Knockout
LDL	Low-density lipoprotein
LDLR	Low-density lipoprotein receptor
LKB1	Liver kinase B1
mHCC	Murine Hepatocellular Carcinoma
MUFA	Monounsaturated fatty acids
MVA	Mevalonate
MVD	Mevalonate-5-pyrophosphate decarboxylase
MVK	Mevalonate-5-kinase
NSCLC	Non-small cell lung cancer
OAA	Oxalacetate
PCR	Polymerase Chain Reaction
PEI	Polyethylenimine
PFA	Paraformaldehyde
PI3K	phosphatidylinositol 3 kinase
PLA	Proximity Ligation Assay
PMVK	Phosphomevalonate kinase
PTM	Post-translational Modification
RING	Really interesting new gene
RNA	Ribonucleic Acid
RPMI	Roswell Park Memorial Institute
RT	Room temperature
SCAP	SREBP cleavage activating protein
SCC	Squamous Cell Carcinoma
SCD1	Stearoyl-CoA desaturase 1

SCLC	Small cell lung cancer
SDM	Site-directed mutagenesis
SDS-PAGE	Sodium dodecylsulfate polyacrylamide gel electrophoresis
SKP	S-phase kinase-associated protein
SQLE	Squalene monooxygenase
SRE	Sterol-regulatory element
SREBP	Sterol regulatory element binding protein
SSD	Sterol-sensing domain
STK11	Serine/threonine kinase 11
STR	Short Tandem Repeats
SUMO	Small ubiquitin-related modifier 1
S1P	Site-1 protease
S2P	Site-2 protease
TAD	Transactivation domain
TAGs	Triglycerides
TCA	Tricarboxylic acid
TCGA	The Cancer Genome Atlas
TF	Transcription Factors
TKI	Tyrosine kinase inhibitor
TPM	Transcripts per million
TSP	Total Soluble Protein
TTF-1	Thyroid transcription factor 1
UBA domain	Ubiquitin-associated domain
UBL domain	Ubiquitin-like domain
UIM	Ubiquitin-interacting motif
UPS	Ubiquitin Proteasome System
USP	Ubiquitin-specific protease
UV	Ultraviolet
VLDL	Very Low Density Lipoprotein
VME	Vinyl methyl ester
WT	Wild-type
5-FU	5-Fluorouracil

8.4 Acknowledgments

There are many who helped me along the way on this journey and I want to make a moment to thank them.

First, I wish to thank Prof. Dr. Almut Schulze for the opportunity to work on this project in her lab, for her guidance and her patience. Almut, without your support, I would have getting off the train and would regret this decision for the rest of my life. Thank you for being supportive on my side whenever I need to discuss data, asked for reviewing and especially in personal exceptional situations.

Further, I want to thank my thesis committee members Prof. Dr. Grzegorz Sumara, Prof. Dr. Popov and Dr. Markus Diefenbacher. Thanks to Prof. Sumara, who attended all my thesis committee meetings and added valuable discussion points by having another perspective on the project leading this to success. Nikita, thank you so much for investigating in some preliminary experiments laying the foundation for this PhD project. I am thankful for your support during the last years and when finalising the manuscript for publication. Markus, when my group moved to Heidelberg in my third year of PhD you offered me to stay further in Würzburg in your group. I was warmly welcomed and enjoyed the lively discussions during the lab meetings. Thank you so much for giving me this opportunity, the great ideas for the project, the close collaboration with your group and your support in all scientific and personal issues.

Additionally, I want to thank Prof. Alexander Buchberger, spokesperson of the GRK2243. I am grateful for the funding of my project by the DFG within this RTG and I am thankful for the opportunity to gain from the well-structured program, the great retreats and the attendance of several international conferences. The GRK2243 created a terrific scientific environment for young scientists in Würzburg. Thanks to Julia Seubert, coordinator of the GRK, for planning and organising such great events.

I want to acknowledge the support of Dr. Lisa Schlicker and Dr. Felix Vogel at the AG Schulze for their help and support on the metabolomics and transcriptomics experiments. Special thanks to the technicians Silke Haid and Celine Reifenberg for their help and support mostly during my pregnancy. I really enjoyed the coffee breaks with you and Anna Lück, who was always there for administrative questions. Thanks to all members of the AG Schulze in Würzburg and later on in Heidelberg. It was a pleasure working with you.

I appreciate the scientific environment of the Department of Biochemistry and Molecular Biology of the Biocenter in Würzburg. Special thanks to the head of the department Prof. Dr. Martin Eilers and the team of the Eilers lab, the Diefenbacher lab, the Wolf lab and the Wiegering lab. Thank you all for the great team work making such projects successful. Thanks to Uschi and Christina supporting the experiments using the operetta system.

Especially, I wanted to say thank you to Cristian Pietro-Garcia and Oliver Hartman of the Diefenbacher lab. Cristian, thank you for your support, the many scientific discussions and also the great exchange of data. Thank you to Oli, for all your contribution in this project by carrying out the mouse experiments and thanks for being patient with me during the histological analysis. Beside the work-related teamwork, I want to thank you for being at my side in all good and bad times in my life and I am looking forward spending the rest of my life with you – thank you for marrying me.
Namely, I wanted to thank Michi (AG Diefenbacher), Isa (AG Eilers), Sarah (AG Wiegering) and Jessi (AG Wolf) for a wonderful friendship and the warm welcome at the Department. Thanks for being there in all situations – at daily work and personally. I really enjoyed the unforgettable Girls' Nights.

Lastly, I want to thank my families. I am sure my parents would be proud finally finishing this chapter. Thanks to my sister Sonja, who still refuses to listen to my scientific problems and my brother Matze. On the other side, I want to thank Anka and Micha Hartmann, welcoming me in their family and persistently asking, when I will be finished – now I am.

8.5 Publications

Kaymak, I., **Maier, C.R.**, Schmitz, W., Campbell, A.D., Dankworth, B., Ade, C.P., Walz, S., Paauwe, M., Kalogirou, C., Marouf, H., et al. (2020). Mevalonate Pathway Provides Ubiquinone to Maintain Pyrimidine Synthesis and Survival in p53-Deficient Cancer Cells Exposed to Metabolic Stress. Cancer Res 80, 189-203. 10.1158/0008-5472.CAN-19-0650.

Triki, M., Rinaldi, G., Planque, M., Broekaert, D., Winkelkotte, A.M., **Maier, C.R.**, Janaki Raman, S., Vandekeere, A., Van Elsen, J., Orth, M.F., et al. (2020). mTOR Signaling and SREBP Activity Increase FADS2 Expression and Can Activate Sapienate Biosynthesis. Cell Rep 31, 107806. 10.1016/j.celrep.2020.107806.

Hartmann, O., Reissland, M., **Maier, C.R.**, Fischer, T., Prieto-Garcia, C., Baluapuri, A., Schwarz, J., Schmitz, W., Garrido-Rodriguez, M., Pahor, N., et al. (2021). Implementation of CRISPR/Cas9 Genome Editing to Generate Murine Lung Cancer Models That Depict the Mutational Landscape of Human Disease. Front Cell Dev Biol 9, 641618. 10.3389/fcell.2021.641618.

Prieto-Garcia, C., Hartmann, O., Reissland, M., Fischer, T., **Maier, C.R.**, Rosenfeldt, M., Schulein-Volk, C., Klann, K., Kalb, R., Dikic, I., et al. (2022). Inhibition of USP28 overcomes Cisplatin-resistance of squamous tumors by suppression of the Fanconi anemia pathway. Cell Death Differ 29, 568-584. 10.1038/s41418-021-00875-z.

Maier, C.R., Hartmann, O., Prieto-Garcia, C., Al-Shami, K.M., Schlicker, L., Vogel, F.C.E., Haid, S., Klann, K., Buck, V., Munch, C., et al. (2023). USP28 controls SREBP2 and the mevalonate pathway to drive tumour growth in squamous cancer. Cell Death Differ 30, 1710-1725. 10.1038/s41418-023-01173-6.

8.6 Affidavit

I hereby confirm that my thesis entitled *Regulation of the Mevalonate Pathway by the Deubiquitinase USP28 in Squamous Cancer* is the result of my own work. I did not receive any help or support from commercial consultants. All sources and / or materials applied are listed and specified in the thesis.

Furthermore, I confirm that this thesis has not yet been submitted as part of another examination process neither in identical nor in similar form.

Würzburg, 28th July 2023
Place, Date Signature

Hiermit erkläre ich an Eides statt, die Dissertation *Regulation des Mevalonat Stoffwechselwegs durch die Deubiquitinase USP28 in Plattenepithelkarzinomen* eigenständig, d.h. insbesondere selbständig und ohne Hilfe eines kommerziellen Promotionsberaters, angefertigt und keine anderen als die von mir angegebenen Quellen und Hilfsmittel verwendet zu haben.

Ich erkläre außerdem, dass die Dissertation weder in gleicher noch in ähnlicher Form bereits in einem anderen Prüfungsverfahren vorgelegen hat.

Würzburg, den 28. Juli 2023
Ort, Datum Unterschrift

8.7 Curriculum Vitae